



The University of  
**Nottingham**

UNITED KINGDOM • CHINA • MALAYSIA

# **Low Molecular Mass Nucleoside Gelators For Intra-Tumoural Drug Delivery**

Kathryn J. Skilling MChem (Hons.)

Submitted to The University of Nottingham for the degree of Doctor of  
Philosophy

September 2015



## Declaration

---

Unless otherwise acknowledged, the work presented in this thesis is my own. No part has been submitted for any other degree at The University of Nottingham or any other institution.

The data presented in Chapters 1 and 2 is based upon previous publications:

Chapter 1: Insights into low molecular mass gelators: a focus on drug delivery and tissue engineering applications. K. J. Skilling, F. Citossi, M. Ashford, T. D. Bradshaw, B. Kellam and M. Marlow, *Soft Matter*, 2014, 10, 237-256

Chapter 2: Gelation properties of self-assembling *N*-acyl modified cytidine derivatives. K. J. Skilling, A. Ndungu, M. Ashford, T. D. Bradshaw, B. Kellam and M. Marlow, *J. Mater. Chem. B*. 2014, 2, 8412-8417

Kathryn J. Skilling

September 2015

## Abstract

---

There are numerous chemotherapeutic agents available today that treat a wide array of tumours. The majority of these compounds are administered *via* intravenous (*i.v.*) infusion in large doses (1000 mg/m<sup>2</sup>), necessary to sustain a desired therapeutic effect. The systemic nature of the drug delivery, the dosage size and non-specific nature of many chemotherapeutic agents however means that they attack any rapidly dividing tissue system, leading to the commonly observed side effects e.g. alopecia, nausea, neutropenia and thrombocytopenia.

Low molecular weight gelators (LMWGs) are increasing in popularity as an alternative platform for drug delivery. They are typically small amphiphilic organic molecules which self-assemble in water forming a 3D gel network; they offer advantages over other drug delivery platforms as they are typically derived from biological polymers and are therefore inherently biocompatible.

Using the nucleoside gemcitabine; a first-line treatment for the treatment of gastric and pancreatic cancer as a model drug, two localised delivery systems were developed. The first, an inert LMWG matrix for the encapsulation and passive release of gemcitabine and the second, a therapeutic molecular gel derived from the chemotherapeutic itself.

Cytidine, an inert analogue of gemcitabine was used to develop a passive delivery system. Regioselective synthesis of *N*-acylated derivatives of varying chain lengths was achieved *via* an activated triazine ester. Using a minimal amount of ethanol and an 'anti-solvent' switch gelation method a gelating system derived from the *N*-myristoyl derivative, containing a solvent volume fraction ( $\Phi_{\text{SOL}}$ ) of 0.40 was found to have the most advantageous mechanical and structural properties; a crosslinked nanofibrillar network, established by rheological measurements and microscopy (TEM). The gel was validated as a drug delivery platform *via* encapsulation and release low molecular weight fluorescein and high molecular weight FITC Dextran, with the gelator matrix releasing the smaller fluorescein and retarding the release of the higher molecular weight dextran.

Further modification and optimisation of the passive system afforded an *N*-octanoyl 2'-deoxycytidine conjugate that underwent molecular reorganisation into a cross-linked nanofibrillar structure in a 100 % aqueous environment. This gel was the first of its kind to assemble in this manner and the rheological measurements demonstrate its self-healing properties, whilst encapsulation of fluorescents once again demonstrated controlled release of low molecular weight fluorescein over a 24 h period. *In vitro* growth inhibition assays validated the platform as biologically compatible against gastric (MKN-7) and pancreatic (MIA PaCa-2) cell lines.

Additional modification of the chemotherapeutic itself laid the foundation for an intra-tumoural targeted therapeutic delivery system. Enzyme cleavable pro-drugs of gemcitabine were created with amphiphilic properties, linkages designed to undergo varying rates of hydrolysis from both the *N*-amino and 5'-hydroxyl positions. Whilst no successful gelating entities were achieved, the *N*-amide and 5'-ester prodrugs were found to have comparable potencies to the parent compound *in vitro* when tested against gastric and pancreatic cell lines.

From the results obtained during this work, it can be concluded that with further chemical modification based upon parameters discussed here on in that a LMWG system could be a viable platform for drug delivery in the future.

## Acknowledgements

---

First and foremost, I would like to thank my supervisors at The University of Nottingham; Dr. Maria Marlow, Prof. Barrie Kellam and Dr. Tracey D. Bradshaw for their unwavering support and guidance throughout the PhD. I would also like to thank my industrial supervisor Dr. Marianne Ashford (AstraZeneca) for her help and guidance throughout the project.

Undoubtedly, the work I have accomplished over the last 3 years wouldn't have been possible were it not for the technical guidance provided by Lee Hibbett, Paul Cooling, Tom Booth and Christine Grainger-Boulton. Many thanks also go to Mike Fay in Nottingham Nanotechnology and Nanoscience Centre for TEM imaging and Shazad Aslam in Department of Chemistry for assistance with VT-NMR.

Additional thanks go to members of C24/25, past and present. They have provided constant encouragement, instilled invaluable knowledge but most importantly, have succeeded in keeping me (relatively) sane. A special mention goes to Dr. Andrea Vernall, who was there to offer a helping hand in the early days.

I owe the largest gratitude to my parents and sister. Without the support of my parents in particular I would never have achieved a fraction of what I am so proud of today. The example they set will forever be a standard to which I aspire, and my hard work is only a reflection of their own.

The last few years would not have been possible without a close circle of friends; thrown together on day one, Jamie Patient, Andreea Iuraş, Naim Hage and Francesco Tres. We have suffered through the hard times and celebrated the good; but there is no doubt that the last four years wouldn't have been the same without you!

My final and biggest thank you extends to my boyfriend, Lee Moir. You're the rock that has provided constant encouragement, plenty of laughs and have never failed to pick me back up whenever I've been at breaking point. This work definitely wouldn't have been possible were it not for you.

This work was funded by EPSRC and AstraZeneca; EPSRC Grant EP/I01375X/1

## Abbreviations

1D	One-dimensional
2'-dC	2'-deoxycytidine
2',3'-ddC	2',3'-dideoxycytidine
3D	Three-dimensional
Ala	Alanine
API	Active Pharmaceutical Ingredient
CAL-B	Lipase B Candida Antarctica
CDA	Cytidine Deaminase
CD	Circular Dichroism
CDMT	2-chloro-4,6-dimethoxy-1,3,5-triazine
COSY	Correlation Spectroscopy
DCC	N,N'-dicyclohexylcarbodiimide
dCK	Deoxycytidine Kinase
dFdC	2',2'-difluoro 2'-deoxycytidine / Gemcitabine
DIPEA	N,N-diisopropylethylamine
DMF	N,N-Dimethylformamide
DMSO- <i>d</i> <sub>6</sub>	Deuterated Dimethylsulfoxide
DNA	Deoxyribonucleic acid
EDC	1-ethyl-3-(3-dimethylaminopropyl)carbodiimide
ESI-MS	Electrospray Ionisation - Mass Spectroscopy
EtOH	Ethanol
Fmoc	9- fluoronylmethoxycarbonyl
FT-IR	Fourier Transformed Infra-red Spectroscopy
G'	Storage/Elastic Modulus
G''	Loss Modulus
GABA	Gamma amino butyric acid
GdL	Glucono $\delta$ Lactone
GI	Gastrointestinal
GNL	Glycosyl Nucleolipid

HATU	O-(7-azabenzotriazol-1-yl)-N,N,N',N'-tetramethyluronium hexafluorophosphate
HBTU	O-benzotriazole-N,N,N',N'-tetramethyluronium-hexafluorophosphate
hNT	Human Nucleoside Transporter
HOBt	1-hydroxybenzotriazole
HPLC	High Pressure Liquid Chromatography
HSQC	Heteronuclear Single Quantum Correlation
LC-MS	Liquid Chromatography - Mass Spectrometry
LMWG	Low Molecular Weight Gelator
LVE	Linear Viscoelastic
μm	micrometre
MMP-2	Metalloproteinase-2
nm	nanometre
NMM	<i>N</i> -methyldmorpholine
NMP	<i>N</i> -methylpyrrolidone
NMR	Nuclear Magnetic Resonance Spectroscopy
Pa	Pascal
PBS	Phosphate Buffered Saline
Phe	Phenylalanine
Ppm	Parts per million
r.t	Room temperature
SAFIN	Self-Assembled Fibrillar Network
SEM	Scanning Electron Microscopy
TEM	Transmission Electron Microscopy
T <sub>gel</sub>	Temperature of Gelation
TLC	Thin Layer Chromatography
t <sub>R</sub>	Retention Time
UV	Ultraviolet

# Table of Contents

Declaration .....	ii
Abstract .....	iii
Acknowledgements .....	v
Abbreviations.....	vi
Table of Contents .....	viii
List of Figures.....	xi
List of Tables .....	xiv
List of Schemes .....	xvi
1. Introduction.....	17
1.1. Low Molecular Weight Gelators .....	17
1.1.1. Molecular Considerations .....	20
1.1.2. The Importance of the Gelation Process.....	21
1.1.3. Methods of Characterisation.....	22
1.1.4. Molecular Gels in Drug Delivery .....	26
1.2. Gemcitabine (Gemzar <sup>®</sup> ).....	43
1.2.1. Uptake and Metabolism .....	43
1.2.2. Mechanism of Action.....	46
1.2.3. Gemcitabine Chemoresistance .....	47
1.2.4. Prodrugs of Gemcitabine.....	47
1.3. Project Aims .....	51
2. Modified Cytidine as a Drug Delivery Platform .....	52
2.1. Synthesis .....	55
2.1.1. A Selective Route for <i>N</i> -acylation of Cytidine .....	55
2.2. Analysing the Macroscopic Behaviour.....	57
2.2.1. Vial Inversion .....	57
2.2.2. Rheology .....	62
2.2.3. Nanostructure Determination.....	67
2.3. <i>In Vitro</i> Release Kinetics.....	71
2.4. Can the Gel Function in a Physiological Environment? .....	73

2.4.1.	<i>In Vitro</i> Growth Inhibition Efficiency of Ethanol .....	73
2.4.2.	<i>In Vitro</i> Growth Inhibition Efficiency of 42c .....	73
2.5.	Summary .....	75
2.6.	Materials and Methods .....	76
2.6.1.	General Chemistry .....	76
2.6.2.	Physicochemical Characterisation.....	82
2.6.3.	<i>In Vitro</i> Release Kinetics of Fluorescein, FITC Dextran 4 and FITC Dextran 10 .....	83
2.6.4.	<i>In Vitro</i> Growth Inhibition Assays.....	84
3.	A Tale of Refinement.....	85
3.1.	Is the Amide Integral to the Successful Self-Assembly Process?.....	86
3.2.	Can Gelation be enhanced by Removing Additional Nucleophilic Groups?....	88
3.2.1.	Gel Development.....	92
3.2.2.	Is the Hydrogel a Good Foundation for a Drug Delivery Platform? .....	101
3.2.3.	Nanostructure Determination.....	106
3.2.4.	Gelation NMR .....	106
3.2.5.	<i>In Vitro</i> Release Kinetics of Fluorescents .....	108
3.2.6.	Will Gelation Occur in Simulated Physiological Conditions? .....	110
3.2.7.	Growth Inhibition Studies on Compound and on Gel .....	112
3.3.	Summary.....	120
3.4.	Materials and Methods .....	122
3.4.1.	General Chemistry .....	122
3.4.2.	Physicochemical Characterisation.....	129
3.4.3.	<i>In Vitro</i> Release Kinetics of Fluorescents .....	133
3.4.4.	<i>In Vitro</i> Growth Inhibition Assays.....	133
4.	Therapeutic Molecular Gels of Gemcitabine .....	138
4.1.	Synthesis .....	141
4.1.1.	A Regioselective Enzymatic Synthesis of Gemcitabine-5'-ester Prodrugs .....	141
4.1.2.	Synthesis of Gemcitabine- <i>N</i> -functionalised prodrugs .....	142
4.1.3.	Can existing LMWGs gelators be used as a mode to facilitate gelation? .....	145

4.2.	Physical Characterisation.....	151
4.2.1.	Gemcitabine-5'-esters .....	155
4.2.2.	Gemcitabine- <i>N</i> -amides.....	159
4.2.3.	Gemcitabine- <i>N</i> -carbamates .....	165
4.2.4.	Gemcitabine- <i>N</i> -ureas .....	169
4.2.5.	Summary.....	174
4.2.6.	Fmoc-protected Gemcitabine- <i>N</i> -amino acids.....	175
4.3.	Determining the Cytotoxic Nature of the Molecular Gels.....	177
4.3.1.	Growth Inhibition Studies .....	177
4.4.	Summary.....	180
4.5.	Materials and Methods .....	181
4.5.1.	General Chemistry.....	181
4.5.2.	Physiochemical Characterisation .....	200
4.5.3.	<i>In vitro</i> Growth Inhibition Assays .....	202
5.	Conclusions and Future Work .....	203
5.1.	General Conclusions .....	203
5.1.1.	Modified Cytidine as a Drug Delivery Platform.....	203
5.1.2.	A Tale of Refinement.....	204
5.1.3.	Therapeutics Molecular Gels of Gemcitabine .....	204
5.2.	Future Work.....	206
5.2.1.	Further functionalisation of nucleosides.....	206
5.2.2.	<i>In vitro</i> release of therapeutics from inert-gel scaffold .....	206
5.2.3.	<i>In vivo</i> imaging of drug release.....	206
5.2.4.	Determining the reason for selectivity seen in MRC-5 fibroblasts .....	207
	References.....	208

## List of Figures

Figure 1: The primary, secondary, tertiary and macrostructure of a self-assembled physical network.....	19
Figure 2: Microscopic analysis of a self-assembled Fmoc–diphenylalanine hydrogel...24	
Figure 3: Methods of drug delivery using low molecular weight gelators.....	28
Figure 4: Amino acid derived scaffold gels for drug delivery .....	29
Figure 5: Hydrophobic drugs; doxorubicin and camptothecin .....	30
Figure 6: Cisplatin and self-assembling peptide amphiphile (GTAGLIGQRGDS) .....	33
Figure 7: Stimuli responsive gel based on cyclohexane <i>tris</i> -amide scaffold .....	34
Figure 8: Non-steroidal anti-inflammatory drugs (NSAIDs) and associated gelators ....	35
Figure 9: Paracetamol, amphiphilic and bola-amphiphilic derivatives .....	36
Figure 10: Taxol and Taxol-SA-GSSG derivative .....	37
Figure 11: Nucleoside derived gelators.....	41
Figure 12: Structure of gemcitabine (2',2'-difluoro-2'-deoxycytidine; dFdC) .....	43
Figure 13: Cellular mechanism of gemcitabine.....	45
Figure 14: Gemcitabine mechanisms of action.....	46
Figure 15: Gemcitabine 4-amino prodrugs .....	48
Figure 16: Gemcitabine 5'-prodrugs.....	50
Figure 17: Structure of chemotherapeutic gemcitabine and inert analogue cytidine. .	53
Figure 18: Rheological data for 42c.....	66
Figure 19: Electron microscopy of 42c $\Phi_{\text{EtOH}} 0.40$ .....	68
Figure 20: FT-IR absorbance of the amide I region of 42c. ....	69
Figure 21: <i>In vitro</i> release kinetics of Fluorescein (0.15 mM), FITC Dextran 4 (0.06 mM) and FITC Dextran 10 (0.01 mM) from the gel matrix of 42c. ....	72
Figure 22: Reduction of MTT to formazan. ....	73
Figure 23: a) anti-conformation of cytidine (39) showing C-2 carbonyl (red) and $\beta$ -glycosidic bond (green) b) a representation of molecular syn-conformation of cytidine. ....	85
Figure 24: Vial inversion and interpretation of intra-molecular hydrogen bonding in 42c. ....	87
Figure 25: Structure of 2'-deoxycytidine (46) and 2',3'-dideoxycytidine (47).....	88

Figure 26: Vial inversion of 48d in $\Phi_{\text{EtOH}}$ 0.00, 0.01, 0.02, 0.05, 0.10, 0.20, 0.30, 0.40 and 0.50 (left to right) at a final compound concentration 0.5 % (w/v).....	99
Figure 27: Screen shot of video of gelation over 10 minutes following solubilisation of 48d. a) Following solubilisation b) 2.5 minutes c) 5 minutes d) 10 minutes and e) 10 minutes inverted. ....	99
Figure 28: Rheological studies of 48d $\Phi_{\text{SOL}}$ 0.00, 0.5 % (w/v). ....	103
Figure 29: Recovery sweeps of 48d $\Phi_{\text{SOL}}$ 0.00, 0.5 % w/v. ....	105
Figure 30: Electron microscopy images of 48d .....	106
Figure 31: VT-NMR of 48d in H <sub>2</sub> O. ....	107
Figure 32: Release kinetics of Fluorescein (0.08 mM), FITC Dextran 4 (0.005 mM) and FITC Dextran 10 (0.005 mM) through the gel matrix of 48d. ....	109
Figure 33: Vial inversion of 48d in phosphate buffered saline and RPMI-1640 media	110
Figure 34: G' values of 48d in water (o), PBS pH 7.4 (□) and RPMI 1640 (Δ). ....	111
Figure 35: Cell on Gel colorimetric MTT .....	113
Figure 36: G' values from the strain sweep of 0.5 % and 1 % (w/v) gelators derived from 48d in RPMI-1640 (o) and RPMI-1640 + 1 % gelatine (□). ....	114
Figure 37: Cell proliferation colorimetric assay on MIA PaCa-2 human pancreatic adenocarcinoma cells .....	116
Figure 38: Methylene Blue assay with Mia PaCa-2 cells (left) and MRC-5 fibroblasts (right). ....	117
Figure 39: Cell proliferation colorimetric assay of gels made from 48d (0.5 % and 1 % w/v) injected on to the cell monolayer and in suspended in RPMI-1640. ....	119
Figure 40: Co-axial insert mounted into NMR tube .....	132
Figure 41: 24 well plate arrangement of MTT cell adhesion assays .....	135
Figure 42: 6 well plate arrangement for gel state, cell proliferation assays. ....	137
Figure 43: Structure of Gemcitabine showing functional groups available for derivatisation. ....	140
Figure 44: Fmoc-amino acid structures. ....	145
Figure 45: Peptide coupling agents EDC, DCC and HATU .....	146
Figure 46: Relationship between cLogP and predicted water solubility for ester (50a – 50e), amide (51a – 51e), carbamate (52a – 52c) and urea (53a – 53e) derivatives of gemcitabine. ....	153

Figure 47: Relationship between cLogP and predicted water solubility for Gemcitabine and Fmoc-amino acid (AA) derived conjugates. ....	154
Figure 48: Rheological measurements (amplitude, frequency and recovery) for 51d $\Phi_{\text{EtOH}}$ 0.05 (0.5 % w/v). ....	163
Figure 49: Transmission Electron micrographs of 51d $\Phi_{\text{EtOH}}$ 0.05 (0.5 % w/v) .....	164
Figure 50: Amplitude sweep of 52a (0.5 % w/v, $\Phi_{\text{EtOH}}$ 0.10).....	167
Figure 51: Transmission electron micrograph images of 52a 0.5 % w/v, $\Phi_{\text{EtOH}}$ 0.10...168	
Figure 52: Amplitude and frequency sweep for 53c $\Phi_{\text{EtOH}}$ 0.20 at 25 °C.....	172
Figure 53: Transmission electron micrograph images of 53c 0.5 % w/v, $\Phi_{\text{EtOH}}$ 0.20 prepared at 25 °C. Samples were prepared 24 h in advance of imaging.....	173
Figure 54: Growth inhibition studies of 30, 50d, 51d, 52a and 53c on Mia PaCa-2 (purple) and MKN-7 (grey) adenocarcinoma cell lines. ....	178

## List of Tables

Table 1: cLogP values of compounds 42a - 42e .....	58
Table 2: Vial inversion of compounds 42a - 42e in DMSO (left) and ethanol (right).....	60
Table 3: Classification of gels of 42a - 42e at $\Phi_{\text{SOL}}$ 0.05 – 0.50, where G (Gel), PG (Partial Gel) and NG (no gel).....	61
Table 4: Diffusion coefficients for dyes release from 42c in pH 7.4 phosphate buffered saline .....	72
Table 5: 50 % Growth Inhibition ( $GI_{50}$ ) data for cytidine (39) and cytidine-N-tetradecanoyl (42c) in HCT-116 and MCF-7 cell lines. Data is representative of n=5. ..	74
Table 6: Amount of solvent and ultra-purified water required to make solvent volume fractions ( $\Phi_{\text{SOL}}$ ) 0.00 – 0.50 to a final sample volume of 500 $\mu\text{L}$ .....	82
Table 7: cLogP and predicted water solubility values for 48a and 49a.....	89
Table 8: Vial inversion of 42c, 48a and 49a.....	91
Table 9: Vial inversion of compounds 42c, 48a and 49a in ethanol (top to bottom) with 0.1, 0.25 and 0.5 % (w/v) compound (left to right).....	94
Table 10: Structure and associated cLogP of compounds in series 48 and 49. Representative structure is shown on the right.....	95
Table 11: Stability to inversion of 48a - 48e (left) and 49a - 49d (right) in ethanol.....	97
Table 12: Diffusion coefficient of Fluorescein, FITC Dextran 4 and FITC Dextran 10 from the hydrogel of 48d. ....	110
Table 13: Solution phase growth inhibition studies for 46 and 48d in MIA PaCa-2, MKN-7 and MCF-7 adenocarcinoma cell lines.....	113
Table 14: Amount of compound needed to make final compound concentrations 0.5, 0.25 and 0.1 % (w/v) in 500 $\mu\text{L}$ . ....	130
Table 15: Calculated yields from peptide coupling reactions with gemcitabine .....	150
Table 16: cLogP and predicted water solubility values for compound 50a - 50e, 51a - 51e, 352a - 52c and 53a - 53e .....	153
Table 17: cLogP and predicted water solubility values for compound 55 - 58 and 66 - 69 .....	153
Table 18: Vial inversion of gels derived for 50a - 50e. ....	158
Table 19: Vial inversion of gels derived for 51a - 51e. ....	160

Table 20: Vial inversion of gels derived from 52a - 52c at 60 °C (left) and room temperature (right). .....	166
Table 21: Vial inversion of gels derived for 53a - 53e, $\Phi_{\text{EtOH}}$ 0.00 – 0.20.....	170
Table 22: cLogP and predicted water solubility values for successful gelating compounds 51d, 52a and 53c. ....	174
Table 23: Vials inversion of gels derived from 66 -69 .....	176
Table 24: Solution phase growth inhibition studies for gemcitabine (34) and conjugates 50d, 51d, 52a and 53c in MIA PaCa-2, MKN-7 and MRC-5 cells. ....	179

## List of Schemes

Scheme 1: Synthesis of <i>N</i> -acylated cytidine from an activated triazine ester.....	55
Scheme 2: Synthesis of a cytidine- <i>N</i> -3-OH-tetradecanoyl (45).....	86
Scheme 3: Synthesis of 2'-deoxycytidine- <i>N</i> -tetradecanoyl (48a) and 2',3'- dideoxycytidine- <i>N</i> -tetradecanoyl (49a) <i>via</i> an activated triazine ester.....	89
Scheme 4: Scheme for the synthesis of Gemcitabine-5'-ester prodrugs.....	142
Scheme 5: Synthesis of Gemcitabine- <i>N</i> -acyl derivatives .....	143
Scheme 6: Synthesis of gemcitabine- <i>N</i> -urea derivatives.....	144
Scheme 7: Synthesis of gemcitabine- <i>N</i> -carbamates .....	144
Scheme 8: Desired and undesired reactions of EDC and DCC peptide coupling .....	147
Scheme 9: Mechanism of EDC/DCC peptide coupling .....	148
Scheme 10: Mechanism of HATU coupling .....	148
Scheme 11: Synthesis of Gemcitabine- <i>N</i> -amino acid Fmoc conjugates .....	149

# 1. Introduction

---

## 1.1. Low Molecular Weight Gelators

Over the last two decades, interest in low molecular weight gelators (LMWGs, molecules arbitrarily linked to having a molecular mass of  $\leq 3000$ ) has significantly increased. With a rapidly growing body of literature, a number of reviews<sup>1-8</sup> have summarised molecules that can act as LMWGs and have characterised the potential applications of the gels in multiple systems, including drug delivery, tissue engineering, catalysis and electronics.<sup>9</sup>

Gels are chemically diverse molecular systems that are frequently acknowledged as being easier to recognise than define.<sup>10,11</sup> Following the introduction of gel theory in 1861 by Thomas Graham,<sup>12</sup> the definition of a gel has continually evolved. One of the most well recognised attempts to define a gel came from Jordan Lloyd, who suggested that gels are comprised of two component systems; a liquid and solid that together must express the mechanical properties of a solid.<sup>13</sup> Whilst this definition was useful for defining a gel it was considered imprecise as the definition relied wholly upon qualitative macroscopic observations. The first comprehensive correlation between microscopic and macroscopic properties, thus defining a gel, came about more than 70 years later.<sup>14,15</sup> Flory stated that 'a substance was a gel if it possessed a continuous microscopic structure with macroscopic dimensions that were permanent and solid-like in rheological behaviour despite being derived from systems that were mostly liquid'. Today, in order to link the microscopic and macroscopic properties, a substance will be only be classified as a gel if (i) it has a continuous microscopic structure with macroscopic dimensions and (ii) is solid-like in its rheological behaviour despite being predominantly liquid.<sup>11</sup>

Unlike the more commonly reported polymeric gels, molecular gels contain small amounts (typically  $< 2\%$  (w/v)) of gelator that can gel under aqueous or organic conditions and combinations thereof. The minor solid and major liquid components self-assemble *via* highly specific non-covalent interactions to form a three dimensional continuous phase,<sup>16</sup> typically, an entangled self-assembled fibrillar

network (SAFIN). Gels are broadly categorised depending upon whether the liquid phase is predominantly aqueous or organic. Those gels that are mainly organic in nature (i.e. gelator molecules in organic solvent) are termed organogels; conversely gels that are aqueous in nature (though often containing a small (< 1 %) amount of solvent to solubilise the gelator molecule) are termed hydrogels. The thermally-activated formation of gels is the most common method for gel formation and commonly follows a multistep procedure, involving initial dissolution of a low percentage (0.1 – 5 % (w/v)) of gelator molecule in a heated solvent to obtain a solution or sol. Upon cooling below the temperature of gelation ( $T_{\text{gel}}$ ) the LMWGs are no longer soluble and so, rather than crystallising into a three-dimensional (3D) ordered crystal lattice, they self-assemble. Super-saturation drives the aggregation of the gelator molecules *via* stochastic nucleation whereby the affinity between gelator and liquid phase decreases and the former self-assembles into a 3D network of solid fibres, immobilising the liquid phase through strong intermolecular forces and allowing it to support its own weight without collapsing.<sup>4</sup> Unlike crystallisation, the nucleation requires highly specific interactions that promote one-dimensional (1D) growth. These interactions include hydrogen bonding,  $\pi$ - $\pi$  stacking, van der Waals interactions, electrostatic interactions and London dispersion forces. The morphology of these assembled networks may take on the appearance of fibres, tapes, rods, ribbons, tubules and sheets, to name a few, with the branching between the SAFIN strands being the ultimate determinant in the final mechanical strength of the gels. In 2000, Estroff and Hamilton<sup>17</sup> successfully dissected the mechanism of fibre formation in predominantly aqueous environments (hydrogels) individually characterising the primary, secondary and tertiary structures of fibrous assemblies. **(Figure 1)**

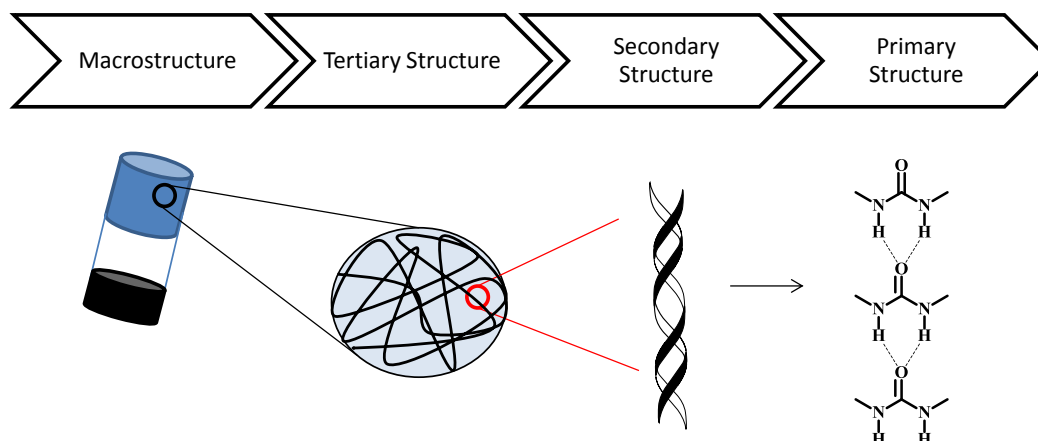


**Figure 1: The primary, secondary, tertiary and macrostructure of a self-assembled physical network.**

Example hydrogen bonding between individual urea molecules represents the primary structure. Under certain conditions e.g. change in temperature, pH, enzymatic influence the gelator will self-assemble *via* non-covalent interactions into an ordered one dimensional network, a secondary structure, represented here by an intertwined helical structure, but may consist of micelles, tapes, vesicles etc. The tertiary structure signifies the overall network; in this case a branching structure of elongated fibres.

Formation of a network of fibres occurs *via* tiered assembly.<sup>18</sup> Initial assembly towards a primary nanostructure is reported to be driven by the aforementioned 1D interactions on the molecular level. These interactions are needed to encourage one dimensional fibre formation over other structures e.g. 3D order in crystallisation, but ultimately gelation is determined by the delicate balance between the molecule's ability to dissolve or aggregate in solution. Whilst it is known that formation of non-covalent interactions such as hydrogen bonds etc. direct the anisotropic self-assembly process, in aqueous environments these interactions are inherently weak, inferring that hydrophobic forces also play a dominant role during the anisotropic aggregation in water. The subsequent transition from secondary to tertiary structure has been described as being the main process by which gel formation is determined. Gelation ultimately requires the creation of a single continuous network, often achieved by the cross-linking of fibres brought about from fibre entanglement or fibre branching, trapping the mobile phase in place. However, even now, the transformation to tertiary structure and association of LMWGs into fibres and the control of cross linking in aqueous solutions are not well understood.<sup>19,20</sup> In 1997, Terech and Weiss<sup>4</sup> described the gelation process in organic media (organogels) and proposed that, unlike in

hydrogel formation, the attractive forces between gelator molecules were largely dipolar interactions but may potentially involve other weak molecular interactions including highly specific intermolecular hydrogen bonds, London dispersion forces, electrostatic forces and  $\pi$ - $\pi$  stacking. They attributed the final lamellar/fibrillar structure of the aggregates to their entropically favoured configuration, specifically the influence of the cross-sectional areas of a hydrocarbon chain, the polar moieties of the gelator and the polarity of the solvent.

Where the result of gelation is a 3D structure, SAFINs favour anisotropic growth along a single axis, the patterns formed consisting of radial arms initiating from a core in a Cayley tree structure. Anisotropy is such that it can be directed *via* the introduction or removal of hydrogen bonding moieties in the gelator molecule e.g. hydroxyl, amide, urea, urethane, sulfide and carboxylic groups. The difference between gelation and solution is often made by only a small change in molecular structure.<sup>21</sup> This was reiterated less than 5 years later by van Esch.<sup>8</sup> However in 2005, Liu<sup>22</sup> reported more recent findings that indicated self-organisation of 3D supramolecular structures was actually controlled by wide angle crystallographic mismatch (non-crystallographic) branching.<sup>23-26</sup> Several models have been developed to explain the transition of amphiphilic gelator molecules from their molecular to primary and secondary aggregate structures.<sup>20,27</sup> but the small number of studies reported do not offer one single mechanism for the complete self-assembly process.

Based on this information we can condense the formation of fibres into three steps: initial fibre nucleation, repeating crystalline fibre branching and fibre growth.

### 1.1.1. Molecular Considerations

Multiple non-covalent interactions are the key to self-assembly of gelator molecules, for this reason, certain functional groups are frequently found in gelator molecules;

- i. Amides (RCONHR') and urea's (RNHCONHR') form complementary hydrogen bonding interactions e.g.  $\text{C}=\text{O}\cdots\text{H}-\text{N}$

- ii. Long chain alkanes generate van der Waals (vdW) forces and solvophobic interactions
- iii. Nucleobases can form hydrogen bonds and  $\pi$ - $\pi$  stacking interactions
- iv. Aromatic rings will facilitate  $\pi$ - $\pi$  stacking interactions
- v. Carbohydrates containing numerous O-H residues are capable of hydrogen bonding.

The role of chirality in gelation is also of particular importance, with a large proportion of existing gelators containing at least one stereogenic centre.<sup>28-31</sup> It is known that mixtures of enantiomers can self-sort and form separate crystals; or a racemic crystal in which the enantiomers form a regular alternating pattern; or a racemic crystal in which the enantiomers are arranged randomly – occurring when there is little-to-no structural difference between enantiomers.<sup>32</sup>

Chirality contributes a stabilising effect to the self-assembly process, playing a role at the scale of individual molecules as well as the completed aggregated state.<sup>33-35</sup> One such example of chirality controlling gelation was demonstrated using the (*S,S*) and (*R,R*) enantiomers of two different oxalamides. The paper showed that the homochiral mixture of (*S,S*) had a rigid ordered structure *via* a hydrogen bonded network; whereas the heterochiral mixture produced a ‘weaker’ network, with lower thermal stability due to polar interactions.<sup>36</sup>

Engelkamp *et al.*<sup>37</sup> demonstrated molecules with chirality, such as crown ethers with a phthalocyanine ring, form helical structures *via*  $\pi$ -stacking and fibres as opposed to the formation of flat aggregates that would have occurred if the molecule was less prone to twisting. Racemic mixtures tend to form these flatter aggregates and are more prone to uncontrollable crystallisation.<sup>29</sup> In general there are limited examples of favourable racemic mixtures i.e. those that are more stable than an enantiomerically pure sample.<sup>4</sup>

### 1.1.2. The Importance of the Gelation Process

Often overlooked, when describing gelation are the specific triggers required to initiate gel formation; a recent review<sup>18</sup> describes these processes. Very often, as

previously discussed, this is a simple process for example a change in temperature (a heating-cooling cycle).<sup>38</sup>

Other common triggers used to promote gelation include a change in pH, (whereby the LWMG has a higher solubility at one pH over another) changes in solvent polarity (whereby, the LMWG has a higher solubility in water-miscible organic solvent over water) or the use of an enzyme to cleave a functional group from a pro-gelator, thus reducing solubility in water when cleaved.

Gelation *via* change in pH can be achieved in one of two ways, either by addition of an additive such as the glucono- $\delta$ -lactone (GdL) demonstrated by the Adams group,<sup>39</sup> alternatively gelation can be achieved by direct addition of an inorganic acid, such as the transition from high pH sodium hydroxide to low pH by addition of hydrochloric acid as reported by the Ulijn group.<sup>40</sup>

Vemula *et al.*<sup>6</sup> introduced encapsulated curcumin into a paracetamol hydrogel and demonstrated its enzyme (lipase) triggered release. Other reports of enzyme triggered gelation include phosphatase triggered gelation of small peptides in phosphate buffered saline,<sup>41</sup> and a hydrolysis triggered Taxol<sup>®</sup> hydrogelation.<sup>42</sup>

### 1.1.3. Methods of Characterisation

Initial characterisation of any gel should be both efficient and informative. For gels used in drug delivery it is important to characterise their mechanical stability, chemical stability and resistance to enzymatic degradation in simulated *in vivo* conditions and diffusion of therapeutics and nutrients through the gel.

Whilst it may not be of utmost importance to have a gel with a high degree of mechanical strength for drug delivery, it is still important to understand how the gel would behave under stresses, such as those exerted *in vivo*<sup>43,44</sup> as the ability of the gel to remain localised *in vivo* in a body cavity or tissue is directly related to stiffness and network structure.<sup>45</sup> Moreover, mechanical properties of gels can influence cell differentiation.<sup>46</sup>

Tabletop rheology provides a good foundation for comparing the strength and flexibility of a given material. It is often used as a preliminary diagnostic test for

gelation aiding in the characterisation of the temperature of gelation ( $T_{\text{gel}}$ ). Multiple methods can be used to determine this value including the 'dropping ball' method in which a small ball bearing is placed on top of a gel while it is heated, the temperature at which the ball breaks through the gel is recorded as the  $T_{\text{gel}}$ . Another simplistic method is the 'tube inversion' test in which a gel is formed at an increased temperature then slowly cooled, the vial is inverted at different temperatures and when the gel no longer flows upon inversion it can be assumed that the sample has established elasticity i.e. has a yield stress. These simple tests make them ideal preliminary screens for molecular gelation. However, due to the qualitative nature of these measurements it is easy to mistake a viscous solution for a gel and conversely to mistake a gel with small yield stress as a solution.

Rheology allows easy quantitative characterisation of flow behaviour, provides information about the tertiary structure of the gel (the type of network responsible for gelation) and supports clear differentiation between mechanically 'strong' and 'weak' gels i.e. those that have no flow-like behaviour and those that show behaviour comparable to a viscous liquid.

Procedures measuring a range of mechanical parameters such as shear stress, oscillation and stress relaxation can be used to obtain a number of important variables;  $G'$  (storage or elastic modulus),  $G''$  (loss modulus) and  $G^*$  (complex modulus) being amongst the most useful. By plotting these against frequency, strain, temperature etc. the way in which the material responds to different stresses and thus the nature of the interactions responsible for aggregation can be ascertained. For solid-like gels  $G'$  needs to demonstrate a linear region i.e. one that is independent of the stress and strain applied. In addition  $G'$  must exceed  $G''$  by at least one order of magnitude.<sup>47</sup> A number of rheological measurements have been adapted from polymer chemistry, enabling accurate determination of the gel point ( $T_{\text{gel}}$ ) of a material,<sup>48</sup> the rate of self-assembly and the viscoelastic properties thereafter,<sup>49-51</sup> with strain sweeps and frequency sweeps being amongst the most utilised methods of characterisation. However rheological data can vary considerably depending on the geometry of the plate used e.g. parallel plates, concentric cylinders, cup and vane<sup>52</sup> etc. and the method of sample preparation *i.e.*

prepared *in advance*<sup>43</sup> or gelled *in situ*.<sup>49</sup> Also important is the characterisation of the pore size between fibres<sup>53</sup> for entrapment of therapeutics or diffusion of nutrients.<sup>54</sup>

Information on the bulk properties of a gel offers only a small insight into the microscopic organisation of the molecules as a result of gelation. Complete characterisation of a gel/solid system requires information at the supramolecular level. The morphology of the 3D network of gel fibres and by extension the nature of the connections can be studied using a multitude of techniques on a scale of 0.01 - 1000 nm. Using a combination of microscopy and spectroscopy a detailed picture of the molecular arrangement can be obtained.

Optical microscopy provides information about gel structure<sup>4,55,56</sup> but is used less frequently than other techniques due to its low spatial resolution (diffraction limit). More widely used imaging methods include electron microscopy (EM) techniques.

Scanning Electron Microscopy (SEM) and Transmission Electron Microscopy (TEM) (**Figure 2**) are high resolution techniques (0.2 nm) and offer an insight into gel micro- and nanostructure providing a detailed view of the morphology of the unidirectional aggregates that result from gelation. Under the standard operating

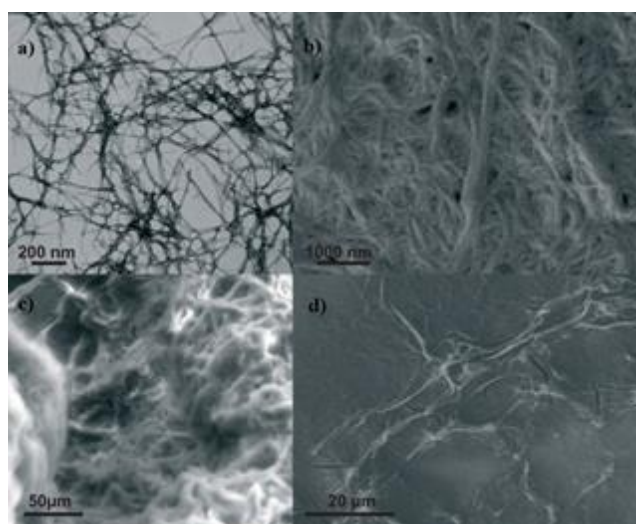


**Figure 2: Microscopic analysis of a self-assembled Fmoc-diphenylalanine hydrogel.**

a) TEM image of the fibrous scaffold. b) Cold-field emission-gun HR scanning electron microscopy (HR-SEM) image of the scaffold fibrils. c, d) Environmental SEM (E-SEM) images of the 3D, natural, spacious structure of the hydrogel. Adapted from reference 50

conditions of both SEM and TEM, the sample is required to be dehydrated (xerogel) which in the case of a LMWG often results in collapse of the structure prior to imaging.<sup>49</sup> Cryogenic techniques (CryoSEM/TEM) are increasingly common methods of analyses, allowing nm resolution images of a gel in its hydrated state.

36,57-59

Electron micrographs are informative but should usually be combined with complementary methods such as scattering techniques. Small-angle scattering (SAS) techniques like small-angle neutron scattering (SANS) or small-angle x-ray scattering (SAXS) provide useful information about spatial organisation of fibrillar networks<sup>60,61</sup> on a mesoscopic scale (1 - 1000 nm).

Scanning probe techniques such as atomic force microscopy (AFM) offer high resolution, suitable for investigating gel fibre thickness and the morphological arrangement of the gel without the need for dehydration and are often used in combination with traditional EM techniques.<sup>7,62</sup>

Spectroscopic techniques such as nuclear magnetic resonance (NMR), UV/vis, fluorescence, circular dichroism (CD) and infra-red (IR) have been applied to gelation systems and offer more information on the intermolecular organisation of the gelators that cannot be seen with other techniques.

Solution state,<sup>63,64</sup> and increasingly solid state NMR is being used as a complementary tool for investigating LMWGs. Analysis of variation in either chemical shifts,<sup>65-68</sup> relaxation times<sup>69,70</sup> or changing temperature can be used to obtain useful information such as the nature of the intermolecular interactions, the critical concentration values or thermodynamic parameters associated with gel formation.<sup>71</sup> UV/vis and fluorescence spectroscopy are used to monitor absorption and fluorescence of a gel and thus obtain a deeper knowledge of the weak bonding interactions;  $\pi$ - $\pi$  stacking, hydrogen bonding and charge transfer. CD involves measuring the absorption of circularly polarised light by a chiral sample as a function of wavelength and is a useful tool when investigating self-assembly processes particularly those of chiral gelators that lead to the formation of helical structures.<sup>66,72</sup> IR is a useful tool for confirming the presence of hydrogen bonding as well as providing useful information regarding the role hydrogen bonding plays

during the process of gelation by studying the characteristic peak shifts between gelators in solution phase and those in the gel phase. Frequently peaks of interest (e.g. NH stretch) would be obscured by the OH stretch of water therefore characterisation by IR is usually carried out on dehydrated samples.

Also important to consider is chemical stability and enzymatic breakdown of the gel matrix. This will be described more fully in section **1.1.4.3** “Therapeutic molecular gels”.

#### **1.1.4. Molecular Gels in Drug Delivery**

Developing new drug delivery systems is paramount to improving the therapeutic efficacy of drugs and the use of any drug delivery vehicle is often beneficial in pharmaceutical development as many marketed compounds are delivered intravenously, relying on the body’s own systemic transport system to deliver drug molecules to their desired site of action. A disadvantage of this conventional method is that under certain circumstances i.e. in the administration of chemotherapeutics, toxic drug molecules interfere with any rapidly dividing cell systems they encounter e.g. hair follicles and epithelial gastrointestinal (GI) lining, not limited to the malignant tumour cells themselves, which results in the commonly observed side effects such as hair loss and vomiting. This off-site targeting is often why chemotherapeutic agents fail, when toxicity to bone marrow prevents the completion of the therapy.<sup>73</sup>

Localised drug delivery offers multiple advantages including reduced toxicity from systemic exposure and improved efficacy.

There exist a few methods by which localised delivery can be achieved: (**Figure 3**)

- i. The compound can be physically entrapped within an inert gelator matrix (defined as a ‘scaffold’) and the released from the gel *via* diffusion - **inert gel scaffold**
- ii. An active pharmaceutical ingredient (API) can be covalently conjugated to a functional group creating a prodrug with amphiphilic characteristics, which will self-assemble. The prodrug will then release the API in response to a stimulus e.g. enzymes – **stimuli-responsive gel-therapeutic delivery system**

- iii. A functionalised linker can be covalently conjugated to an API creating an amphiphilic prodrug which can self-assemble. This method doesn't rely upon diffusion controlled or stimulus triggered release, the gel itself is the therapeutic – **therapeutic molecular gel**

Each of these approaches will be discussed in detail below.

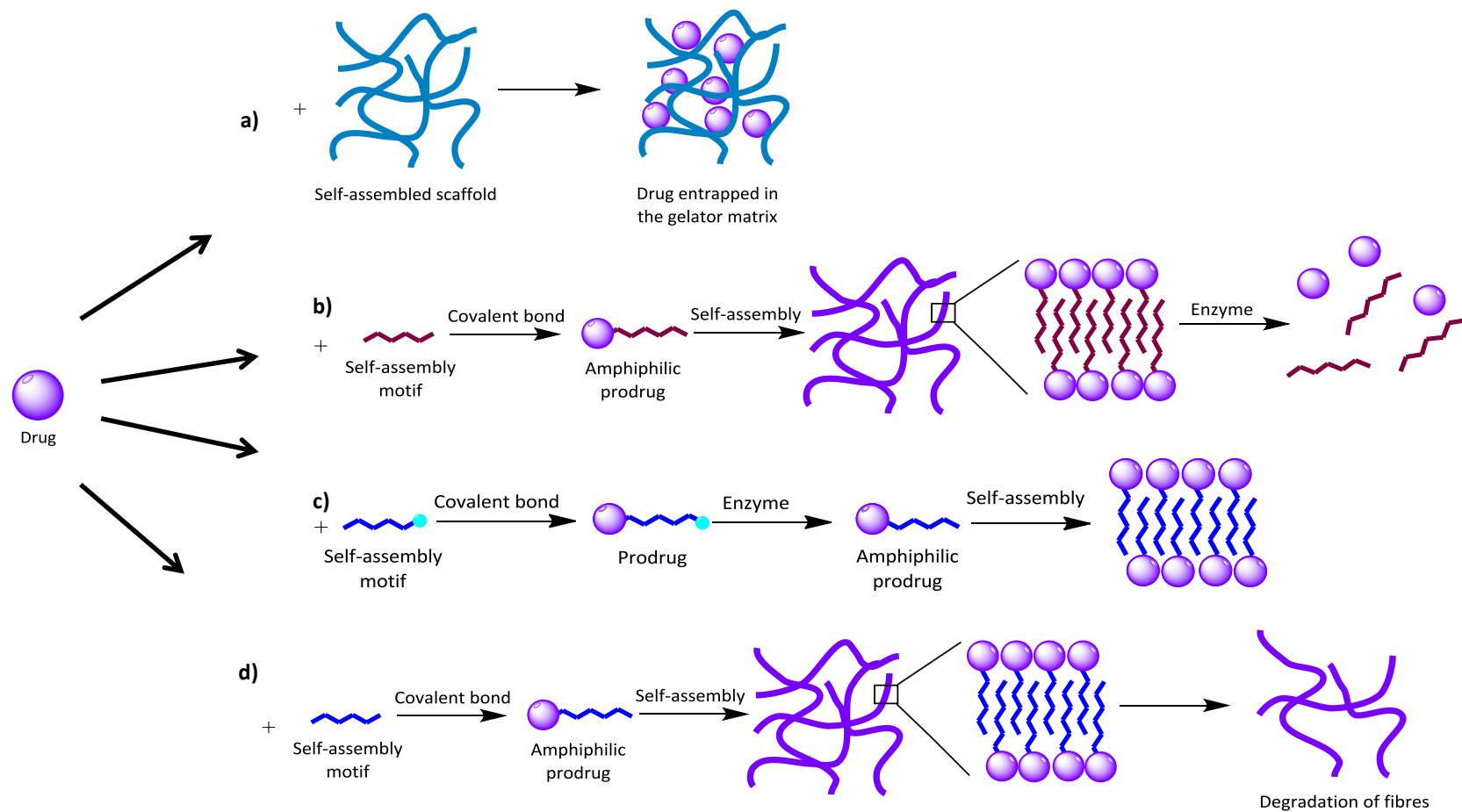


**Figure 3: Methods of drug delivery using low molecular weight gelators.**

a) The compound is physically entrapped within the gelator matrix ('scaffold') and released from the gel *via* diffusion. b) The drug can be covalently conjugated to a functional group, inducing amphiphilicity, this can then self-assemble *in situ* and release the drug *via* an external stimulus e.g. enzymes. c) A functionalised linker can be covalently conjugated to a therapeutic, following enzymatic cleavage of part of the linker, the amphiphilic prodrug can self-assemble d) A functionalised linker can be covalently conjugated to a therapeutic, this method doesn't rely upon diffusion controlled release or stimulus triggered release; the gel itself is the therapeutic.

### 1.1.4.1. Molecular Gel Scaffolds

Controlled release (diffusion or degradation mediated) delivery of therapeutics encapsulated in an inert molecular gel scaffold is the simplest method by which drugs can be delivered. However, controlling the rate at which the therapeutic is released and degradation of materials is still a challenge.

The most utilised scaffolds for this approach are self-assembled amino-acid/peptide hydrogels, which have been widely studied and reviewed by several authors.<sup>74-76</sup>

Two decades prior, Vegners reported one of the first examples of drug incorporation into a dipeptide conjugate. Adamantanamine derivatives were loaded into Fmoc-Leu-Asp (**1**) hydrogels and injected into rabbits; they were found to affect the rabbit's immune system, resulting in a production of highly specific antibodies against the drug.<sup>77</sup>

More recently Zhang and his group used a commercially available long chain peptide [Acetyl-(Arg-Ala-Asp-Ala)<sub>4</sub>-CONH<sub>2</sub>, RADA 16] (**2**) to study the release kinetics of model drugs such as the dyes phenol red and bromophenol blue, and

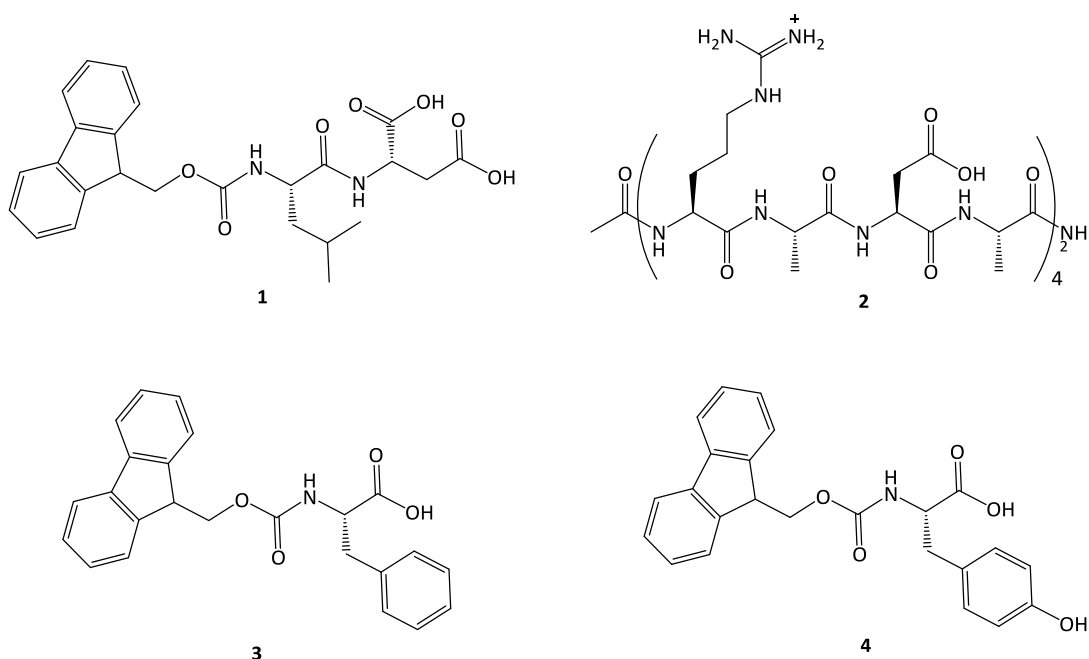


Figure 4: Amino acid derived scaffold gels for drug delivery

certain proteins, i.e. lysozyme and trypsin inhibitors, from these self-assembling peptide hydrogels. It was found that the choice of peptide scaffold is fundamental and that tailor-made peptide hydrogels should be synthesised for each compound based upon the molecular structure to ensure that the release can be controlled.<sup>78,79</sup> A similar study with L-peptide hydrogels as carriers demonstrated that drug size and lipophilicity influenced controlled release from the scaffold. Adams *et al.* used Fmoc protected amino acid hydrogels to monitor the release of model drugs from these gels. Fmoc-phenylalanine (**3**) and Fmoc-tyrosine (**4**) gels were formed by switching the pH of solution with GdL, followed by calculation of the amount and the rate of drug release, indicating that drug release followed Fick's law of diffusion. Thus, it was demonstrated that commercially available Fmoc-amino acids can be used as suitable platforms for drug delivery.<sup>80</sup> Though it should be noted that in this case sustained release of a drug occurred over only a period of hours (not days); release times of longer than a couple of hours have yet to be recorded. Recently some anticancer drugs were delivered *via* peptide hydrogels. The use of gels as carriers for chemotherapeutic agents is increasingly becoming an effective strategy to increase both therapeutic concentration and efficacy and to reduce side effects associated with systemic drug delivery. Doxorubicin (Dox, **5**) has been evaluated as model drug and has been incorporated into two different oligopeptides that formed pH and thermo-sensitive hydrogels: this anticancer agent was released slowly and at physiological pH.<sup>81</sup> Stupp *et al.* encapsulated the hydrophobic drug camptothecin (**6**) into a self-assembled peptide, resulting in

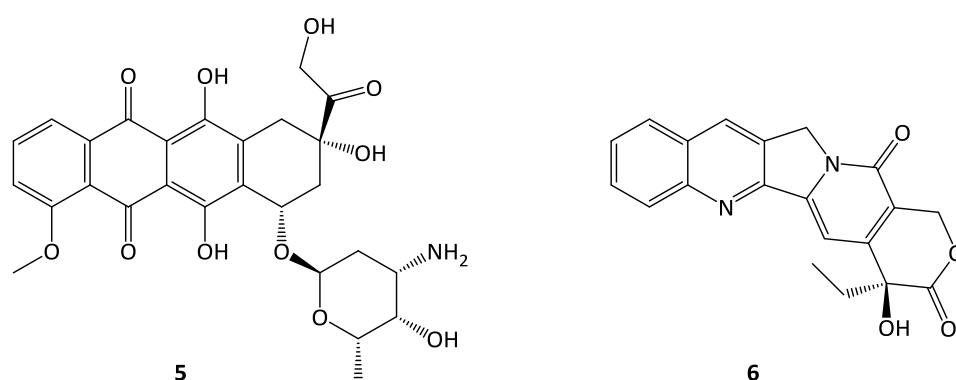


Figure 5: Hydrophobic drugs; doxorubicin and camptothecin

enhanced aqueous solubility (> 50-fold). *In vitro* and *in vivo* tests showed also the ability of these amphiphilic nanofibres to inhibit tumour growth, thus demonstrating the potential of these systems to deliver hydrophobic drugs.<sup>82</sup>

In contrast to established and developed delivery systems based on low molecular weight hydrogels, recent studies describing applications of organogels in drug delivery are limited. This is due to the fact that some components of organogels (i.e. benzene, toluene, vegetable oils etc.) can lead to irritation or inflammation. In spite of these limitations, organogels have some advantages; the lack of aqueous media in formulations can deter microbial growth and also render them suitable for carrying oil-soluble drugs.<sup>83</sup>

One of the first examples reported was the delivery of the non-steroidal anti-inflammatory drug (NSAID) piroxicam, which was dispersed in organogels formed with Miglyol<sup>®</sup> and solid fatty acid esters. The anti-inflammatory effect, based on inhibition of oedema after treatment, of topical applied piroxicam organogels to the skin was studied *in vivo*. Organogel formulations demonstrated increased efficacy compared to placebo controls.<sup>84</sup> Leroux and his group, as previously mentioned, pioneered the use of L-alanine and tyrosine based organogels for *in situ* delivery. They synthesised *N*-lauroyl L-alanine derivatives and formed organogels by dissolving the native molecules first in ethanol (a water-diffusible inhibitor of gelation) and then into soybean oil or a medium chain triglyceride; the solutions were subcutaneously injected at room temperature into rats, forming a solid implant *in situ* within minutes after ethanol diffusion.<sup>85</sup> A subsequent study on organogels based on L-alanine derivatives in safflower oil, evaluated the biocompatibility of these *in situ* forming implants, revealing minimal and limited inflammatory reactions, in accordance with the normal body response to biocompatible materials.<sup>86</sup>

These promising results led to the concept that organogels of L-alanine could be used as scaffolds for site-specific controlled drug delivery. Indeed, leuprolide, a synthetic hormone used in prostate cancer, uterine fibroid tumour and endometriosis treatment, was delivered *in situ* using L-alanine derivatives in safflower oil. The peptide was shown to be gradually released over a period of 14 to

25 days and the drug's efficacy was demonstrated in prostate cancer patients by induction of chemical castration for up to 50 days (due to inhibition of testosterone secretion).<sup>87</sup>

Subsequently, the same group reported organogels of L-tyrosine prepared using the same method as with the L-alanine systems: amino acid derivatives were initially dissolved in safflower oil and then *N*-methyl pyrrolidone (NMP, a biocompatible water-diffusible inhibitor of gelation) was added. The solution was subcutaneously injected resulting in gel formation after NMP diffusion into adjacent tissues. Since L-tyrosine organogels were shown to form implants with strong mechanical properties,<sup>88</sup> they were used to investigate the sustained release of rivastigmine, an acetylcholinesterase inhibitor used in treatment of Alzheimer's disease. *In vivo* studies showed that L-tyrosine-based organogels could gradually deliver rivastigmine up to 35 days after subcutaneous administration producing only limited chronic inflammation and inhibiting acetylcholinesterase production in the hippocampus for at least 14 days. These findings confirm that tyrosine-based organogels can be used as an alternative to commercially available depot formulations of cholinesterase inhibitors.<sup>89</sup>

Lastly, an oral controlled release formulation based on a 12-hydroxystearic acid organogel in soybean oil has been prepared for delivery of hydrophobic compounds. Ibuprofen was chosen as a model drug for this study. The LMWG and ibuprofen gelled in the vegetable oil by temperature switch. *In vivo* studies were performed on rats; ibuprofen was administered orally both as an organogel and as an aqueous suspension control: compared to the latter formulation, results showed that organogel formulation allowed sustained release of ibuprofen due to retention in the gel and low intestinal absorption.<sup>90</sup>

In all the studies described above, it has been demonstrated that low molecular weight organogels are potential and efficient drug delivery systems for controlled release.

### 1.1.4.2. Stimuli-Responsive Molecular Therapeutic Gels

As previously mentioned, the most utilised scaffolds for drug delivery are self-assembled peptide hydrogels in which drugs are encapsulated.<sup>75,91</sup> However, despite such advantageous properties demonstrated by these systems, certain weaknesses have been encountered such as inadequate encapsulation efficiency, low and limited drug loading and burst drug release.

In order to overcome these limitations, in recent years a novel strategy of drug delivery using the concept of LMWGs has been introduced. As already indicated, this strategy consists of a synthesis of prodrugs that are able to self-assemble in water forming a hydrogel, releasing the active compound either *via* hydrolysis or enzymatic degradation. In this way, drug loading is markedly increased because the gel is derived from the drug molecules themselves. Additionally, no excipients are used, thus excipient-drug interactions are prevented and putative side effects caused by the presence of stabilising agents are circumvented.<sup>6</sup>

There are two ways in which this can be achieved; first, the drug can be covalently conjugated to a functional group, inducing amphiphilicity, this can then self-assemble *in situ* and release the drug *via* an external stimulus e.g. enzymes. Second, a functionalised linker can be covalently conjugated to a therapeutic, following enzymatic cleavage of part of the linker, the amphiphilic prodrug can self-assemble.

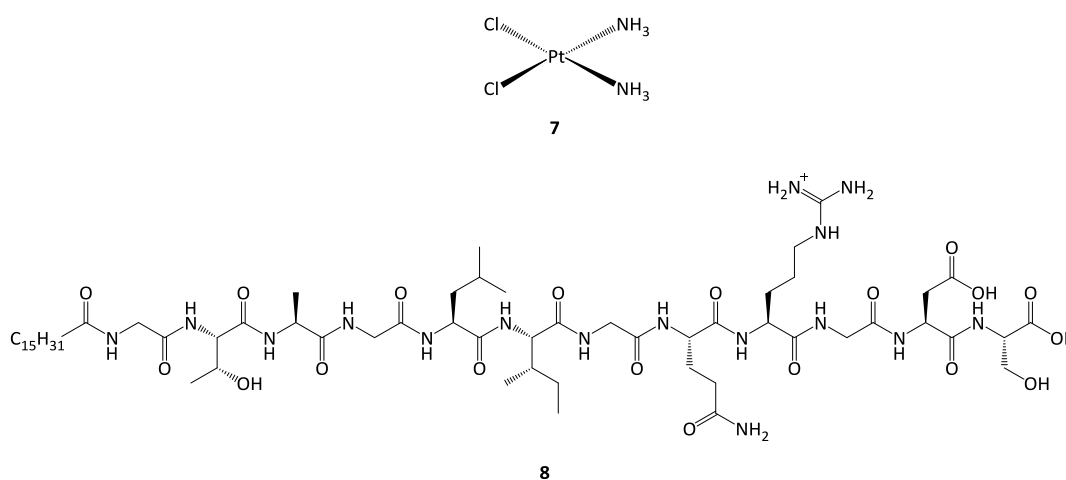


Figure 6: Cisplatin and self-assembling peptide amphiphile (GTAGLIGRQDGS)

The choice of functional moiety by which to promote gelation is critical: several molecules that have been reported to gel independently can be used to synthesise self-assembled prodrugs such as amino acids, di- or tri-peptides, and fatty acids. The most commonly used linkers in prodrug synthesis are ester bonds and it has been found that release of almost 49 % of all marketed prodrugs is triggered by enzymatic hydrolysis by esterases. However, drugs can be functionalised with other groups forming amides, carbamates or oximes, though their use is limited by higher enzymatic stability *in vivo* compared to esters.<sup>92</sup>

#### 1.1.4.2.1. API Release in Response to Enzymatic Breakdown of Gelating Prodrug

Kim and co-workers described a new method for the delivery of cisplatin (**7**),<sup>93</sup> conjugating the active compound to a self-assembling peptide amphiphile (GTAGLIGQRGDS, **8**) sensitive to matrix metalloproteinase-2 (MMP-2) by formation of complexes between the drug and carboxylic acids of the peptide; its successful enzymatic degradation from the gel has been confirmed by TEM analyses.

Van Esch *et al.* synthesised low molecular weight hydrogelators capable of gelling at 0.03 % (w/v), based on a cyclohexane tris-amide (**9**) scaffold previously reported as a gelator.<sup>94</sup> In order to demonstrate the potential applications of the two-step drug release system, the enzyme  $\alpha$ -chymotrypsin was incorporated into the gel matrix and the rate of hydrolysis of the prodrug was compared to that of a model substrate. The results showed that when the enzyme was included into the hydrogel, drug molecules were protected from hydrolysis but at the same time  $\alpha$ -chymotrypsin activity was preserved. However, when the gel underwent a gel-sol transition upon increasing the temperature, the prodrug molecule was released

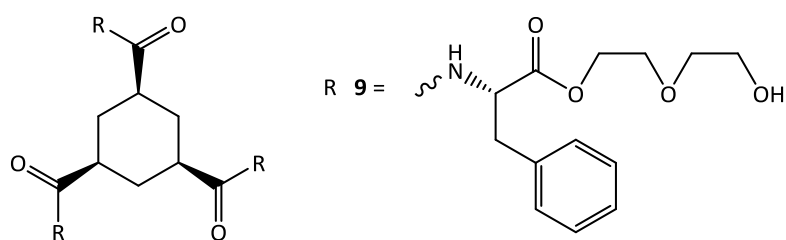
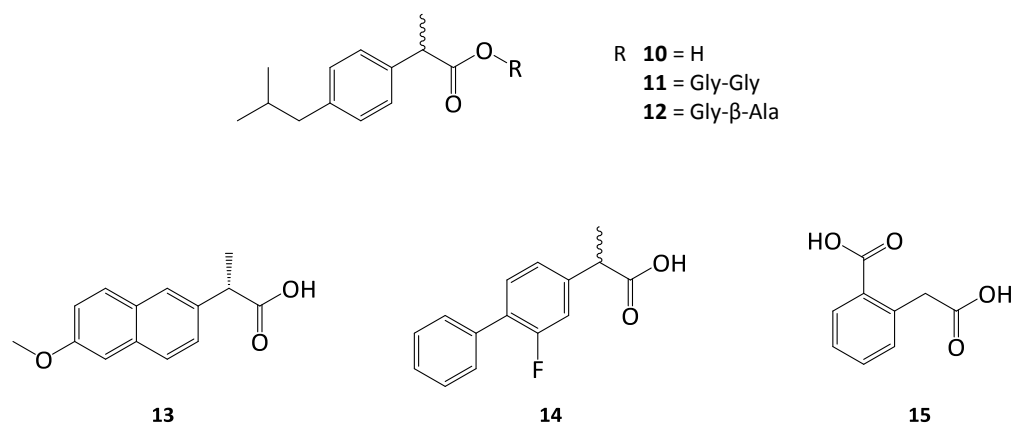


Figure 7: Stimuli responsive gel based on cyclohexane *tris*-amide scaffold



**Figure 8: Non-steroidal anti-inflammatory drugs (NSAIDs) and associated gelators**

into solution and hydrolysed enzymatically.

Bhuniya *et al.* have developed successful low molecular weight hydrogelators based on the non-steroidal anti-inflammatory drug (NSAID) ibuprofen, covalently bound to various dipeptides.<sup>95</sup> They reported the synthesis of six ibuprofen (**10**) prodrugs, but only the Gly-Gly derivative (**11**) demonstrated an ability to self-assemble in water forming a translucent gel whereas the β-alanine moiety (**12**) formed an opaque hydrogel. The other candidates failed to reach a sufficient hydrophilicity-hydrophobicity balance to facilitate gelation in aqueous media. The group also performed a study of drug release from the gel in the presence of a carboxypeptidase solution, finding that after only one day of incubation the gel weakened as a result of the enzymatic degradation of the prodrug. Xu *et al.* recently reported the synthesis of other NSAID hydrogelators based on naproxen (**13**), flurbiprofen (**14**), aspirin (**15**) and **10** (**Figure 8**): they were obtained by conjugation to aromatic di- or tri-peptides.<sup>96</sup> However they concluded that the most stable gelators would be produced *via* conjugation with the di-peptide diphenylalanine due to the stability from the di-aromatic system.

Vemula, another pioneering author in self-assembled prodrugs chose the simple and widely used drug paracetamol (**16**) to demonstrate the concept of enzymatically triggered prodrug-based gelators (**Figure 9**).<sup>97</sup> Amphiphilic (**17**) and bola-amphiphilic (**18, 19**) derivatives of paracetamol were readily synthesised in a single step from native paracetamol. Subsequent gelation studies demonstrated

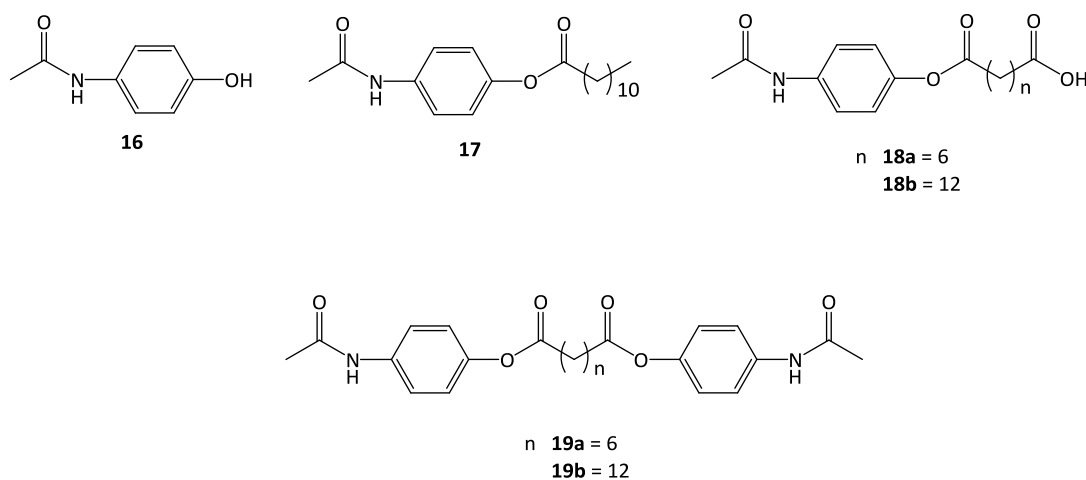


**Figure 9: Paracetamol, amphiphilic and bola-amphiphilic derivatives**

that most compounds formed hydrogels at low concentrations (0.4 - 1.5 % (w/v)) by temperature switch, and microscopy studies revealed the presence of nanofibres organised into entangled gel networks. In order to prove the effectiveness of these hydrogelators in delivering single and multiple drugs, a series of enzyme-mediated gel degradation studies was performed showing that after 48 h of incubation of paracetamol derivatives with lipase, the gels degraded forming a clear solution, indicating paracetamol release from the prodrugs by hydrolysis of the ester bond. The drug curcumin was also incorporated into the hydrogels and the same enzymatic degradation test was carried out with similar results, confirming the ability of these gels to release multiple drugs. Lastly, mesenchymal stem cells (MSCs) treated with these paracetamol-based prodrugs were able to preserve properties such as viability, proliferation and adhesion, demonstrating the highly cyto-compatible nature of the hydrogel.

The examples reported above are prodrugs of antibacterial and anti-inflammatory drugs; however, there is increasing interest towards development of anticancer prodrug gelators, since cancer is one of the main causes of morbidity and mortality worldwide. In 2008, 12.7 million new cancer cases were diagnosed globally, with 7.6 million deaths from this disease. Existing chemotherapeutic strategies are not efficient enough to eradicate these malignancies due to factors including tumour aggressiveness, inherent or acquired resistance, and increased tumour size. Along

with continuous research in discovering novel compounds with potent anticancer activity, other important goals include improving poor solubility, limited bioavailability, formulation properties and delivery of existing and widely used antineoplastic agents to allow direct intra-tumoural injection. Consequently, drug delivery systems, such as hydrogels, can be employed to locally release these drugs simultaneously reducing side effects associated with systemic treatment and increasing *in situ* concentration.

#### 1.1.4.2.2. Self-Assembly of a Gel and Release of API *via* Cleavage of Precursor

Xu and co-workers were the first to report a triggered-enzyme synthesis of a supramolecular paclitaxel (**20**) (marketed as Taxol®) derivative hydrogel.<sup>98</sup> According to structure-activity studies of this antineoplastic drug, the compound was covalently bound to the self-assembly motif 2-naphthalen-Phe-Phe-Lys-Tyr-phosphate through a succinic acid linker yielding a phosphate precursor. In the

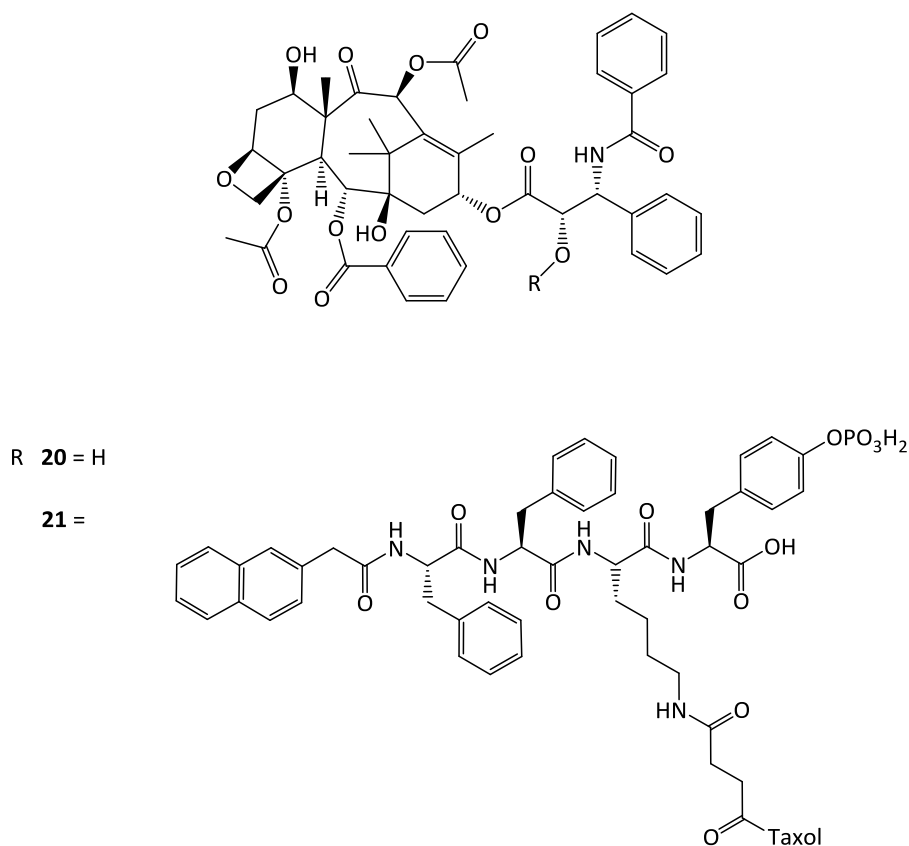


Figure 10: Taxol and Taxol-SA-GSSG derivative

presence of an alkaline phosphatase enzyme, dephosphorylation occurred after few minutes and transformed the precursor into a hydrogelator consisting of a Taxol<sup>®</sup> derivative capable of self-assembly into nanofibres in aqueous media. Moreover, this hydrogel preserved the anti-tumour activity of native compound and was cyto-compatible.

Inspired by this work, Wang *et al.*<sup>99</sup> used the same anticancer drug to synthesise a folic acid-Taxol conjugate: they chose folic acid as the terminal moiety because of its propensity to form a stable tetramer; it was linked to Taxol<sup>®</sup> *via* a phosphorylated and succinated tripeptide Gly-Tyr-Lys, which enhanced water solubility and acted as a substrate for the phosphatase. In fact, as in Xu's work, only the dephosphorylated paclitaxel derivative, obtained after incubation with phosphatase enzyme demonstrated self-assembly properties in water at a minimum concentration of 0.08 % (w/v), thus forming a transparent hydrogel consisting of uniform nanospheres. Moreover, the weight percentage of Taxol<sup>®</sup> in the nanospheres was calculated to be almost 50 %, more than every other Taxol<sup>®</sup>-conjugate delivery system reported in the literature. The hydrogelator demonstrated an ability to conserve activity similar to that of Taxol<sup>®</sup> when incubated with HepG2 cells. All these encouraging results demonstrate that folic acid can be used as a versatile molecule to synthesise hydrogelators of hydrophobic drugs, such as Taxol<sup>®</sup>, which can be locally injected into the tumour site allowing sustained drug release.<sup>100</sup>

In support of this study, Yang *et al.* reported the conjugation of folic acid to the hydrophobic therapeutic agent rapamycin (an immunosuppressive and anticancer drug) and triamcinolone acetonide (TA; a corticosteroid). These conjugates were synthesised linking folic acid to the drugs through a Lys-ss-Glu-Glu peptide; the disulfide bond was used as a linker for the hydrophilic and hydrophobic moieties and it was necessary to guarantee a substrate for glutathione. Indeed, the hydrogelators (1-2 % (w/v)) formed after treatment with glutathione; the native drugs were then released after hydrolysis of the ester bond between the linker and the drugs. *In vivo* studies of the folic acid-TA gel were also performed in rabbits

eyes to assess biocompatibility of this hydrogelator: it demonstrated sustained release and no changes were observed in the retina or sclera.<sup>101</sup>

The same group recently reported a molecular hydrogel of Taxol<sup>®</sup>, consisting of the native compound connected *via* an ester bond to succinic acid linked to oxidised glutathione (**21**). The ester bond was introduced into the molecule to allow release of Taxol<sup>®</sup> after ester hydrolysis; the hydrophilic oxidised glutathione was used to enhance compound water solubility and was selected for its *in vivo* compatibility. Gelation tests were carried out in phosphate buffer solution containing 2 % (w/v) of the compound; gelation occurred at room and physiological temperatures after undergoing ester bond self-hydrolysis. The molecular hydrogel was also tested *in vitro*, showing a sustained release profile. The truly innovative nature of these studies, compared to previous studies with Taxol<sup>®</sup> based gelators, was demonstrated using *in vivo* studies in mice bearing solid breast tumours: local injection of Taxol<sup>®</sup> - derivatised hydrogels clearly impaired tumour growth in the first 6 days after administration and delayed it further in the 6 days that followed; Taxol<sup>®</sup> hydrogels also prevented breast cancer metastasis. Moreover, this compound inhibited lymphoma tumour growth more efficiently than the commercially and clinically used intravenous Taxol<sup>®</sup> formulation. This work thus proves the high potential of chemotherapeutic hydrogels in the treatment of solid tumours.<sup>42</sup>

A very recent example was of an injectable camptothecin hydrogel;<sup>102</sup> a naphthalene-Phe-succinic acid pro-moiety was conjugated to camptothecin. The resulting compound, though poorly soluble was able to undergo solubilisation and cleavage of the succinic acid linker in weakly basic conditions to generate a compound that was able to self-assemble at concentrations of 0.1 % (w/v). The gel was tested *in vitro* and the efficacy of the hydrogel was found to be increased in comparison to the parent compound in MCF-7 cells.

#### **1.1.4.3. Therapeutic Molecular Gels**

Therapeutic molecular gels are defined as API's including, but not limited to, antibiotics and chemotherapeutics that have been modified to include large aromatic systems, peptides or any predominantly lipophilic system that will

promote the gelation process under aforementioned appropriate conditions. These systems have demonstrated enhanced controlled release profiles for drug delivery applications when directly compared to the diffusion mediated release from encapsulated systems.<sup>103</sup> The first example reported in the literature of a self-assembled prodrug was the antibiotic vancomycin, which was converted into a hydrogelator by introduction of a pyrene group to the C-terminal of the vancomycin backbone *via* an amide bond.<sup>104</sup> The prodrug showed an 11-fold increase in activity compared to the unmodified vancomycin.

Therapeutic molecular gel complexes have the potential to make a huge impact in the treatment of cancer owing to the localised delivery and sustained release, particularly when combined with tumour resection, applying the gel into the cavity of a resected tumour. Alternative therapies already exist that could be used in a similar manner during resection surgery. Ellis-Behnke reported an alternative use for a known self-assembling peptide<sup>105</sup> Ac-(RADA)<sub>4</sub>-NH<sub>2</sub> (**5**) which forms a molecular gel in under 15 seconds upon coming into contact with bodily fluids, including blood, establishing a nanofibrous barrier.

The therapeutic potential of peptide amphiphiles has been further explored by Stupp and co-workers<sup>106</sup> who developed a dexamethasone (Dex) gelator conjugated *via* labile hydrazone linkage. The hydrazone linkage was shown to modulate the release of Dex over a 32 day period with a total 40 % release, minimal burst release and a zero-order kinetic profile. Wang *et al.* reported a bioactive molecular gel of Taxol<sup>®</sup> (**20**) covalently linked to short peptide chains and amino acids.<sup>107</sup> The ability of the Taxol<sup>®</sup>-peptide systems to form molecular gels allowed for the localised delivery of hydrophobic chemotherapeutics without the need for polymeric based carriers. Furthermore the gel could be tailored to self-assemble in response to tumour-specific environmental conditions, in this instance, reduction of the disulphide bond by glutathione.

Another example of a molecular gel with potential biomedical application was reported by Lee *et al.*<sup>108</sup> who successfully fabricated a molecular gel from DNA based upon a single strand non-covalent pairing, thus meaning the gel process was reversible.

#### 1.1.4.4. Nucleoside Gelators

Nucleoside-based compounds (**Figure 11**) represent another significant advance in the design of hydrogelators. The first studies were in the 1960's with guanosine derivatives. Gellert and later Sasisekharan reported that 5' and 3' isomers of guanylic acid (also known as guanosine monophosphate (GMP)) formed gels in 0.1 M KCl, with 5'-GMP self-assembling as a continuous helix whilst 3'-GMP self-assembled as a cyclic tetramer (**22**).<sup>109-111</sup> More recently, diacyluridinophosphocholine derivatives (**23**) containing different acyl chains were synthesised and formed stable hydrogels in aqueous solutions.<sup>112</sup>

Nucleoside-based bolaamphiphiles i.e. amphiphilic compounds containing two hydrophilic groups (one at each end) connected by a hydrophobic hydrocarbon

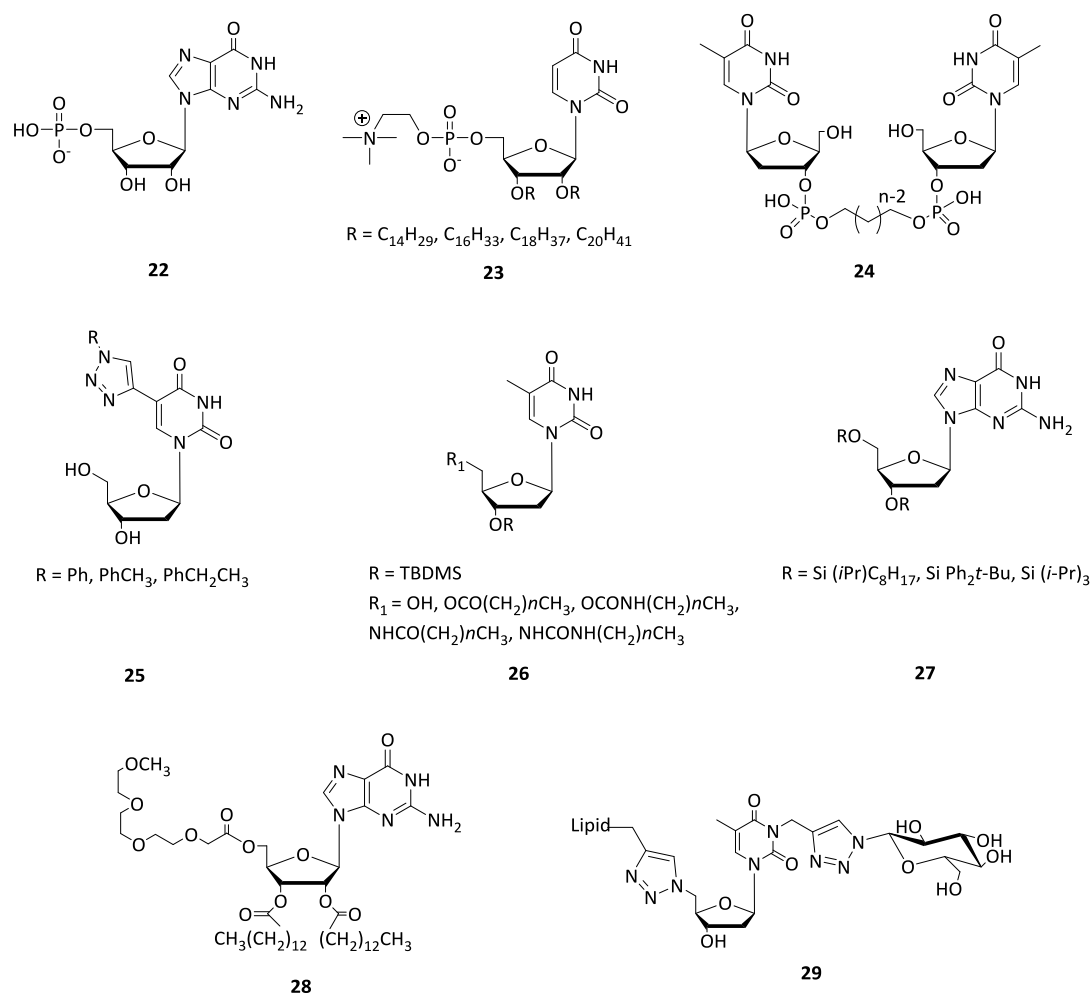


Figure 11: Nucleoside derived gelators

chain have also been evaluated by Shimizu et al. They prepared bola-amphiphiles based on 3'-phosphorylated thymidine moieties linked at both ends to a variable length oligomethylene spacer (C<sub>18</sub>-C<sub>20</sub>) (**24**) which self-assembled into nanofibres at specific pH's and temperatures.<sup>113</sup> Recently, Kim and co-workers focused on another nucleoside, synthesising benzyltriazole appended 2'-deoxyuridine hydrogelators (**25**) which gel in water at concentrations of 0.2 % w/v aggregating into fibres and lamellae.<sup>114</sup>

Nucleoside-based organogelators were first reported by Kim and co-workers, who demonstrated the gelation ability of thymidine functionalised with urea, amides, carbamate and ester groups (**26**).<sup>115</sup> Later, alkylsilylated guanosine derivatives (**27**)<sup>116</sup> and guanosine-based amphiphiles (**28**)<sup>117</sup> were reported to gel in most nonpolar solvents. More recently, a new class of organogelators has emerged consisting of glycosyl nucleoside lipids (GNLs) (**29**), synthesised by double-click chemistry, that exhibit both organo- and hydrogelating abilities at very low concentrations (0.1 % w/w) of gelator molecule.<sup>118,119</sup> Xu *et al*, recently reported enzyme labile gelating structures derived from existing known peptide gelators, functionalised at the 5'-position of the nucleoside guanosine and the nucleobase uridine.<sup>120,121</sup> Another route less often taken is modification of the nucleobase at the 5-position, an example of which is that taken by Park<sup>122</sup> to derivatise ribo- and deoxyuridine.

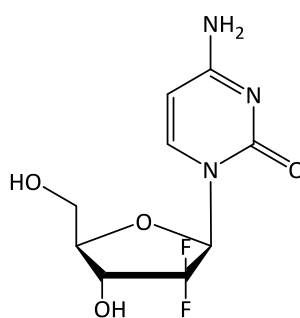
## 1.2. Gemcitabine (Gemzar<sup>®</sup>)

Gemcitabine <sup>123</sup> (2',2'-difluoro-2'-deoxycytidine; dFdC) (**30**) is a nucleoside analogue that is currently indicated as first line treatment for both locally advanced and metastatic pancreatic cancers. However, it is increasingly being utilised in the treatment of other cancers, including, gastric, breast and non-small cell lung cancer (NSCLC), notably in combination with the platinum based drugs cisplatin and carboplatin. <sup>124</sup>

Pancreatic cancer remains one of the most devastating cancers with a median survival rate of less than five months following initial diagnosis and with a survival rate after remission of less than 5 % over five-years. <sup>125</sup> The poor prognosis can be attributed to poor penetration of drugs, high degree of acquired chemoresistance and because in almost 80 % of patients, surgical resection is not possible. <sup>126</sup>

### 1.2.1. Uptake and Metabolism

dFdC is a cytidine analogue with numerous modes of action inside a cell (**Figure 13**). Cellular uptake of dFdC is mediated by a family of membrane proteins; human nucleoside transporters (hNTs), overcoming the inherent barrier to diffusion and allowing the hydrophilic nucleoside to cross the cell membrane. It has been previously shown the human (sodium-independent) equilibrative nucleoside transporter (hENT) hENT1 is the primary mediator of transport with hENT2 and the (sodium dependant) concentrative transporters hCNT1 and hCNT3 playing a minor



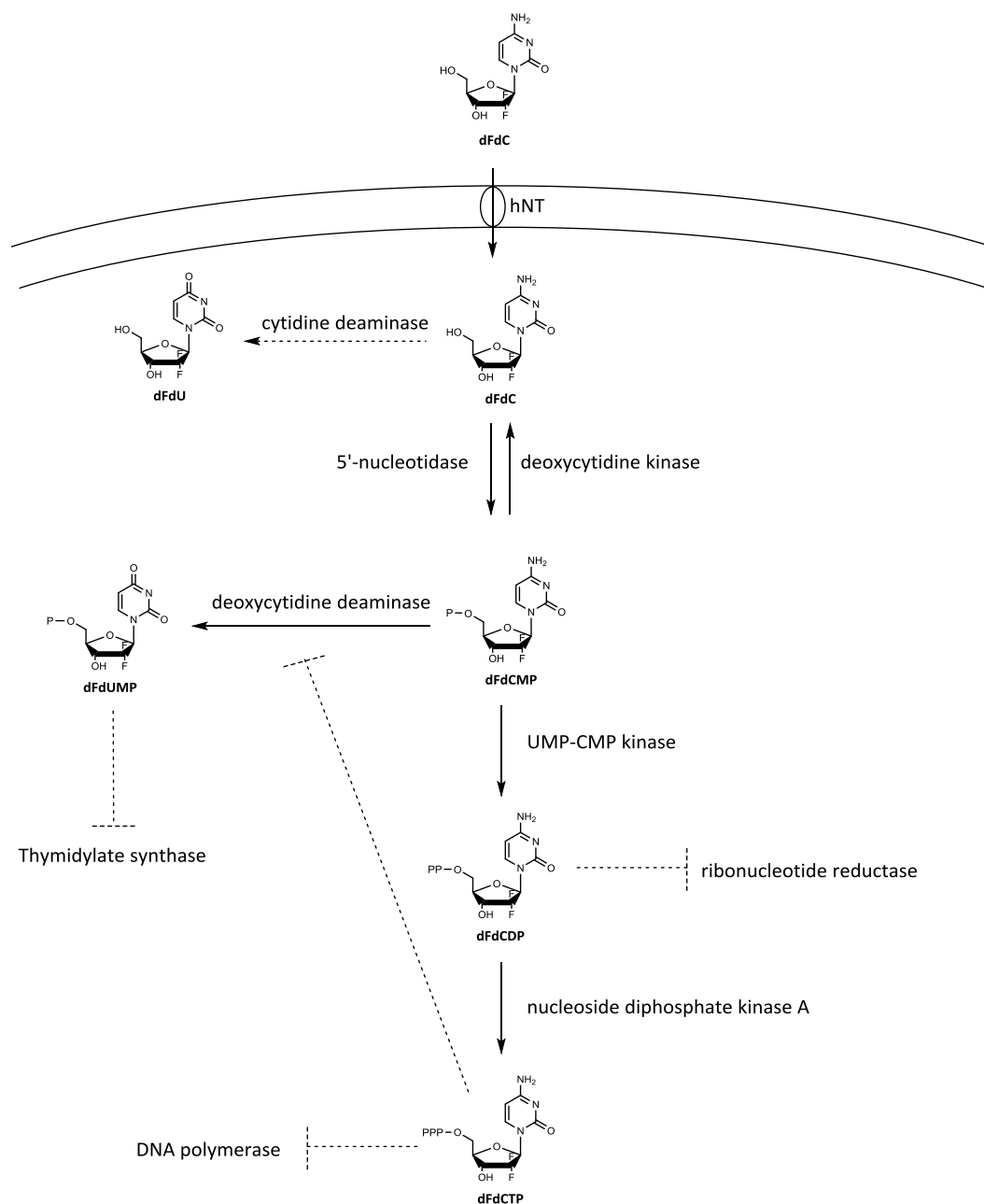
30

Figure 12: Structure of gemcitabine (2',2'-difluoro-2'-deoxycytidine; dFdC)

role in the uptake.<sup>127</sup>

Upon entering the cell, dFdC is phosphorylated by deoxycytidine kinase (dCK) to generate the monophosphorylated dFdCMP before being further phosphorylated by a pyrimidine monophosphate kinase (UMP-CMP kinase) to give the dephosphorylated dFdCDP.<sup>128,129</sup> However, Hu *et al.* recently reported that up- or down-regulation of UMP-CMP kinase bears no effect upon the levels of dFdCDP and dFdCTP in human colorectal cancer,<sup>130</sup> indicating that other previously unreported enzymes may play a role in the secondary phosphorylation. The enzyme responsible for the final phosphorylation step to the active dFdCTP is still unclear, however it is the initial transformation to dFdCMP that is considered the rate limiting step for production of both dFdCDP and dFdCTP.<sup>131</sup>

Gemcitabine is readily metabolised by cytidine deaminase (CDA) and deoxycytidine deaminase (dCDA) to generate the 2',2'-difluoro-2' deoxyuridine (dFdU) and 2',2'-difluoro-2'-deoxyuridine monophosphate (dFdUMP), respectively. dFdU has several postulate intracellular roles including the regulation of transport, accumulation and cytotoxicity of gemcitabine, whilst dFdUMP has been reported to inhibit thymidylate synthetase activity.<sup>132</sup> Gemcitabine may also become deactivated by dephosphorylation of the monophosphate derivatives by 5'-nucleotidases (5'-NTs) converting the nucleotides back into nucleosides, affect the rate limiting step and thus the overall cytotoxic effect of gemcitabine.



**Figure 13: Cellular mechanism of gemcitabine.**

hNT: human nucleoside transporter; dFdCMP: gemcitabine monophosphate; dFdCDP: gemcitabine diphosphate; dFdUTP: gemcitabine triphosphate; dFdU: 2',2'-difluoro-2'-deoxyuridine, dFdUMP: 2', 2'-difluoro-2'-deoxyuridine monophosphate. Adapted from reference 125

### 1.2.2. Mechanism of Action

The primary mode of action of gemcitabine is the inhibition of DNA synthesis. (Figure 14)<sup>133</sup> When dFdCTP is incorporated into an elongating chain of DNA, the non-terminal locale allows for only one additional deoxy-nucleotide triphosphate (dNTP) to be incorporated into the chain before chain elongation is terminated in a process called ‘masked-chain termination’ which additionally shields dFdCTP from removal by DNA repair enzymes.<sup>134</sup>

An additional mechanism of action is self-potentialisation *via* the inhibition of enzymes associated with deoxynucleotide metabolism. dCDA is inhibited directly by dFdCTP and indirectly by dFdCDP. The indirect reduction is due to a reduction in the pool of intracellular dNTP. Ribonucleotide reductase (RR) is inhibited by dFdCDP by covalent binding to the enzyme active site.<sup>135</sup> Additionally, since dCK activity is modulated by dCTP, lowering the amount of dNTP promotes dFdC phosphorylation, thereby increasing the level of dFdCTP to the ratio of dCTP, making dFdCTP

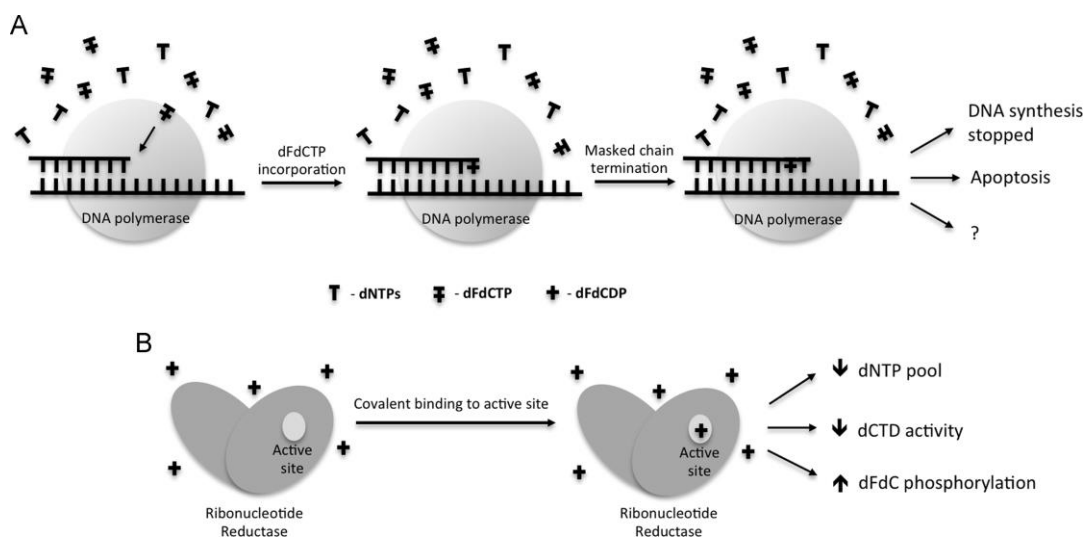


**Figure 14: Gemcitabine mechanisms of action.**

a) A representation of the masked chain termination. DNA polymerase incorporates gemcitabine triphosphate (dFdCTP) during DNA synthesis. Following this, another nucleotide triphosphate (dNTP) is incorporated, inhibiting the polymerase and terminating chain elongation. Although many cellular responses to dFdCTP incorporation are known, the exact downstream pathways are not well understood. b) Gemcitabine self-potentialisation. Covalent binding of gemcitabine diphosphate (dFdCDP) to leads to ribonucleotide reductase (RR) leads to inactivation, decreasing the pool of dNTP pool and deoxycytidylate deaminase (dCTD) activity, making gemcitabine more likely to be activated by nucleotide metabolising enzymes and therefore incorporated into DNA. Adapted from reference 123

increasingly likely to be successfully incorporated into DNA.

A further mechanism is the induction of apoptosis thorough caspase signalling.<sup>136</sup> Gemcitabine triggers apoptosis *via* activation of the p-38 mitogen-activated protein kinase (MAPK) in response to cellular stress.

There is some additional evidence that activation of p-38 MAPK can induce phosphorylation of heat shock protein (hsp-27), responsible for growth suppression *in vitro*.<sup>137</sup>

### **1.2.3. Gemcitabine Chemoresistance**

Like many other marketed drugs used in chemotherapy, resistance to gemcitabine may be intrinsic or acquired during (a) treatment cycle(s).

As the mechanisms of chemoresistance are highly complex it can be difficult to understand precise consequences of each mechanism.<sup>138,139</sup> Several mechanisms have been proposed in the literature to confer resistance, including the balance of dCK, RRM1, RRM2, and hENT1 gene expression. A decrease in this ratio reflects both inherent and acquired chemoresistance of pancreatic cancer cells to gemcitabine.<sup>140</sup> Limited intracellular uptake of gemcitabine through hENT1 expression is an established resistance mechanism *in vitro*<sup>141</sup> and low levels of hENT1 has been shown to decrease median survival rates of patients *in vivo*. Over-expression of RR, responsible for DNA synthesis, is an additional mechanism of gemcitabine chemoresistance, however, the dominant mechanism is the over-expression of the plasma membrane drug efflux pumps P-glycoprotein (P-gP), the product of the *mdr1* gene, and multidrug resistance-associated protein (MRP)<sup>142,143</sup>

As noted above, there are many reasons why gemcitabine could fail as a therapy. Overcoming these resistance mechanisms has become a major challenge to improving the therapeutic efficacy of the drug. One way in which this can be achieved is by developing a prodrug strategy.

### **1.2.4. Prodrugs of Gemcitabine**

Nucleoside analogues are often poorly active following oral administration because of their limited intestinal permeability and rapid first pass metabolism. Gemcitabine

derived prodrugs have recently been reviewed.<sup>144</sup> Covalent coupling to the 4-amino of the cytosine ring has multiple advantages, including increasing stability to both chemical and enzymatic hydrolysis and improving bioavailability by blocking the site of potential deamination by CDA and dCDA.

Bergman *et al.* reported an elaidic acid derivative of gemcitabine (**31**).<sup>145</sup> The group tested new conjugates in leukaemic (BLCO and L5) and solid tumour cells (ovarian A2780 and colon C26-A). They reported no significant difference in efficacy when directly compared to gemcitabine but noted a decrease in the amount of measurable dFdU formed; demonstrating a resistance to CDA. Further prodrugs, functionalising with an acyclic isoprenoid chain of squalene (**32**)<sup>146</sup> were found to have a slower metabolism in plasma and a higher cytotoxicity than gemcitabine. Due to their increased lipophilicity, these derivatives are also expected to have an increased oral bioavailability when compared to gemcitabine. Another reported

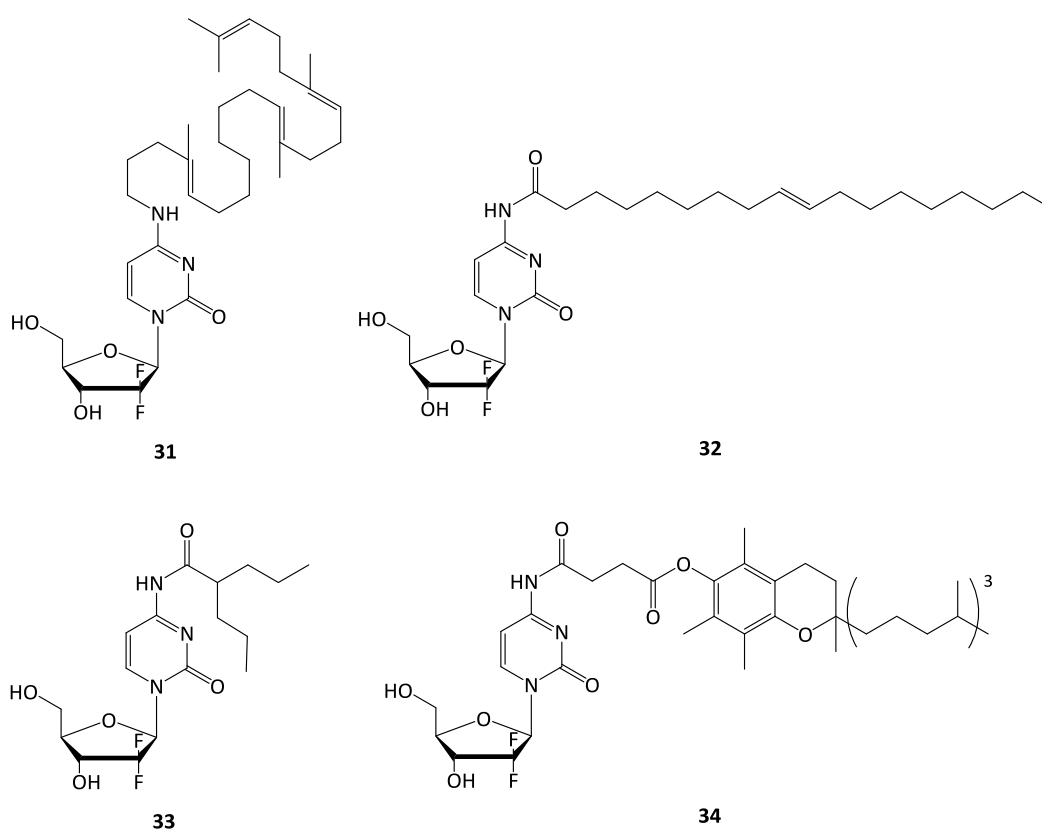


Figure 15: Gemcitabine 4-amino prodrugs

amide-based prodrug, LY2334737 (**33**),<sup>147</sup> a gemcitabine-valproic acyl prodrug was found to be more stable to hydrolysis in early preclinical studies leading to an enhanced bioavailability by blocking the site of deamination. This led to prolonged systemic exposure of gemcitabine compared to both i.v. and oral administration of gemcitabine. Subsequent pharmacokinetic studies showed that the prodrug was absorbed mainly intact across the intestinal membrane before being delivered to systemic circulation. The hydrolysis of LY2334737 was relatively slow, leading to sustained plasma presence of gemcitabine *in vivo*.

A recent publication reported a vitamin E succinate (VES) gemcitabine prodrug (**34**) that displayed a successful intracellular release of dFdC and more efficient uptake by BxPC-3 pancreatic adenocarcinoma cells, thus increased its cytotoxicity to tumour cells.<sup>148</sup>

5'-hydroxyl prodrugs are an alternative to the 4-amino derivatives, however they lack the dCDA blocking mechanism of the 4-amino derivatives.

Song *et al.*<sup>149</sup> created a series of 5'-ester prodrugs in an attempt to exploit the human peptide transporter (hPEPT1). Conjugates of L-valyl (**35**) and L-isoleucyl (**36**) both exhibited enhanced transportation, furthermore the chemical stability and rapid bioconversion seen *in vitro* of **38** suggested enhanced oral absorption.

CP-4126 (**37**),<sup>150</sup> an elaidic acid prodrug was reported to have an efficacy similar to gemcitabine itself in gemcitabine-resistant cell lines also displaying a 200-fold increase in potency.

Another phosphoramidite conjugate (**38**) was found to bypass the rate limiting monophosphorylation step<sup>151</sup> The prodrug demonstrated a 4-fold increase in activity over gemcitabine in dCK deficient cell lines.

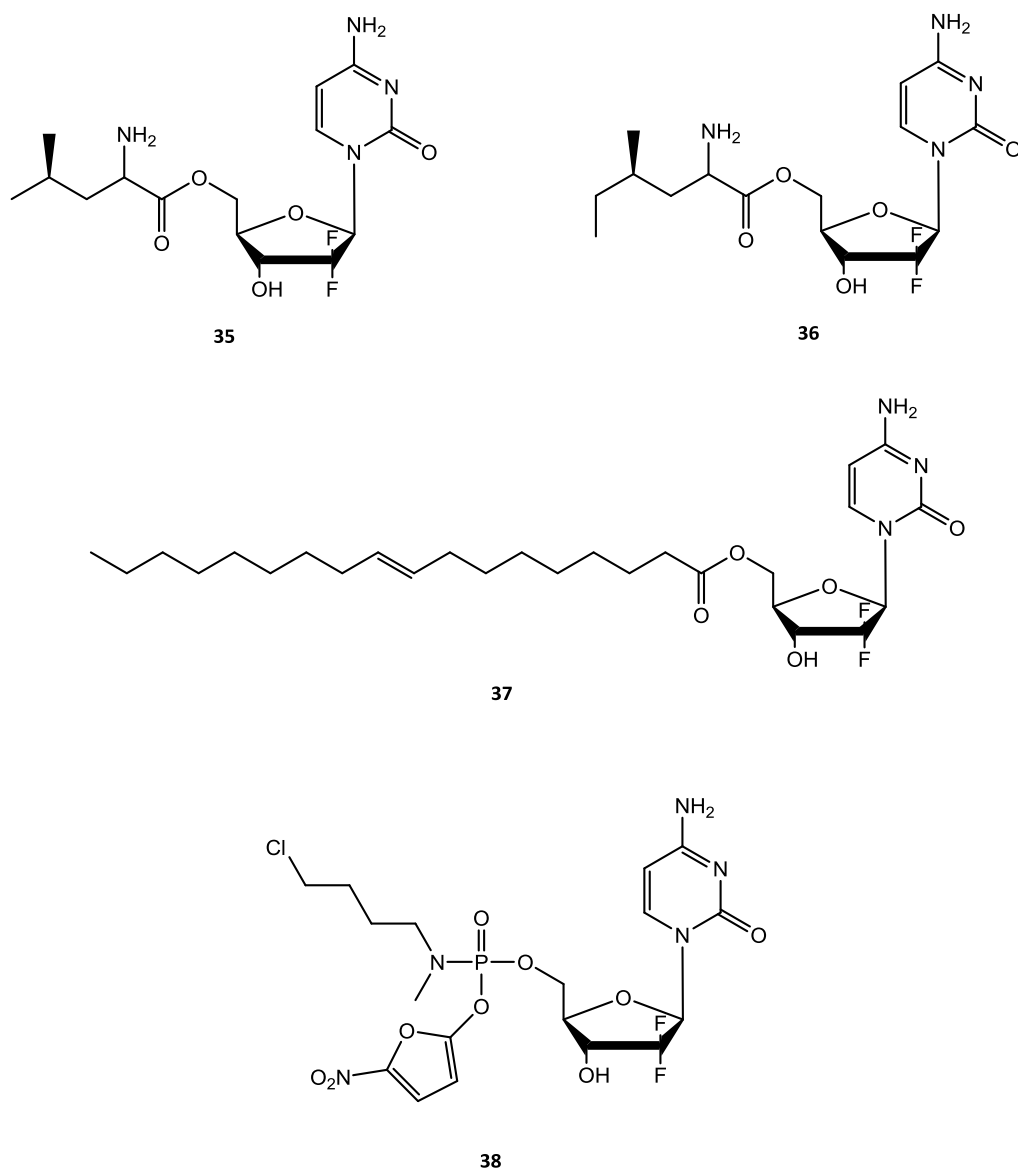


Figure 16: Gemcitabine 5'-prodrugs

### 1.3. Project Aims

As previously described (**Section 1.1.4**) there are multiple approaches that can be taken to formulate a gel for drug delivery; the 'passive' approach by which a drug is encapsulated in an inert gelator matrix and the drug released *via* diffusion or the 'therapeutic gel' approach, by which the gel itself is derived from a therapeutically active compound.

With gemcitabine (**30**) indicated as a first line treatment for pancreatic and gastric cancer and it undergoing significant first pass metabolism, the compound was easily rationalised as a starting compound with which to develop a LMW gelating controlled release drug delivery system.

The ultimate project aims were to design a platform system for the controlled release of **30** following intra-tumoural delivery. This would entail developing an amphiphilic nucleoside gelator, with a minimal solvent concentration (for biocompatibility) and moderate mechanical strength (for injectability). Additionally, the gelator would need to display good diffusion mediated release for the inert gelator matrix or cytotoxic properties, for the therapeutic molecular gel.

The following chapters detail the design, synthesis, characterisation and biological test of two diffusion mediated systems and therapeutic molecular gels for the intra-tumoural delivery and release of gemcitabine.

## 2. Modified Cytidine as a Drug Delivery Platform

---

Inert gelator matrices are an increasingly common way to encapsulate active pharmaceutical ingredients (APIs) for drug delivery as they afford opportunities to bypass the off target toxicity related effects typically associated with systemic delivery. (**Section 1.1.4.1**) These systems are usually either stable systems in which the API release is diffusion mediated or containing cleavable linkages, whereby either pH or enzymatic stimuli control matrix breakdown and API release from the gelator matrix.

Nucleoside derived LMW gelators have received little interest for the specific purpose of drug delivery with the majority of reports describing peptide derived LMW hydrogelators.<sup>52,152,153,154</sup> However, the abundance of nucleosides in nature makes them inherently biocompatible and thus an ideal foundation for a drug delivery platform. Additionally, nucleosides contain specific functional groups that make them particularly well suited to becoming LMW gelators; the nucleobase forming intermolecular interactions in a perpendicular direction, whilst hydrogen bonding and  $\pi$ - $\pi$  stacking brought about from the heterocyclic ring holds together the higher order structure. However, the intrinsic hydrophilicity of nucleosides means a considerable amount of lipophilicity is usually required to instil enough overall amphiphilic character to facilitate gelation.

There is a literature precedent for using nucleosides as the foundation of a drug delivery platform. Previous studies have reported modified nucleosides that form gelator networks in water.<sup>155</sup> For many years it has been known that guanosine makes a good hydrogelator in a  $K^+$  dependent system.<sup>156</sup> Other gelators arose *via* the modification of the ribose sugar, a strategy employed by Yun, Godeau<sup>118,157,158</sup> and most recently, Xu.<sup>50,121,159</sup>

Cytidine (**39**, **Figure 17**) is an inert analogue of the chemotherapeutic gemcitabine (**30**). It consists of a hydrophilic sugar moiety and the same cytosine nucleobase as

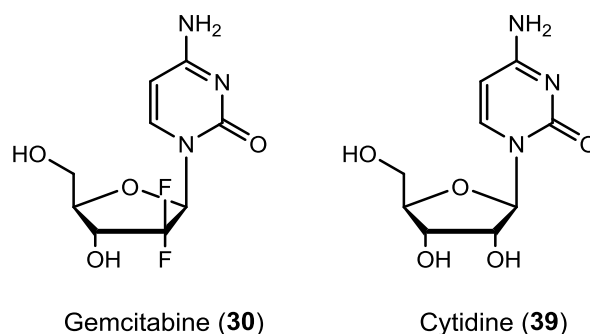


Figure 17: Structure of chemotherapeutic gemcitabine and inert analogue cytidine.

**30**, possessing the hydrogen bond donor and acceptor groups necessary to promote hydrogen bonding and facilitate the one dimensional order required for gelation. The chemical modification of cytidine is least commonly reported amongst nucleoside gelators; one of the earliest reports was of 5-triazoldeoxycytidines however the report was brief and neglected to comment on gelation procedures.<sup>160</sup> More recently an azide modified cytidine derivative was synthesised,<sup>161</sup> however there are no other reported cytidine derived gelators.

Here, a new inert cytidine-based LMW gelating scaffold is reported for the encapsulation and diffusion mediated delivery of small molecule therapeutics.

Previously described in **Chapter 1** was the relationship between the self-assembly process and the presence of certain functional groups (e.g. amides) within the gelating molecule, where a number of gelation preferred functional groups were identified based on their ability to accept and donate electrons and promote hydrogen bonding.

Amphiphilic lipids are well known for spontaneously forming a variety of architectures in aqueous solutions, depending on their overall molecular structure, though simple amphiphilic compounds often fall short in terms of their capacity for molecular recognition and self-assembly. However, nucleobase moieties are known for their ability to recognise their counterparts with high affinity and specificity towards hydrogen bonding.<sup>162</sup>

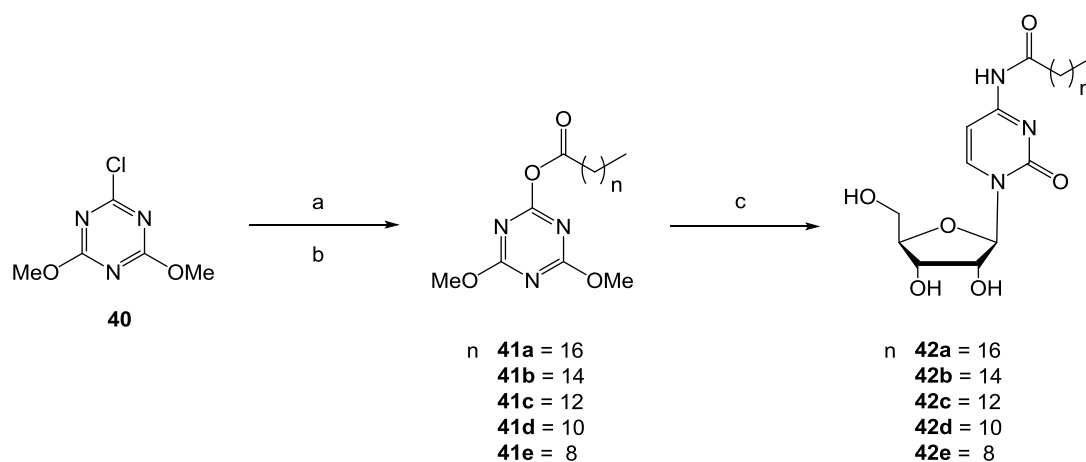
The initial focal point of this project was to create a series of cytidine gelators, based upon chemical modification with a variety of medium and long chain carboxylic acids. This addition would provide the required lipophilic character to create amphiphilicity and introduce a foundation for intramolecular solvophobic interactions, with which the gelator network would eventually be stabilised.

## 2.1. Synthesis

Cytidine contains 4 nucleophilic groups available for potential functionalisation; a primary amine on the cytosine nucleobase and three hydroxyls (2', 3' and 5') on the ribose sugar. To introduce the stable amide bonds mentioned above, the most expeditious route to achieve this was *via* modification of the 4-amino group on the cytosine nucleobase.

### 2.1.1. A Selective Route for *N*-acylation of Cytidine

There are a number of synthetic routes to similar compounds reported in literature.<sup>163,164</sup> However, they either require the use of highly toxic reagents (e.g. phosgene) or are simply undesirable due to the ratio between the number of synthetic steps to projected achievable yield. The primary interfering factor to consider in this synthesis is the presence of multiple nucleophilic groups both on the nucleobase and as part of the furanose ring. In 2000, 2-chloro-4,6-dimethoxy-1,3,5-triazine (CDMT, **40**) was found to have applications as a condensing agent in peptide chemistry.<sup>165</sup> By adapting previous literature<sup>166</sup> used for the synthesis of other nucleoside derivatives, the nucleoside conjugates **42a** – **42e** were synthesised each in a one-pot, single-step procedure with a predominant selectivity for acylation of the 4-amino group. Instead of using acyl halides or anhydrides, this strategy



**Scheme 1: Synthesis of *N*-acylated cytidine from an activated triazine ester**

Reagents and Conditions: (a) *N*-methylmorpholine, CH<sub>2</sub>Cl<sub>2</sub>, 0 °C, 1h (b) R-COOH, CH<sub>2</sub>Cl<sub>2</sub>/DMF, 0 °C, 1h (c) Cytidine (**39**), DMF, 0 °C - 50 °C, 20 h.

involved an alternative enhancement of reactivity of the carbonyl group of the carboxylic acid moiety. The reaction proceeded by reaction of **40** with *N*-methylmorpholine (NMM) to form 4-(4,6-dimethoxy-1,3,5-triazin-2-yl)-4-methylmorpholinium chloride, followed by addition of a medium or long chain carboxylic acid to generate the activated triazine ester **41a – 41e**. The resulting mixture was then treated with cytidine to afford the *N*-acylated nucleoside in moderate yield. (**Scheme 1**)

Despite the presence of three additional nucleophilic groups (2', 3' and 5'-hydroxyl) the reaction conditions favoured acylation of the exocyclic amine. A similar observation was made <sup>167</sup> during the selective acylation of 2-hydroxy ethyl piperazine. Due to the steric hindrance present in the CDMT intermediate (**41**), no *bis-N*-acylation was detected. Interestingly, no *O*-acylated product was detected either, this is suggestive of a reaction mechanism involving a direct nucleophilic attack of the 4-amino. The selectivity may be explained by the intrinsic stability of the acylating intermediate (**41**) or by the difference in nucleophilicity of the *N/O* nucleophiles of cytidine.

## 2.2. Analysing the Macroscopic Behaviour

### 2.2.1. Vial Inversion

Following successful synthesis and characterisation, the compounds underwent qualitative testing to determine their capacity to act as self-supporting gel systems. 'Table-top' rheology is an advantageous technique as it can be carried out in any laboratory, without the need for specialised or sophisticated equipment. This technique is particularly useful for determining the gel-sol phase boundary as the conversion can be visually assessed. The simplest method for monitoring gel-sol transitions involves the inversion of a vial to determine flow behaviour.

Developing a gelator compound that forms a stable gel in a 100 % aqueous environment, a hydrogel, is the ultimate challenge. **42a – 42e** were assessed for their stability to inversion in water alone; 0.5 % (w/v) of compound was dispersed in ultra-purified water (500  $\mu$ L) and heated to 60 °C in sealed vials for 30 minutes, before allowing to cool.

Gelation is a solubility driven process; under the tested conditions complete solubilisation was not achieved for any of **42a – 42e**, likely due to the high cLogP values (**Table 1**) indicating the high lipophilic content of the conjugates and thus reduced water solubility. A common solution to this problem is to introduce a minimal amount (< 5 % (v/v)) of organic solvent to enable solubilisation of the compound prior to facilitating gelation *via* the addition of water, this is termed 'anti-solvent' or 'solvent switch'.<sup>43,168,49,169</sup> Common solvents used to create organogels include hexafluoroisopropanol (HFIP), acetone and dimethylsulfoxide (DMSO),<sup>51</sup> with DMSO being the first choice solvent in most cases.

For this investigation DMSO and ethanol were selected. Under normal circumstances solvents will only ever be used sparingly due to associated toxicity; however for a cancer drug delivery platform such as this, increased concentrations of solvent are potentially advantageous. DMSO has been shown to reduce growth of a human ovarian carcinoma (HOC-7) cell line reversibly in a dose and time dependent manner<sup>170</sup> and to reduce the tumorigenicity of human pancreatic cell lines.<sup>171</sup> Only a few papers exist that claim to use ethanol as a gelating medium.

**Table 1: cLogP values of compounds 42a - 42e**

	n	cLogP
<b>42a</b>	16	6.43
<b>42b</b>	14	5.37
<b>42c</b>	12	4.31
<b>42d</b>	10	3.25
<b>42e</b>	8	2.20

A rare, recent example uses a gel formulated with 40 % (v/v) ethanol to show the enhanced release profile of indomethacin; a controlled release (~25 %) over 300 h demonstrating its use for dermatological applications.<sup>172</sup> Additionally, ethanol has been used extensively as a pharmaceutical co-solvent for solubilisation of poorly soluble drugs,<sup>173</sup> and there is associated clinical guidance recommending intra-tumoural ethanol injection in oesophageal, gastric and pancreatic tumours as a method of ablation.<sup>174</sup>

Solvent volume fractions ( $\Phi_{\text{SOL}}$ ) of 0.05 - 0.50 (5 – 50 % (v/v)) were explored so that the gel would potentially generate some of the characteristics representative of a hydrogel and would therefore be beneficial for this application. Results for **42a - 42e** at  $\Phi_{\text{SOL}}$  0.05, 0.10, 0.20, 0.30, 0.40 and 0.50 in DMSO and ethanol are shown in **Table 2** and at a low final compound concentration of 0.5 % (w/v). Each of the samples was classified based upon their stability to inversion, where G (gel), PG (partial gel) and NG (no gel) denotes the three classes. (**Table 3**)

Gels were prepared by solubilising a small amount (2.5 mg) of compound in a volume of solvent at 60 °C before introducing water also at an elevated temperature to make the final volume up to 500  $\mu\text{L}$ , as per **Table 6**. The vials were left to cool to room temperature before examining by vial inversion.

Reported for Fmoc-dipeptides<sup>175,176</sup> is the observation that upon the addition of water to a minimal concentration of organic solvent a turbid solution results, this clarifies over time to give a stable gelator. For this series, instantaneous gelation was observed. It is thought this may be due to rapid restructuring of an initial self-assembled structure from many irregular aggregates into more highly ordered structures potentially representing a high  $T_{\text{gel}}$ . It was noticed that the greater the

lipophilic character of the nucleoside conjugate the less stable the gels were to inversion at lower solvent volume fractions. This was the most apparent in **42d** and **42e** across both the DMSO and ethanol series', each series only offering one seemingly stable gelator seen at  $\Phi_{\text{EtOH}}$  0.40 and  $\Phi_{\text{DMSO}}$  0.50, respectively.

Table 2: Vial inversion of compounds 42a - 42e in DMSO (left) and ethanol (right).

Each image show is  $\Phi_{\text{SOL}}$  0.05, 0.1, 0.2, 0.3, 0.4 and 0.5 (left to right). Representative image of n = 4.

	DMSO	Ethanol
42a		
42b		
42c		
42d		
42e	-	

**Table 3: Classification of gels of 42a - 42e at  $\Phi_{\text{SOL}}$  0.05 – 0.50, where G (Gel), PG (Partial Gel) and NG (no gel).**

$\Phi_{\text{SOL}}$	Conjugate									
	DMSO					Ethanol				
	42a	42b	42c	42d	42e	42a	42b	42c	42d	42e
<b>0.05</b>	NG	NG	NG	NG	-	NG	NG	NG	NG	NG
<b>0.10</b>	NG	NG	NG	G	-	NG	NG	PG	G	NG
<b>0.20</b>	PG	PG	PG	G	-	PG	PG	G	G	NG
<b>0.30</b>	PG	G	PG	G	-	PG	PG	G	G	NG
<b>0.40</b>	PG	G	G	G	-	PG	G	G	G	NG
<b>0.50</b>	G	PG	G	G	-	PG	G	G	G	NG

The ‘stable to inversion’ studies (**Table 2**) confirmed that there is a window in which gelation will occur successfully for this series, in both DMSO and in ethanol. Gels of **42a**, **42b** and **42e** do not meet the criteria, that is, they do not produce either homogenous or stable gels. This can be explained by looking at the degree of lipophilicity introduced in each case.

The cLogP is a representation of the amount of lipophilic character a compound possesses. The closer the cLogP value is to zero the less lipophilic the compound and thus the more water soluble. The cLogP values of **42a** and **42b** are 6.43 and 5.37, respectively, indicating a high proportion of lipophilic character within the molecule and lack of aqueous and organic solubility. For this reason, aggregates suspended in the ‘gels’ are visible and a heterogeneous phase i.e. a partition between solvent phase and aqueous phase, is apparent. The converse is seen in the gels derived from **42e**; a lower cLogP (2.20) indicates less lipophilic character and thus increased water solubility. This is seen in the representative gel samples; there is a lack of stability to inversion, and even though the gels appear homogenous the increased solubility reduced the amount of intermolecular bonding required for gelation.

The ‘best’ gelators were seen in series **42c** and **42d**. There was no observed gelation at  $\Phi_{\text{SOL}}$  0.05 in any instance; however at  $\Phi_{\text{SOL}}$  0.10 the appearance of stable gelators was noted, particularly in ethanol. An increased turbidity was noted in these samples, that can be attributed to lower lipophilic content and therefore decreased organic solubility, this was particularly apparent in those gels containing **42d**, where a

homogenous transparent system didn't appear even at the highest solvent volume fraction,  $\Phi_{\text{SOL}}$  0.50. In gels of **42c** a visually stable clarified sample occurred at  $\Phi_{\text{SOL}}$  0.40.

An enhanced 'stability to inversion' profile was also noted for samples of **42c** prepared in ethanol over their DMSO counterparts. This observation may be attributed to the disruption in hydrogen bonding caused by DMSO.

Solvent structure is known to play an important, yet often underappreciated role in gel formation. A recent example highlights how a change in solvent can lead to drastic changes in both dissolution and gelation ability.<sup>177</sup> In this instance weak solvent/gelator interactions were seen in DMSO/H<sub>2</sub>O and strong solvent/gelator interactions in EtOH/H<sub>2</sub>O, as reported here.

From this initial bench-top study the preference for cytidine nucleoside analogues to form stable gelators in ethanol over their DMSO counterparts was concluded. Furthermore, the increased propensity for gelation was seen in **42c** over each of the other conjugates, surprising due to its increased lipophilicity. Hence, for the remainder of this chapter the work focused on the physical and biological characterisation of **42c**.

### 2.2.2. Rheology

Upon confirming the lead candidate for an acceptable gelator the mechanical properties were probed using rheology.

Oscillatory measurements are used to examine primarily viscoelastic materials. They offer advantages over rotational testing as the data is based upon two independent sets of data; storage modulus ( $G'$ ) and loss modulus ( $G''$ ) with  $G'$  being a measure of deformation energy stored within the sample and representing elastic behaviour.  $G''$  is a measure of deformation energy used up by the sample during the shear process and therefore is 'lost' from the sample and represents the viscous behaviour of a sample. Other information about the sample can be recovered from these measurements; the loss factor ( $\tan \delta$ ) represents the ratio of the viscous and elastic portions. (**Equation 1**) Reaching a  $\tan \delta = 1$  is an important criteria during gel formation as this indicates the

sol/gel transition. If  $\tan \delta < 1$  ( $G' > G''$ ) then the gel-like state dominates. The converse is true for samples with  $\tan \delta > 1$  ( $G'' > G'$ ) in which case the liquid state prevails.

**Equation 1: Derivation of the loss factor  $\tan \delta$  from oscillatory measurements.**

$$\tan \delta = G'' / G'$$

Initial oscillatory measurements are usually amplitude sweeps, performed at variable amplitudes with constant frequency. The frequency is often set as angular frequency ( $\omega = 10$  rad/s) since  $\omega = 2\pi \cdot f$  and frequency (Hz) is not an SI-unit. At low amplitudes, the linear viscoelastic (LVE) region exists, this term is derived from the proportionality of pre-set and measured parameters and as a consequence the resulting curve occurs as a straight line. Analysing the behaviour of a sample in the LVE range, the viscoelastic behaviour of a sample can be described. As these systems are gel like in behaviour, we would expect  $G' > G''$  and  $\tan \delta < 1$ . Here the elastic behaviour dominates the viscous behaviour in the LVE range.

Frequency sweeps are oscillatory tests performed at variable angular frequencies but at a constant strain, determined by the centre of the LVE range found during an amplitude sweep. In stable viscoelastic materials/gels, intermolecular interactions build up the three dimensional (3D) network. These materials demonstrate  $G' > G''$  across the whole frequency sweep in the form of almost parallel straight lines and typically, for an ordered system will show a  $\tan \delta = 0.1 - 0.01$ .

#### **2.2.2.1. Amplitude sweep**

Initial oscillatory measurements ( $n = 5$ ) were carried out on each of the gels found from stability to inversion studies of **42c**. (**Section 2.2.1**) Amplitude sweeps of **42c**  $\Phi_{\text{EtOH}} 0.20 - 0.50$  confirmed a good correlation between visual stability and the associated quantitative mechanical strengths of the gels derived from **42c**. The amplitude sweeps (**Figure 18a**) show a consistent storage modulus ( $G'$ ) of between 1000 and 5000 Pa, <sup>178</sup> the presence of a linear region within the centre of the

amplitude sweep as well as a difference of one order of magnitude between  $G'$  and the loss modulus ( $G''$ ).

$\Phi_{\text{EtOH}} 0.40$  demonstrated the greatest overall mechanical strength in giving a maximum  $G'$  of 5000 Pa. Previous reports have alluded to the effect of solvent type and concentration on gel formation of Fmoc-PhePhe-OH gels, demonstrating a more uniform network when  $\Phi_{\text{EtOH}}$  was above 0.30.<sup>179</sup> The main observation from these studies is the extent to which the LVE region extends. In each of  $\Phi_{\text{EtOH}} 0.20, 0.30$  and  $0.50$  the LVE region stretched to  $0.1 - 0.2\%$  after which point the mechanical strength decreased slightly. In the case of  $\Phi_{\text{EtOH}} 0.50$  this observation can be attributed to the increased solubility of **42c** in the amount of solvent whilst for  $\Phi_{\text{EtOH}} 0.20$  and  $0.30$ , this experimental observation is likely due to the decreased solubility in both aqueous and organic phases. The mechanical properties ( $G'$  and  $G''$ ) of the gels were reproducible (means and standard deviations are of 3 independent samples).

At this point, taking into account the 'stable to inversion' studies,  $\Phi_{\text{EtOH}} 0.40$  appeared to be the most favourable solvent volume fraction at which to form a stable gelator.

#### 2.2.2.2. Frequency Sweeps

Frequency sweeps were carried out on **42c**  $\Phi_{\text{EtOH}} 0.40$  at  $\omega = 0.5\%$ , based upon the centre of the LVE region defined during the amplitude sweep. Angular frequency was varied between  $0.1$  and  $100$  rad/s and the temperature was kept constant at a physiologically relevant  $37\text{ }^\circ\text{C}$ . **Figure 18b** shows a high degree of linearity between  $1$  and  $100$  rad/s with a  $\tan \delta = 0.18$ , indicating that the material is viscoelastic in behaviour and behaves independently of the frequency applied.

#### 2.2.2.3. Temperature of gelation

Finally the temperature of gelation ( $T_{\text{gel}}$ ) was examined. From the initial bench top 'stable to inversion' study we know that the gelation temperature should be above  $60\text{ }^\circ\text{C}$ , due to the method of preparation and observations during the cooling process i.e. instantaneous gelation upon mixing with water. In this instance the temperature was increased from  $35 - 105\text{ }^\circ\text{C}$  at  $0.5\text{ }^\circ\text{C}/\text{min}$  increments, maintaining a constant strain ( $\gamma = 0.5\%$ ) and angular frequency ( $\omega = 10$  rad/s) (**Figure 18c**). Noted is a stability; approximately an order of magnitude between  $G'$  and  $G''$  below  $90\text{ }^\circ\text{C}$ , after this point

the gel begins to decrease in strength, evident by the intersecting of  $G'$  and  $G''$  and the reversing of solid and liquid priority caused by the disconnection of the cross-linked network and solubilisation of the gelator compound, **42c**. From this study, we quantified the  $T_{gel}$  to be 98 °C; moreover we are able to say that the gelator will remain stable at physiological temperatures, an important consideration when designing a drug delivery platform.

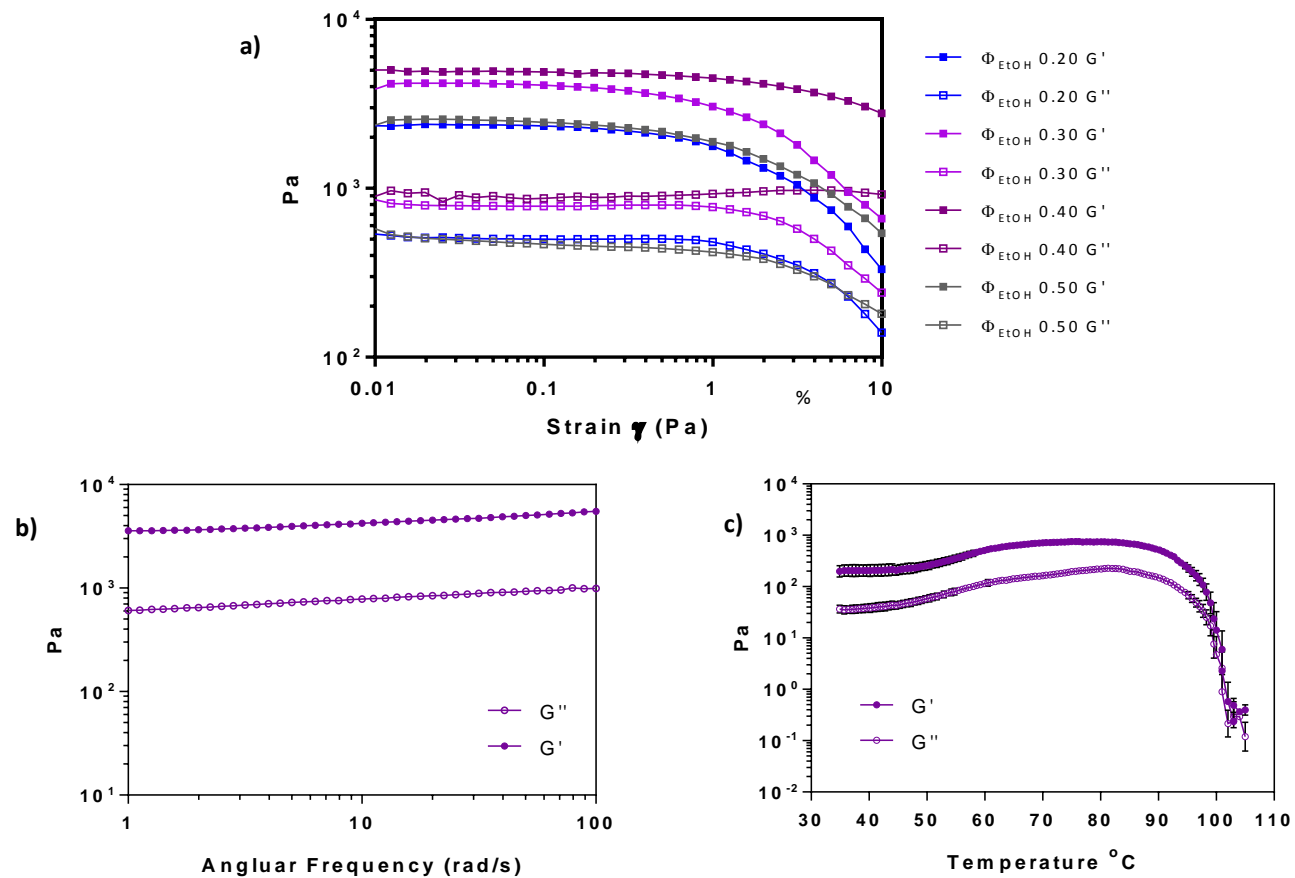


**Figure 18: Rheological data for 42c**

a) Amplitude sweeps ( $G'$  and  $G''$ ) of **42c**  $\Phi_{EtOH}$  0.2, 0.3, 0.4 and 0.5,  $n = 5$  at 37  $^{\circ}C$ ,  $\gamma = 0.01 - 10\%$  and  $\omega = 10$  rad/s. Standard Deviations  $< 10\%$  b) frequency sweep of **42c**  $\Phi_{EtOH}$  0.40,  $n = 5$  at 37  $^{\circ}C$ ,  $\gamma = 1\%$  and  $\omega = 1-100$  rad/s. Standard Deviation  $2500 \pm 300$  Pa % c) Temperature sweep of **42c**  $\Phi_{EtOH}$  0.40,  $\gamma = 0.5\%$   $\omega = 10$  rad/s, 35- 105  $^{\circ}C$  heating at 0.5  $^{\circ}C/min$  increments.

### 2.2.3. Nanostructure Determination

Understanding and probing the nanostructure of a gelator is key to understanding its potential applications. As mentioned in **Chapter 1** there are many forms a gelator can take depending on the kinetics of the cooling process such as tapes, ribbons, fibres etc. However, based upon the rheological measurements, an ordered/cross-linked series of nanofibres was anticipated for this series.

#### 2.2.3.1. Electron Microscopy

Scanning electron microscopy (SEM) was utilised to give a broad overview of the gelator structure. **Figure 19a** shows a highly cross-linked fibrillar network, however at this magnification and voltage the individual fibres were not visible. Transmission electron microscopy (TEM) was considered the more suitable system for imaging the nanostructure of these gels. **Figure 19b** shows a much clearer representation of the nanostructure; the cross-linked network of fibres was seen in more detail and the porosity between the fibres was now evident. Further analysis of these images quantified each fibre to have an approximate width of between 20 - 25 nm and a length of approximately 200  $\mu\text{m}$ . However, due to sample preparation and the high vacuum drying conditions involved in TEM it can't be assumed that these features are completely representative of the matrix in its hydrated state.

Based upon the results of microscopic imaging, a hypothetical model of self-assembly can be proposed. (**Figure 19c**) One molecule of **42c** is approximately 10 – 15 Å; it was thought that during the self-assembly of a single fibre, the hydrophilic cytidine moiety would align outwardly whilst the hydrophobic acyl chain would align as the core of the fibre, with each individual molecule of **42c** being offset, resonating as a 'twist' caused by electrostatic repulsive forces. Therefore the final radius of a single fibre would have approximately double the width of a single molecule (20 – 30 Å). Each of these fibres would subsequently aggregate and intertwine with additional fibres to create a fibrous 'bundle' with a nanometre width.

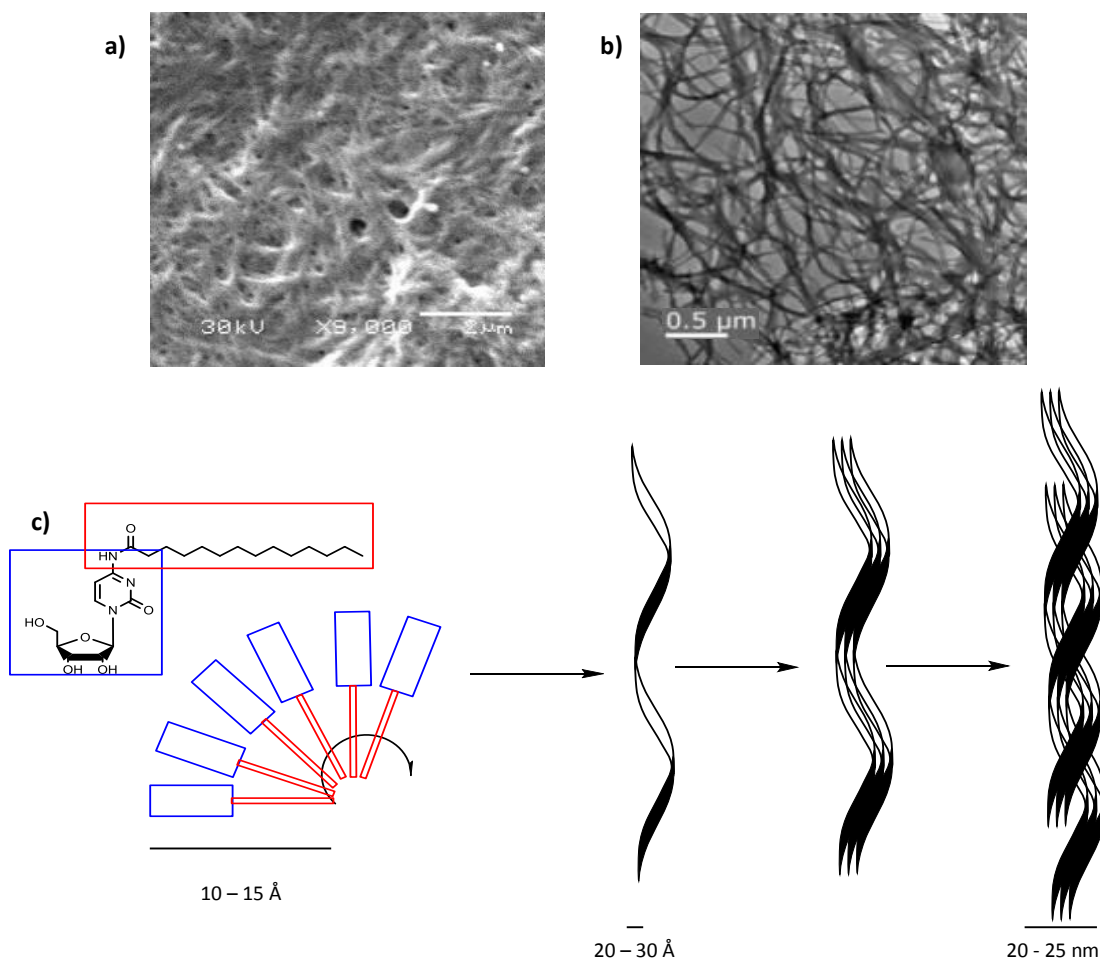


**Figure 19: Electron microscopy of 42c  $\Phi_{\text{EtOH}}$  0.40**

a) Scanning electron microscopy where scale bar is 2  $\mu\text{m}$  and b) Transmission electron microscopy where the scale bar is 0.5  $\mu\text{m}$ . c) Hypothetical model of self-assembly. The hydrophilic cytidine moiety aligns on the outside of the helix and the hydrophobic acyl chain aligns as the core of the fibre. One fibre is approximately 10 – 15  $\text{\AA}$  in width. Each of these fibres aggregates and intertwines with additional fibres to create a fibrous ‘bundle’

### 2.2.3.2. Fourier transformed infra-red (FT-IR) spectroscopy

FT-IR measurements were conducted to determine which of the functional groups present in the gelating molecule **42c** were involved in the gelation process. **Figure 20** shows  $\Phi_{\text{EtOH}}$  0.50, 0.40, 0.30 and 0.20 (top to bottom) with IR peaks at 1681 and 1642  $\text{cm}^{-1}$  representing the amide I region of **42c**. As the solvent volume fraction increased from  $\Phi_{\text{EtOH}}$  0.20 to 0.30 a clear change in the molecular packing was observed. The peak at 1681  $\text{cm}^{-1}$  was seen to broaden and attenuate, shifting slightly from 1681  $\text{cm}^{-1}$  to 1678  $\text{cm}^{-1}$ . An additional shift was seen from the peak at 1652  $\text{cm}^{-1}$  shifting and

broadening into a peak at  $1642\text{ cm}^{-1}$ . The peak shifts and broadening observed *via* FTIR are indicative of hydrogen bonding and have been observed for other gelating molecules.<sup>43,122</sup> These findings imply the change from ‘free’ single molecules to a hydrogen bonded networks. Other interactions were anticipated from this series, including hydrogen bonding from the ribose hydroxyls and  $\pi$ - $\pi$  stacking interactions brought about from inter-molecular interaction between nucleobases. However owing to the number of hydroxyl residues present in the gelating molecule and the lack of specificity in FTIR it isn’t possible to define exactly which, if any of them play a role in the self-assembly and stabilisation of the gel network.

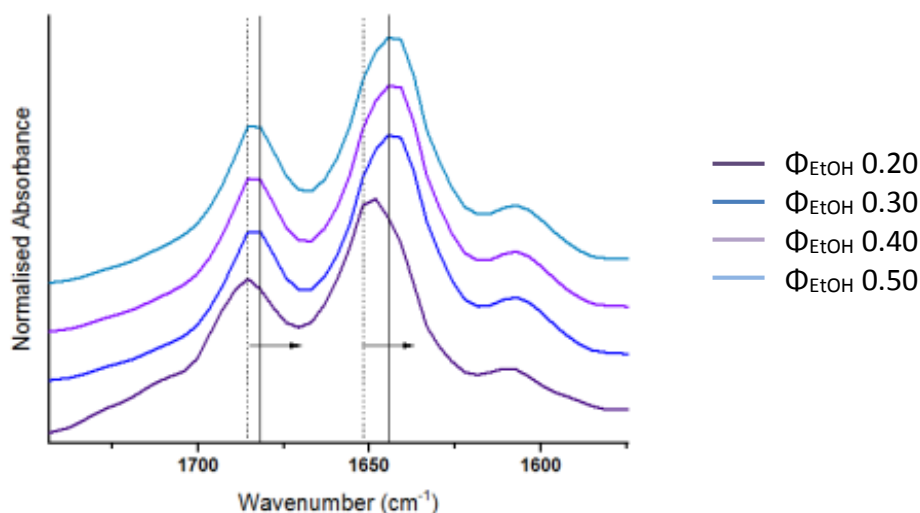


**Figure 20: FT-IR absorbance of the amide I region of 42c.**

Top to bottom  $\Phi_{\text{EtOH}}$  0.50, 0.40, 0.30 and 0.20. Spectra are off set to demonstrate peak shifts and peak broadening.

The FTIR study further supports the rheological and microscopic findings, of a cross-linked fibrillar network stabilised through hydrogen bonding. The extent of the hydrogen bonding was not determined as the FTIR was acting only a model to conclude that hydrogen bonding was present within the system.

It was noted during imaging that the cross-linked fibrillar networks contain a number of microscopic cavities, further confirming the hypothesis that this system had potential applications as a scaffold in which to encapsulate APIs for drug delivery.

In order to explore the possible applications of **42c** as a reservoir for therapeutic materials, the gel was self-assembled in the presence of fluorescent particles of various molecular dimensions.

### 2.3. *In Vitro* Release Kinetics

Fluorescein (332 Da), Fluorescein Isothiocyanate Dextran 4000 Da (FITC Dextran 4) and Fluorescein Isothiocyanate Dextran 10000 Da (FITC Dextran 10) were used to examine the encapsulation and release efficiency from the  $\Phi_{\text{EtOH}}$  0.40 gel. The fluorescent molecule was solubilised in the aqueous phase and the gel formulated as per the earlier procedure (**Section 2.2.1**) up to the volume of 2 mL. Phosphate Buffered Saline (PBS, 5 mL) was pipetted on top of the gel and the release monitored by removing aliquots (150  $\mu\text{L}$ ) at specific intervals and measuring the relative fluorescence in order to calculate the percentage of each fluorescent molecule released.

The volume of water removed for sampling was extremely low with respect to the total volume of the system. The release of the dye from the gel was monitored with time and the diffusion coefficients ( $D$ ) of the dyes in the gel matrix were calculated using the non-steady-state diffusion model equation (**Equation 2**) where  $M_t$  is the total amount of molecules released during the measurement,  $M_\infty$  is the total number of molecules kept in the matrix,  $\lambda$  is the hydrogel thickness,  $t$  is the time of the measurement, and  $D$  is the diffusion coefficient of the molecule.

**Equation 2: Non-steady state diffusion model equation**

$$M_t / M_\infty = 4(Dt/\pi\lambda^2)^{0.5}$$

No change to the hydrogel was visually apparent (e.g. shrinkage or swelling). The release profiles showed typical sustained release behaviour with the total percentage release of fluorescein (88 %) far exceeding that of the two FITC Dextran compounds (< 10 %). **Figure 21a** shows the release data as a plot of mass released fraction ( $M_t / M_\infty$ ) as a function of time ( $t$ ). When the amount of dye released is plotted against the square root of time, a good linear relationship was found ( $r^2 > 0.97$ ), indicating that the release of the dyes from the hydrogel matrix is following Fickian diffusion control.<sup>180</sup> The diffusion coefficients for each of the tested dyes were calculated (**Table 4**). The

release rate of FITC Dextran 10 was so low that a diffusion coefficient couldn't be calculated.

**Table 4: Diffusion coefficients for dyes release from 42c in pH 7.4 phosphate buffered saline**

Dye	Diffusion Coefficient (m <sup>2</sup> /s)
Fluorescein	$3.32 \times 10^{-11} \pm 0.19 \times 10^{-11}$
FITC Dextran 4	$3.84 \times 10^{-13} \pm 0.36 \times 10^{-13}$
FITC Dextran 10	<i>n.d</i>

Release from a gel matrix can be controlled by many factors, including pore size and molecular weight of the drug. The calculated diffusion coefficients here reflect similar values reported in literature for the release of drug like molecules for similar gelator systems,<sup>54</sup> however in this system the values are slightly lower indicating slower release. This could be attributed to the close packing of the fibres within the gel matrix significantly retarding the free diffusion of these larger molecules. We can therefore make a general assumption from this that the gel of **42c**  $\Phi_{\text{EtOH}}$  0.40 will retain molecules with a large mass and molecules with smaller masses (100's Da) will be released; a theory in agreement with others who have also shown similar retention of higher molecular mass molecules from a gelating dipeptide based hydrogel.<sup>49,181</sup>

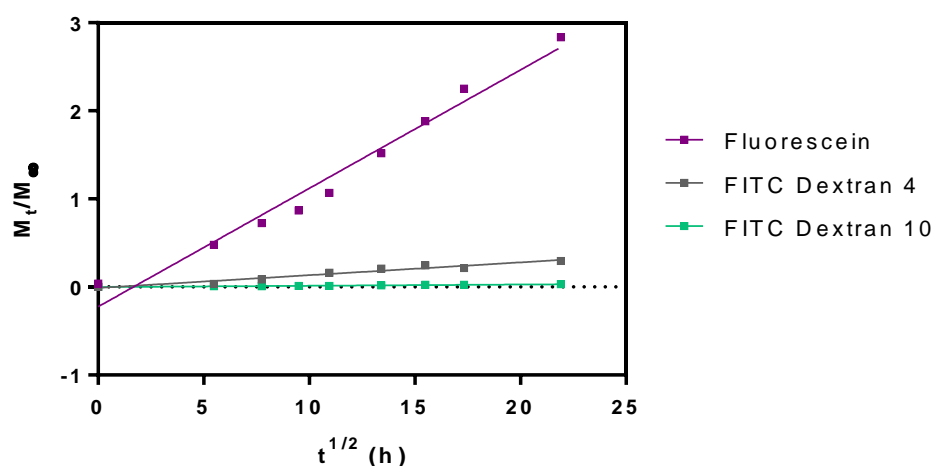


**Figure 21: *In vitro* release kinetics of Fluorescein (0.15 mM), FITC Dextran 4 (0.06 mM) and FITC Dextran 10 (0.01 mM) from the gel matrix of 42c.**

a) Plot of released dye against square root of time. b) Figure is representative of 5 repeat release experiments, n = 4 in each experiment.

## 2.4. Can the Gel Function in a Physiological Environment?

Having completed the physicochemical characterisation and demonstrated the non-steady state diffusion of small molecules from the gel matrix *in vitro* mammalian cell studies were carried out to determine the applicability as a drug delivery platform.

### 2.4.1. *In Vitro* Growth Inhibition Efficiency of Ethanol

Initially the effect of the solvent concentration upon two cell lines; HCT-116, a human colorectal carcinoma cell line and MCF-7, a human breast adenocarcinoma cell line was determined. The cell lines were tested against ethanol concentrations from 0.01 - 10 % (v/v). An n=3 gave an average 50 % growth inhibition (GI<sub>50</sub>) at 3.8 % and 2.8 % (v/v) ethanol in HCT-116 and MCF-7 cell lines, respectively.

Ideally this gelator scaffold would be non-toxic as the 'cytotoxic' character would be introduced using the encapsulated drug. Growth inhibition assays were carried out using the HCT-116 and MCF-7 cell lines. Due to the preliminary solvent screen we can say that in the HCT-116 and MCF-7 cell lines, the gels derived from **42c** would not be well tolerated due to the high solvent volume fraction ( $\Phi_{\text{EtOH}}$  0.40), for that reason the following assays were carried out on **42c** in its solid state and not **42c** in its gel state.

### 2.4.2. *In Vitro* Growth Inhibition Efficiency of **42c**

The compound was tested against a cytidine (**39**) alone, as a control. Obtaining a high

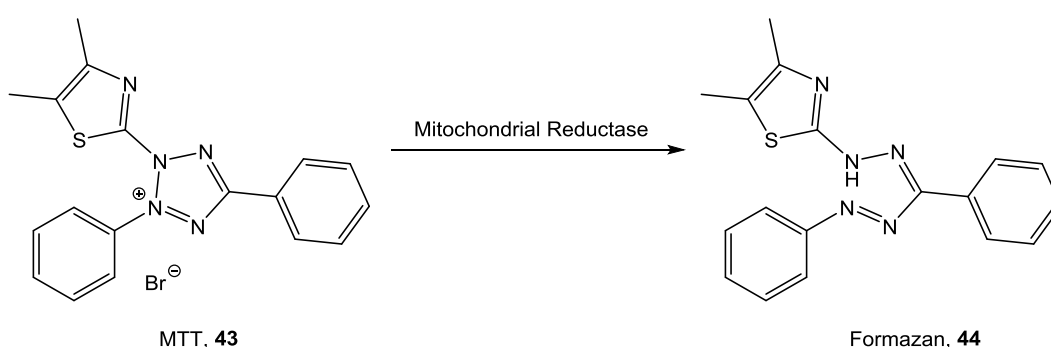


**Figure 22: Reduction of MTT to formazan.**

Yellow 3-(4,5-dimethylthiazol-2-yl)-2,5-diphenyltetrazolium bromide (MTT) is reduced to insoluble purple (E,Z)-5-(4,5-dimethylthiazol-2-yl)-1,3-diphenylformazan (formazan) crystals *via* mitochondrial reductase.

degree of growth inhibition from either of these compounds was not anticipated due to being either wholly biologically compatible or being derived from 2 biologically compatible parts. A standard colorimetric MTT assay was used; the cells were split into a nuncwell 96 well plate (3000 cells/ well) and incubated for 24 h at 37 °C and 5 % CO<sub>2</sub> before introducing the test agent, either cytidine (**39**) or **42c**. The cells and test compound were incubated for a further 72 h before adding 3-(4,5-dimethylthiazol-2-yl)-2,5-diphenyltetrazolium bromide (MTT, **43**). Living and dead cells were quantified by measuring UV absorbance, living cells metabolise the yellow MTT to insoluble purple (E,Z)-5-(4,5-dimethylthiazol-2-yl)-1,3-diphenylformazan (formazan, **44**) crystals (**Figure 22**) that could then be solubilised with DMSO and measured at 570 nm.

**Table 5** suggests a biocompatibility between the conjugate, **42c**, and the parent compound cytidine (**39**) in both HCT-116 and MCF-7 with both compounds with the conjugate **42c**, demonstrating GI<sub>50</sub> values of 5.88 mM and 5.92 mM, respectively. Therefore it can be assumed that any toxicity associated with the gel scaffold *in vitro* could be attributed solely to the high ethanol content of the formulation.

**Table 5: 50 % Growth Inhibition (GI<sub>50</sub>) data for cytidine (39) and cytidine-N-tetradecanoyl (42c) in HCT-116 and MCF-7 cell lines. Data is representative of n=5.**

	GI <sub>50</sub> (mM)	
	HCT-116	MCF-7
<b>39</b>	9.34 ± 4.44	5.62 ± 3.51
<b>42c</b>	5.88 ± 2.56	5.92 ± 0.95

## **2.5. Summary**

Shown here is a new LMW nucleoside gelator with demonstrated applications in drug delivery. Simple chemical modification of the exocyclic *N*-position on the cytosine nucleobase afforded a suitably amphiphilic compound. When prompted by a change in solvent polarity, the compound was able to self-assemble in a rapid gelation process resulting in the formation of a stable self-assembled cross-linked fibrillar network.

Through rheological testing, TEM imaging and FTIR the importance of the solvent: water ratio to the self-assembly process was demonstrated; specifically showing that a gel containing a solvent volume fraction,  $\Phi_{\text{EtOH}}$  0.40, displayed enhanced self-assembly capabilities, arranging itself into an ordered highly cross-linked fibrillar structure with an increased mechanical strength. FT-IR spectroscopy alluded to the critical importance of the amide functionality in the self-assembly process, though it was not able to provide more information about the interaction on a molecular level beyond this. Molecular modelling would provide a more accurate alternative, however owing to the complexity of the dual component solvent phase, modelling would ultimately prove difficult.

The possible application of such gels as reservoirs for both large and small bio macromolecular therapeutics was fully demonstrated. And the biocompatibility of the solid compound explored using growth inhibition assays.

However, there are significant drawbacks to this gelator formulation; its increased ethanol concentration is a hindrance, particularly when considering this gelator/gel for drug delivery applications beyond intra-tumoural or topical drug delivery. Developing a gelator with minimal (< 5 %) or no solvent interference i.e. a complete hydrogel, would be a way to overcome this. This would require increasing the water solubility/hydrophilicity of the compound or conversely decreasing the amount of lipophilic character introduced during the conjugation.

## 2.6. Materials and Methods

### Materials

Cytidine was purchased from Sigma Aldrich (Europe) and all other chemicals and solvents were purchased from commercial suppliers and used without further purification.

1.5 mL sample vials and 7 mL Sterilin vials were purchased from Fischer Scientific, 7 mL aluminium rheology vials were purchased from Anton Paar GmbH and Transmission Electron Micrograph (TEM) grids were purchased from EM Resolutions.

### Methods

#### 2.6.1. General Chemistry

Reactions were monitored by thin layer chromatography (TLC) on commercially available pre-coated aluminium-backed plates (Merck Kieselgel 60 F<sub>254</sub>). Visualisation was by examination either under UV light (254 nm and 366 nm) or by staining with potassium permanganate (KMnO<sub>4</sub>) or ninhydrin (solution in ethanol) dip. Flash chromatography was performed using Merck Kieselgel 60, 230-400 mesh (Merck KGaA, Darmstadt, Germany).

Melting points (m.p) were recorded on a Gallenkamp Melting point apparatus and were corrected using benzoic acid as a standard (121 – 123 °C).

Fourier-transform infra-red (FT-IR) spectra were recorded on an Agilent Cary-360 spectrophotometer with diamond ATR attachment in the range of 4000 cm<sup>-1</sup> - 650 cm<sup>-1</sup>.

<sup>1</sup>H NMR spectra were recorded on a Bruker 400 Ultrashield at 400.13 MHz at 25 °C. <sup>13</sup>C NMR spectra were recorded on a Bruker AV(III) at 500 MHz at 25 °C. Unless stated otherwise, solvent used for NMR analysis was DMSO-*d*<sub>6</sub> ((CHD)<sub>2</sub>SO at δ<sub>H</sub> 2.50 ppm, (CD<sub>3</sub>)<sub>2</sub>SO at 39.52 ppm). Chemical shifts (δ) are recorded in parts per million (ppm). Coupling constants (*J*) are recorded in Hz (rounded to one decimal place) and any significant multiplicities described by singlet (s), doublet (d), triplet (t), quadruplet (q),

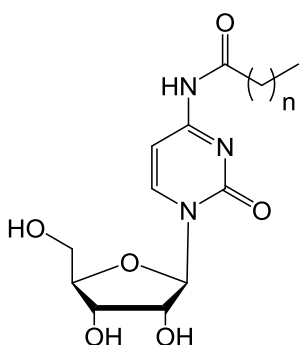
broad (br), multiplet (m), doublet of doublets (dd) and doublet of triplets (dt). Spectra were assigned using correlation spectroscopy (COSY) sequences.

High Resolution Mass Spectroscopy (HRMS) time of flight, electrospray (TOF ES +/-) was recorded on a Waters 2795 separation module micro-mass LCT platform.

Analytical Liquid chromatography-mass spectroscopy (LC-MS) was carried out on a Shimadzu UFLCXR system coupled to an Applied Biosystems API2000. A Phenomenex Gemini-NX C<sub>18</sub> column (50mm × 2mm × 3μm-110 Å) was used. Mobile phases were prepared as follows Solvent A – 0.1 % Formic acid in water and Solvent B – 0.1 % formic acid in acetonitrile (CH<sub>3</sub>CN) and sonicated for 30 min. The retention time (t<sub>R</sub>) was reported using a pre-equilibration run (1 min) at 10 % B, the 10 % B for 0.5 min, 10 – 98 % B for 8 min, 98 % B for 2 min then 98 – 10 % B for 0.5 min and 10 % B for a further 1 min.

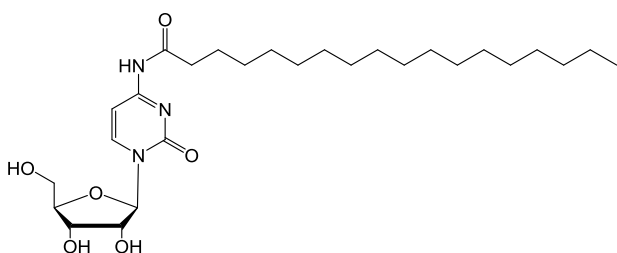
Analytical Reverse Phase High Performance Liquid Chromatography (RP-HPLC) mobile phases were prepared as follows: Eluent A – 0.05 % trifluoroacetic acid (TFA) (v/v) in water sonicated for 30 min; Eluent B – Eluent A in CH<sub>3</sub>CN (1:9) sonicated for 30 min. All RP-HPLC gradients were performed using a Waters 2767 sample manager, Waters 2525 binary gradient module and visualised at 254 nm with a Waters 2487 dual wavelength absorbance detector and spectra were analysed using MassLynx. A YMC-Pack C<sub>8</sub> column (150 mm × 4.6 mm × 5 μm) at a flow rate of 1 mL/min was used to collect the data. The retention time (t<sub>R</sub>) of the final product is reported in minutes using a gradient of 0 – 1 min 5 % solvent B in solvent A, 2 – 26 min gradient of 5 % to 90 % solvent B in solvent A, 27 – 35 min held at 90 % solvent B in solvent A, 35 - 36 min 90 % to 5 % solvent B in solvent A, 36 - 38 min held at 5 % solvent B in solvent A (solvent A = 0.05 % TFA in H<sub>2</sub>O, solvent B = 0.05 % TFA in 9:1 v:v CH<sub>3</sub>CN:H<sub>2</sub>O). Purities of all compounds tested were determined by RP-HPLC to be ≥ 95 %.

**General Procedure for the synthesis of substituted 4-amino-1-((2*R*, 3*R*, 4*S*, 5*R*)-3,4-dihydroxy-5-(hydroxymethyl)tetrahydrofuran-2-yl)pyrimidin-2(1*H*)-one**



To a solution of 2-chloro-4,6-dimethoxy-1,3,5-triazine (**40**) (CDMT, 20 mmol, 1 eqv, 3.50 g) in anhydrous  $\text{CH}_2\text{Cl}_2$  (60 mL) at 0 °C, was added *N*-methylmorpholine (NMM, 27.2 mmol, 1.36 eqv, 2.99 mL) with continuous stirring until a white suspension had formed. The mixture was then left to stir for 1 h. A medium or long chain carboxylic acid (20 mmol, 1 eqv) was added directly into the mixture as a solution in anhydrous DMF (20 mL) and stirred for a further h. A solution of cytidine (**39**) (20 mmol, 1 eqv, 4.86 g) in anhydrous DMF (20 mL) was made up at 0 °C. The cold triazine solution was added drop wise to the cooled cytidine solution over 30 mins, before heating to 50 °C and stirring for 14 - 24 h. The cooled solution was evaporated *in vacuo*. The mixture was triturated with distilled water to remove excess CDMT, NMM and cytidine, followed by trituration with  $\text{CH}_2\text{Cl}_2$  to remove any excess carboxylic acid. The product was purified using flash silica column chromatography, eluting at 5 - 7 % methanol in  $\text{CH}_2\text{Cl}_2$ .

***N*-(1-((2*R*,3*R*,4*S*,5*R*)-3,4-dihydroxy-5-(hydroxymethyl)tetrahydrofuran-2-yl)-2-oxo-1,2-dihydro-pyrimidin-4-yl)stearamide (**42a**)**



Octadecanoic acid (20 mmol, 1 eqv, 5.69 g). Reaction took 24 h as octadecanoic acid took 2 h to fully dissolve upon heating. Final compound was an off-white powder.

n.b. Purity of compound determined *via* NMR due to insolubility, unable to pass down HPLC column.

**Yield:** 39.8 %

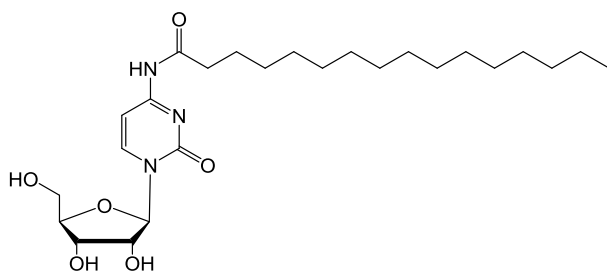
**NMR Purity:** 97.8 %

**<sup>1</sup>H NMR (DMSO-*d*<sub>6</sub>)** δ 0.85 (t, *J* = 7.2 Hz, 3H, CH<sub>3</sub>), 1.23 (br-m, 28H, CH<sub>2</sub>-(CH<sub>2</sub>)<sub>14</sub>-CH<sub>3</sub>), 1.52 (m, 2H, C=O-CH<sub>2</sub>-CH<sub>2</sub>), 2.37 (t, *J* = 6.9 Hz, 2H, C=O-CH<sub>2</sub>), 3.56 - 3.76 (m, 2H, 5'-CH<sub>2</sub>), 3.87 - 3.91 (m, 1H, 4'-CH), 3.93 - 3.99 (m, 2H, 2'-CH, 3'-CH), 5.03 (d, *J* = 5.4 Hz, 1H, 3'-OH), 5.14 (t, *J* = 4.7 Hz, 1H, 5'-OH), 5.46 (d, *J* = 4.7 Hz, 1H, 2'-OH), 5.77 (d, *J* = 2.7 Hz, 1H, 1'-CH), 7.20 (d, *J* = 7.6 Hz, 1H, 5-CH), 8.41 (d, *J* = 7.6 Hz, 1H, 6-CH), 10.82 (s, 1H, NH)

**m/z:** HRMS (TOF ES<sup>+</sup>) C<sub>27</sub>H<sub>48</sub>N<sub>3</sub>O<sub>6</sub> [M+H]<sup>+</sup> calculated 510.3538; found 510.3655.

**m.p:** 154 - 155 °C

***N*-(1-((2*R*,3*R*,4*S*,5*R*)-3,4-dihydroxy-5-(hydroxymethyl)tetrahydrofuran-2-yl)-2-oxo-1,2-dihydro-pyrimidin-4-yl)palmitamide (42b)**



Hexadecanoic acid (20 mmol, 1 eqv, 5.13 g). Product was an off-white powder.

**Yield:** 44.2 %

**HPLC purity:** 95.4 %

**HPLC t<sub>R</sub>:** 18.1 min

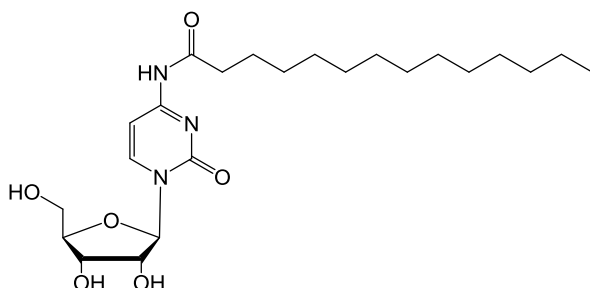
**<sup>1</sup>H NMR (DMSO-*d*<sub>6</sub>)** δ 0.85 (t, *J* = 6.7 Hz, 3H, CH<sub>3</sub>), 1.23 (br-m, 22H, CH<sub>2</sub>-(CH<sub>2</sub>)<sub>11</sub>-CH<sub>3</sub>), 1.53 (m, 2H, C=O-CH<sub>2</sub>-CH<sub>2</sub>), 2.38 (t, *J* = 7.4 Hz, 2H, C=O-CH<sub>2</sub>), 3.57 - 3.76 (m, 2H, 5'-CH<sub>2</sub>), 3.88 - 3.91 (m, 1H, 4'-CH), 3.93 - 3.99 (m, 2H, 2'-CH, 3'-CH), 5.04 (d, *J* = 5.6 Hz, 1H, 3'-OH), 5.14 (t, *J* = 5.0 Hz, 1H, 5'-OH), 5.45 (d, *J* = 5.0 Hz, 1H, 2'-OH), 5.77 (d, *J* = 2.9 Hz, 1H, 1'-CH), 7.20 (d, *J* = 7.5 Hz, 1H, 5-CH), 8.41 (d, *J* = 7.5 Hz, 1H, 6-CH), 10.83 (s, 1H, NH).

**<sup>13</sup>C NMR (DMSO-*d*<sub>6</sub>)** δ 14.89, 23.05, 25.38, 29.38, 29.62, 29.79, 29.99, 32.27, 37.29, 60.88, 69.62, 75.50, 85.14, 91.08, 96.16, 146.18, 155.61, 163.24, 174.84

**m/z:** HRMS (TOF ES<sup>+</sup>) C<sub>25</sub>H<sub>44</sub>N<sub>3</sub>O<sub>6</sub><sup>+</sup> [M+H]<sup>+</sup> calculated 482.3225; found 482.3046

m.p: 150 - 151 °C

***N*-(1-((2*R*,3*R*,4*S*,5*R*)-3,4-dihydroxy-5-(hydroxymethyl)tetrahydrofuran-2-yl)-2-oxo-1,2-dihydro-pyrimidin-4-yl)tetradecanamide (42c)**



Tetradecanoic acid (20 mmol, 1 eqv, 4.57 g). The product was a white powder.

**Yield:** 46.0 %

**HPLC Purity:** 97.6 %

**HPLC  $t_R$**  = 16.3 min

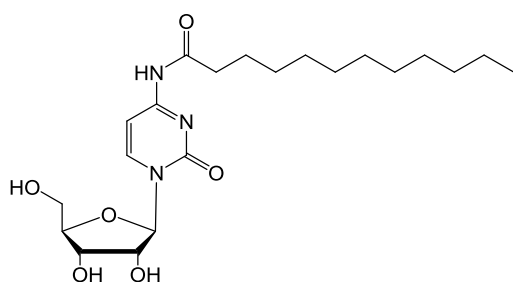
**$^1\text{H NMR}$  (DMSO- $d_6$ )**  $\delta$  0.85 (t,  $J$  = 6.6 Hz, 3H,  $\text{CH}_3$ ), 1.24 (br-m, 20H,  $\text{CH}_2$ - $(\text{CH}_2)_{10}$ - $\text{CH}_3$ ), 1.53 (m, 2H,  $\text{C}=\text{O}$ - $\text{CH}_2$ - $\text{CH}_2$ ), 2.38 (t,  $J$  = 7.3 Hz, 2H,  $\text{C}=\text{O}$ - $\text{CH}_2$ ), 3.56 - 3.76 (m, 2H, 5'- $\text{CH}_2$ ), 3.88 - 3.91 (m, 1H, 4'- $\text{CH}$ ), 3.93 - 3.99 (m, 2H, 2'- $\text{CH}$ , 3'- $\text{CH}$ ), 5.03 (d,  $J$  = 5.6 Hz, 1H, 3'- $\text{OH}$ ), 5.14 (t,  $J$  = 5.1 Hz, 1H, 5'- $\text{OH}$ ), 5.46 (d,  $J$  = 4.9 Hz, 1H, 2'- $\text{OH}$ ), 5.77 (d,  $J$  = 2.9 Hz, 1H, 1'- $\text{CH}$ ), 7.20 (d,  $J$  = 7.5 Hz, 1H, 5- $\text{CH}$ ), 8.40 (d,  $J$  = 7.4 Hz, 1H, 6- $\text{CH}$ ), 10.83 (s, 1H,  $\text{NH}$ )

**$^{13}\text{C NMR}$  (DMSO- $d_6$ )**  $\delta$  13.92, 22.10, 24.45, 28.46, 28.72, 28.88, 29.02, 29.06, 30.67, 36.36, 59.91, 68.66, 74.55, 84.20, 90.18, 95.21, 145.32, 154.69, 162.33, 173.91

**m/z:** HRMS (TOF ES<sup>+</sup>)  $\text{C}_{23}\text{H}_{40}\text{N}_3\text{O}_6$   $[\text{M}+\text{H}]^+$  calculated 454.2192; found 454.2376.

m.p: 154 - 155 °C

***N*-(1-((2*R*,3*R*,4*S*,5*R*)-3,4-dihydroxy-5-(hydroxymethyl)tetrahydrofuran-2-yl)-2-oxo-1,2-dihydro-pyrimidin-4-yl)dodecanamide (42d)**



Dodecanoic acid (20 mmol, 1 eqv, 4.01 g). The product was a white powder

**Yield:** 48.4 %

**HPLC purity:** 98.0 %

**HPLC  $t_R$ :** 14.7 min

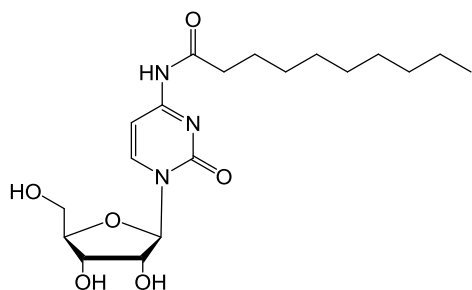
**$^1\text{H}$  NMR (DMSO- $d_6$ )**  $\delta$  0.85 (t,  $J$  = 6.6 Hz, 3H,  $\text{CH}_3$ ), 1.24 (br-m, 16H,  $\text{CH}_2$ - $(\text{CH}_2)_8$ - $\text{CH}_3$ ), 1.53 (m, 2H,  $\text{C}=\text{O}$ - $\text{CH}_2$ - $\text{CH}_2$ ), 2.38 (t,  $J$  = 7.4 Hz, 2H,  $\text{C}=\text{O}$ - $\text{CH}_2$ ), 3.56 - 3.76 (m, 2H, 5'- $\text{CH}_2$ ), 3.89 - 3.91 (m, 1H, 4'- $\text{CH}$ ), 3.93 - 3.99 (m, 2H, 2'- $\text{CH}$ , 3'- $\text{CH}$ ), 5.03 (d,  $J$  = 5.7 Hz, 1H, 3'- $\text{OH}$ ), 5.14 (t,  $J$  = 5.1 Hz, 1H, 5'- $\text{OH}$ ), 5.46 (d,  $J$  = 4.9 Hz, 1H, 2'- $\text{OH}$ ), 5.77 (d,  $J$  = 2.8 Hz, 1H, 1'- $\text{CH}$ ), 7.20 (d,  $J$  = 7.5 Hz, 1H, 5- $\text{CH}$ ), 8.41 (d,  $J$  = 7.5 Hz, 1H, 6- $\text{CH}$ ), 10.83 (s, 1H,  $\text{NH}$ ).

**$^{13}\text{C}$  NMR (DMSO- $d_6$ )**  $\delta$  13.98, 22.13, 24.47, 28.49, 28.76, 28.88, 29.03, 30.68, 31.31, 36.41, 59.95, 68.62, 74.56, 84.22, 90.21, 95.22, 145.33, 154.69, 162.34, 173.92,

**$m/z$ :** HRMS (TOF ES<sup>+</sup>)  $\text{C}_{21}\text{H}_{36}\text{N}_3\text{O}_6$   $[\text{M}+\text{H}]^+$  calculated 426.2599; found 426.1529

**$m.p.$ :** 151 - 152 °C

***N*-(1-((2*R*,3*R*,4*S*,5*R*)-3,4-dihydroxy-5-(hydroxymethyl)tetrahydrofuran-2-yl)-2-oxo-1,2-dihydro-pyrimidin-4-yl)decanamide (42e)**



Reaction carried out on a 0.76 mmol scale.

Decanoic acid (0.76 mmol, 1 mmol, 131 mg).

The product was a white powder.

**Yield:** 24.0 %

**HPLC purity:** 96.6 %

**HPLC  $t_R$ :** 18.6 min

**$^1\text{H}$  NMR (DMSO- $d_6$ )**  $\delta$  0.85 (t,  $J$  = 6.8 Hz, 3H,  $\text{CH}_3$ ), 1.24 (br-m, 12H,  $\text{CH}_2$ - $(\text{CH}_2)_6$ - $\text{CH}_3$ ), 1.53 (m, 2H,  $\text{C}=\text{O}$ - $\text{CH}_2$ - $\text{CH}_2$ ), 2.38 (t,  $J$  = 7.2 Hz, 2H,  $\text{C}=\text{O}$ - $\text{CH}_2$ ), 3.56 - 3.76 (m, 2H, 5'- $\text{CH}_2$ ), 3.88 - 3.91 (m, 1H, 4'- $\text{CH}$ ), 3.93 - 3.99 (m, 2H, 2'- $\text{CH}$ , 3'- $\text{CH}$ ), 5.03 (d,  $J$  = 5.5 Hz, 1H, 3'- $\text{OH}$ ), 5.14 (t,  $J$  = 5.1 Hz, 1H, 5'- $\text{OH}$ ), 5.46 (d,  $J$  = 4.8 Hz, 1H, 2'- $\text{OH}$ ), 5.77 (d,  $J$  = 2.8 Hz, 1H, 1'- $\text{CH}$ ), 7.20 (d,  $J$  = 7.5 Hz, 1H, 5- $\text{CH}$ ), 8.41 (d,  $J$  = 7.5 Hz, 1H, 6- $\text{CH}$ ), 10.82 (s, 1H,  $\text{NH}$ ).

**$^{13}\text{C}$  NMR (DMSO- $d_6$ )**  $\delta$  22.56, 24.91, 28.91, 29.11, 29.18, 29.29, 31.73, 36.82, 40.24, 69.15, 74.99, 84.67, 90.6, 95.69, 145.82,

**m/z:** HRMS (TOF ES<sup>+</sup>) C<sub>19</sub>H<sub>32</sub>N<sub>3</sub>O<sub>6</sub> [M+H]<sup>+</sup> calculated 398.2280; found 398.6219

## 2.6.2. Physicochemical Characterisation

### 2.6.2.1. Stability to Inversion

**42a - 42e** (2.5 mg) were weighed using an A and D GR-202 semi micro-analytical balance into 1.5 mL sample vials so that a final compound concentration would be 0.5 % (w/v) and the final sample volume was 500  $\mu$ L. The compound was solubilised in either DMSO or ethanol as per **Table 6** and sonicated for 1-2 minutes. Solutions were heated to 60 °C, using a made to measure aluminium heating vessel to solubilise the compound before adding pre-heated (60 °C) ultra-purified water. The samples were left to cool to room temperature for 18 h, prior to inversion.

**Table 6:** Amount of solvent and ultra-purified water required to make solvent volume fractions ( $\Phi_{\text{sol}}$ ) 0.00 – 0.50 to a final sample volume of 500  $\mu$ L.

Final Solvent Volume Fraction ( $\Phi_{\text{sol}}$ )	Final Solvent Volume ( $\mu$ L)	Final Water Volume ( $\mu$ L)
0.00	0	500
0.05	25	475
0.10	50	450
0.20	100	400
0.30	150	350
0.40	200	300
0.50	250	250

### 2.6.2.2. Rheological Experiments

Rheology was carried out using an Anton Paar MCR302 Modular Compact Rheometer. A four-bladed vane geometry was used with a diameter of 8.5 mm and length 8.5 mm in a cup with a diameter of 14.5 mm. The solution of gelator was prepared in a 7 mL Sterilin™ plastic sample vial to a final sample volume of 2 mL. Once the gel was prepared, the sample vial was mounted in the lower plate (cup) of the rheometer; the vane (attached to the upper part) was lowered into place, at a depth of 3 mm. This arrangement gave a total sample depth of approximately 16 mm in the 14.5 mm diameter cup which allowed positioning of the vane in the centre of the sample.

All strain amplitude measurements were carried out between 0.05 – 100 %. The  $G'$  and  $G''$  (storage modulus and loss modulus, respectively) were measured at a constant angular frequency of 10 rad/s. The temperature was set to 37 °C to mimic physiological conditions.

Frequency sweeps were performed at an angular frequency of 0.1 to 100 rad s<sup>-1</sup> under a strain of 0.5 %, derived from the linear viscoelastic region found during the strain sweep. The temperature was set at 37 °C to mimic physiological conditions.

Temperature of gelation ( $T_{gel}$ ) measurements were carried out under constant strain (0.5 %) and constant frequency (10 rad/s), found from strain and frequency sweeps. Gels were prepared in 7 mL aluminium vials as per the method above and the vane positioned at a 2 mm depth, to account for the reduction in vial thickness. Temperature measurements were carried out between 20 °C and 100 °C at a heating rate of 0.5 °C/min.

#### **2.6.2.3. Scanning Electron Microscopy (SEM)**

SEM was performed on a JEOL JSM-6060LV compact scanning electron microscope. All samples were loaded onto suitable stub holders with a 200 µL micropipette fitted with sterile tips. The point of the tip was cut to increase the diameter and thus minimise the shear stress applied to the gels. The stubs were sputter coated with gold (Balzers Benchtop sputter coater SCD 030) under an argon atmosphere (50 Pa) at 30 mA for 4 minutes before imaging. Images were acquired using an electron beam of 7 - 22 kV.

#### **2.6.2.4. Transmission Electron Microscopy (TEM)**

TEM was carried out by dispersing a small amount of gel in 150 µL of ultra-purified water and pipetting on to a carbon-coated copper grid (No. 400). Excess sample was blotted with Whatman 50 filter paper. The grid was subjected to high vacuum in a Gatan dry pumping station (model 655) prior to inserting into the machine and imaging at an accelerated voltage of 100 kV.

#### **2.6.3. *In Vitro* Release Kinetics of Fluorescein, FITC Dextran 4 and FITC Dextran 10**

Gels (**42d**,  $\Phi_{EtOH}$  0.40) containing fluorescent dyes were prepared in 7 mL Sterilin™ cups to a final gel volume of 2 mL with the dye phase replacing the aqueous phase in

each instance. Stock solutions of each dye were prepared so that the fluorescent output would be within the linear region of the calibration curves (0.15 mM Fluorescein and 0.06 mM Fluorescein isothiocyanate (FITC) Dextran 4 kDa and 0.08 mM FITC Dextran 10 kDa). Having prepared the gels as per method **2.6.2.1** the gel volume was allowed to stand for 18 h to allow time for complete gelation. Ultra-purified water (5 mL) was gently placed on top of each gel and the initial time point taken (150  $\mu$ L,  $T_0$ ), subsequent readings (150  $\mu$ L) were taken at further time points and the fluorescence measured (excitation of 485 nm with the emission measured at 521 nm) using a Perkin Elmer plate reader.

#### **2.6.4. *In Vitro* Growth Inhibition Assays**

HCT-116 colorectal carcinoma and MCF-7 breast adenocarcinoma cell lines were cultured in RPMI-1640 medium supplemented with 10 % Foetal Bovine Serum (FBS). Cells were passaged upon reaching 60- 80 % confluency and not used past passage number 50. MTT was made in sterile PBS at a concentration of 2 mg/mL.

For MTT assays, cells were seeded at a density of  $3 \times 10^3$  cells per well into 96-well microtiter plates and allowed to adhere for 24 h before test agent was introduced (0.1 nM – 100  $\mu$ M,  $n = 8$ ). Stock solutions of each compound were prepared in DMSO (10 mM) to aid solubilisation and further dilutions were prepared in RPMI medium prior to each assay. Viable cells at the time of drug addition, (time zero ( $T_0$ )) and following 72 h incubation period with test agents, were determined by cell-mediated MTT reduction (final concentration 400  $\mu$ g/mL) to generate a  $T_0$  sample reading. Cells were incubated with test agent for 72 h at 37 °C and 5 % CO<sub>2</sub> to allow the reduction of MTT to an insoluble formazan, which was solubilised by DMSO(150  $\mu$ L). Cell growth and agent activity were determined by measuring absorbance at 550 nm using an Anthos Labtec systems plate reader. Non-linear regression analysis was used to calculate compound concentrations required to inhibit 50 % of cell growth ( $GI_{50}$ ).

### 3. A Tale of Refinement

---

The foundation for a good gelator was described in **Chapter 2**, however there were still modifications that could be made to the overall structure in order to enhance the aqueous solubility and to improve the self-assembly process. Previously considered, was the option of modelling the compound to determine which moieties were crucial to the gelation process and which were available for modification. However, other than a non-specific coarse grain model, the modelling process was considered too complicated given the complexity of the multicomponent system. The most appropriate way to determine the changeable parameters was to review each one experimentally.

Before considering structural modifications it was important to first understand the nucleoside itself and in particular the potential intra-molecular interactions that exist inherently within the molecule. Unlike some nucleosides, cytidine is known to only adopt the anti-conformation. (**Figure 23**) The carbonyl oxygen at the C-2 position (red) produces a significant amount of steric hindrance and prevents significant rotation around the  $\beta$ -glycosidic bond (green) as it invades the space occupied by the hydroxyl at 2'-C, potentially causing intra-molecular hydrogen bonding.

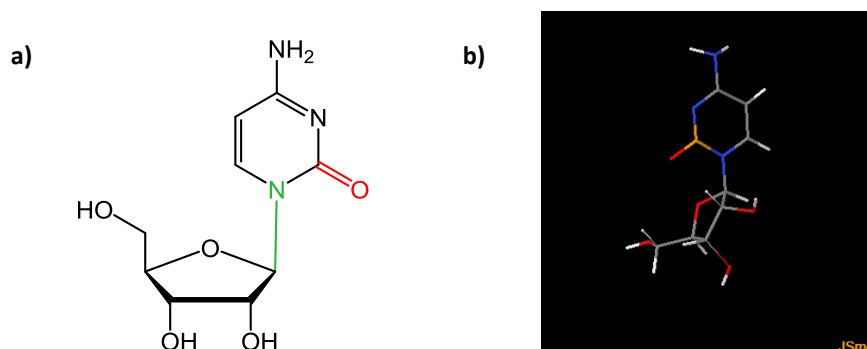
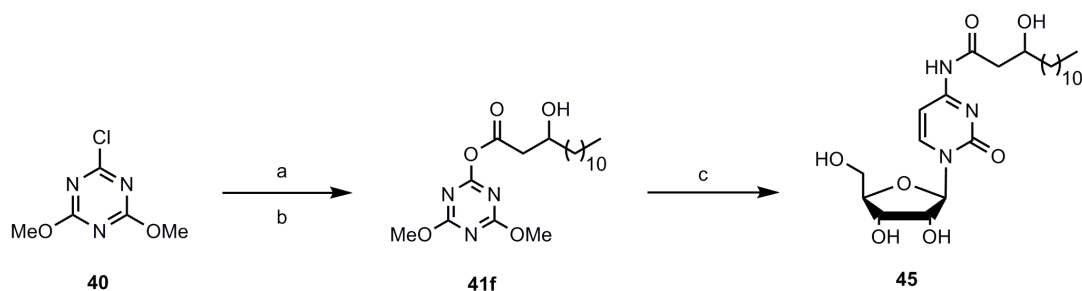


Figure 23: a) anti-conformation of cytidine (39) showing C-2 carbonyl (red) and  $\beta$ -glycosidic bond (green) b) a representation of molecular syn-conformation of cytidine.

### 3.1. Is the Amide Integral to the Successful Self-Assembly Process?

Initial studies were carried out to determine whether the amide functionality introduced during the acylation of the exocyclic amine was an integral part of the self-assembly process. This work was complementary to FT-IR studies (**Figure 20**) carried out previously that demonstrated the broadening and attenuation of peaks in the amide-I region following gelation. Synthesis of **45** was achieved in a similar manner to the initial reported reaction, the main alteration being the presence of an additional hydroxyl at the 3-position of the tetradecanoic acid introduced during step b. (**Scheme 2**)



**Scheme 2: Synthesis of a cytidine-*N*-3-OH-tetradecanoyl (**45**)**

Reagents and Conditions: (a) *N*-methylmorpholine, CH<sub>2</sub>Cl<sub>2</sub>, 0 °C, 1h (b) 3-OH-tetradecanoic acid, CH<sub>2</sub>Cl<sub>2</sub>/DMF, 0 °C, 1h (c) cytidine, DMF, 0 °C - 50 °C, 20 h.

The synthesis proceeded *via* an activated triazine ester and achieved regioselective acylation of the 4-amino group of the nucleobase as described previously (**Chapter 2**) with the final compound being produced in a good yield of 60 %. Stable to inversion studies of **45** were carried out by solubilising 2.5 mg of **45** in varying solvent volume fractions ( $\Phi_{\text{EtOH}}$  0.05 – 0.50) of ethanol at 60 °C, to generate gels of 0.5 % (*w/v*). Upon complete solubilisation of **45** in the solvent, pre-heated (60 °C) ultra-purified water was added to make a final gel volume of 500  $\mu\text{L}$  and the vials left to cool to room temperature for approximately 18 h prior to inverting.

Unlike gels prepared previously from **42c** the gelation of **45** did not occur instantaneously following addition of the pre-heated water. **Figure 24a** shows an observable change in gel stability between those gels prepared from **42c**; cytidine-*N*-tetradecanoyl (top) and those derived from **45**; cytidine-*N*-3-OH-tetradecanoyl (bottom). **45** shows enhanced solubility due to the addition of the hydrophilic 3-hydroxyl; this change is more apparent at the increased solvent volume fractions, particularly  $\Phi_{\text{EtOH}}$  0.40 and 0.50 where the compound appears completely soluble. At a lower  $\Phi_{\text{EtOH}}$  there is visual evidence of a precipitate, though with less apparent aggregation than in **42c**. The lack of gelation from **45** in the samples that contain a lower  $\Phi_{\text{EtOH}}$  can be attributed to intramolecular hydrogen bonding (**Figure 24b**) between the amide carbonyl and the 3-hydroxyl. The presence of the hydroxyl obstructs the intramolecular hydrogen bonding and prevents self-assembly, but it also validates the amide as a key functionality in the self-assembly process. As noted above, subtle changes to a molecular structure of a gelator can unpredictably disrupt gel formation; recent examples exist for a family of benzene 1,3,5-

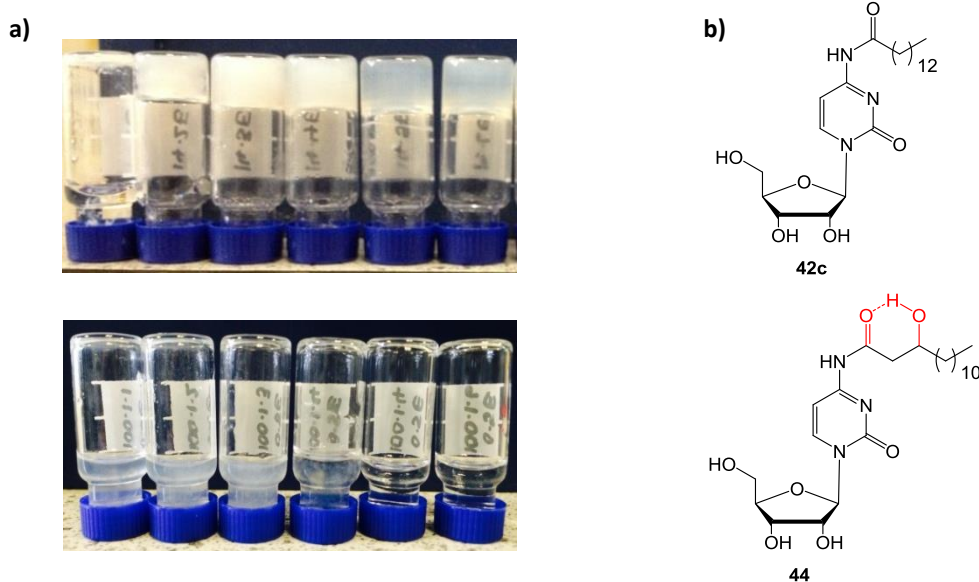


**Figure 24:** Vial inversion and interpretation of intra-molecular hydrogen bonding in **42c**.

a) Vial inversion of compound **42c** (top) and **45** (bottom) in ethanol. Image shows  $\Phi_{\text{EtOH}}$  0.05, 0.1, 0.2, 0.3, 0.4 and 0.5 (left to right). Representative image of  $n=4$ . b) Structure of **42c** (top) and **45** (bottom); cytidine-*N*-3-OH-tetradecanoyl showing intra-molecular hydrogen bonding (red) between amide carbonyl and 3-hydroxyl.

tricarboxamide hydrogels that demonstrated different gel properties depending upon aromatic terminal group utilised.<sup>182</sup> Additional pertinent examples includes work by Awhida *et al.*<sup>183</sup> on the substitution of Fmoc-dipeptides, it was concluded that gelation was more likely to occur when at least one aromatic peptide was present due to enhanced  $\pi$ -stacking stabilisation.

### 3.2. Can Gelation be enhanced by Removing Additional Nucleophilic Groups?

Logical progression indicates that ribose hydroxyls, being free hydrogen bonding functionalities should subsequently be validated for their involvement in the self-assembly process. By creating similar gelators from 2'-deoxycytidine (**46**) and 2',3'-

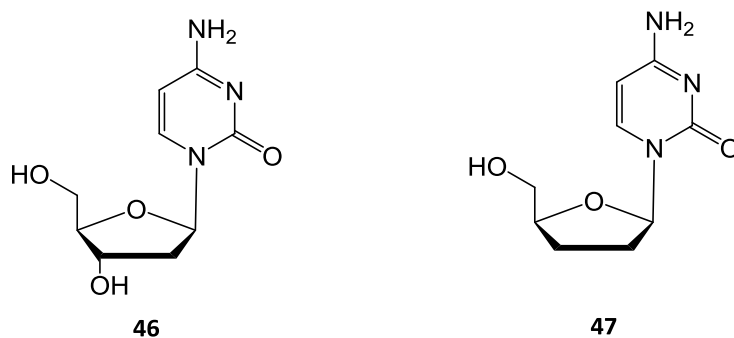
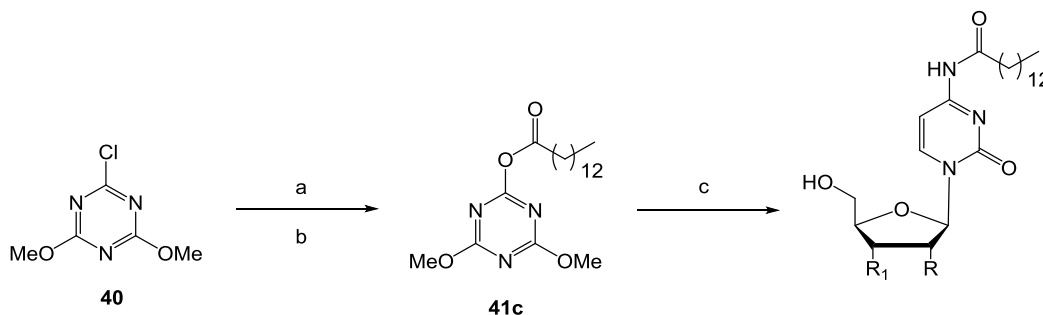


Figure 25: Structure of 2'-deoxycytidine (**46**) and 2',3'-dideoxycytidine (**47**)

dideoxycytidine (**47**, **Figure 25**) it is possible to mimic the effect the sequential removal of the 2'- and 3'-hydroxyl moieties would pose to gelation by synthesising 2'-deoxycytidine-*N*-tetradecanoyl (**48a**) and 2',3'-dideoxycytidine-*N*-tetradecanoyl (**49a**). However, it is important to consider that as well as potentially interfering with the self-assembly process; removing each of the hydroxyls will result in an increase in cLogP, which would be reflected in the decreased aqueous solubility of each compound.

**48a** and **49a** were synthesised as in **Scheme 3** *via* an activated triazine ester, using 2'-deoxycytidine (**46**) to generate **48a** and 2',3'-dideoxycytidine (**47**) to produce **49a**.



**Scheme 3: Synthesis of 2'-deoxycytidine-*N*-tetradecanoyl (48a) and 2',3'-dideoxycytidine-*N*-tetradecanoyl (49a) via an activated triazine ester**

Reagents and Conditions: (a) *N*-methylmorpholine, CH<sub>2</sub>Cl<sub>2</sub>, 0 °C, 1h (b) tetradecanoic acid, CH<sub>2</sub>Cl<sub>2</sub>/DMF, 0 °C, 1h (c) **46** or **47**, DMF, 0 °C - 50 °C, 16 - 24 h.

Each of the compounds was achieved in good yields of 40.0 % and 56.9 %, respectively.

Gelation was promoted by dissolving 2.5 mg of compound (**48a** and **49a**) in varying amounts of solvent (DMSO or EtOH), depending upon the final solvent volume fraction required ( $\Phi_{\text{SOL}}$  0.05 – 0.50) at an elevated temperature of 60 °C. Upon complete solubilisation pre-heated (60 °C) ultra-purified water was added (final gel volume 500  $\mu\text{L}$ ) thus facilitating gelation. The vials were left to cool down to ambient temperature over 18 h before inverting.

**Table 7: cLogP and predicted water solubility values for 48a and 49a**

	R	R <sub>1</sub>	cLogP	Predicted LogS <sub>w</sub>
<b>42c</b>	OH	OH	4.31	- 5.09
<b>48a</b>	H	OH	4.61	- 5.19
<b>49a</b>	H	H	5.26	- 5.27

**Table 8** shows the results from the gelation of **42c**, **48a** and **49a**. Immediately apparent is the difference in visual structural integrity between the gels made in DMSO and those made with ethanol.

For compound **48a**  $\Phi_{\text{DMSO}}$  0.05 and 0.10 there is significant precipitation, comparable to the same samples derived from **42c**. In contrast, the same solvent

volume fractions in **49a** display some stability to inversion, a surprising result, given the increased cLogP and therefore decreased aqueous solubility. Another unusual result from the DMSO series of **49a** is the syneresis at  $\Phi_{\text{DMSO}}$  0.20 and 0.30 which was evident in a number of repeats. Gels are typically metastable materials, kinetically trapped within a certain conformation; however there are a few reports of gels that are generally unstable with respect to aggregation, which can lead to a destabilisation of a gel upon standing,<sup>184,185</sup> as noted in these samples.

The ethanol series displayed increased stability to gelation when **48a** was the gelating entity used, showing a propensity for gelation even at  $\Phi_{\text{EtOH}}$  0.05. All gelators in the **48a** series display turbidity up to  $\Phi_{\text{EtOH}}$  0.50 upon which point the balance between solubility and lipophilicity peaks and the gel appears transparent. Ethanol samples of **49a** show a reduced propensity for gelation in comparison to those made with **48a**, this is in contrast to the observations noted for the DMSO series. At  $\Phi_{\text{EtOH}}$  0.05 in **49a** a precipitate is seen, whereas at  $\Phi_{\text{EtOH}}$  0.10 we see the only homogenous gelator of the series. The remaining samples in the series, particularly in  $\Phi_{\text{EtOH}}$  0.50 we see a phase separation between the aqueous and solvent phases which actually leads to unstable gel when inverted for longer than 1 minute.

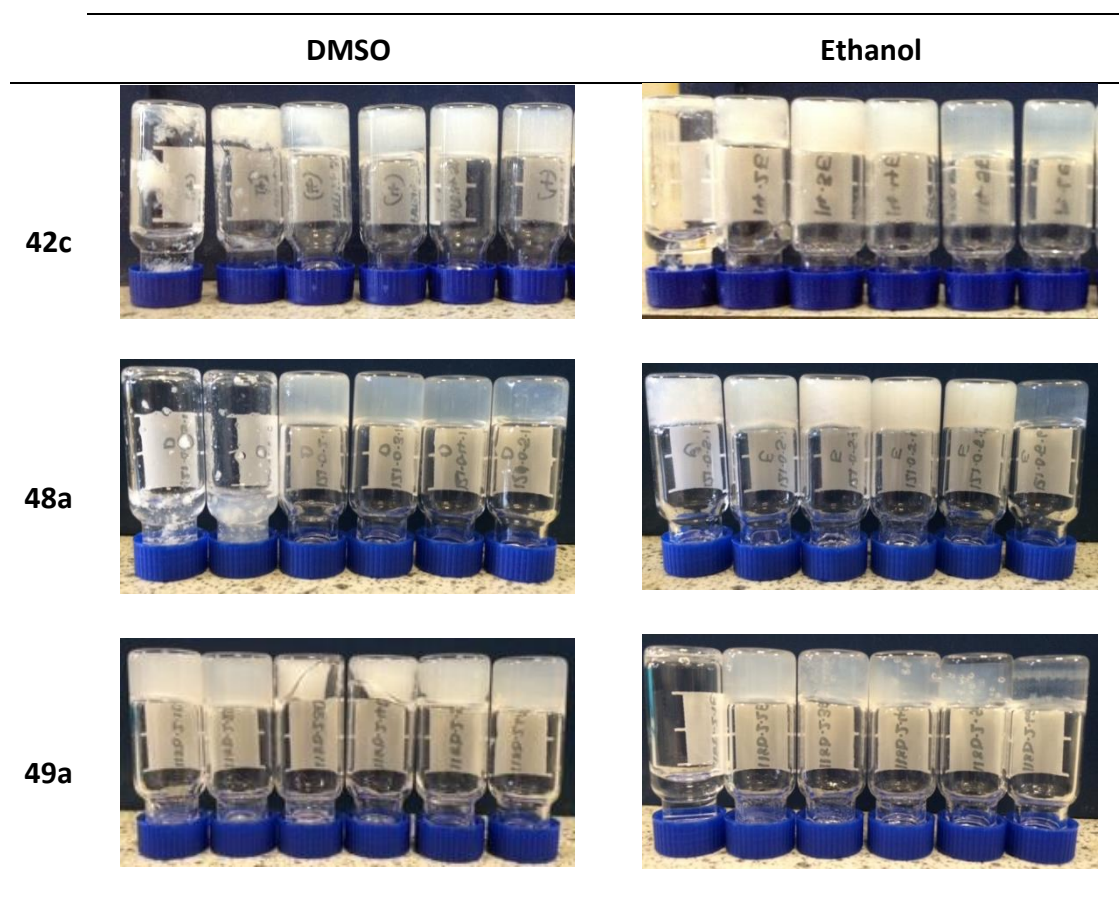
The overall results from gelation are suggestive of the 2' and 3'-hydroxyls playing a significant role in gelation as the profile of each gelator differs depending on the number of hydroxyls present when all other conditions remain constant. As mentioned previously, cytidine adopts the *anti*-conformation around the glycosidic bond, it is entirely possible, that removal of the 2'-OH decreases the steric bulk around the 2'-C position and thus interferes with the intra-molecular hydrogen bonding between the 2-C carbonyl and the 2'-C hydrogen, thus allowing a greater degree of rotation around the glycosidic bond and arrangement of the gelator molecule into a more favourable kinetically trapped conformation.

When neither 2' nor 3' hydroxyls are present (**49a**) there is a reduction in gelation at the lower solvent volume fractions, correlating with the increased CLogP and lower aqueous solubility of the gelator. However the samples seen appear to be

more transparent than the **42c** and **48a** counterparts. This observation can be explained by the puckering of the ribose sugar.<sup>186</sup> A reduction in steric bulk around the 2'-C and 3'-C allows for a conformational change to a more stable C3'-exo, C4'-endo conformation, this change means that the 5'-OH switches from an equatorial to an axial position without affecting the position of the base and thus allows the gelator molecules to assemble into 'flatter' structures represented by the transparent gels.

**Table 8: Vial inversion of 42c, 48a and 49a.**

0.5 % (w/v) in DMSO (left) and ethanol (right). Images shown  $\Phi_{\text{sol}}$  0.05, 0.1, 0.2, 0.3, 0.4 and 0.5 (left to right) are representative images of n=3.



From this study we were able to rationalise retaining the 2'-deoxycytidine and 2',3'-dideoxycytidine series and developing them further, in order to find a true hydrogelator. Driving gelation towards the lower end of the solvent volume fraction

by increasing compound solubility was probed. As with **42a** - **42e**, the gels mentioned above were progressed only using ethanol as an anti-solvent, due to the general observed instability in the DMSO samples.

### 3.2.1. Gel Development

#### 3.2.1.1. Lowering Compound Concentration to Improve Gelation

One way to potentially force the kinetics of the gelation towards a more homogenous gel without any precipitate was to decrease the overall compound concentration. Gels of **48a** and **49a** were made as 0.1 and 0.25 % (w/v) gels in ethanol; the results of which are shown in **Table 9**.

Initial observations suggest an increased homogeneity and reduced precipitation in samples upon decreasing the compound concentration from 0.5 – 0.1 % (w/v), also apparent is the decreased stability in lower solvent volume fractions.

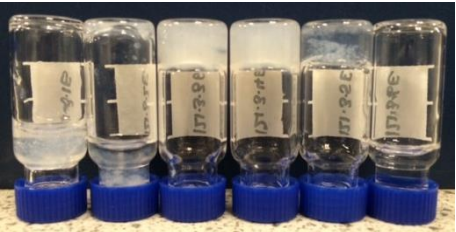
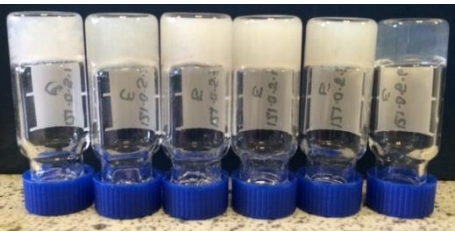
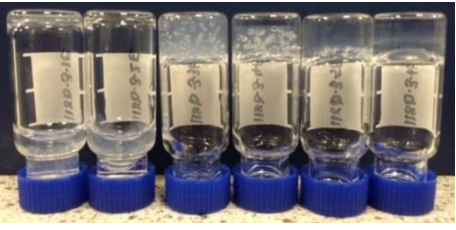
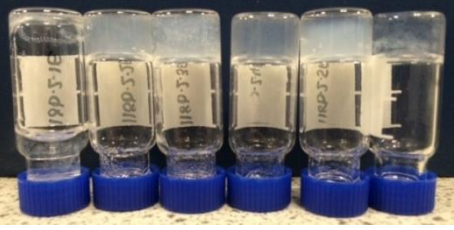
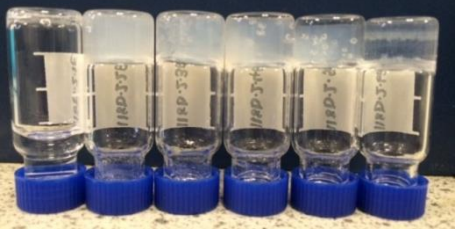
On decreasing the concentration from 0.5 % to 0.25 % there is initially an observed increase in transparency of the gels in each series. In **49a** there is little observed change in overall gel stability across the series, however the presence of heterogeneous systems at  $\Phi_{\text{EtOH}}$  0.40 and 0.50 are still indicative of kinetically unstable gels as this indicates a metastable state. Gels of **48a** display a general decrease in gel stability with the samples at both ends of the solvent spectrum (i.e.  $\Phi_{\text{EtOH}}$  0.05, 0.10 and 0.50). This observation is entirely expected and can be justified by the solvent driven nature of the gel formation. At lower solvent concentrations the high lipophilic content of compound **48a** hinders solubilisation and thus, gelation, whereas the converse is true at the higher solvent concentration. The increased solvent volume fraction is able to fully solubilise the compound at lower compound concentrations, which too hinders the gelation process.

In both series the most stable gelators, over a sustained time period, were observed when the final compound concentration was 0.5 % (w/v), indicating that decreasing the final compound concentration is not a viable way to force gelation towards the lower solvent fractions for these series.

An alternative way to influence gelation was to adjust the cLogP of the compound; decreasing the lipophilic content of the overall gelator would still result in an amphiphilic compound needed to promote gelation but would increase solubility in aqueous media.

Table 9: Vial inversion of compounds 42c, 48a and 49a in ethanol (top to bottom) with 0.1, 0.25 and 0.5 % (w/v) compound (left to right).

Each image shows  $\Phi_{\text{EtOH}}$  0.05, 0.1, 0.2, 0.3, 0.4 and 0.5 (left to right). Representative image of n = 3

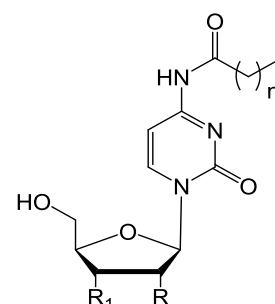
	0.1 % (w/v)	0.25 % (w/v)	0.5 % (w/v)
42c	-	-	
48a			
49a			

### 3.2.1.2. Decreasing Lipophilicity to Improve Gelation

The most efficient way to decrease lipophilicity was to decrease the length of the acyl chain introduced *via* the exocyclic primary amine and monitor the effect this had upon gelation in ethanol. This meant that the synthetic route used previously could remain the same, achieving the compounds *via* the activated triazine ester, (**Scheme 3**) with the only modification to the reaction being a change in the carboxylic acid introduced in step b. An additional advantage to this is that the samples could be made in parallel. **Table 10** details the compounds synthesised using this method and their associated cLogP values.

**Table 10:** Structure and associated cLogP of compounds in series 48 and 49. Representative structure is shown on the right.

Compound	R	R <sub>1</sub>	n	cLogP	Predicted LogS <sub>w</sub>	Yield (%)
<b>42c</b>	OH	OH	12	4.31	-5.09	46.0
<b>48a</b>	H	OH	12	4.61	-5.19	40.0
<b>48b</b>	H	OH	10	3.55	-4.61	59.0
<b>48c</b>	H	OH	8	2.49	-4.02	54.2
<b>48d</b>	H	OH	6	1.44	-3.41	70.8
<b>48e</b>	H	OH	4	0.38	-2.79	39.8
<b>49a</b>	H	H	12	5.26	-5.27	56.9
<b>49b</b>	H	H	10	4.20	-4.68	70.7
<b>49c</b>	H	H	8	3.14	-4.08	68.3
<b>49d</b>	H	H	6	2.09	-3.46	58.9



Decreasing the lipophilicity by one ethylene unit would result in a decrease in cLogP of approximately 1.05. Each compound was achieved in a reasonable yield of 39 – 71 % for **48a - 48e** and 56 – 71 % for **49a – 49d**. The results of the stability to inversion studies are shown in **Table 11**. Each gel was promoted by solubilising compound (2.5 mg) in pre-heated ethanol (60 °C), in varying quantities before

adding pre-heated water to create a gel with total volume of 500  $\mu\text{L}$  and a final compound concentration of 0.5 % (w/v). The samples were left to cool gradually down to ambient temperature and left to stand for 18 h before inverting.

In the 2'-deoxycytidine series (**48a** - **48e**) enhanced gelation is seen as the lipophilic content of the compound is decreased, correlating with the previously mentioned solubility driven nature of the self-assembly process. This is evident through an increased transparency of the samples. The largest visible difference between compounds in this series occurs between **48b** and **48c**, where a complete reduction in the number of turbid samples present from three to zero, occurs as the cLogP drops below 3. This is an interesting observation as it tallies with a similar observation which suggests a gelator has a greater chance of assembling when the cLogP of the molecule lies between 1 and 3 for an individual system. This observation is supported by the visible structural difference between those samples prepared from **48d** and those from **48e**. In **48d** a good structural integrity is observed, even at  $\Phi_{\text{EtOH}}$  0.05, whereas in **48e**; where the cLogP falls below 1 (cLogP 0.68) there is no evidence of gelation or precipitation.

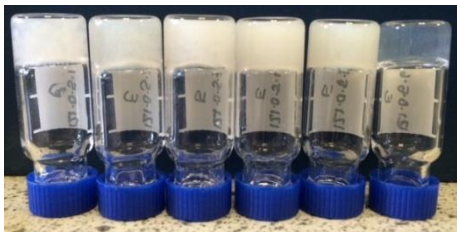
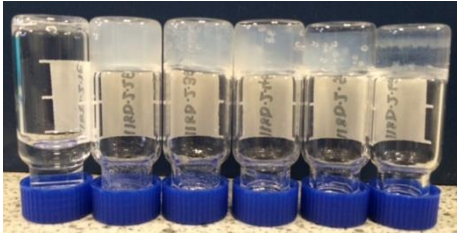
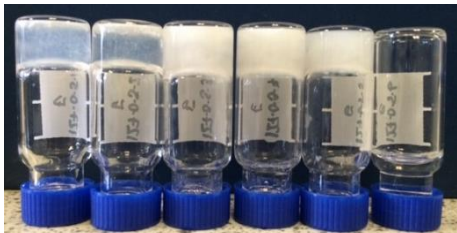
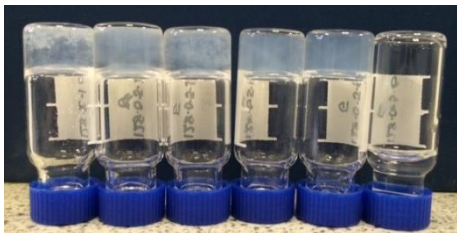
In the 2',3'-dideoxycytidine series (**49a** - **49d**) there isn't a noticeable difference in structural integrity between **49a** and **49b**. There is an increased transparency seen at the higher solvent volume fractions due to a decreased lipophilicity (and increased organic solubility) but no change at the lower end of the solvent scale. Upon decreasing the lipophilic content further, towards a cLogP of 2 - 3 a decrease in gelation is observed; the gels become increasingly turbid and although (particularly in the case of **49d**) they appear stable at the lower solvent fractions are actually assembled from aggregates of precipitate.

This observation contradicts everything previously mentioned regarding cLogP and aqueous solubility. However, this observation can be explained by considering the inter-molecular interactions. Previously mentioned in **Section 3.2** was the absence of intra-molecular interactions between molecules of **47**. This suggests that in this case the 4-amide and acyl chain essentially dominates the self-assembly process. As

we decrease the lipophilicity some of the solvophobic forces generated by the acyl chain are lost, leading to a destabilised system.

**Table 11: Stability to inversion of 48a - 48e (left) and 49a - 49d (right) in ethanol.**

n is the number of carbons in the acyl chain. A final compound concentration of 0.5 % (w/v). Each image shows  $\Phi_{\text{EtOH}}$  0.05, 0.1, 0.2, 0.3, 0.4 and 0.5 (left to right). Representative image of n=3

n	2'-deoxycytidine series	2', 3'-dideoxycytidine series
12 48a		
10 48b		
8 48c		
6 48d		
4 48e		-

For the purpose of this work, this series was disregarded at this point and not explored further.

As **48d** was found to have the most stable gelator with the greatest hydrophilicity, predicted water solubility and formed gels with the lowest solvent volume fraction, this was the gelator selected for further investigation.

**48d** formed stable gelators at the lowest measured solvent volume fraction ( $\Phi_{\text{EtOH}}$  0.05) in the initial solvent screen, for that reason lower solvent volume fractions were explored ( $\Phi_{\text{EtOH}}$  0.02, 0.01 and 0.00). **Figure 26a** shows gelation from  $\Phi_{\text{EtOH}}$  0.01 – 0.05; these gelators were promoted in the usual manner at 60 °C, to a final gel volume of 500  $\mu\text{L}$  and concentration (0.5 % w/v). Immediately apparent is the presence of a transparent, stable gel at  $\Phi_{\text{EtOH}}$  0.01. By reducing the solvent content a truly homogenous system devoid of any precipitate or metastable character had been generated.

As lowering the overall solvent concentration has been successful, a 100 % hydrogelator was made, creating a sample with 100 % water meant it could be heated above the 'standard' gelation temperature for these series' (60 °C). The compound was heated to just before boiling point (~ 95 °C) in order to fully solubilise the compound, it was then left to cool for 18 h prior to inversion. **Figure 26b** shows the resulting gel; a transparent, homogenous and self-supporting gelator.

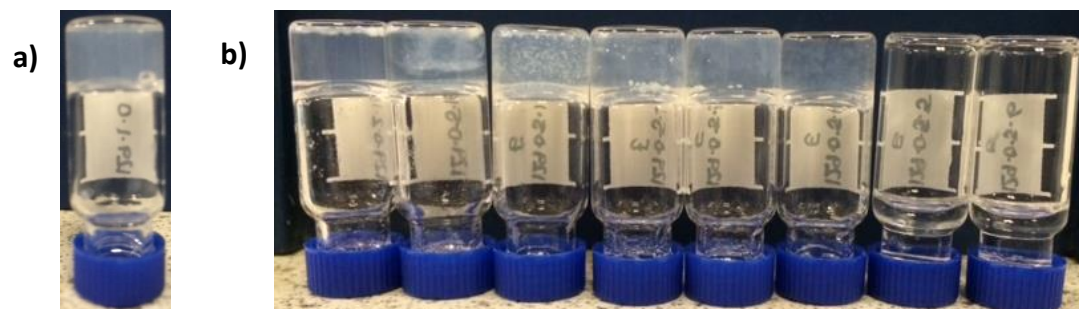


Figure 26: Vial inversion of 48d in  $\Phi_{\text{EtOH}}$  0.00, 0.01, 0.02, 0.05, 0.10, 0.20, 0.30, 0.40 and 0.50 (left to right) at a final compound concentration 0.5 % (w/v)

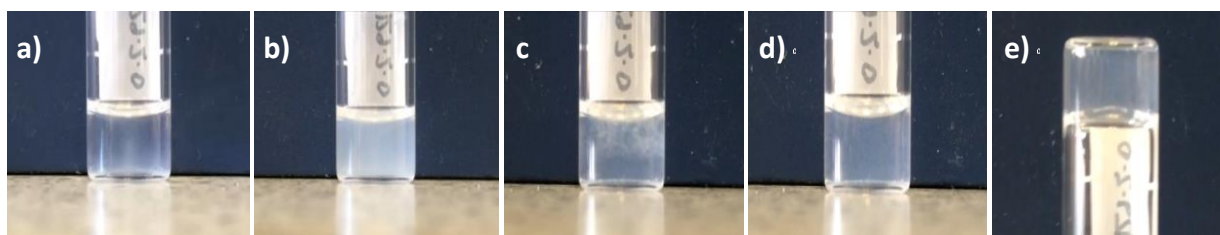


Figure 27: Screen shot of video of gelation over 10 minutes following solubilisation of 48d. a) Following solubilisation b) 2.5 minutes c) 5 minutes d) 10 minutes and e) 10 minutes inverted.

Gelation was monitored immediately following solubilisation of compound **48d** into ultra-purified water. Overall, an increase in turbidity was noted followed by steady decrease over a 10 minute period.

**Figure 27a** depicts the gel following solubilisation; within 30 seconds, as the solution begins to cool, the evolution of an opaque sample is noted, beginning from the bottom of the sample vial, after 2.5 minutes (**Figure 27b**) a homogenous, slightly translucent system is noted. Following this, approximately 5 minutes later (**Figure 27c**) the gel is once again developing a transparency from the bottom of the vial and after a total of 10 minutes (**Figure 27d** and **Figure 27e**) the gel is a homogenous transparent system, capable of retaining structural integrity upon inversion. These observations are representative of a system that, upon cooling, undergoes molecular reorganisation of the building blocks within the fibres following gelation; creating a more kinetically trapped assembly.

Similar systems have previously been reported in literature; Shi *et al.* reported a phenylalanine and cinnamoyl derivative that underwent molecular reorganisation over 10 days.<sup>187</sup> Chen *et al.* reported an Fmoc-diphenylalanine hydrogel that underwent molecular reorganisation over a few minutes,<sup>52</sup> observable by clarification from a turbid solution to a clear gel, whilst Orbach *et al.* demonstrated that varying ratios of Fmoc-amino acids would determine the turbidity of a sample and rate of molecular reorganisation over 75 mins.<sup>175</sup> Most recently Draper *et al.* reported a 2-thiophene diphenylalanine that showed gel aging over 3 days.<sup>188</sup> This gelator (**48d**) can therefore be considered to undergo a fast molecular reorganisation, occurring over 10 mins. This observation is a good indicator of a mechanically strong gel<sup>43</sup> in which the metastable aggregates are trapped kinetically within the gel and is not something that was seen during the formation of any other 2'-deoxycytidine gelators.

Following initial qualitative stability to inversion tests, **48d** displayed idealistic behaviour for a potential drug delivery platform, therefore it was carried forward through to physicochemical characterisation to quantify its mechanical strength.

### 3.2.2. Is the Hydrogel a Good Foundation for a Drug Delivery Platform?

For a gel to be considered as a platform for drug delivery, it is required to display a degree of mechanical strength whilst displaying encapsulation efficiency and physiological tolerability.

#### 3.2.2.1. Rheological Analysis

Initially oscillatory tests were used to characterise the viscoelastic behaviour of the materials. **Figure 28a** depicts the results of a strain/amplitude sweep, performed at variable amplitudes whilst keeping the angular frequency at a constant value. In this case the strain ( $\gamma$ ) was measured between 0.5 and 100 % whilst the frequency ( $\omega$ ) and temperature (T) remained constant at 10 rad/s and 37 °C, respectively. When the storage modulus ( $G'$ ) (a measure of deformation energy stored during the shear process), exceeds the loss modulus ( $G''$ ) (a measure of deformation energy used up by the sample) then the elastic behaviour dominates the viscous behaviour, signifying a certain rigidity in the sample. This is what was seen in this instance, there was an order of magnitude between  $G'$  and  $G''$  which is characteristic of LMWG's. A maximal  $G'$  value of 20 Pa was observed for this sample, making it mechanically weaker than its cytidine counterpart (**42c, Chapter 2**). However it still retains some of the linearity expected for viscoelastic gels. An unusual observation is the slight decrease in  $G''$  at  $\gamma = 8 - 9$  %; this can be attributed to 'wall slip' which commonly occurs in cylindrical measuring systems upon exceeding the LVE range.<sup>178</sup>

Strain sweeps are mostly carried out for the sole purpose of determining the limit of the linear viscoelastic (LVE) region, this is the region in which the strain remains linearly constant i.e. no yield stress/deformation is seen. This is then applied to another oscillatory measurement, the frequency sweep. The LVE in this case was calculated (using Anton Paar GmbH, Rheoplus software) to be 5 %.

A downside of an amplitude sweep is that it doesn't show the behaviour of a sample at rest as it is carried out at a constant frequency of 10 rad/s. The frequency sweep gives a good indication of how a sample will respond to variable angular frequencies. Here, **Figure 28b** indicates that the gel matrix is cross-linked due to the

linearity of the slope, indicating that the  $G'$  and  $G''$  are proportional to one another; however the intersection of the  $G'$  and  $G''$  slopes at the higher frequencies is suggestive of transient crosslinks and that the system is not entirely frequency independent.

**Figure 28c** represents the temperature sweep at constant strain ( $\gamma = 5\%$ ) and frequency ( $\omega = 10$  rad/s) between 37 and 70 °C, with the temperature increasing at intervals of 0.5 °C/min. The sweep shows a steady deformation of the hydrogel beginning at 55 °C, with complete intra-molecular breakdown observed at 65 °C. This is in contrast to the previous cytidine (**42c**) gelator which displayed a much harsher 95 °C gelation temperature.

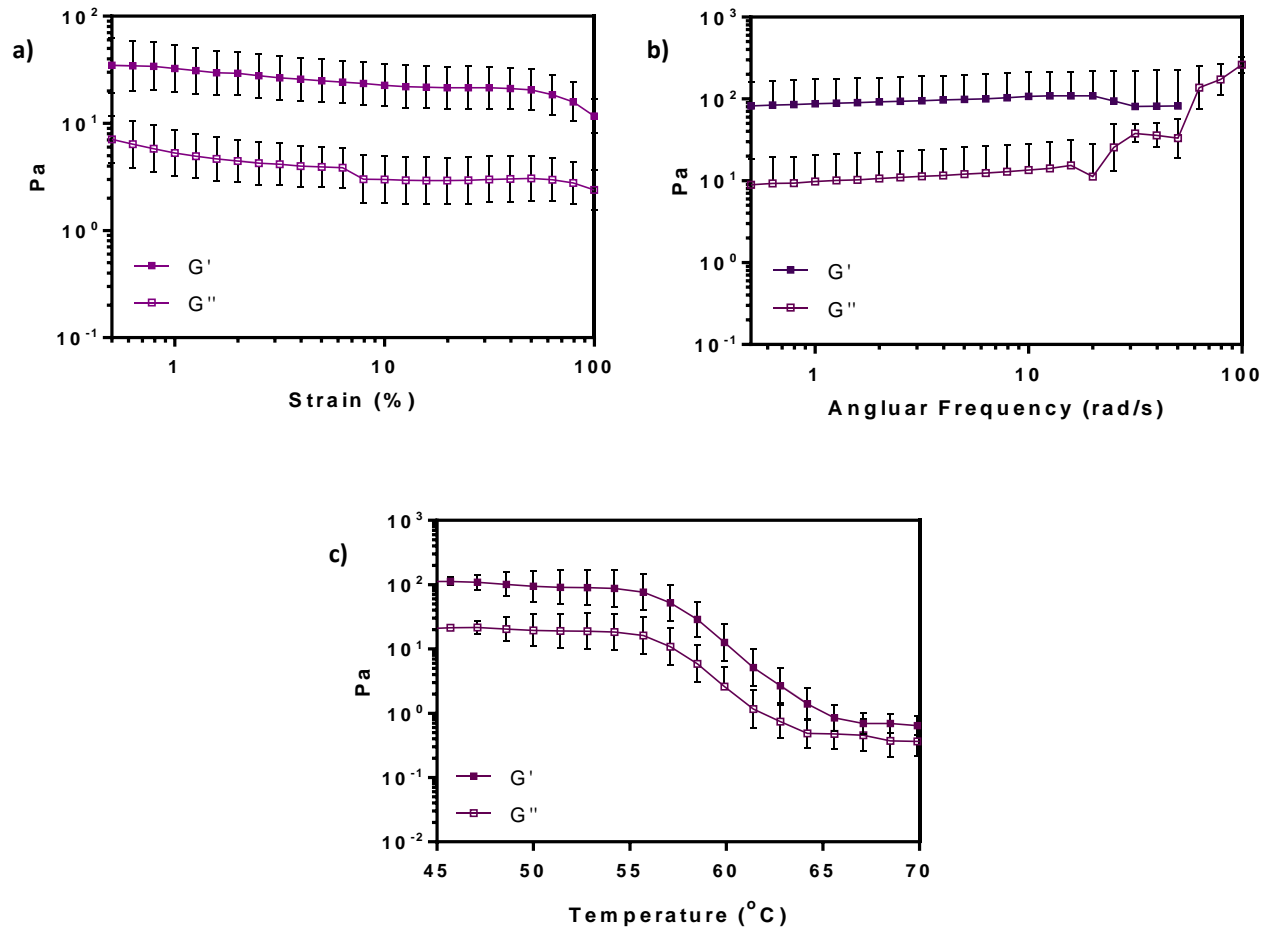


Figure 28: Rheological studies of 48d  $\Phi_{\text{sol}}$  0.00, 0.5% (w/v).

a) Amplitude sweep  $\gamma = 0.05 - 100\%$ ,  $\omega = 10$  rad/s,  $T = 37$   $^{\circ}\text{C}$  b) Frequency sweep  $\gamma = 5\%$ ,  $\omega = 0.1 - 100$  rad/s,  $T = 37$   $^{\circ}\text{C}$  c) Temperature sweep  $\gamma = 5\%$ ,  $\omega = 10$  rad/s,  $T = 37 - 70$   $^{\circ}\text{C}$ . In all cases  $n = 4$

Temperature profiling (**Figure 29a**) was done initially to determine whether the number of heat cool cycles would alter previously observed mechanical strengths. In this instance the temperature was alternated between ambient temperature (20 °C) at which the hydrogel was self-supporting and 80 °C at which the gelator would be in solution. All other variables remained constant ( $\gamma = 5\%$  and  $\omega = 10$  rad/s). There was no significant reduction in mechanical strength following 3 heat-cool cycles and the gel was quick to recover.

Self-healing gels; materials that are capable of autonomous healing upon damage have recently become a focus of many gel research groups – the majority of systems rely upon the permanent cross-linking properties of polymeric systems.<sup>189,190</sup> However the same principal can be applied to LMW gelating systems.

**Figure 29b** depicts a time dependant-recovery test; the recovery being when the molecules are no longer under strain and return to a comparable rest position seen prior to deformation. The gels were subjected to alternating strains; 5 % at which the gel is at within the LVE region (1200 s) and 500 %, at which point we expect complete breakdown of the gelator network (300 s). All other conditions remain constant ( $\omega = 10$  rad/s and  $T = 37$  °C). The shear recovery cycles were performed 4 times for each sample to determine reproducibility. In the majority of LMWG's the recovery ratio would equal zero, indicating a network that was unable to recover from deformation. However, in this case we see retarded recovery. That is, after releasing a high strain and after a rest phase, a certain extent of deformation remains, shown here by a slight decrease in  $G'$  after each cycle of deformation and a recovery ratio of 0.70. This is particularly pertinent as this material needs to be able to withstand physiological pressure and will undergo shear *in situ*. This represents an additional encouragement as there are currently no other reported nucleoside gelators with these properties.<sup>191</sup>

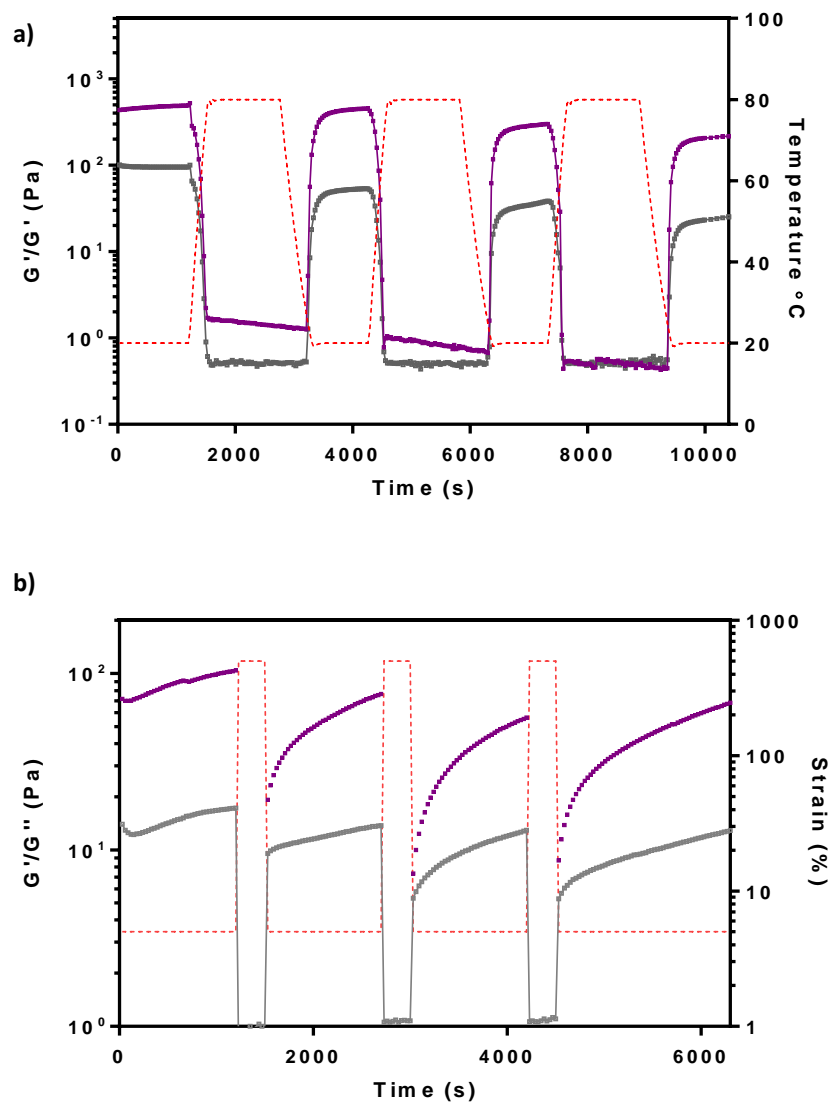


**Figure 29: Recovery sweeps of 48d  $\Phi_{\text{SOL}}$  0.00, 0.5 % w/v.**

a) Temperature profiling ( $T_{\text{prof}}$ ) sweep. 48d ( $\Phi_{\text{SOL}}$  0.00) was measured over 10000 seconds at a constant strain  $\gamma = 1\%$  and frequency  $\omega = 10$  rad/s.  $G'$  (purple) and  $G''$  (grey) were measured between 20 and 80 °C (red) Standard Deviation ( $G'$ )  $234 \pm 80$  Pa. b) Shear/Recovery profile over 6000 seconds at a constant frequency ( $\omega = 10$  rad/s) and temperature ( $T = 37$  °C) alternating (red) between a stable strain (5%) and strain resulting in complete deformation of the gel (500%). Standard Deviation ( $G'$ )  $188 \pm 90$  Pa.  $G'$  (purple) and  $G''$  (grey). In all cases  $n = 4$ .

### 3.2.3. Nanostructure Determination

Both Transmission electron microscopy (TEM) (**Figure 30a** and **Figure 30b**) and Scanning Electron Microscopy (SEM) (**Figure 30c**) were utilised to give an insight into the nanostructure of **48d** ( $\Phi_{\text{SOL}}$  0.00). Both methods are suggestive of a cross-linked fibrillar network, containing cavities suitable for encapsulation of therapeutic materials. Further analysis of these images quantifies each fibre to have an approximate width of between 20 - 25 nm, and a length of approximately 200  $\mu\text{m}$  as with the network found for **42c**, **Section 2.2.3.1**.

### 3.2.4. Gelation NMR

NMR is a powerful technique for studying gels on the molecular scale, as it provides a way of quantifying what is present in the 'liquid-like' phase, and what is immobilised

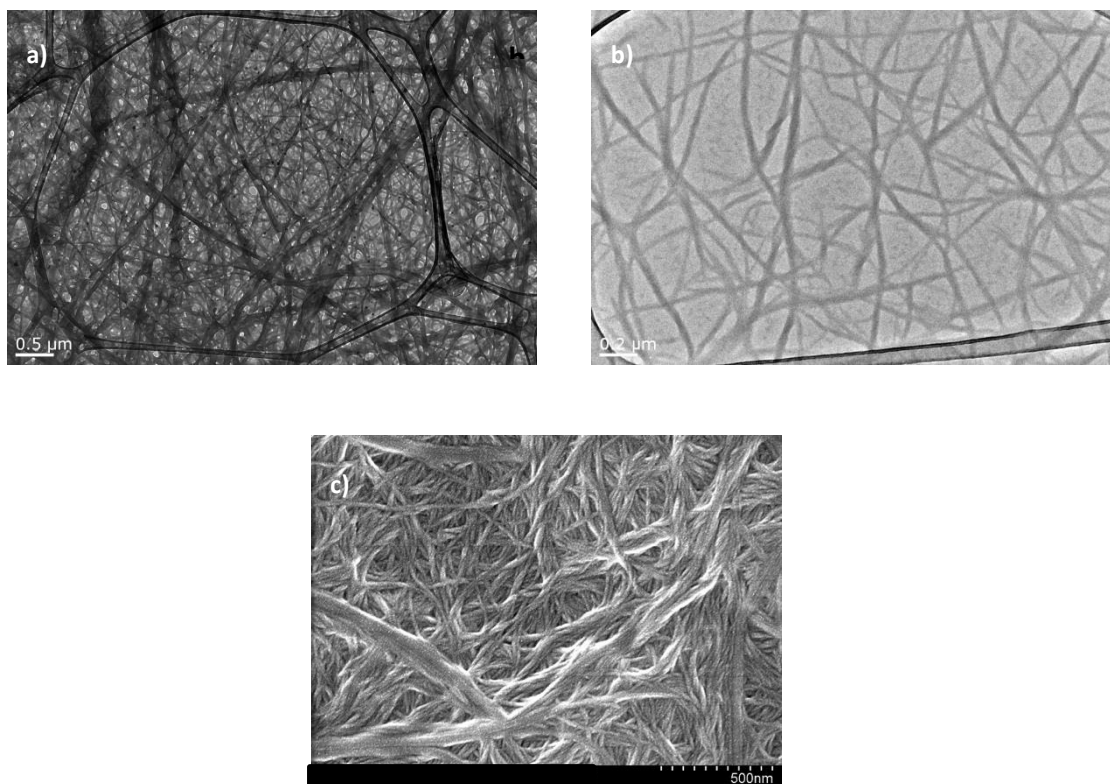


**Figure 30: Electron microscopy images of 48d**

a) Transmission electron microscope (TEM) image of 48d a) highly entangled fibrillar network; scale bar is 0.5  $\mu\text{m}$ ; b) detailed view of entangled network scale bar 0.2  $\mu\text{m}$  and c) scanning electron microscope (SEM) image of gelator surface; scale bar 500 nm.

in the 'solid-like' gel fibres, as documented previously by Hirst *et al.*<sup>192</sup> and Smith *et al.*

193

NMR peaks are observed for mobile components, whereas anything immobilised, for example within gel fibres, effectively broadens into the baseline. Variable temperature (VT) NMR was used to examine the response of **48d** to change in temperature. 2.5 mg of **48d** in H<sub>2</sub>O (500 µL) and a co-axial insert containing a reference standard (D<sub>2</sub>O) was measured using <sup>1</sup>H NMR at increasing temperatures (25 – 70 °C).

The addition of D<sub>2</sub>O directly into the sample and promoting gelation you would see H-D exchange and thus many of the key features of the gelator would disappear, for this reason the reference standard was contained separately to the sample so as to minimise any deuterium exchange.

**Figure 31** shows the solution state <sup>1</sup>H NMR of **48d** in DMSO-*d*<sub>6</sub> at the top and the gel sample in D<sub>2</sub>O/H<sub>2</sub>O at different temperatures from 70 °C to 25 °C (top to bottom). As

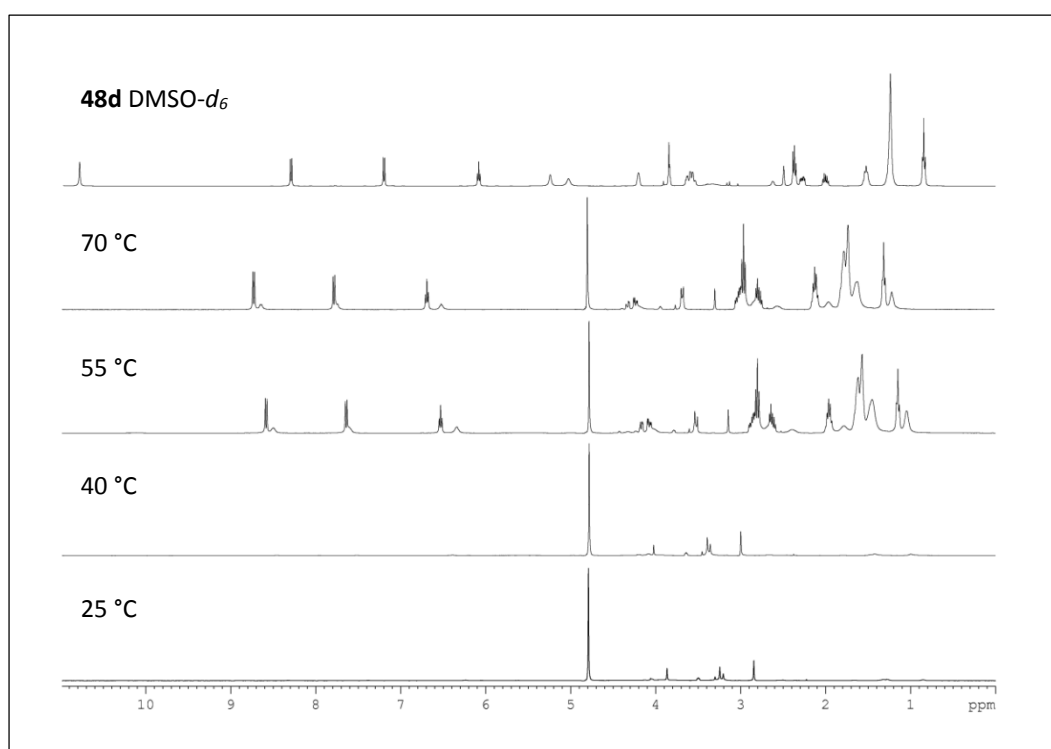


**Figure 31:** VT-NMR of **48d** in H<sub>2</sub>O.

Proton spectra of **48d** dissolved in DMSO-*d*<sub>6</sub> (top); Proton spectra of **48d** in D<sub>2</sub>O/H<sub>2</sub>O with pre-saturation of the water signal at 70, 55, 40 and 25 °C (top to bottom)

D<sub>2</sub>O and H<sub>2</sub>O are considerably more polar than DMSO an overall downfield change in chemical shift is seen, when compared to the NMR in solution state.

At 25 °C and 40 °C there is very little mobility within the samples as it is complexed into the gel structure. Upon increasing temperature, the evolution of the compound to the 'liquid' state is observed. This NMR correlates with the temperature sweep in **Figure 28** suggesting that the temperature of gelation is approximately 55 °C. However, there still appears to be some degree of H-D exchange, as even at the elevated temperature the OH, NH and even adjacent proton signals are absent from the spectrum.

### 3.2.5. *In Vitro* Release Kinetics of Fluorescents

Noted from the microscopy studies is the presence of microscopic cavities within the gelator matrix of **48d** ( $\Phi_{\text{SOL}}$  0.00), as with the **42c** in **Section 2.2.3.1**. For this reason it was thought that the gel may have the same encapsulation efficiency and controlled release as was demonstrated by **42c**. Thus *in vitro* release was evaluated using Fluorescein (332 Da), Fluorescein isothiocyanate Dextran 4000 Da (FITC Dextran 4) and Fluorescein isothiocyanate Dextran 10000 Da (FITC Dextran 10). The fluorescent molecules were dissolved in the aqueous phase during gel preparation and formulated at 0.5 % (w/v) using the aforementioned procedure up to a final gel volume of 2 mL. Upon cooling to ambient temperature, Phosphate Buffered Saline (PBS, 5 mL) was placed on top of the gel and the release monitored over 24 h by removing aliquots (150  $\mu$ L) of the free aqueous phase at specific intervals and measuring the relative fluorescence. The sample volume was small relative to the final volume of the free aqueous phase so as not to disturb the environment. The release of the dye was monitored over time by calculating the diffusion coefficients using the non-steady state diffusion equation (**Equation 2**) reported elsewhere,<sup>181</sup> where  $M_t$  is the total number of molecules released from the matrix between time points,  $M_\infty$  is the total number of molecules left in the matrix,  $\lambda$  is the hydrogel thickness,  $t$  is the time of measurement and  $D$  is the diffusion coefficient of the molecule.

Release from a hydrogel can be controlled by many factors, including the size of the cavities in the mesh network, the surface area to volume ratios, molecular weight of

trapped compounds and interactions between the gel matrix and entrapped molecules. Over the time course of the release no change was observed in the macro structure of the gel i.e. no swelling, shrinking or gel degradation. **Figure 32** shows the amount of dye released plotted against the square root of time. There is a good linear relationship between the amounts of fluorescein dye released over time showing  $R^2 > 0.97$  indicating that again the release profile follows Fickian diffusion.<sup>180</sup> The total percentage release of each fluorescein from the gel matrix was 67 % after 24 h, whereas the release of the two FITC Dextran compound was  $< 5$  %. The retarded release of the FITC Dextran compounds can be attributed to their high molecular weight and the close packed structure of the fibres within the gel matrix trapping them in place. Diffusion coefficients (**Table 12**) were calculated from the linear regression analysis of the fluorescein release profile. The calculated diffusion coefficient of fluorescein is similar to that previously reported in literature for other drugs and drug-like molecules, where values were seen to be in the range of  $2.9 \times 10^{-11}$  and  $5.6 \times 10^{-10}$  m<sup>2</sup>/s.<sup>194</sup> This value also correlates to those previously reported in literature for the release of fluorescein from Fmoc-dipeptide hydrogels.<sup>49,181</sup> The diffusion coefficients of FITC Dextran 4 and FITC Dextran 10 were not calculated as minimal release was detected over 24 h.

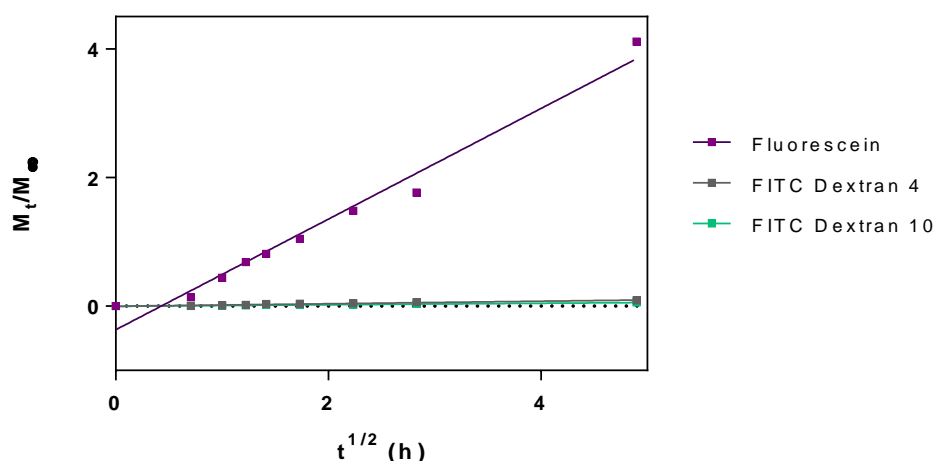


**Figure 32:** Release kinetics of Fluorescein (0.08 mM), FITC Dextran 4 (0.005 mM) and FITC Dextran 10 (0.005 mM) through the gel matrix of 48d.

Plot of dye released against square root of time. This figure is representative of 3 repeat release experiments,  $n = 4$  in each experiment.

Table 12: Diffusion coefficient of Fluorescein, FITC Dextran 4 and FITC Dextran 10 from the hydrogel of 48d.

Dye	Diffusion Coefficient $\times 10^{-10}$ (m <sup>2</sup> /s)
Fluorescein	0.19 $\pm$ 0.004
FITC Dextran 4	<i>n.d</i>
FITC Dextran 10	<i>n.d</i>

### 3.2.6. Will Gelation Occur in Simulated Physiological Conditions?

Unlike *in vitro* cell based assays carried out in previous chapters, studies of gelator **48d** can be carried out both in solution and in gel form owing to the lack of solvent presence in the formulation. Initially it was prudent to explore the structure of the gel in biological conditions to obtain whether conditions can be enhanced towards cell growth.

Gelation was carried out in both PBS pH 7.4 buffer and in RPMI 1640 growth medium at varying compound concentrations (0.1, 0.25, 0.5 and 1 % (w/v)), utilising the method mentioned previously for **48d** in water. **Figure 33** shows the results from the 'stable to inversion' test. Immediately obvious is the absence of gelation when final compound concentration equalled 0.1 % in both PBS and in RPMI 1640. The samples at 1 % were difficult to solubilise even at elevated temperature of 95 °C which is reflected in the opacity of the resulting gels. RPMI 1640 resulted in superior gels over those formed when PBS was used as the medium to facilitate gelation, this is apparent particularly in the 0.25 and 0.5 % gels. These observations can be attributed to the

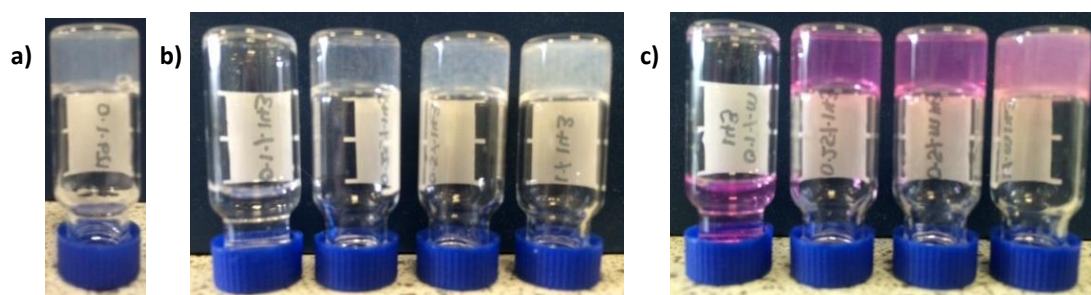


**Figure 33: Vial inversion of 48d in phosphate buffered saline and RPMI-1640 media**

a) **48d**  $\Phi_{\text{SOL}}$  0.00, 0.5 % (w/v) b) **48d** (PBS 7.4) 0.1, 0.25, 0.5 and 1 % w/v (left to right) c) **48d** (RPMI 1640) 0.1, 0.25, 0.5 and 1 % w/v (left to right)

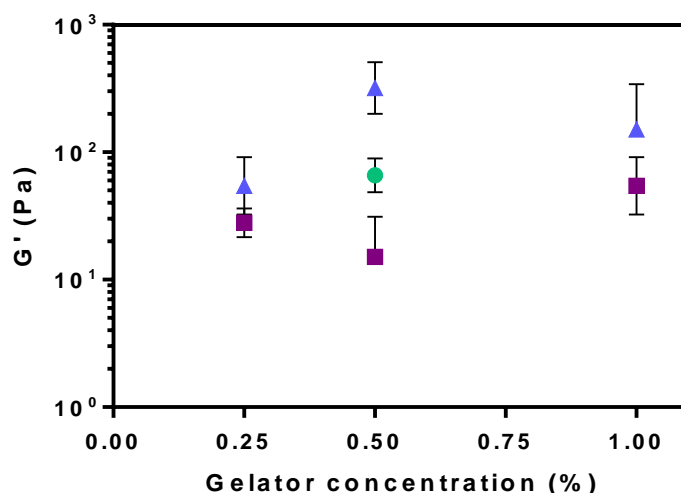


Figure 34:  $G'$  values of **48d** in water (o), PBS pH 7.4 (□) and RPMI 1640 (Δ).

Measurements carried out at varying gelator concentration (0.25, 0.5 and 1 % (w/v) at a strain of 5 %. Each point is representative of  $n=4$  and the standard deviation < 5 %.

difference in ionic strength between PBS and RPMI 1640 medium. RPMI 1640 contains an increased concentration of salts that aid the solubilisation and aggregation of the amphiphilic conjugate **48d**, once in solution the presence of salts promote stability of colloidal interactions.

The mechanical strengths of the self-supporting gels found from the 'stable to inversion' study were measured using oscillatory rheology as described earlier for **48d** (0.5 % w/v) in water using the strain amplitude sweep at a constant angular frequency of 10 rad/s. **Figure 34** shows that at a strain of 5 % strain (indicated by the centre of the LVE region) across each gelator concentration RPMI 1640 displayed the highest mechanical strength, with the highest measured  $G'$  value occurring when the final compound concentration was 0.5 % (w/v). When PBS was used as the gelating medium the gels produced had the lowest overall mechanical strengths at each gelator concentration.

Others have also reported hydrogelators made using various buffers for the purpose of cell culture. Liebmann *et al.*<sup>195</sup> reported gelation of Fmoc-diphenylalanine (Fmoc-FF) in PBS and demonstrated its use as a scaffold for tissue engineering, no rheological data was reported for this system, however, it was reported that differing buffer

concentrations negatively affected the visual stability of the gels. Similar findings were reported by Raeburn *et al.*<sup>51</sup> who reported the mechanical strengths of Fmoc-FF at various pH's using phosphate and acetate buffers. It was found that above pH 7 the use of phosphate buffers in particular significantly reduced the mechanical strength ( $G'$ ) of the Fmoc-FF hydrogels. Recently, a glycosyl-nucleoside amphiphile was reported<sup>196</sup> again for the purpose of tissue culture, this gel was found to be stable in the presence of PBS and demonstrated moderate mechanical strengths, similar to those reported above for **48d** in PBS.

However, due to the increased mechanical strengths ( $G'$ ) of the gels of **48d** made with RPMI medium, this system was used to carry out cell based assays.

### 3.2.7. Growth Inhibition Studies on Compound and on Gel

#### 3.2.7.1. Solution State

A colorimetric cell proliferation assay (MTT) was used to evaluate the toxicity of **48d** against the parent compound, 2'-deoxycytidine (**46**) in 3 different cell lines; MCF-7 human breast adenocarcinoma, MIA PaCa-2 human pancreatic carcinoma and MKN-7 human stomach adenocarcinoma to determine the 50 % growth inhibition concentration ( $GI_{50}$ ). MIA PaCa-2 and MKN-7 represent 2 gemcitabine susceptible cell lines that can be used to test the effectiveness of the delivery system in subsequent experiments, however initially we needed to confirm that the **48d** gelator didn't display any adverse toxicity in its solution state. The cells were split into a nuncwell 96 well plate (3000 cells/well) and incubated for 24 h at 37 °C and 5 % CO<sub>2</sub> before introducing the test agent. The cells and test compound were incubated for a further 72 h before adding 3-(4,5-dimethylthiazol-2-yl)-2,5-diphenyltetrazolium bromide (MTT). Living and dead cells were quantified by measuring UV absorbance, living cells metabolise the yellow MTT to insoluble purple (E,Z)-5-(4,5-dimethylthiazol-2-yl)-1,3-diphenylformazan (formazan) crystals that can then be solubilised with DMSO and measured at 570 nm. **Table 13** shows the millimolar  $GI_{50}$  concentration values found for both **46** and **48d** in each of the tested cell lines, with the conjugate **48d** being minimally more toxic than the parent compound in every tested cell line.

These results were promising moving forward, however to fully qualify the **48d** hydrogel as a viable drug delivery platform it needed to be tested in the gel state.

**Table 13:** Solution phase growth inhibition studies for 46 and 48d in MIA PaCa-2, MKN-7 and MCF-7 adenocarcinoma cell lines.

Compound	GI <sub>50</sub> (mM)		
	MIA PaCa-2	MKN-7	MCF-7
<b>46</b>	9.55 ± 3.65	9.99 ± 2.81	4.14 ± 2.47
<b>48d</b>	6.58 ± 1.40	7.74 ± 3.26	3.94 ± 0.74

### 3.2.7.2. Probing Cell Adhesion – A Gel State Colorimetric Assay

One limitation of the MTT assay is that if cells are unable to adhere to the surface of the gel matrix then they cannot proliferate and therefore will have reduced absorbance readings when directly compared to a control surface. Many existing hydrogels exhibit cell adherence behaviour and have demonstrated applications in

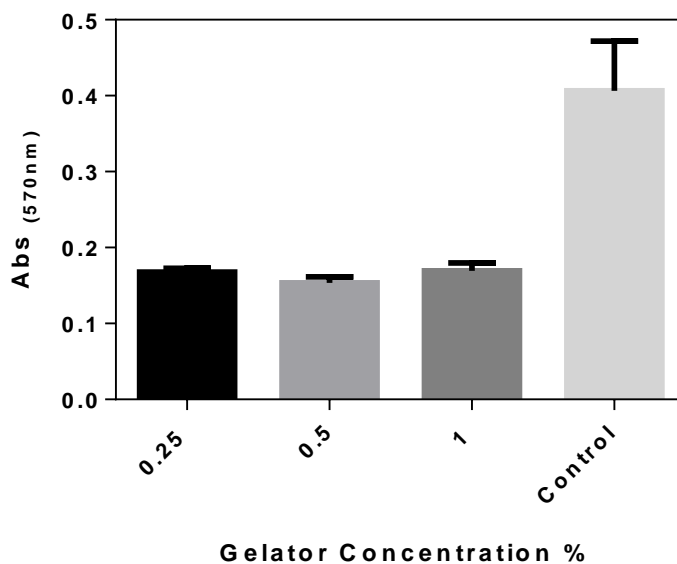


**Figure 35:** Cell on Gel colorimetric MTT

MIA-PaCa-2 after 72 h with 0.25 and 0.5 and 1 % w/v, equivalent to 0.5 $\times$ , 1 $\times$  and 2 $\times$  GI<sub>50</sub>

tissue engineering.<sup>195,197,198</sup> Initial studies were designed to determine cell adherence; **48d** was prepared under sterile conditions to 0.25, 0.5 and 1 % w/v and distributed into 24 well plates with a final gel volume of 50  $\mu$ L gel/well. The samples were incubated at 37 °C and 5 % CO<sub>2</sub> for 24 h prior to the introduction of cells.  $1 \times 10^4$  cells were suspended in 700  $\mu$ L medium on top of the gel and incubated for a further 72h. Following the 72 h incubation, MTT was added to the wells and incubated for a further 2 h before aspirating the wells and adding DMSO, the cell viability was quantified by UV at 570 nm. **Figure 35** indicates a degree of toxicity associated with all of the gelators. As we know for the solution state assays the GI<sub>50</sub> ( $6.58 \pm 1.40$  mM) corresponds to a final gelator concentration of 0.5 % therefore we would expect a significant difference in cell viability between each of the tested gelator concentrations ( $0.5 \times$ ,  $1 \times$  and  $2 \times$  GI<sub>50</sub>). As the absorbance after 72 h was almost identical for each of the gelator concentrations, the data is suggestive that the cells may not be completely adhering to the surface of the gels.

To validate the cell adherence, a 2 % gelatine solution was introduced into the gelator formulation (to a final gelatine concentration of 1 %) to enhance cell adhesion. Gelatine is not expected to elicit any additional survival advantages in the cells, as demonstrated previously using an acetyl guanosine hydrogelator,<sup>198</sup> however, as we

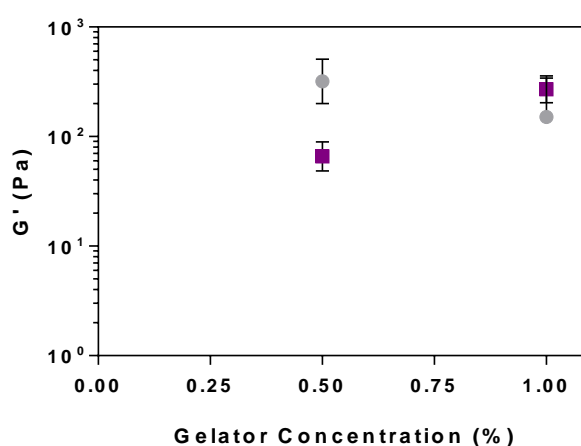


**Figure 36:** G' values from the strain sweep of 0.5 % and 1 % (w/v) gelators derived from **48d** in RPMI-1640 (o) and RPMI-1640 + 1 % gelatine ( $\square$ ).

Each data point is a representation of  $n = 3$ .

had a formulation change it was pertinent to re-assess the mechanical strength of the gels by the way of a strain sweep ( $\gamma = 0.05 - 100\%$ ) carried out at constant frequency  $\omega = 10$  rad/s . **Figure 36** shows that the addition of 1 % gelatine to the RPMI gels didn't provide any additional benefits to gel stability, in the case of 0.5 % (w/v) the addition of the 1 % gelatine decreased the overall mechanical strength of the gelator.

The gel based assays were repeated with the newly formulated gelatine (1 %) gels. The assays were carried out in two ways; introducing the cells in suspension on top of the gels and introducing the gels to a pre-prepared monolayer of cells. Having two individual assays would help distinguish between the inherent growth inhibitory effect of the gels and the effect cell adherence plays in apparent growth inhibition. For the cell adherence the assay was performed as described above. For the assay in which gels are injected on top of cells, the cell suspension was added into the 24 well plates and incubated at (37 °C and 5 % CO<sub>2</sub>) for 24 h before addition of the gels directly on to the cell monolayer. Cell viability was quantified at 24, 48 and 72 h; **Figure 37a** shows the results of the cell adherence assay, the DMSO control represents 100 % dead cells. As is apparent there is a significant reduction in cell growth from 0.5 % and 1 % gels after 72 h, with the 1 % (w/v) gel displaying complete cell death, this indicates a lack of cell adherence to the gel of **48d** even with the addition of 1 % gelatine. This observation is likely due to the method of gel preparation and the degradation of gelatine at this temperature.<sup>199</sup> **Figure 37b** shows the comparative assay in which the gels were injected directly onto the cells. The cells responded well to the gels in this environment, displaying comparable growth inhibition to the solution state assays above. These results indicate that at these concentrations the gels are well tolerated and aren't 'suffocating' the cell monolayer i.e there is a flow of nutrients from media through the gel to the cells on the plate below. At a final gelator concentration of 0.5 % there is little change in the overall interruption of growth inhibition between 24 and 72 h, whereas when the final gelator concentration is 1 % there is an observable decrease in cell viability.

For the remainder of the assays the gels were formulated without 2 % gelatine solution

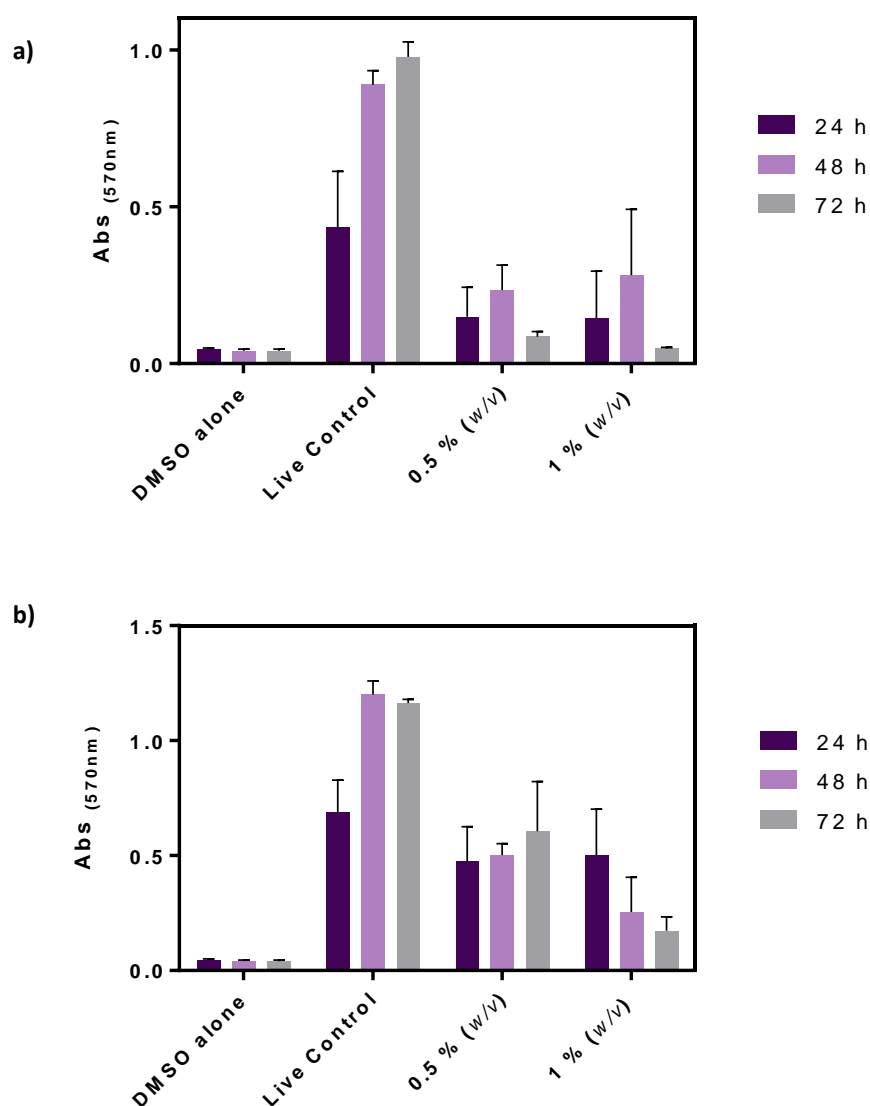


Figure 37: Cell proliferation colorimetric assay on MIA PaCa-2 human pancreatic adenocarcinoma cells

Gelator concentrations 0.5 and 1 % (w/v), where gels are made with 1 % gelatine to aid adherence a) Cells distributed on gels b) Gels distributed on cells

### 3.2.7.3. Global Effect of a Hydrogel *In Vitro*

Another valid way to qualify the hydrogel **48d** as a drug delivery platform is to determine its effect on cell proliferation over a larger cell monolayer. A qualitative assay was designed that can be used in conjunction with other quantitative methods to determine activity of specific agents. Gels of **48d** were prepared in sterile conditions to final compound concentrations of 0.5 % and 1 % (w/v) in RPMI-1640. The gels were deposited into syringes, before allowing to cool to ambient temperature over 18 h.

MIA PaCa-2 carcinoma cells and MRC-5 fibroblasts were seeded at a density of  $1 \times 10^5$  and  $5 \times 10^5$  cells/well, respectively. Plates were incubated ( $37^\circ\text{C}$  and  $5\% \text{CO}_2$ ) for 24 h prior to introduction of the gel. MRC-5 cells were chosen as a control cell line, representative of healthy tissue, in which gemcitabine should not show activity. Both concentrations (0.5 % and 1 % w/v) were tested as i) a deposit on to the cell monolayer and ii) a raft into the cell culture medium, to determine the environmental effects of the gels. **Figure 38** shows the result of the qualitative methylene blue assay,

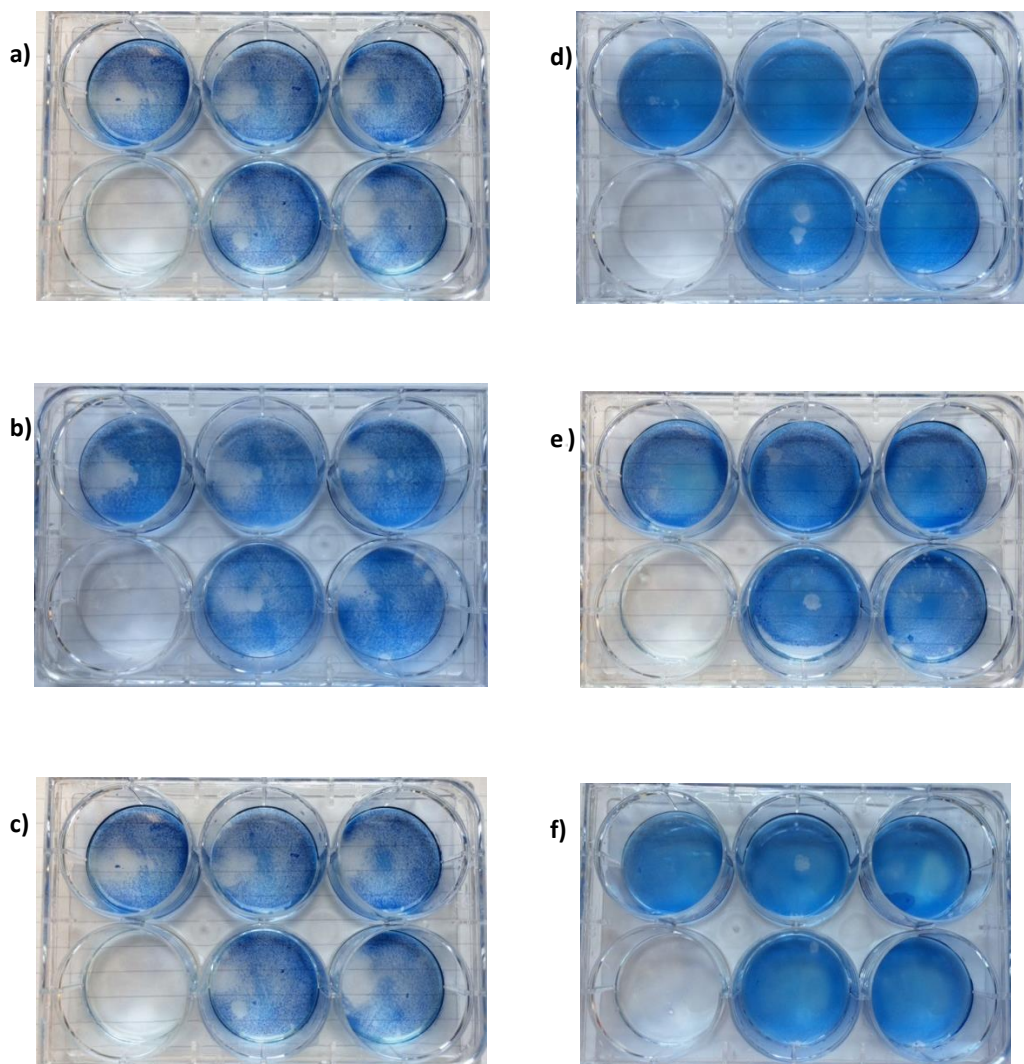


**Figure 38: Methylene Blue assay with Mia PaCa-2 cells (left) and MRC-5 fibroblasts (right).**

24, 48 and 72 h time points (top to bottom). Each image shows a live control, (top left), 0.5 % (w/v) injected on to cells (top middle), 0.5 % (w/v) gel injected into media (top right), a dead control (no cells)(bottom left), 1 % (w/v) gel injected onto cells (bottom middle) and 1 % (w/v) injected into media (bottom right).

the result from the MIA PaCa-2 cell line is shown on the left and the MRC-5 result is shown on the right with the 24, 48 and 72 h time points shown from top to bottom. The MRC-5 assays show an absence of growth inhibition, at both concentrations (0.5 and 1 % (w/v) when gels were applied to the cells directly and when deposited in medium. There was a small artefact in the cell monolayer underneath where the gel had been deposited on to the monolayer. However, the overall results from the MRC-5 control assay were a good indicator that the gels were non-toxic and didn't prevent proliferation. MIA PaCa-2 results show that the gel has an increased effect on growth inhibition when compared with the same assay performed on MRC-5 fibroblasts. It appears that after 48 hours cell proliferation is increased, with **48d** only displaying cytostatic activity beyond this point. A quantitative MTT colorimetric assay was additionally performed. The results of which are shown in **Figure 39**. The impact of 0.5 % and 1 % (w/v) gels; as a deposit onto a cell monolayer and as a 'raft' in medium, on MIA PaCa-2 cells is shown in **Figure 39a**. The results after 24 h show a notable difference in the observed absorbance between those cells in contact with the gel and those exposed to the gel 'raft', with the gels injected on to the cell monolayer displaying an approximate 50 % reduction in cell growth. However, there is little difference in the growth inhibition between 0.5 % and 1 % w/v gels, suggesting that the long-term effect of the compound concentration isn't immediate. As observed in **Figure 38** there is an increased proliferation of cells up to 48 h under all gel conditions, signifying that the viable cells are quick to recover from the initial exposure to the gels after 24 h. However, following 72 h exposure, MIA PaCa-2 cells display growth inhibition once more. The samples prepared from injection of gels into media follow an expected inhibition based upon gel concentration i.e. 1 % w/v inhibits cell proliferation approximately 50 % more than 0.5 % w/v. However, samples prepared from injection onto the cell monolayer don't agree with previous predictions based upon solution state assays; a 2-fold decrease would have been expected from the 1 % w/v ( $2 \times GI_{50}$ ) gel based upon previous calculated  $GI_{50}$  values. Observed was a comparable growth inhibition suggesting that the compound has a maximum threshold for cytotoxicity, and concentration above this will result in the same growth inhibition.

MRC-5 results are shown in **Figure 39b**. Fibroblasts were seen to grow to a maximum density after 24 h for the volume of the well. This density was maintained for a further 48 h and the presence of the gel was found to have no adverse effect on the proliferation of cells under any of the tested conditions.

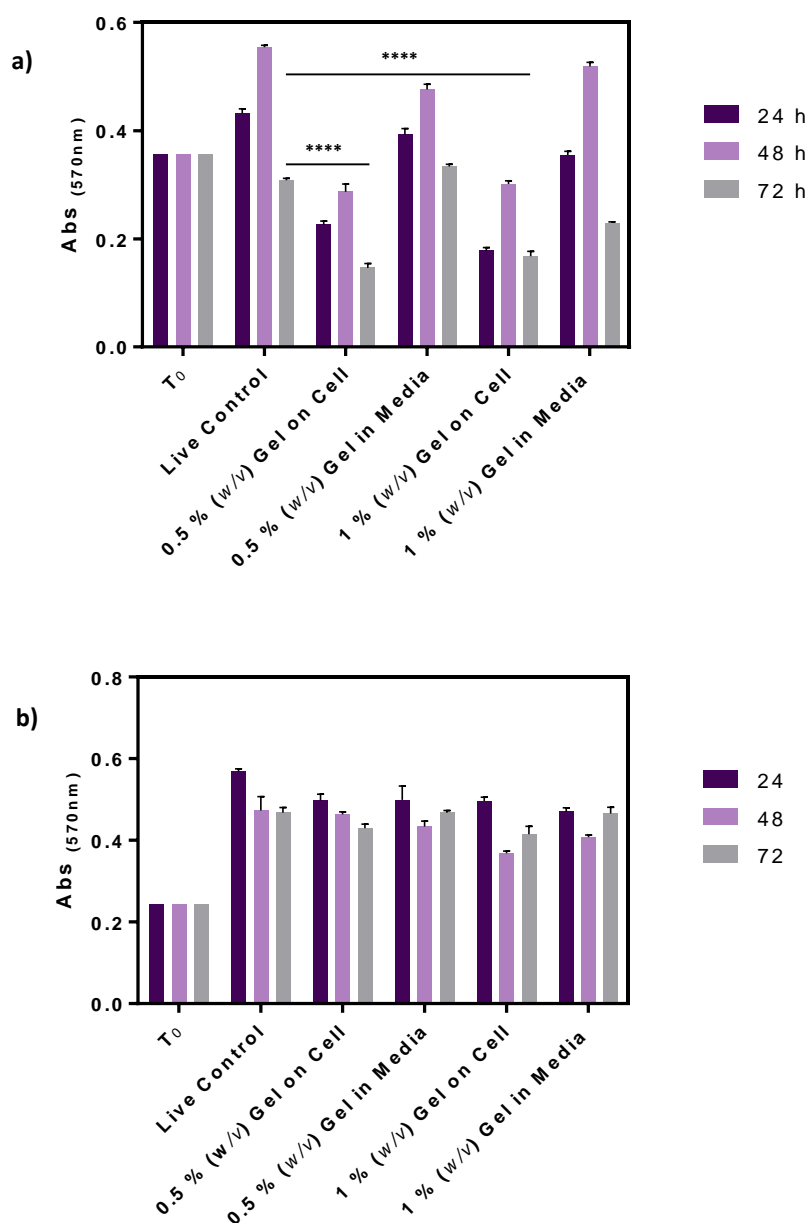


**Figure 39: Cell proliferation colorimetric assay of gels made from 48d (0.5 % and 1 % w/v) injected on to the cell monolayer and in suspended in RPMI-1640**

a) MIA PaCa-2 human pancreatic adenocarcinoma cells and b) MRC-5 human fibroblast cells. Gels were made with 1 % gelatine to aid adherence. Assays were carried out in n = 3. Paired t-test analyses were run on the 72 h time points \*\*\*\* p < 0.0001

### 3.3. Summary

The foundation for a good gelator was described in **Chapter 2**, however to enhance aqueous solubility and to improve the self-assembly process i.e. drive it towards hydro-gelation; modifications to the overall structure were needed. Using molecular modelling to determine key functional group to the gelation process had been deemed too complicated based upon the complex binary system seen for gelators. Instead an experimental method was utilised.

Initial findings confirmed the existing amide functionality of **42c** as a key functionality in the gelation process, by introducing an additional hydroxyl on the tetradecanoyl chain, intra-molecular hydrogen bonding was introduced and the self-assembly process was disrupted.

Additional studies focused on the sequential removal of the 2' and 3' hydroxyls from the ribose sugar of cytidine. Synthesis of 2'-deoxycytidine (**46**) and 2',3'-dideoxycytidine (**47**) afforded gelators with the same amide functionality as above but introduced shorter chain lengths so that the predicted water solubility ( $\text{LogS}_w$ ) would be decreased and as a result the solubility would be enhanced, thus driving gelation towards a predominantly aqueous system.

When gelation was promoted using the 'anti-solvent' system, a preference for gelation was seen in the 2'-deoxycytidine series (**48a** - **48e**). Further studies alluded to a gelator (**48d**) that could be completely solubilised in water thus generating a 100 % hydrogelating system.

Rheological testing confirmed this system to be stable under relatively high strains (LVER ~ 5 %) and demonstrated the propensity of the gel to act as a 'self-healing' material, thus validating it for use as an intra-tumoural drug delivery system. Further electron microscope imaging confirmed the nanostructure to be a cross-linked fibrillar network and *in vitro* release studies once again demonstrated a diffusion mediated release of small molecular weight fluorescein from the gelator matrix, whilst larger molecular weight FITC Dextran 4 and 10 were retained.

In vitro growth inhibition assays finally established the gelator compound and the gel scaffold as an inert matrix and thus validated the device for drug delivery.

### 3.4. Materials and Methods

#### Materials

Cytidine, 2'-deoxycytidine and 2',3'-dideoxycytidine were all purchased from TCI Chemicals (Europe) and all other chemicals and solvents were purchased from commercial suppliers and used without further purification.

1.5 mL sample vials were purchase from Fischer Scientific, 7 mL aluminium rheology vials were purchased from Anton Paar GmbH and Transmission electron micrograph grids were purchased from EM Resolutions.

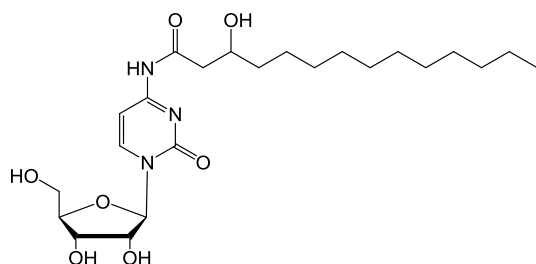
#### Methods

##### 3.4.1. General Chemistry

TLC, NMR, HRMS, LC-MS and analytical RP-HPLC were all carried out as reported in Section 2.6.1.

##### **General procedure for the synthesis of *N*-(1-((2*R*,3*R*,4*S*,5*R*)-3,4-dihydroxy-5-(hydroxymethyl)tetrahydrofuran-2-yl)-2-oxo-1,2-dihydropyrimidin-4-yl)-3-hydroxytetradecanamide (45)**

To a solution of 2-chloro-4,6-dimethoxy-1,3,5-triazine (**40**) (CDMT, 0.9 mmol, 1 eqv, 158 mg) in anhydrous CH<sub>2</sub>Cl<sub>2</sub> (10 mL) at 0 °C, was added *N*-methylmorpholine (NMM, 27.2 mmol, 1.36 eqv, 98 µL) with continuous stirring until a white suspension had formed. The mixture was then left to stir for 1 h. 3-hydroxy-tetradecanoic acid (0.9 mmol, 1 eqv, 207 mg) was added directly into the mixture as a solution in anhydrous DMF (5 mL) and stirred for a further h. A solution of cytidine (**39**) (0.9 mmol, 1 eqv, 219 mg) in anhydrous DMF (6 mL) was made up at 0 °C. The cold triazine solution was added drop wise to the cooled cytidine solution over 30 mins, before heating to 50 °C and stirring for 12 h. The cooled solution was evaporated *in vacuo*. The product was purified using flash silica column chromatography, eluting at 5 - 7 % methanol in CH<sub>2</sub>Cl<sub>2</sub>. Product was a white powder. Purity was determined by NMR.



**Yield:** 21 %

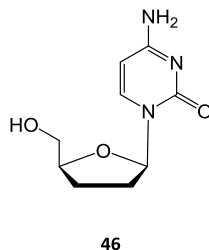
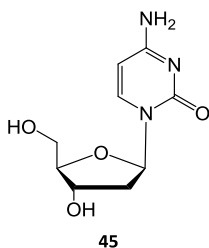
**NMR purity:** 98.2 %

**<sup>1</sup>H NMR (DMSO-*d*<sub>6</sub>)** δ 0.85 (t, *J* = 6.8 Hz, 3H, CH<sub>3</sub>), 1.15 - 1.41 (m, 20H, CH<sub>3</sub>-(CH<sub>2</sub>)<sub>10</sub>-CH(OH)), 2.25 (ddd, *J* = 22.6, 14.8, 6.5 Hz 1H, C=O-CH<sub>2</sub>-CH(OH)), 2.45 (d, *J* = 6.7 Hz, 2H, C=O-CH<sub>2</sub>), 3.55 - 3.78 (m, 2H, 5'-CH<sub>2</sub>), 3.85 (m, 1H, 4'-CH), 3.95 (m, 1H, 3'-CH), 4.71 (t, *J* = 5.3 Hz, 1H, acyl-3-OH) 5.04 (t, *J* = 5.4 Hz, 1H, 3'-OH), 5.15 (d, *J* = 5.2 Hz, 1H, 5'-OH), 5.47 (d, *J* = 4.7 Hz, 1H, 2'-OH), 5.77 (d, *J* = 2.4 Hz, 1H, 1'-CH), 7.21 (d, *J* = 7.4 Hz, 1H, 5-CH), 8.41 (d, *J* = 7.4 Hz, 1H, 6-CH), 10.73 (s, 1H, NH).

**<sup>13</sup>C NMR (DMSO-*d*<sub>6</sub>)** δ 22.56, 29.18, 29.49, 29.52, 31.76, 40.04, 40.25, 40.46, 40.67, 67.55, 69.12, 75.00, 84.66, 90.64, 65.73, 141.71, 145.82, 183.11

**m/z:** HRMS (TOF ES<sup>+</sup>) C<sub>23</sub>H<sub>40</sub>N<sub>3</sub>O<sub>7</sub> [M+H]<sup>+</sup> calculated 470.2861; found 470.1759

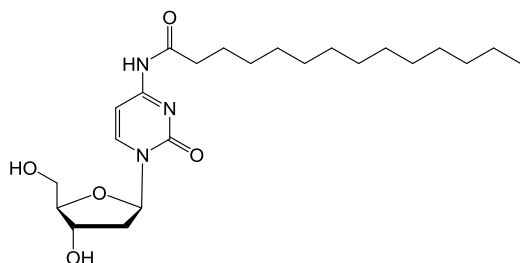
**General Procedure for the synthesis of substituted 4-amino-1-((2*R*,4*S*,5*R*)-4-hydroxy-5-(hydroxymethyl)tetrahydrofuran-2-yl)pyrimidin-2(1*H*)-one (46) and 4-amino-1-((2*R*,5*S*)-5-(hydroxymethyl)tetrahydrofuran-2-yl)pyrimidin-2(1*H*)-one (47)**



To a solution of 2-chloro-4,6-dimethoxy-1,3,5-triazine (**40**) (CDMT, 1.1 mmol, 1 eqv, 193 mg) in anhydrous CH<sub>2</sub>Cl<sub>2</sub> (3.5 mL) at 0 °C, was added *N*-methylmorpholine (NMM, 1.50 mmol, 1.36 eqv, 171 μL) with continuous stirring until a white suspension had formed. The mixture was then left to stir for 1 h. Medium or short chain carboxylic acids (1.1 mmol, 1 eqv) were added directly into the mixture as a solution in anhydrous DMF (1 mL) and stirred for a further h. A solution of either **46** or **47** (1.1 mmol, 1 eqv) in anhydrous DMF (2 mL) was made up at 0 °C. The cold triazine solution was added drop wise to the cooled cytidine solution over 30 mins, before heating to 50 °C and stirring for 7-8

h. The cooled solution was evaporated *in vacuo*. The product was purified using flash silica column chromatography, eluting at 5 - 8 % methanol in CH<sub>2</sub>Cl<sub>2</sub>.

***N*-(1-((2*R*,4*S*,5*R*)-4-hydroxy-5-(hydroxymethyl)tetrahydrofuran-2-yl)-2-oxo-1,2-dihydropyrimidin-4-yl)tetradecanamide (48a)**



Tetradecanoic acid (1.1 mmol, 1 eqv, 251 mg), **45** (1.1 mmol, 1 eqv, 250 mg)

**Yield:** 40.0 %

**HPLC purity:** 98.0 %

**HPLC t<sub>R</sub>:** 24.1 min

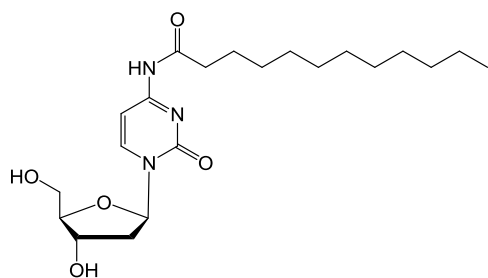
**<sup>1</sup>H NMR (DMSO-*d*<sub>6</sub>)** δ 0.86 (t, *J* = 6.7 Hz, 3H, CH<sub>3</sub>), 1.23 (br-m, 20H, CH<sub>2</sub>-(CH<sub>2</sub>)<sub>10</sub>-CH<sub>3</sub>), 1.54 (m, 2H, C=O-CH<sub>2</sub>-CH<sub>2</sub>), 1.98 - 2.32 (m, 2H, 2'-CH<sub>2</sub>), 2.38 (t, *J* = 7.3 Hz, 2H, C=O-CH<sub>2</sub>), 3.54 - 3.65 (m, 2H, 5'-CH<sub>2</sub>), 3.87 (q, *J* = 3.7 Hz, 1H, 4'-CH), 4.20 - 4.24 (td, *J* = 7.7, 3.9 Hz, 1H, 3'-CH), 5.03 (t, *J* = 5.3 Hz, 1H, 5'-OH), 5.25 (d, *J* = 4.3 Hz, 1H, 3'-OH), 6.11 (t, *J* = 6.3 Hz, 1H, 1'-CH), 7.22 (d, *J* = 7.7 Hz, 1H, 6-CH), 8.32 (d, *J* = 7.5 Hz, 1H, 5-CH), 10.81 (s, 1H, NH).

**<sup>13</sup>C NMR (DMSO-*d*<sub>6</sub>)** δ 13.95, 22.09, 24.44, 28.43, 28.70, 28.85, 28.98, 29.00, 29.05, 31.29, 36.33, 40.89, 60.94, 69.93, 86.12, 87.89, 95.24, 144.94, 154.45, 162.27, 173.92

**m/z:** HRMS (TOF ES<sup>+</sup>) C<sub>23</sub>H<sub>40</sub>N<sub>3</sub>O<sub>5</sub> [M+H]<sup>+</sup> calculated 438.2965; found 438. 4150

**m.p:** 141 - 142 °C

***N*-(1-((2*R*,4*S*,5*R*)-4-hydroxy-5-(hydroxymethyl)tetrahydrofuran-2-yl)-2-oxo-1,2-dihydropyrimidin-4-yl)dodecanamide (48b)**



Dodecanoic acid (1.1 mmol, 1 eqv, 242 mg), **45** (1.1 mmol, 1 eqv, 250 mg)

**Yield:** 59.0 %

**HPLC purity:** 98.7 %

**HPLC t<sub>R</sub>:** 21.5 min

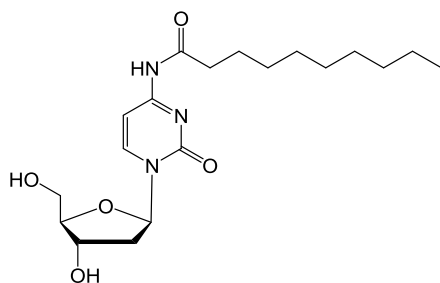
**<sup>1</sup>H NMR (DMSO-*d*<sub>6</sub>)** δ 0.85 (t, *J* = 6.9 Hz, 3H, CH<sub>3</sub>), 1.25 (br-m, 16H, CH<sub>2</sub>-(CH<sub>2</sub>)<sub>8</sub>-CH<sub>3</sub>), 1.47-1.54 (m, 2H, C=O-CH<sub>2</sub>-CH<sub>2</sub>), 1.95-2.32 (m, 2H, HO-CH-CH<sub>2</sub>), 2.37 (t, *J* = 7.3 Hz, 2H, C=O-CH<sub>2</sub>), 3.54 - 3.5 (m, 2H, 5'-CH<sub>2</sub>), 3.86 (q, *J* = 3.8 Hz, 1H, 4'-CH), 4.20 -4.24 (td, *J* = 7.6, 3.9, 1H, 3'-CH), 5.03 (t, *J* = 5.2 Hz, 1H, 5'-OH), 5.26 (d, *J* = 4.3 Hz, 1H, 3'-OH), 6.10 (t, *J* = 6.3 Hz, 1H, 1'-CH), 7.22 (d, *J* = 7.4 Hz, 1H, 6-CH), 8.32 (d, *J* = 7.4 Hz, 1H, 5-CH), 10.82 (s, 1H, NH).

**<sup>13</sup>C NMR (DMSO-*d*<sub>6</sub>)** δ 13.95, 22.08, 24.44, 28.42, 28.68, 28.70, 28.85, 28.97, 28.98, 31.28, 36.33, 40.88, 55.29, 60.94, 69.92, 86.11, 87.88, 95.24, 144.94, 154.45, 162.27, 173.92

**m/z:** HRMS (TOF ES<sup>+</sup>) C<sub>21</sub>H<sub>36</sub>N<sub>3</sub>O<sub>5</sub> [M+H]<sup>+</sup> calculated 410.2649; found 410.2086

**m.p:** 135 – 137 °C

***N*-(1-((2*R*,4*S*,5*R*)-4-hydroxy-5-(hydroxymethyl)tetrahydrofuran-2-yl)-2-oxo-1,2-dihydropyrimidin-4-yl)decanamide (48c)**



Decanoic acid (1.1 mmol, 1 eqv, 189 mg), **45** (1.1 mmol, 1 eqv, 250 mg)

**Yield:** 54.0 %

**HPLC purity:** 97.2 %

**HPLC t<sub>R</sub>:** 19.0 min

**<sup>1</sup>H NMR (DMSO-*d*<sub>6</sub>)** δ 0.85 (t, *J* = 6.6 Hz, 3H, CH<sub>3</sub>), 1.24 (br-m, 12H, CH<sub>2</sub>-(CH<sub>2</sub>)<sub>6</sub>-CH<sub>3</sub>), 1.53 (m, 2H, C=O-CH<sub>2</sub>-CH<sub>2</sub>), 1.97-2.31 (m, 2H, HO-CH-CH<sub>2</sub>), 2.38 (t, *J* = 7.2 Hz, 2H, C=O-CH<sub>2</sub>), 3.52 - 3.66 (m, 2H, 5'-CH<sub>2</sub>), 3.85 (q, *J* = 3.7 Hz, 1H, 4'-CH), 4.19-4.23 (m, 1H, 3'-CH), 5.03 (t, *J* = 5.3 Hz, 1H, 5'-OH), 5.25 (d, *J* = 4.1 Hz, 1H, 3'-OH), 6.10 (t, *J* = 6.4 Hz, 1H, 1'-CH), 7.21 (d, *J* = 7.4 Hz, 1H, 6-CH), 8.31 (d, *J* = 7.5 Hz, 1H, 5-CH), 10.81 (s, 1H, NH).

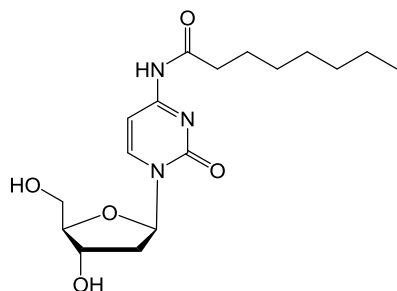
**<sup>13</sup>C NMR (DMSO-*d*<sub>6</sub>)** δ 13.95, 22.09, 24.45, 28.44, 28.65, 28.71, 28.82, 31.26, 36.34, 40.88, 55.32, 60.94, 69.92, 86.12, 87.89, 95.25, 144.95, 154.45, 162.27, 173.93

**m/z:** HRMS (TOF ES<sup>+</sup>) C<sub>19</sub>H<sub>32</sub>N<sub>3</sub>O<sub>5</sub> [M+H]<sup>+</sup> calculated 382.2336; found 381.7577

**m.p:** 133 – 134 °C

***N*-(1-((2*R*,4*S*,5*R*)-4-hydroxy-5-(hydroxymethyl)tetrahydrofuran-2-yl)-2-oxo-1,2-dihydropyrimidin-4-yl)octanamide (48d)**

Octanoic acid (1.1 mmol, 1 eqv, 159 mg, 179  $\mu$ L), **45** (1.1 mmol, 1 eqv, 250 mg)



**Yield:** 42.0 %

**HPLC purity:** 97.3 %

**HPLC  $t_R$ :** 16.4 min

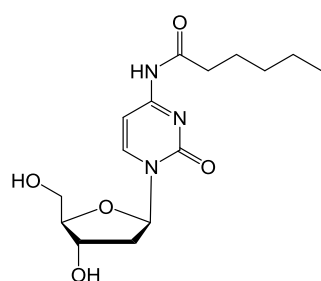
**$^1\text{H NMR}$  (DMSO- $d_6$ )**  $\delta$  0.86 (t,  $J$  = 6.8 Hz, 3H,  $\text{CH}_3$ ), 1.25 (br-m, 8H,  $\text{CH}_2$ - $(\text{CH}_2)_4$ - $\text{CH}_3$ ), 1.46-1.60 (m, 2H,  $\text{C}=\text{O}$ - $\text{CH}_2$ - $\text{CH}_2$ ), 1.98-2.31 (m, 2H,  $\text{HO}$ - $\text{CH}$ - $\text{CH}_2$ ), 2.38 (t,  $J$  = 7.4 Hz, 2H,  $\text{C}=\text{O}$ - $\text{CH}_2$ ), 3.53 - 3.64 (m, 2H,  $5'$ - $\text{CH}_2$ ), 3.85 (q,  $J$  = 3.8 Hz, 1H,  $4'$ - $\text{CH}$ ), 4.21 (m, 1H,  $3'$ - $\text{CH}$ ), 5.03 (t,  $J$  = 5.3 Hz, 1H,  $5'$ - $\text{OH}$ ), 5.25 (d,  $J$  = 4.2 Hz, 1H,  $3'$ - $\text{OH}$ ), 6.10 (t,  $J$  = 6.3 Hz, 1H,  $1'$ - $\text{CH}$ ), 7.22 (d,  $J$  = 7.4 Hz, 1H,  $6$ - $\text{CH}$ ), 8.31 (d,  $J$  = 7.5 Hz, 1H,  $5$ - $\text{CH}$ ), 10.81 (s, 1H,  $\text{NH}$ )

**$^{13}\text{C NMR}$  (DMSO- $d_6$ )**  $\delta$  14.40, 22.51, 24.93, 28.85, 28.89, 31.58, 36.81, 61.41, 70.40, 86.59, 88.36, 95.72, 145.42, 150.38, 154.93, 162.74, 174.39

**$m/z$ :** HRMS (TOF ES $^+$ )  $\text{C}_{17}\text{H}_{28}\text{N}_3\text{O}_5$   $[\text{M}+\text{H}]^+$  calculated 354.2023; found 353.7968

**m.p:** 122 – 125 °C

***N*-(1-((2*R*,4*S*,5*R*)-4-hydroxy-5-(hydroxymethyl)tetrahydrofuran-2-yl)-2-oxo-1,2-dihydropyrimidin-4-yl)hexanamide (48e)**



Hexanoic acid (1.1 mmol, 1 eqv, 127 mg, 138  $\mu$ L), **45** (1.1 mmol, 1 eqv, 250 mg)

**Yield:** 21.5 %

**HPLC purity:** 97.8 %

**HPLC  $t_R$ :** 13.2 min

**$^1\text{H NMR}$  (DMSO- $d_6$ )**  $\delta$  0.86 (t,  $J$  = 6.9 Hz, 3H,  $\text{CH}_3$ ), 1.22 – 1.31 (m, 4H,  $\text{CH}_2$ - $(\text{CH}_2)_2$ - $\text{CH}_3$ ), 1.50 – 1.58 (m, 2H,  $\text{C}=\text{O}$ - $\text{CH}_2$ - $\text{CH}_2$ ), 1.98 - 2.31 (m, 2H,  $\text{HO}$ - $\text{CH}$ - $\text{CH}_2$ ), 2.38 (t,  $J$  = 7.4 Hz,

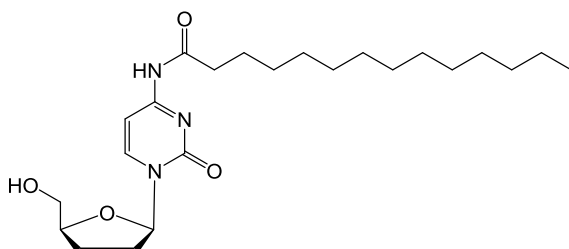
$^1\text{H}$  NMR (DMSO- $d_6$ )  $\delta$  2.31-2.42 (m, 2H, C=O-CH<sub>2</sub>), 3.55 - 3.63 (m, 2H, 5'-CH<sub>2</sub>), 3.85 (q,  $J$  = 3.8 Hz, 1H, 4'-CH), 4.19-4.23 (m, 1H, 3'-CH), 5.03 (t,  $J$  = 4.2 Hz, 1H, 5'-OH), 5.25 (d,  $J$  = 3.8 Hz, 1H, 3'-OH), 6.10 (t,  $J$  = 6.3 Hz, 1H, 1'-CH), 7.22 (d,  $J$  = 7.5 Hz, 1H, 6-CH), 8.31 (d,  $J$  = 7.5 Hz, 1H, 5-CH), 10.82 (s, 1H, NH).

$^{13}\text{C}$  NMR (DMSO- $d_6$ )  $\delta$  13.81, 21.83, 24.14, 30.67, 36.30, 40.87, 60.94, 69.92, 86.12, 87.88, 95.24, 144.95, 154.45, 162.27, 173.92

$m/z$ : HRMS (TOF ES<sup>+</sup>) C<sub>15</sub>H<sub>24</sub>N<sub>3</sub>O<sub>5</sub> [M+H]<sup>+</sup> calculated 326.1710; found 326.3216

$m.p$ : 120 – 125 °C

***N*-(1-((2*R*,5*S*)-5-(hydroxymethyl)tetrahydrofuran-2-yl)-2-oxo-1,2-dihydropyrimidin-4-yl)tetradecanamide (49a)**



Tetradecanoic acid (1.18 mmol, 1 eqv, 269 mg), **46** (1.18 mmol, 1 eqv, 250 mg)

**Yield:** 56.9 %

**HPLC purity:** 98.9 %

**HPLC t<sub>R</sub>:** 25.5 min

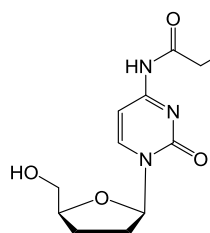
$^1\text{H}$  NMR (DMSO- $d_6$ )  $\delta$  0.85 (t,  $J$  = 6.7 Hz, 3H, CH<sub>3</sub>), 1.23 (br-m, 20H, CH<sub>2</sub>-(CH<sub>2</sub>)<sub>10</sub>-CH<sub>3</sub>), 1.46 - 1.59 (m, 2H, C=O-CH<sub>2</sub>-CH<sub>2</sub>), 1.69 – 1.89 (m, 2H, 3'-CH<sub>2</sub>), 1.90 – 2.00 (m, 1H, 2'-CH<sub>2</sub>), 2.31-2.42 (m, 1H, 2'-CH<sub>2</sub>), 2.37 (t,  $J$  = 7.3 Hz, 2H, C=O-CH<sub>2</sub>), 3.56 - 3.78 (m, 2H, 5'-CH<sub>2</sub>), 4.10 (m, 1H, 4'-CH), 5.10 (t,  $J$  = 5.3 Hz, 1H, 5'-OH), 5.92 (dd,  $J$  = 6.7, 2.5 Hz, 1H, 1'-CH), 7.19 (d,  $J$  = 7.4 Hz, 1H, 6-CH), 8.46 (d,  $J$  = 7.4 Hz, 1H, 5-CH), 10.78 (s, 1H, NH)

$^{13}\text{C}$  NMR (DMSO- $d_6$ )  $\delta$  13.95, 22.09, 23.96, 24.47, 28.43, 28.70, 28.85, 28.97, 29.00, 29.04, 31.28, 32.85, 36.32, 55.16, 61.54, 82.68, 86.86, 94.60, 145.03, 154.49, 162.22, 173.87

$m/z$ : HRMS (TOF ES<sup>+</sup>) C<sub>23</sub>H<sub>40</sub>N<sub>3</sub>O<sub>5</sub> [M+H]<sup>+</sup> calculated 422.3103; found 422.2637

$m.p$ : 127 – 130 °C

***N*-(1-((2*R*,5*S*)-5-(hydroxymethyl)tetrahydrofuran-2-yl)-2-oxo-1,2-dihydropyrimidin-4-yl)dodecanamide (49b)**



Dodecanoic acid (1.18 mmol, 1 eqv, 236 mg), **46**  
(1.18 mmol, 1 eqv, 250 mg)

**Yield:** 70.7 %

**HPLC purity:** 96.9 %

**HPLC  $t_R$ :** 22.9 min

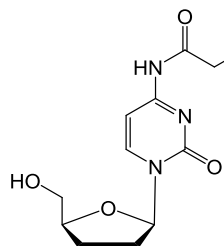
**$^1\text{H NMR}$  (DMSO- $d_6$ )**  $\delta$  0.85 (t,  $J$  = 6.8 Hz, 3H,  $\text{CH}_3$ ), 1.24 (br-m, 16H,  $\text{CH}_2$ - $(\text{CH}_2)_8$ - $\text{CH}_3$ ), 1.45 - 1.60 (m, 2H,  $\text{C}=\text{O}-\text{CH}_2-\text{CH}_2$ ), 1.71 - 1.89 (m, 2H, 3'- $\text{CH}_2$ ), 1.91 - 2.01 (m, 1H, 2'- $\text{CH}_2$ ), 2.30-2.42 (m, 1H, 2'- $\text{CH}_2$ ), 2.37 (t,  $J$  = 7.3 Hz, 2H,  $\text{C}=\text{O}-\text{CH}_2$ ), 3.54 - 3.80 (m, 2H, 5'- $\text{CH}_2$ ), 4.05 - 4.15 (m, 1H, 4'- $\text{CH}$ ), 5.10 (t,  $J$  = 5.3 Hz, 1H, 5'- $\text{OH}$ ), 5.92 (dd,  $J$  = 6.7, 2.5 Hz, 1H 1'- $\text{CH}$ ), 7.19 (d,  $J$  = 7.4 Hz, 1H, 6- $\text{CH}$ ), 8.46 (d,  $J$  = 7.4 Hz, 1H, 5- $\text{CH}$ ), 10.78 (s, 1H,  $\text{NH}$ )

**$^{13}\text{C NMR}$  (DMSO- $d_6$ )**  $\delta$  13.95, 22.09, 23.97, 24.47, 28.43, 28.70, 28.86, 28.97, 31.29, 32.85, 36.33, 55.17, 61.54, 82.69, 86.87, 94.60, 145.04, 154.49, 162.23, 173.86

**$m/z$ :** HRMS (TOF ES<sup>+</sup>)  $\text{C}_{21}\text{H}_{36}\text{N}_3\text{O}_4$   $[\text{M}+\text{H}]^+$  calculated 394.2700; found 394.5134

**$m.p$ :** 114 - 118 °C

***N*-(1-((2*R*,5*S*)-5-(hydroxymethyl)tetrahydrofuran-2-yl)-2-oxo-1,2-dihydropyrimidin-4-yl)decanamide (49c)**



Decanoic acid (1.18 mmol, 1 eqv, 189 mg), **46**  
(1.18 mmol, 1 eqv, 250 mg)

**Yield:** 68.3 %

**HPLC purity:** 92.1 %

**HPLC  $t_R$ :** 20.2 min

**$^1\text{H NMR}$  (DMSO- $d_6$ )**  $\delta$  0.85 (t,  $J$  = 6.8 Hz, 3H,  $\text{CH}_3$ ), 1.26 (br-m, 12H,  $\text{CH}_2$ - $(\text{CH}_2)_6$ - $\text{CH}_3$ ), 1.45 - 1.60 (m, 2H,  $\text{C}=\text{O}-\text{CH}_2-\text{CH}_2$ ), 1.69 - 1.89 (m, 2H, 3'- $\text{CH}_2$ ), 1.91 - 1.99 (ddt,  $J$  = 13.2, 7.6, 2.8 Hz, 1H, 2'- $\text{CH}_2$ ), 2.25-2.42 (m, 1H, 2'- $\text{CH}_2$ ), 2.36 (t,  $J$  = 7.1 Hz, 2H,  $\text{C}=\text{O}-\text{CH}_2$ ), 3.56 - 3.77 (ddd,  $J$  = 68.0, 12.1, 3.7 Hz, 2H, 5'- $\text{CH}_2$ ), 4.07 - 4.13 (dq,  $J$  = 6.0, 3.4 Hz, 1H, 4'-

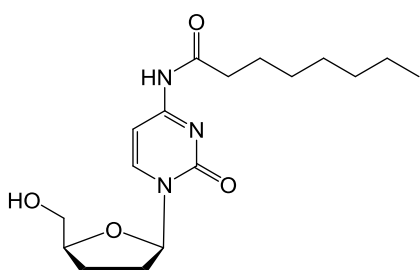
$^1\text{H}$  NMR (DMSO- $d_6$ )  $\delta$  5.10 (br-s, 1H, 5'-OH), 5.92 (dd,  $J$  = 6.7, 2.5 Hz, 1H 1'-CH), 7.19 (d,  $J$  = 7.4 Hz, 1H, 6-CH), 8.46 (d,  $J$  = 7.4 Hz, 1H, 5-CH), 10.78 (s, 1H, NH)

$^{13}\text{C}$  NMR (DMSO- $d_6$ )  $\delta$  13.95, 22.09, 23.97, 24.48, 28.44, 28.65, 28.71, 28.83, 31.26, 32.85, 36.33, 61.54, 82.69, 86.87, 94.61, 145.04, 154.50, 162.23, 173.88

$m/z$ : HRMS (TOF ES $^+$ )  $\text{C}_{19}\text{H}_{32}\text{N}_3\text{O}_4$  [M+H] $^+$  calculated 366.2387; found 366.2419

$m.p$ : 110 - 111  $^\circ\text{C}$

***N*-(1-((2*R*,5*S*)-5-(hydroxymethyl)tetrahydrofuran-2-yl)-2-oxo-1,2-dihydropyrimidin-4-yl)octanamide (49d)**



Octanoic acid (1.18 mmol, 1 eqv, 159 mg, 174  $\mu\text{L}$ ),

**46** (1.18 mmol, 1 eqv, 250 mg)

**Yield:** 58.9 %

**HPLC purity:** 90.1 %

**HPLC  $t_R$ :** 17.4 min

$^1\text{H}$  NMR (DMSO- $d_6$ )  $\delta$  0.87 (t,  $J$  = 6.9 Hz, 3H, CH $_3$ ), 1.27 (br-m, 8H, CH $_2$ -(CH $_2$ ) $_4$ -CH $_3$ ), 1.50 - 1.57 (m, 2H, C=O-CH $_2$ -CH $_2$ ), 1.69 - 1.91 (m, 2H, 3'-CH $_2$ ), 1.91 - 2.00 (m, 1H, 2'-CH $_2$ ), 2.25-2.45 (m, 1H, 2'-CH $_2$ ), 2.37 (t,  $J$  = 7.4 Hz, 2H, C=O-CH $_2$ ), 3.55 - 3.79 (ddd,  $J$  = 68.0, 12.1, 3.7 Hz, 2H, 5'-CH $_2$ ), 4.10 (dq,  $J$  = 6.1, 3.4 Hz, 1H, 4'-CH), 5.10 (br-s, 1H, 5'-OH), 5.92 (dd,  $J$  = 6.7, 2.5 Hz, 1H 1'-CH), 7.19 (d,  $J$  = 7.4 Hz, 1H, 6-CH), 8.46 (d,  $J$  = 7.4 Hz, 1H, 5-CH), 10.78 (s, 1H, NH)

$^{13}\text{C}$  NMR (DMSO- $d_6$ )  $\delta$  13.93, 22.04, 24.00, 24.48, 28.83, 28.42, 31.10, 32.84, 36.33, 61.54, 82.69, 86.66, 94.60, 145.05, 154.49, 162.22, 173.87

$m/z$ : HRMS (TOF ES $^+$ )  $\text{C}_{17}\text{H}_{28}\text{N}_3\text{O}_4$  [M+H] $^+$  calculated 338.2074; found 338.2345

$m.p$ : 103 - 106  $^\circ\text{C}$

### 3.4.2. Physicochemical Characterisation

#### 3.4.2.1. Stability to Inversion

Stability to inversion was carried out by weighing samples using an A and D GR-202 semi micro-analytical balance into 1.5 mL sample vials. Unless stated otherwise,

compound was solubilised at an elevated temperature and left to cool to room temperature for 18 h, prior to inversion.

Below are the individual methods used in **Chapter 3**, depending on solvent volume fraction used.

**Procedure for solvent promoted gelation:** Compounds **44**, **47a - 47e** and **48a - 48d** were weighed using an A and D GR-202 semi micro-analytical balance into 1.5 mL sample vials so that a final compound concentration would be either 0.1, 0.25 or 0.5 % (w/v) as per **Table 14** with a final sample volume was 500  $\mu$ L. The compound was solubilised in either DMSO or ethanol as per **Table 6** and sonicated for 1-2 minutes. Solutions were heated to 60  $^{\circ}$ C, using a made to measure aluminium heating vessel, to solubilise the compound before adding pre-heated (60  $^{\circ}$ C) ultra-purified water. The samples were left to cool to room temperature for 18 h, prior to inversion.

**Table 14:** Amount of compound needed to make final compound concentrations 0.5, 0.25 and 0.1 % (w/v) in 500  $\mu$ L.

Final Compound concentrations (% w/v)	Compound (mg)	Final Volume ( $\mu$ L)
0.5	2.5	500
0.25	1.25	500
0.1	0.5	500

**Procedure for solvent free gels ( $\Phi_{\text{sol}}$  0.00):** Compounds were weighed as per **Table 14** and made by addition of either ultra-purified water or RPMI 1640 (500  $\mu$ L). Samples were sonicated for 1 – 2 minutes before being heated to approximately 95  $^{\circ}$ C or until compound had completely solubilised. Sample was then left to cool.

**Gelation for cell culture procedures:** Compounds were weighed so as to generate gels with final compound concentrations of 0.5 and 1 % (w/v). A 2 % gelatine solution (250  $\mu$ L) was added to the solution followed by RPMI-1640 (250  $\mu$ L) so that the final gelatine concentration was 1 % as reported elsewhere.<sup>198</sup> The solution was sonicated for 1-2 minutes to solubilise the compound. The solution was heated to 95  $^{\circ}$ C to completely solubilise the compound before leaving the sample to cool.

### **3.4.2.2. Rheological Experiments**

Rheology was carried out using an Anton Paar MCR302 Modular Compact Rheometer. A four-bladed vane geometry was used with a diameter of 8.5 mm and length 8.5 mm in a cup with a diameter of 14.5 mm. The solution of gelator was prepared in 7 mL aluminium cups to a final sample volume of 2 mL, as per the method described in **Section 3.4.2.1**. Once the gel was prepared, the sample vial was mounted in the lower plate (cup) of the rheometer; the vane (attached to the upper part) was lowered into place, at a depth of 3 mm. This arrangement gave a total sample depth of approximately 16 mm in the 14.5 mm diameter cup which allowed positioning of the vane in the centre of the sample.

All rheological measurements were carried out in 7 mL aluminium vials to allow for heating of the sample prior to measurement.

Strain sweeps were carried out between  $\gamma = 0.05 - 100 \%$  at a constant angular frequency of 10 rad/s. Frequency sweeps were executed from 0.1 to 100 rad/s at a constant strain of 5 %, as dictated by the linear viscoelastic region from the strain sweep. Both strain and frequency measurements were carried out at 37 °C to mimic physiological conditions.

Gelation temperature ( $T_{\text{gel}}$ ) measurements were carried out at constant strain (5 %) and frequency (10 rad/s) between 25 and 80 °C at increasing intervals of 0.5 °C/min. Temperature profile ( $T_{\text{profile}}$ ) measurements were carried out by alternating the system temperature between 20 and 80 °C at 20 minute intervals at constant strain (5 %) and constant frequency (10 rad/s). Time dependant recovery measurements were carried out by alternating the strain between 5 % and 500 %; a system that could guarantee a stable gel at the lower strain and complete deformation at the higher strain. The strains were applied in 20 minute (5 %) and 5 minute (500 %) cycles. The frequency (10 rad/s) and temperature (37 °C) were kept constant throughout.

### **3.4.2.3. Scanning Electron Microscopy**

Scanning electron microscopy was performed on a JEOL JSM-6060LV compact scanning electron microscope. All samples were loaded onto suitable stub holders

with a 200  $\mu\text{L}$  micropipette fitted with sterile tips. The point of the tip was cut to increase the diameter and thus minimise the shear stress applied to the gels. The stubs were sputter coated with gold (Balzers Benchtop sputter coater SCD 030) under an argon atmosphere (50 Pa) at 30 mA for 4 minutes before imaging. Images were acquired using an electron beam of 7–22 kV.

#### 3.4.2.4. Transmission Electron Microscopy

Transmission electron microscopy (TEM) was carried out by dispersing a small amount of gel in 150  $\mu\text{L}$  of ultra-purified water and pipetting on to a graphene oxide, lacey carbon coated copper grid (No. 300). Excess sample was blotted with Whatman 50 filter paper. The grid was subjected to high vacuum in a Gatan dry pumping station (model 655) prior to inserting into the machine and imaging at an accelerated voltage of 100 kV.

#### 3.4.2.5. $^1\text{H}$ NMR of Gel to Sol state

**47d**  $\Phi_{\text{SOL}}$  0.00 was made in  $\text{H}_2\text{O}$  to a volume of 500  $\mu\text{L}$  into a 528-pp-7 NMR tube. A Wilmad<sup>®</sup> co-axial mounted capillary (50 mm, capacity 60  $\mu\text{L}$ ) containing  $\text{D}_2\text{O}$  was inserted into the middle of the NMR tube, as per **Figure 40**.

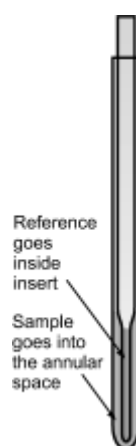


**Figure 40:** Co-axial insert mounted into NMR tube

The Sample was run on a Bruker AV400 NMR with a BBFO z-gradient probe. A  $^1\text{H}$  NMR was run with 1 scan with a 1 second relaxation delay so an accurate 90 degree pulse could be obtained for the samples being measured. The pulse sequence used to run the samples was a  $^1\text{H}$  pre-saturation experiment with excitation sculpting to allow a

better suppression of the HOD peak. These were measured at 25, 40, 55 and 70 °C allowing 15 minutes to equilibrate at each temperature, ensuring the temperatures used were both above and below measured gelation temperature.

#### **3.4.3. *In Vitro* Release Kinetics of Fluorescents**

Gels (**47d**  $\Phi_{\text{EtOH}}$  0.00) containing fluorescent dyes were prepared in 7 mL Aluminium cups to a final gel volume of 2 mL with the dye phase replacing the aqueous phase in each instance. Stock solutions of each dye were prepared so that the fluorescent output would be within the linear region of the calibration curves (0.15 mM Fluorescein and 0.06 mM Fluorescein isothiocyanate (FITC) Dextran 4 kDa and 0.08 mM FITC Dextran 10 kDa). Having prepared the gels as per method **3.4.2.1**, the gel volume was allowed to stand for 18 h to allow time for complete gelation. Phosphate Buffered Saline (PBS) (5 mL) was gently placed on top of each gel and the initial time point taken (150  $\mu\text{L}$ ,  $T_0$ ), subsequent readings (150  $\mu\text{L}$ ) were taken at further time points. After each time point the buffer volume (150  $\mu\text{L}$ ) was replaced and the fluorescence measured (excitation of 485 nm with the emission measured at 521 nm) using a Perkin Elmer plate reader.

#### **3.4.4. *In Vitro* Growth Inhibition Assays**

MCF-7 human breast adenocarcinoma, MIA PaCa-2 human pancreatic carcinoma and MKN-7 human stomach adenocarcinoma cell lines were cultured in RPMI-1640 medium supplemented with 10 % Foetal Bovine Serum (FBS). MRC-5 human fibroblast cells were cultured in modified eagles medium (MEM, containing sodium bicarbonate) supplemented with 10 % heat inactivated foetal calf serum, 1 % penicillin/streptomycin, 1 % L-glutamine (200 mM), 1 % non-essential amino acids (0.1 nM), 1 % 4-(2-hydroxyethyl)-1-piperazineethanesulfonic acid (HEPES) buffer (1 M) and 1 % sodium bicarbonate (7.5 %).

Cells were passaged upon reaching 60 - 80 % confluency and not used passed passage number 50. MTT was made in sterile PBS at a concentration of 2 mg/mL.

#### 3.4.4.1. Solution State

Cells were seeded at a density of  $3 \times 10^3$  cells per well into 96-well microtiter plates and allowed to adhere for 24 h before test agent was introduced (0.1 nM – 100  $\mu$ M,  $n = 8$ ). Stock solutions of each compound were prepared in DMSO (10 mM) to aid solubilisation and further dilutions were prepared in RPMI-1640 medium prior to each assay. At the time of agent addition a control sample was treated with 3-(4,5-dimethylthiazol-2-yl)-2,5-diphenyltetrazolium bromide (MTT) (final concentration 400  $\mu$ g/mL) to generate our  $T_0$  sample reading. Cells were incubated with test agent for 72 h at 37 °C and 5 %  $CO_2$ . Following this exposure MTT was added to each well (final concentration 400  $\mu$ g/mL) and re-incubated at 37 °C for 2.5 h to allow reduction of MTT by viable cells (mitochondrial dehydrogenases) to insoluble formazan crystals. Well supernatants were removed, and intracellular formazan solubilized by addition of DMSO (150  $\mu$ L). Absorbance was read at 550 nm using a Perkin Elmer plate reader. Non-linear regression analysis was used to calculate compound concentrations required to inhibit 50 % of cell growth ( $GI_{50}$ ).

#### 3.4.4.2. Gel state, Cell Adhesion Assays

##### 3.4.4.2.1. Cells Seeded onto Gels

Gels were made as per the procedure listed in 6.3.2.3. However, before leaving to cool the solution was aliquoted into a 24-well plate as per **Figure 6.2** to a final gel volume of 50  $\mu$ L well; enough to cover the bottom of the well plate. Two final concentrations were used based upon the solution state MTT a gel with concentration matching the  $GI_{50}$  and a gel with  $2 \times GI_{50}$  concentration. The gels were left to cool for 18 h in a sterile environment before incubating at 37 °C and 5 %  $CO_2$  for 2 h. MIA PaCa-2 cells were seeded at a density of  $1 \times 10^4$  cells/well into the 24-well microtiter plates and incubated at 37 °C and 5 %  $CO_2$ . At 24, 48 and 72 h time points, 3-(4,5-dimethylthiazol-2-yl)-2,5-diphenyltetrazolium bromide (MTT) (final concentration 400  $\mu$ g/mL) was added to each cell containing well and the plates again incubated for a further 2.5 h to allow reduction of MTT by viable cells (mitochondrial dehydrogenases) to insoluble formazan crystals. Well supernatants were removed, and intracellular

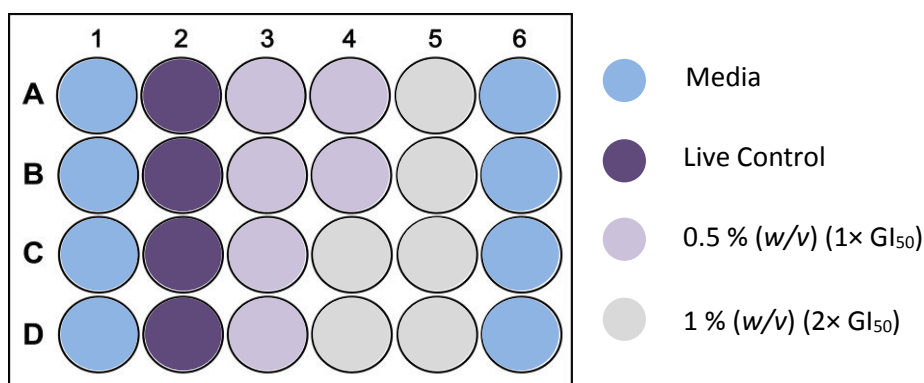


Figure 41: 24 well plate arrangement of MTT cell adhesion assays

formazan solubilized by addition of DMSO (300  $\mu$ L). Absorbance was read at 550 nm using a Perkin Elmer plate reader.

#### 3.4.4.2.2. Gels injected onto cells

Gels were made as per the procedure listed in 6.3.2.3. However, before leaving to cool the solution was transferred into a 1 mL syringe through a 19G needle.

MIA PaCa-2 cells were seeded  $1 \times 10^4$  cells/ well into the 24-well microtiter plates and incubated at 37 °C and 5 % CO<sub>2</sub> for 24 h allowing cells to adhere before adding the pre-prepared gels.

Medium was aspirated and 50  $\mu$ L of each gel injected on to the cells as per **Figure 41**. Two final concentrations were used based upon the solution state MTT a gel with concentration matching the GI<sub>50</sub> and a gel with  $2 \times$  GI<sub>50</sub> concentrations. Media was re-introduced onto the gel/cell system and the plates incubated at 37 °C and 5 % CO<sub>2</sub>. At the time of agent addition a control sample was treated with MTT (final concentration 400  $\mu$ g/mL) to generate a T<sub>0</sub> sample reading. At 24, 48 and 72 h time points MTT (final concentration 400  $\mu$ g/mL) was added to each cell containing well and the plates again incubated for a further 2.5 h to allow reduction of MTT by viable cells (mitochondrial dehydrogenases) to insoluble formazan crystals. Well supernatants were removed, and intracellular formazan solubilised by addition of DMSO (300  $\mu$ L). Absorbance was read at 550 nm using a Perkin Elmer plate reader.

### 3.4.4.3. Gel state, Cell Proliferation Assays

Assays were carried out using either MIA PaCa-2 pancreatic adenocarcinoma cells or a control MRC-5 human fibroblast cell line. Cell proliferation was monitored and quantified using the colorimetric MTT assay and a methylene blue staining assay, measuring cell viability at 24, 48 and 72 h following treatment with the hydrogel. Cells were prepared in a 6 well cell culture plate as shown in **Figure 42**. Each gel was prepared in sterile tissue culture conditions by solubilising gelator (by heating to 95 °C) in RPMI-1640 to the desired final compound concentration (0.5 or 1 % (w/v)). Upon complete solubilisation the gels were deposited into syringes and left to cool for 18 h prior to use.

*n.b. 0.5 % and 1 % represent 1 × and 2 × GI<sub>50</sub> found from solution state MTT assay.*

MIA PaCa-2 cells were seeded at a density of  $1 \times 10^4$  cells/well and MRC-5 cells were seeded at  $5 \times 10^4$  cells/well in 3 mL of medium. Cells were incubated for 24h at 37 °C and 5 % CO<sub>2</sub> to allow time for adhesion. After 24 h media was aspirated and the test agent added to a final volume of 50 µL through a 19G needle. For those wells in which gel was injected directly on to the cells; gels were injected directly into the centre of the well and allowed to re-assemble for 1 minute following shear before adding media (3 mL) to the well again. For those wells in which gel was injected into media; media (3 mL) was re-introduced to the well following aspiration and the gel (50 µL) introduced into the medium towards the centre of the well, forming a raft.

**MTT Colorimetric assay:** At 24, 48 and 72 h time points 3-(4,5-dimethylthiazol-2-yl)-2,5-diphenyltetrazolium bromide (MTT) (final concentration 400 µg/mL) was added to each cell containing well and the plates again incubated for a further 2.5 h to allow reduction of MTT by viable cells (mitochondrial dehydrogenases) to insoluble formazan crystals. Well supernatants were removed, and intracellular formazan solubilized by addition of DMSO (5000 µL). Aliquots (150 µL) were removed from the wells and the absorbance was read at 550 nm using a Perkin Elmer plate reader.

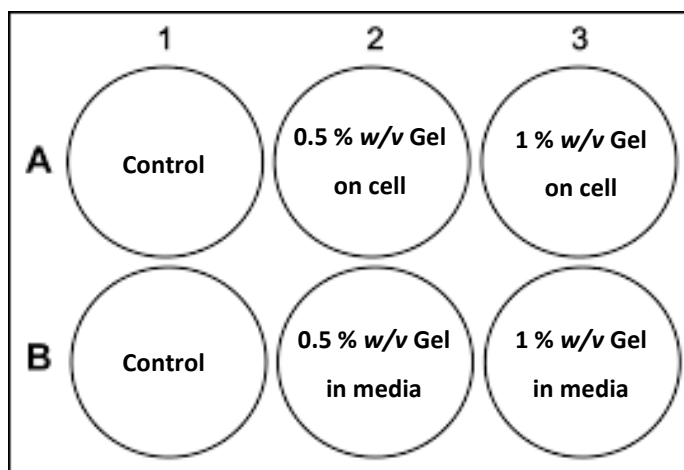


Figure 42: 6 well plate arrangement for gel state, cell proliferation assays.

**Methylene blue proliferation assay:** At 24, 48 and 72 h time points medium was aspirate from the wells and the wells washed in cold phosphate buffered saline (PBS)(1 mL  $\times$  2). The PBS was aspirated and the cells fixed with methanol (500  $\mu$ L) for 10 minutes. Methanol was aspirated and 0.05 % methylene blue (50:50 water: methanol) staining solution was added and the plates left at room temperature for 10 minutes. Colonies were rinsed in water and air dried. Individual colonies were photographed under an optical microscope.

## 4. Therapeutic Molecular Gels of Gemcitabine

---

Therapeutic self-assembled gels represent a novel class of active biomaterial, whereby a functionalised linker can be covalently conjugated to a therapeutic, this method doesn't rely upon diffusion controlled release or stimulus triggered release; the gel itself is the therapeutic. **(Figure 3)** Prodrug based self-assembled materials are advantageous as they provide an opportunity to alter the solubility of a drug, enhance drug loading and eliminate the use of potentially harmful excipients. Additionally, self-assembled prodrugs can be tailored to undergo controlled release or breakdown in response to particular biological cues.

Several factors must be taken into consideration when designing a low molecular weight (LMW) gelating prodrug:

- i. Which functional groups are available for prodrug derivatisation
- ii. The choice of pro-moiety; unless the drug is inherently lipophilic, this should be safe and easily excreted, it should also be lipophilic to create the necessary amphiphilicity. It should also be safe and easily excreted
- iii. The pro-moiety should be relevant to disease state, dose and duration of therapeutic need i.e. the enzyme cleavability of the linker between should be designed

Traditional drug discovery says that some of the most common functionalities amenable to prodrug design include carboxylic, hydroxyl, amine, phosphate and carbonyl groups. From this core functionality we can create prodrugs containing esters, carbonates, carbamates, amides, phosphates and oximes.<sup>92</sup>

Initially, it was hypothesised that creating an amphiphilic prodrug of the chemotherapeutic gemcitabine would enhance its delivery, with emphasis placed upon the management of difficult to treat cancers, including gastric and pancreatic cancers. Adopting this method a therapy for intra-tumoural chemotherapeutic delivery could be generated. Another motivation for this approach was the

opportunity to prevent or retard the first pass metabolism of gemcitabine by cytidine deaminase (CDA) and deoxycytidine deaminase (dCDA). (**Section 1.2.1**)

Gemcitabine (**30**) (dFdC) contains 3 nucleophilic groups available for prodrug development (**Figure 43**) whilst also containing the hydrophilic sugar moiety and cytosine nucleobase that was hypothesised to possess the necessary hydrogen bonding donor and acceptor groups required to create the one dimensional order needed to initiate gelation.

Envisaged were libraries of analogues with differing cleavable linkages conjugated to either the exocyclic primary amine of the cytosine nucleobase or the hydroxyl moieties of the ribose sugar that could be synthesised with ease, were biocompatible but had therapeutic efficacy and could be broken down either enzymatically or by a change in pH both *in vitro* and *in vivo*.

Currently there are no such gelating entities existing for the treatment of pancreatic and gastric cancers.

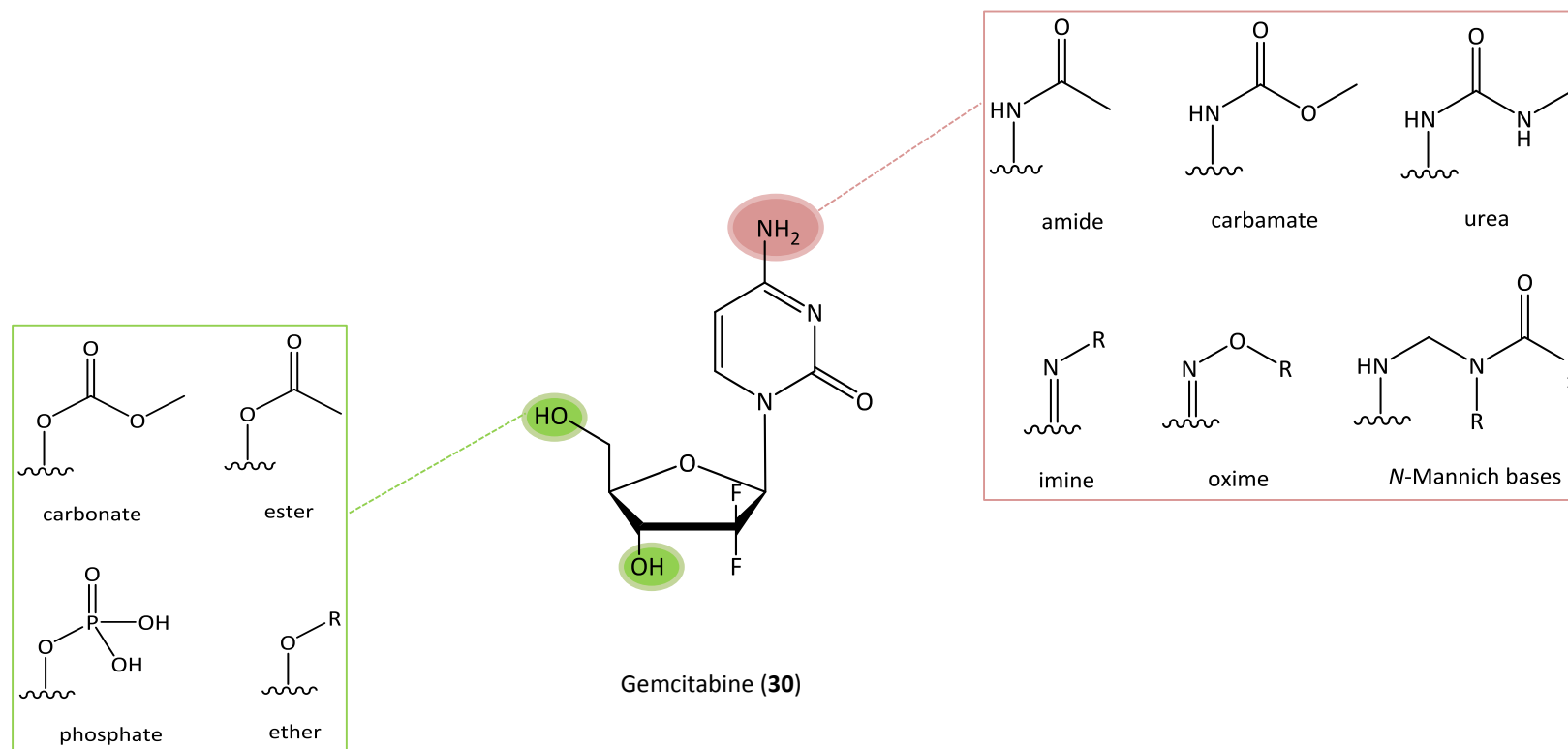


**Figure 43: Structure of Gemcitabine showing functional groups available for derivatisation.**

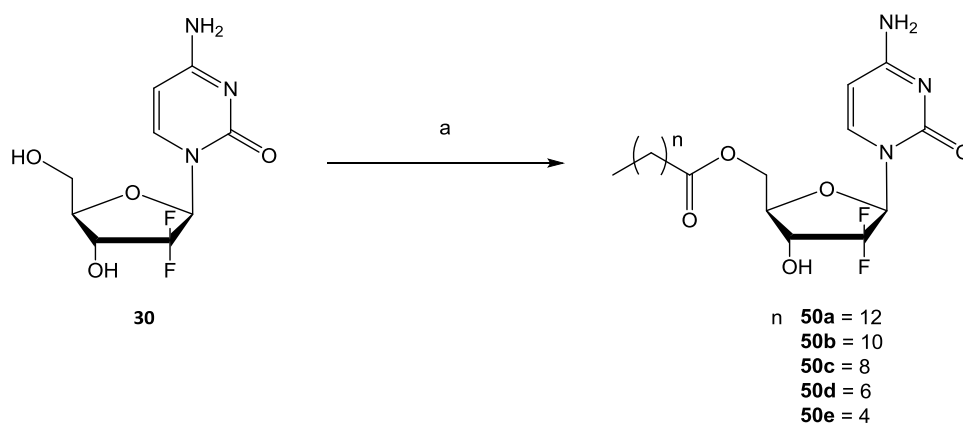
Components in green represent potential pro-moieties for 5' and 3'-hydroxyls. Components in pink represent potential pro-moieties for *N*-functionalisation

## 4.1. Synthesis

### 4.1.1. A Regioselective Enzymatic Synthesis of Gemcitabine-5'-ester Prodrugs

Ester prodrugs are the most common functionalities used in prodrug design as they proffer the opportunity to enhance lipophilicity, improving passive membrane permeability of water soluble drugs.<sup>200</sup> Additionally, the synthesis of an ester prodrug is often a very simple process and once in the body the ester bond is readily hydrolysed by ubiquitous esterases. There already exist examples of efficacious gemcitabine-ester prodrugs,<sup>149,150,201</sup> functionalised off either the 3' or 5'-hydroxyl. However, referring back to the studies carried out in **Chapter 3** describing the importance of both the 2'- and 3'-hydroxyl groups to the gelation process of the inert gemcitabine analogue 2'-deoxycytidine, the attention was instead focused on the development of prodrugs derivatised from the 5'-hydroxyl.

Modification of the ribose sugar has been reported previously for the nucleoside chemotherapeutic cytarabine.<sup>202</sup> However, this strategy involved a sequence of protection-deprotection measures and resulted in a limited overall yield. Additionally, owing to the cytotoxic nature of gemcitabine, it was desirable to contain all synthesis to one-pot. Therefore, 5'-hydroxyl functionalisation was carried out using a one-pot method reported previously for the acylation of uracil derivatives.<sup>203,204</sup> Gemcitabine (**30**) was stirred at 50 °C in the presence of a vinyl ester with differing carbon chain lengths in an azeotrope of hexane and pyridine (1:3), catalysed by the enzyme Lipase B *Candida Antarctica* (CAL-B, Novozyme 435<sup>®</sup>), recombinant from yeast to generate **50a - 50e**. (**Scheme 4**) The presence of the immobilised enzyme ensuring that the reaction is extremely clean, requiring only a simple vacuum filtration to remove the immobilised lipase, followed by purification through a silica plug. This method is particularly advantageous as the stability and reusability of immobilised CAL-B in organic solvents is very high, as was reported before for similar biocatalytic processes,<sup>203,205,206</sup> making it very cost effective. Furthermore, in contrast to chemical synthesis, the enzymatic procedure presented with regioselectivity for the 5'-hydroxyl.



**Scheme 4: Scheme for the synthesis of Gemcitabine-5'-ester prodrugs**

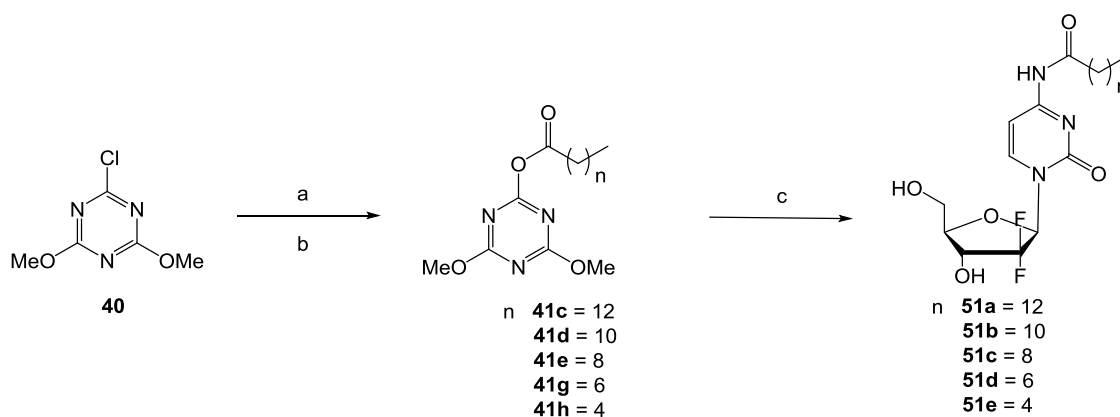
Reagents and Conditions: Gemcitabine, hexane/pyridine (v/v 1:3), vinyl ester (C=C-OCOR), lipase B *Candida Antarctica* (CAL-B), 50 °C, 6h

X-ray crystallographic studies<sup>207,208</sup> have shown that regioselective acylation at the 5'-hydroxyl is possible as the CAL-B contains a medium sized pocket in which the nucleoside binds. The size of the pocket can only compensate for a functional group at the 2'-position, when it is no larger than a propyl. The additional bulk introduced by the presence of the 2', 2'-difluoro on the ribose sugar potentially causes a steric clash resulting in a destabilisation of the ribose conformation forcing the 3'-hydroxyl toward the outside of the pocket and rendering the 5'-hydroxyl the only available hydroxyl for functionalisation.

The ester prodrugs were synthesised with chain lengths ranging from a tetradecanoyl to a hexanoyl, for varying degrees of lipophilicity.

#### 4.1.2. Synthesis of Gemcitabine-*N*-functionalised prodrugs

As mentioned previously covalently coupling to the 4-amino position is a route often taken when designing prodrugs of gemcitabine due to the opportunity to increase both chemical and enzymatic stability and to block the site of potential deamination, thus improving overall therapeutic efficacy. Amides, carbamates and ureas were chosen as appropriate derivatives to achieve this aim. Each one is considerably more stable to enzymatic breakdown *in vivo* than an ester, with the ureas being the least likely to undergo rapid hydrolysis.



**Scheme 5: Synthesis of Gemcitabine-N-acyl derivatives**

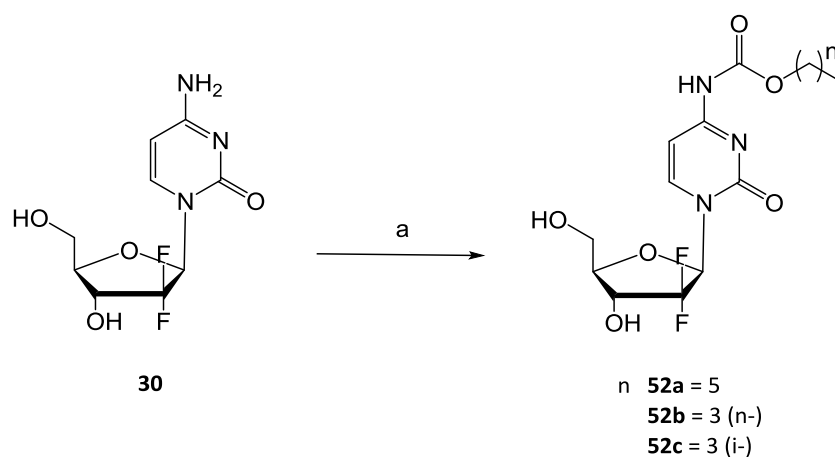
Reagents and Conditions: (a) *N*-methylmorpholine, CH<sub>2</sub>Cl<sub>2</sub>, 0 °C, 1h (b) carboxylic acid, CH<sub>2</sub>Cl<sub>2</sub>/DMF, 0 °C, 1h (c) gemcitabine, DMF, 0 °C - 50 °C, 18 - 24 h

Stability: Ester > Amide > Carbamate > Urea

Although amides undergo hydrolysis by esterases *in vitro*, the rates are usually too slow and insufficiently competitive to be considered useful *in vivo*. For this reason and due to a limited promiscuity of mammalian amidases, amides are not commonly used in prodrug design; however, there are examples of gemcitabine-*N*-amides that are not considered prodrugs but due to an increased lipophilicity (usually introduced *via* a long chain fatty acid) exhibit an enhanced therapeutic effect as a result of increased passive diffusion.<sup>209-211</sup> Increased stability to hydrolysis would too be advantageous from a controlled release perspective, particularly when delivering highly potent compounds such as gemcitabine, as this would enable the delivery of much lower doses and may prolong the therapeutic effect.

Amide derivatives were synthesised using the procedure reported in previous chapters. (**Scheme 5**) An activated triazine ester was used as an intermediate to regioselectively functionalise the exocyclic amine of the cytosine nucleobase with fatty acid chains of variable lengths; tetradecanoyl to hexanoyl.

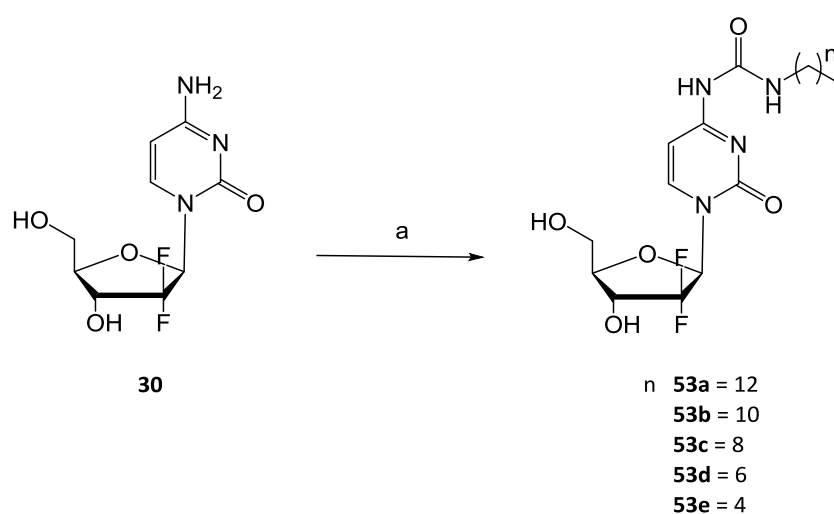
Although they are considerably more stable to enzymatic breakdown than esters, carbamates do not differ significantly in structure; where the ester contains a single



**Scheme 7: Synthesis of gemcitabine-N-carbamates**

Reagents and Conditions: gemcitabine, CH<sub>2</sub>Cl<sub>2</sub>, R-OCOCl, pyridine, 0 °C – r.t., 3h

oxygen heteroatom adjacent to the carbonyl, a carbamate contains an additional nitrogen on the opposite side of the carbonyl carbon to that of the oxygen. The carbamate series was synthesised in a single step; gemcitabine and acyl chloroformates, either hexyl or butyl (*n*- or *i*-) were solubilised in CH<sub>2</sub>Cl<sub>2</sub> at 0 °C in the presence of a small amount of pyridine, acting in a basic capacity, before increasing the temperature to r.t. and allowing the reaction to proceed for 3-4 h. (Scheme 7)



**Scheme 6: Synthesis of gemcitabine-N-urea derivatives.**

Reagents and Conditions: gemcitabine, DMF, N<sub>2</sub>, R-N=C=O, r.t., 3h

Ureas are very rarely used in prodrug design due to significant stability to *in vivo* enzyme degradation; however urea derivatives have long been known to facilitate gelation<sup>212</sup> and may potentially be hydrolysed by ubiquitous ureases. Urea derivatives were synthesised in a single step by solubilising gemcitabine and acyl isocyanates of varying chain lengths in DMF under a nitrogen atmosphere before stirring for 3 h.<sup>213</sup> (Scheme 6)

#### 4.1.3. Can existing LMWGs gelators be used as a mode to facilitate gelation?

Further to a simple 'prodrug' strategy, it was thought that functionalising gemcitabine with an existing LMW gelator could enhance the self-assembly process, whilst retaining the cytotoxic character of the chemotherapeutic. Many of the more established LMWG systems stem from amino acid/di-peptide derivatives.<sup>49,152,214,215</sup> Fluorenylmethoxycarbonyl chloride (Fmoc, **54**) protected amino acids make up the bulk of these known amino acid gelating entities due to the large aromatic system contributing stabilising  $\pi$ - $\pi$  interactions. Below, (Figure 44) four potential gelating entities; Fmoc-gamma amino butyric acid (Fmoc-GABA-OH, **55**), Fmoc-alanine (Fmoc-Ala-OH, **56**), Fmoc-phenylalanine (Fmoc-Phe-OH, **57**) and the most well documented Fmoc-diphenylalanine (Fmoc-Phe-Phe-OH, **58**) were chosen

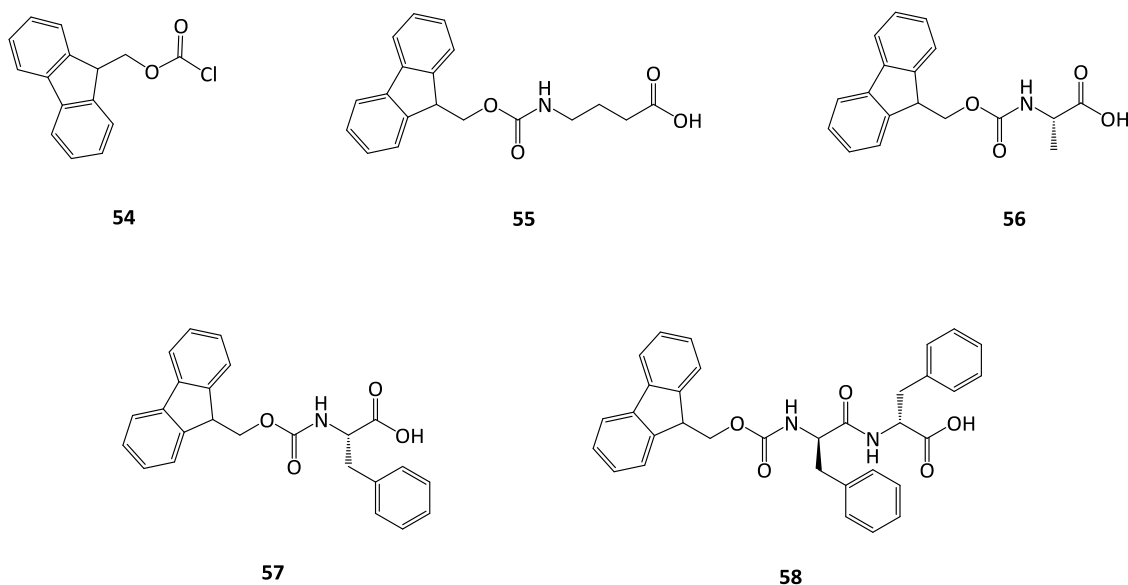


Figure 44: Fmoc-amino acid structures

as potential functionalities. **55** and **56** have very similar cLogP values ( $\sim 3.5$ ) but differ in the way they would potentially assemble; **54** has additional van der Waals forces contributed by the carbon chain of the butyric acid and so should theoretically display an increased stability. **57** was the most hydrophobic of the Fmoc-protected amino acids due to the presence of two phenyl rings, giving a cLogP value of 6.13.

#### 4.1.3.1. 4-amino coupling of Fmoc-protected amino acids

Given the variety of available peptide coupling reagents<sup>216</sup> (**Figure 45**), **56** was used to determine which, amongst, 1-ethyl-3-(3-dimethylaminopropyl)carbodiimide, (EDC, **59**) N,N'-dicyclohexylcarbodiimide (DCC, **60**) and 1-[Bis(dimethylamino)methylene]-1*H*-1,2,3-triazolo[4,5-*b*]pyridinium 3-oxidhexafluorophosphate, *N*-[(Dimethylamino)-1*H*-1,2,3-triazolo-[4,5-*b*]pyridin-1-ylmethylene]-*N*-methylmethanaminium hexafluorophosphate *N*-oxide (HATU, **61**) would deliver the 4-amino gemcitabine amino acid conjugate in the best yield with greatest regioselectivity.

The EDC and DCC reactions proceeded by solubilisation of Fmoc-Ala-OH (**56**), EDC (**59**) or DCC (**60**) and hydroxybenzotriazole (HOBt) in anhydrous DMF at 0 °C. A solution of gemcitabine and DMAP were added before increasing the temperature to r.t. The yields from the EDC and DCC reactions were 9.6 % and 21.9 %, respectively. The limited conversion and reduced yields is likely due to the potential side reactions associated with these coupling agents. (**Scheme 8**) Typical formation of the amide is relatively straightforward. The carboxylate anion, (produced

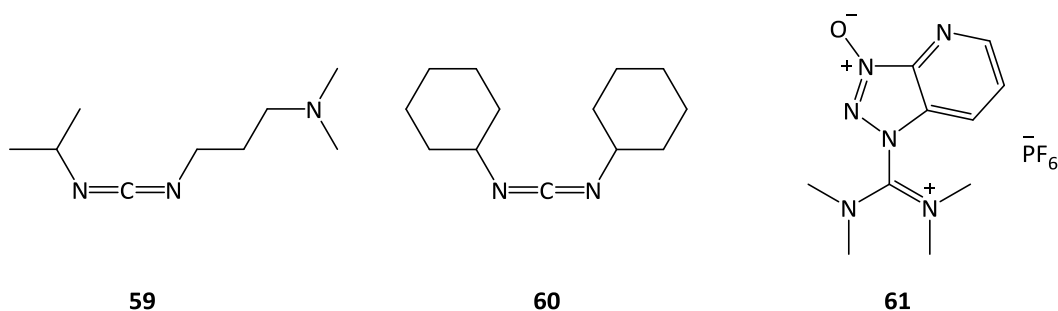
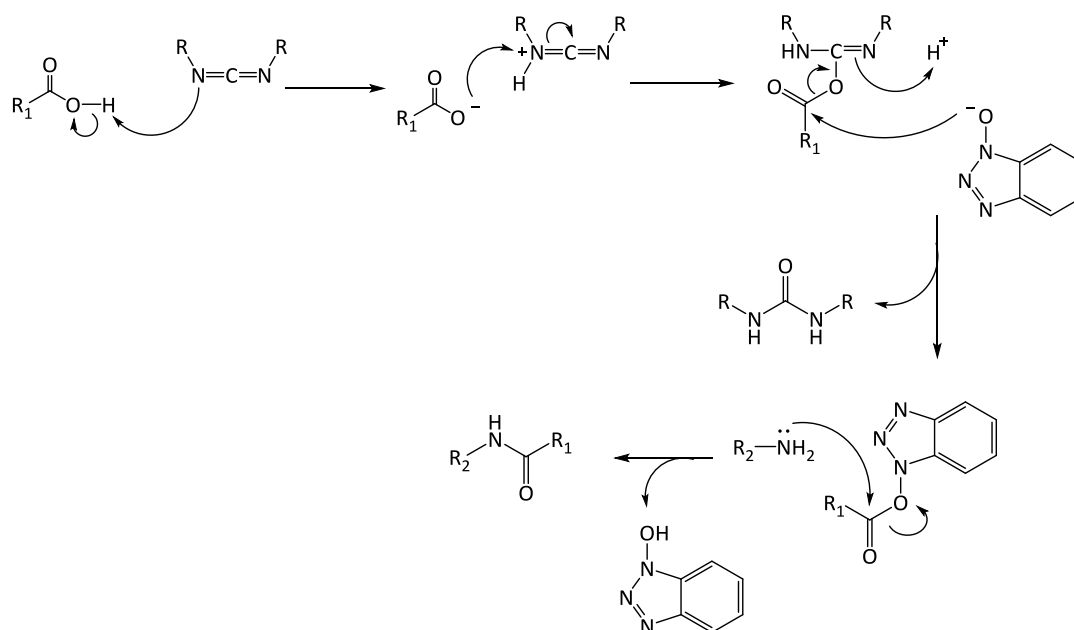


Figure 45: Peptide coupling agents EDC, DCC and HATU

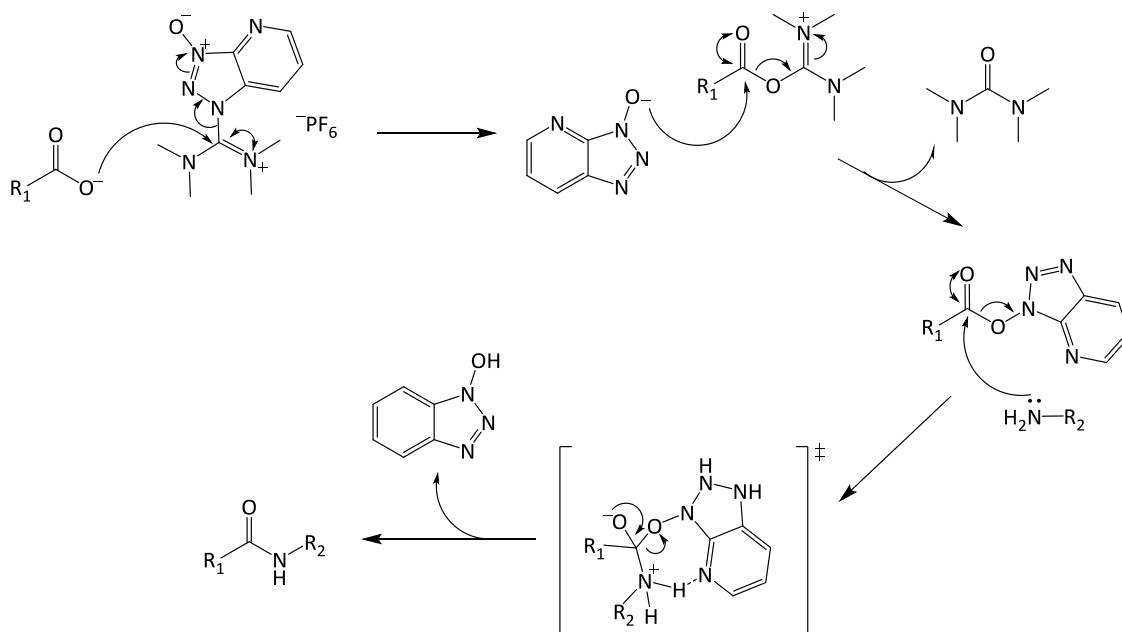




Scheme 9: Mechanism of EDC/DCC peptide coupling

amide (**67**) giving the desired product. Were the intermediate **62** to undergo an intramolecular rearrangement then a stable *N*-acylurea (**65**) would be generated; the undesired product.

However, peptide coupling activated by HATU proceeded by solubilisation of **56** and HATU (**61**) in anhydrous DMF at 0 °C. Gemcitabine, *N,N*-diisopropylethylamine



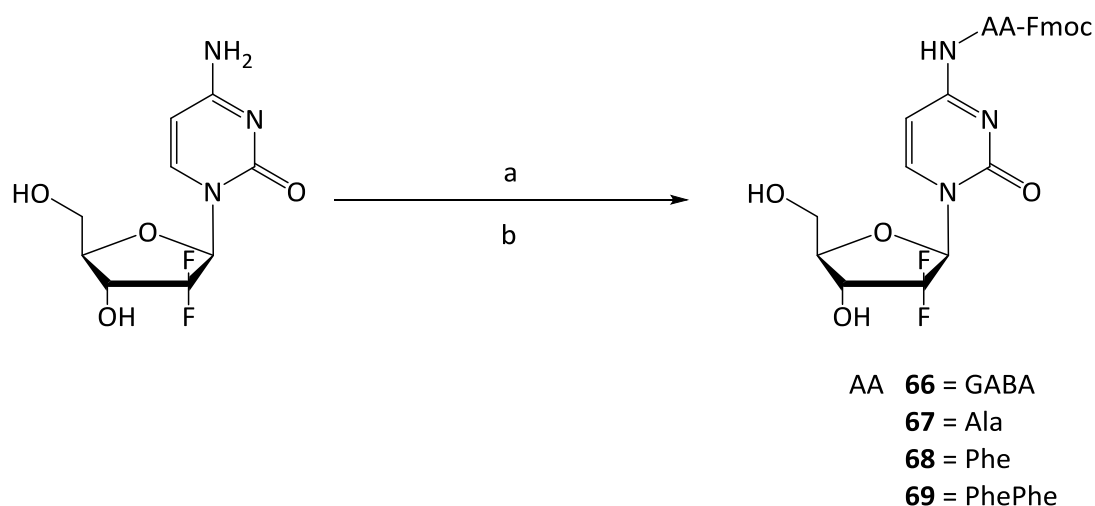
Scheme 10: Mechanism of HATU coupling

(DIPEA) was added as a solution in DMF prior to increasing the temperature to r.t. achieving the desired product in a 77 % yield following silica column purification. The proposed mechanism is shown in **Scheme 10**. The carboxylate anion of **56**, generated by basic deprotonation using DIPEA, attacks the highly reactive **61** to form the unstable *o*-acyl(tetramethyl)isouronium salt, which undergoes rapid nucleophilic attack by the liberated 1-oxy-7-azabenzotriazole anion to afford the corresponding azabenzotriazole ester and a stoichiometric quantity of tetramethylurea. Addition of a nucleophile (**30**) results in amination to afford **67**.

The efficiency of this coupling process over and above that of EDC and DCC arises from a neighbouring group effect brought about by stabilisation of the incoming amine by the pyridine nitrogen atom, through a 7-membered ring transition state.

Given the vast difference in achievable yields between the reaction of **56** with EDC/DCC and HATU, there was no doubt that the most efficient way to generate a library of peptides was to use HATU as the primary coupling agent. (**Scheme 11**)

**66 - 69** were synthesised as per the previously mentioned procedure, with an additional preparative HPLC purification step to fully remove any remaining urea



**Scheme 11: Synthesis of Gemcitabine-N-amino acid Fmoc conjugates**

Reagents and Conditions: a) Fmoc-AA-OH, HATU, anhydrous DMF, N<sub>2</sub>, 0 °C, 1 h b) Gemcitabine, DIPEA, anhydrous DMF, N<sub>2</sub>, 0 °C – r.t. 22h

Table 15: Calculated yields from peptide coupling reactions with gemcitabine

Compound	Yield (%)		
	EDC	DCC	HATU
66	-	-	67.1
67	9.6	21.9	77.0
68	-	-	53.3
69	-	-	59.8

by-products that weren't removed during standard silica column chromatography. Following this purification, Fmoc-protected gemcitabine-*N*-amino acids were generated in 53 – 77 % yields (**Table 15**).

## 4.2. Physical Characterisation

It is known that gelation is a solubility driven process and that there is a close relationship between lipophilicity (cLogP) and the predicted water solubility (LogS<sub>w</sub>). LogS<sub>w</sub> (water solubility values to the logarithm (base 10)); represents the predicted water solubility of a compound measured in mol/litre at pH 7.4 and 25 °C.

The lower the cLogP value (typically 1 – 3) the more aqueous soluble a compound will be therefore the higher the chance of obtaining a hydrogelator. As cLogP increases gelation becomes dependent on solubility in organic media and thus preference is directed towards a binary organic solvent/water system. Similarly, the higher the LogS<sub>w</sub> value the more water soluble the compound and thus the greater the chance of displaying desirable aqueous solubility driven gelation properties. The calculations of LogS<sub>w</sub> were carried out using ACD labs prediction software.

Listed in **Table 16** are the cLogP and LogS<sub>w</sub> values series **50a - 50e**, **51a - 51e**, **52a - 52c** and **53a - 53e** including the values for the successful gelators (**42c** and **48d**) from previous chapters, as a comparison.

Despite containing a free primary amine on the cytosine nucleobase the predicted LogS<sub>w</sub> values of the ester series (**50a - 50e**) in water are relatively low. cLogP values of the 5'-esters range from 5.88 for the longest chain tetradecanoyl conjugate (**50a**) to 1.65 for the shortest chain hexanoyl conjugate (**50e**) and based upon the previous chapter we would anticipate seeing gelation for **50e** under the same heating conditions used for **48d**.

Water solubility was again predicted using ACD labs for series **51**, **52** and **53**, and we can see that the compounds with the highest cLogP have the lowest predicted water solubility value. Based on these analyses we would expect efficient gelation to occur in **51e** due to the similarity in both cLogP values and LogS<sub>w</sub> values; both being within 10 % of the lipophilicity and solubility found in (**48d**). Additional gelators were anticipated from **52a** and **52d** based upon the similarity of predicted water solubility, though there is an apparent difference in cLogP (> 10 %)

A similar analysis of solubility was carried out for compounds **66 – 69** (**Table 17**). In contrast to the compounds mentioned above, the addition of a hydrophobic Fmoc-protected amino acid sequence to gemcitabine considerably reduces the predicted water solubility of each compound. (**Figure 47**) Additionally, there seems only a minimal improvement in cLogP of the amino acid gelators by the addition of gemcitabine, noting an average decrease in cLogP of around 0.39. These features suggest that these gelators may not possess the necessary physical characteristics to successfully undergo gelation however, as they have the lowest cLogP and highest LogS<sub>w</sub> **66** and **67** stand the best chance of being successful gelators.

Table 16: cLogP and predicted water solubility values for compound 50a - 50e, 51a - 51e, 52a - 52c and 53a - 53e

Compound	n	cLogP	Predicted LogS <sub>w</sub> (ACD labs)
30	-	-0.71	-0.56
42c	12	4.31	-5.09
48d	6	1.44	-2.56
50a	12	5.88	-4.78
50b	10	4.82	-4.55
50c	8	3.77	-4.03
50d	6	2.71	-3.20
50e	4	1.65	-2.37
51a	12	5.80	-5.77
51b	10	4.74	-5.19
51c	8	3.68	-4.59
51d	6	2.62	-3.97
51e	4	1.56	-3.33
52a	5	2.36	-2.83
52b	3 ( <i>n</i> -)	1.3	-2.00
52c	3 ( <i>i</i> -)	1.17	-1.83
53a	12	5.38	-5.10
53b	10	4.32	-4.28
53c	8	3.26	-3.45
53d	6	2.21	-2.62
53e	4	1.15	-1.79

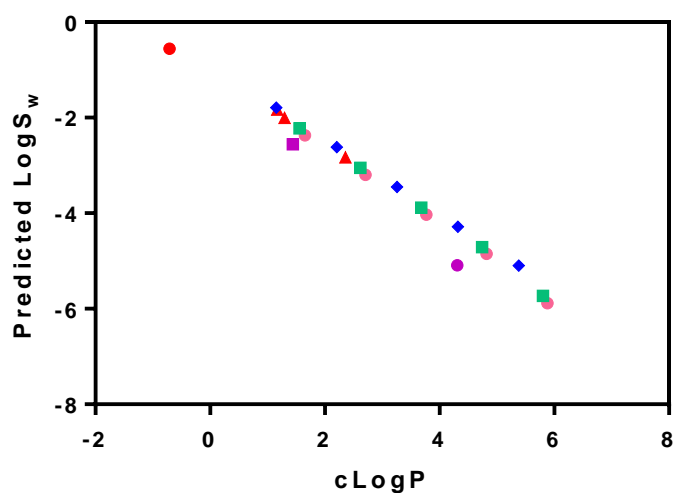


Figure 46: Relationship between cLogP and predicted water solubility for ester (50a – 50e), amide (51a – 51e), carbamate (52a – 52c) and urea (53a – 53e) derivatives of gemcitabine.

Gemcitabine (red circle), 42c cytidine gelator (purple circle) 48d 2'-deoxycytidine hydrogelator (purple square), ester series (pink circle), amide series (green square), carbamate series (red triangle), urea series (blue diamond)

Table 17: cLogP and predicted water solubility values for compound 55 - 58 and 66 - 69

Compound	cLogP	Predicted LogS <sub>w</sub> (ACD labs)
30	-0.71	-0.56
42c	4.31	-5.09
48d	1.44	-2.56
55	3.58	-3.94
56	3.46	-3.90
57	4.87	-5.56
58	6.13	-7.50
66	3.38	-5.14
67	3.02	-5.11
68	4.44	-6.78
69	5.60	-8.71

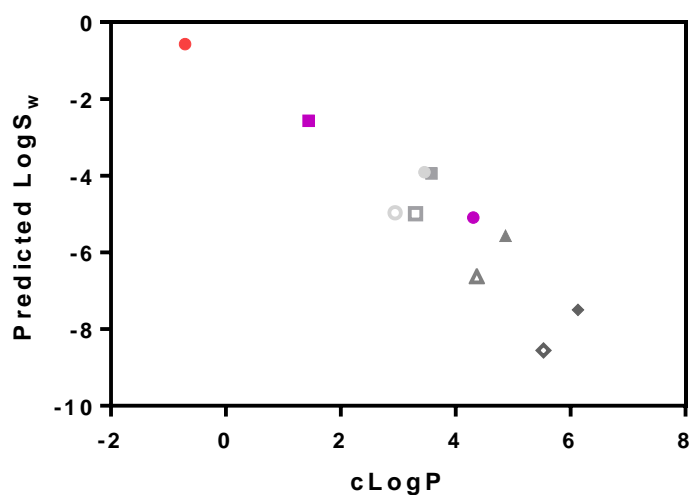


Figure 47: Relationship between cLogP and predicted water solubility for Gemcitabine and Fmoc-amino acid (AA) derived conjugates.

Gemcitabine (red circle), 42c cytidine gelator (purple circle), 48d 2'-deoxycytidine hydrogelator (purple square), Fmoc-Amino acid known gelators (filled in), Gemcitabine-*N*-AA-Fmoc (hollow). Fmoc-Ala (circle), Fmoc-GABA (square), Fmoc-Phe (triangle), Fmoc-Phe-Phe (diamond).

Owing to the relatively high cLogP values of compounds in each series the gelation was initially approached using an 'anti-solvent' system. This would enable solubilisation of the more lipophilic compounds in an organic solvent prior to the addition of water and would proffer the best opportunity for successful gelation. Although a chemotherapeutic molecular gel should be inherently cytotoxic, having a low solvent (ethanol) concentration as part of the gel formulation is still considered a high priority, therefore only solvent volume fractions ( $\Phi_{\text{SOL}}$ ) up to  $\Phi_{\text{EtOH}}$  0.20 were considered for this work.

From this point forward the physical characterisation of each series will be discussed independently.

#### **4.2.1. Gemcitabine-5'-esters**

##### **4.2.1.1. Stability to Inversion**

In alignment with previous gelation studies, the first approach towards gelation of compounds **50a** – **50e** was the temperature mediated solvent-switch approach. Small amounts (0.5 % w/v) of compound were dissolved in ethanol at 60 °C in solvent volume fractions ( $\Phi_{\text{SOL}}$ ) 0.05 - 0.20. Gelation was facilitated by the addition of pre-heated (60 °C) water to achieve a final gel volume of 500  $\mu\text{L}$ , before allowing samples to cool to room temperature for 18 h prior to inversion. Results are depicted in **Table 18**.

It was hypothesised based upon cLogP (1.65) and logS<sub>w</sub> (-2.37) predictions that **50e** would present the best opportunity for successful gelation; however this theory was quickly refuted. Only one gelator was observed from the 5'-ester series; **50a** ( $\Phi_{\text{EtOH}}$  0.20 (cLogP: 5.88, logS<sub>w</sub>: -4.78). This observation is hypothesised to be the result of a combination of increased solubility, imposed by the presence of the free exocyclic primary amine and by the removal of the 5'-hydrogen bonding functionality from the ribose sugar limiting the stabilising interactions noted in previous conjugates. To overcome the loss of the 5'-hydroxyl and the associated hydrogen bonding interactions, a significant increase in lipophilicity is required at

the 5'-hydroxyl position to obtain the increased van der Waals interactions necessary to create the same degree of stability within the gelator network.

The one observable gel from this series was left to stand for 1 h in the inverted position, shown below. However following the inversion period, it was found not to be completely stable to inversion but instead a metastable, fast crystallising system under these conditions, losing any observable stability. This is a common observation for systems facilitated by heating.<sup>217,218</sup>

Owing to the enhanced solubility accrued when gelation was facilitated using an elevated temperature, the gelation was repeated using softer conditions, room temperature (25 °C) and minimal sonication (~30s) as a mode of solubilisation in ethanol.

Ultrasonication as a method of external stimulation has been employed frequently in gel formulation as a way to solubilise compounds.<sup>219,220</sup> A recent example<sup>221</sup> described the self-assembly of an adamantine/cholesterol derivative in ethanol. The morphology of the resulting gel was found to alternate between ribbons and vesicles dependent upon the external stimulus (heating or sonication).

The self-assembly process was once again facilitated using water as the gelating medium and the samples left to stand for approximately 18 h prior to inversion. As is evident from **Table 18**, no gelation was observed in any of the samples under these conditions and an observable increase in propensity for precipitation, suggesting that the harsher conditions imposed by increased temperature were necessary to enhance solubilisation of **50a – 50e** in ethanol.

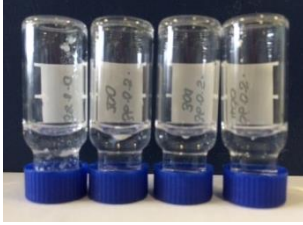
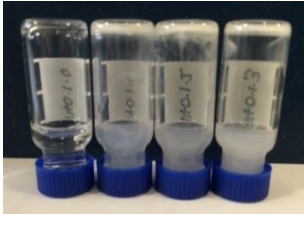
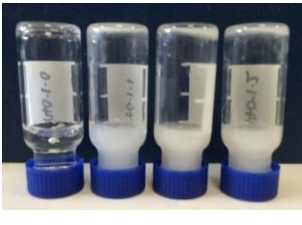
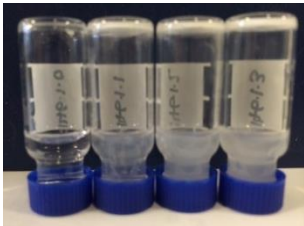
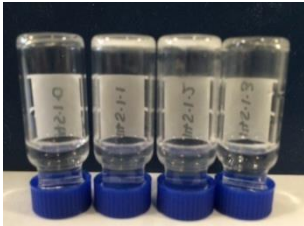
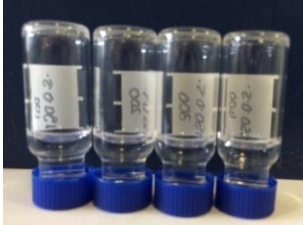
Recently reported was a guanosine-based hydrogelator, containing a free primary amine that formed stable gels in physiological relevant salt concentrations (NaCl, 100 - 400 mM).<sup>198</sup> These conditions were replicated using our amphiphilic conjugates (**50a – 50e**). Compounds were suspended in sodium chloride solution (100 – 400 mM) the samples were then heated to just below boiling point (approximately 95 °C) until dissolution had been achieved. The sample was cooled to room temperature, prior to inverting. **Table 18** shows the results of the salt

mediated gelation. The presence of NaCl (100 – 400 mM) restricted the gelation of **50a – 50e** at each tested concentration. Instead, it appeared that the presence of salt enabled the increased solubilisation of the compounds.

As there were no quantifiable gels derived from this series using three individual gelation procedures, the series wasn't progressed through to further physical characterisation.

Table 18: Vial inversion of gels derived for 50a - 50e.

Gels made at 60 °C (left hand column) and room temperature (middle column). In each case the images shown represent  $\Phi_{EtOH}$  0.05 to 0.20 (left to right). Gels were also promoted using sodium chloride (right hand column) where each image shows 100 – 400 mM NaCl (left to right). All gels were made to a final compound concentration of 0.5 % w/v and a final volume of 500  $\mu$ L. Each image is a representation of n = 3

	Heated (60 °C)	Room temperature (25 °C)	NaCl (100 mM – 400 mM)
50a			
50b			
50c			
50d			
50e			

## 4.2.2. Gemcitabine-*N*-amides

### 4.2.2.1. Stability to Inversion

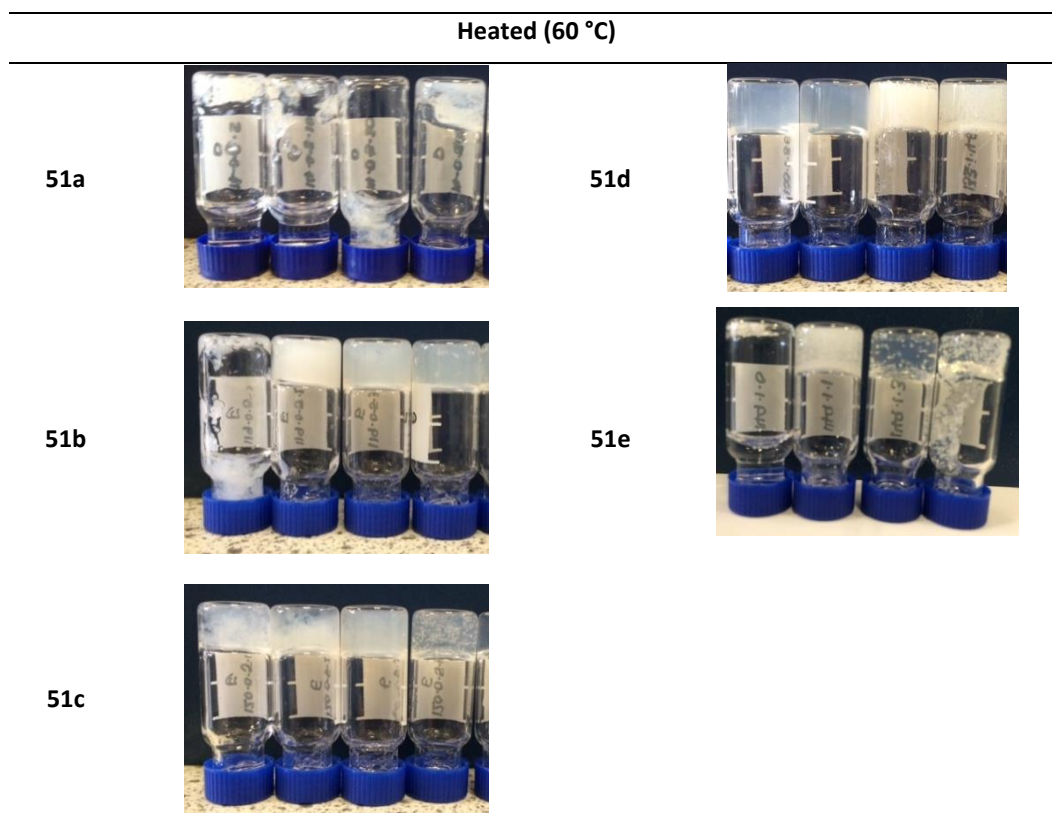
The second gemcitabine series (**51a** – **51e**) is the most closely related to those reported in previous chapters therefore stability to inversion is expected, based upon the cLogP, **51d** (cLogP: 2.62) and **51e** (cLogP: 1.56), following gelation stimulated by typical ethanol anti-solvent gelation conditions ( $\Phi_{\text{EtOH}}$  0.05 – 0.30, 60 °C, 500  $\mu\text{L}$ ). **Table 19** depicts gelation of **51a** – **51e** under these conditions. As predicted, gels derived from **51a** showed a reduced propensity for gelation owing to the high degree of lipophilicity in the compound from the introduction of tetradecanoic acid. Compound **51b** demonstrated stability to inversion at  $\Phi_{\text{EtOH}}$  0.10, 0.20 and 0.30, however at the lower solvent volume fractions ( $\Phi_{\text{EtOH}}$  0.05) the increased lipophilicity dominated over the solubilisation process, resulting in a precipitate. A similar observation was made for samples of **51e**, however in this instance the compound displayed enhanced water solubility at this concentration and so was unable to support network formation. Samples **51c** and **51d** both showed stability to inversion across all tested solvent volume fractions ( $\Phi_{\text{EtOH}}$  0.05 – 0.30). However a number of these samples were either heterogeneous (**51c**  $\Phi_{\text{EtOH}}$  0.05, 0.10, 0.20) or were metastable aggregates (**51d**  $\Phi_{\text{EtOH}}$  0.20, 0.30). The gel that displayed sustained stability and with the lowest solvent volume fraction was **51d**  $\Phi_{\text{EtOH}}$  0.05; the gel was also made at  $\Phi_{\text{EtOH}}$  0.00 (not pictured) however no stability was observed at this concentration. As the most desirable sample from this series **51d**  $\Phi_{\text{EtOH}}$  0.05 was carried through to mechanical measurements.

### 4.2.2.2. Rheological Measurements

Oscillatory measurements were used to examine the behaviour of the viscoelastic material and to determine overall mechanical strength of the **51d**  $\Phi_{\text{EtOH}}$  0.05 gel. Samples were prepared in 7 mL aluminium sample vials to a final gel volume of 2 mL so that the vane would be positioned in the centre of the gel.

**Table 19: Vial inversion of gels derived for 51a - 51e.**

Made at 60 °C. Each image shows  $\Phi_{\text{EtOH}}$  0.05 to 0.30 (left to right). All gels were made to a final compound concentration of 0.5 % w/v and a final volume of 500  $\mu\text{L}$ . Each image is a representation of  $n = 3$



The gelation procedure was as reported above. Amplitude sweeps (**Figure 48a**) were carried out using variable strain ( $\gamma = 0.1 - 100\%$ ) at a constant frequency ( $\omega = 10\text{ rad/s}$ ) and temperature (37 °C). The results give an indication of gel stability; whilst sample structure is maintained, the complex modulus ( $G'$ ) is constant; when the applied stress becomes too high, breakdown occurs in the 3D fibrillar network and the modulus decreases. This gel sample (**51d**  $\Phi_{\text{EtOH}}$  0.05) did not display prolonged stability under increasing strain, with the linear viscoelastic region extending up to  $\sim 3\%$ , however the  $G'$  value didn't lose its dominance over  $G''$  even at  $\gamma = 100\%$ , suggesting that the major cross-linkages between nanofibres remained intact.

Frequency sweeps (**Figure 48b**) were used to determine the overall nature of the tested material with measurements carried out at constant strain as determined by

the centre of the linear viscoelastic region from the amplitude sweep ( $\gamma = 1\%$ ). Angular frequency was the changing variable ( $\omega = 0.1 - 100$  rad/s), whilst temperature remained constant at a physiologically relevant  $37\text{ }^{\circ}\text{C}$ . For a typical highly cross-linked nanofibrillar structure, a difference of one order of magnitude between the storage modulus ( $G'$ ) and loss modulus ( $G''$ ) would be expected. Additionally,  $G'$  was expected to be the dominant parameter throughout the measurements. This sample shows the dominance of  $G'$  over  $G''$  however the difference of an order of magnitude isn't present. A calculated value of  $\tan \delta$  (0.20 – 0.30) (**Equation 1**) represents the ordered state in which the gel or solid state exists. This is suggestive of a cross-linked network but with few stabilising linkages between morphologies.<sup>178</sup>

In a similar manner to that reported in **Chapter 3**, strain/recovery measurements were carried out on this sample to mimic the conditions that would be encountered during endoscopic injection into a tumour site. The measurements were carried out by varying the strain between  $1\%$ , whereby the sample would exist in a stable condition (as quantified by the LVE region found during the amplitude sweep) and  $500\%$ , upon which the gel would undergo complete deformation. By monitoring the recovery between deformation and stability we can quantify how the gel would behave following shear stress i.e. injection.

Angular frequency was once again kept constant at  $10$  rad/s and the temperature remained at a physiological  $37\text{ }^{\circ}\text{C}$ . (**Figure 48c**) The gel was found to undergo complete deformation, as expected by exposure to  $500\%$  strain. However, following the recovery phase, whereby the strain was decreased to  $1\%$ , the gel failed to fully recover its initial mechanical strength, instead losing  $50\%$  of the acquired stability, implying that the important stabilising cross links aren't able to fully reform. A secondary cycle of strain/recovery was applied to the same sample and once again, a  $50\%$  decrease in quantifiable mechanical strength following the recovery phase was observed.

Following these mechanical measurements, transmission electron microscopy (TEM) was employed to probe the nanostructure of the samples and confirm the presence of a minimally crosslinked network.

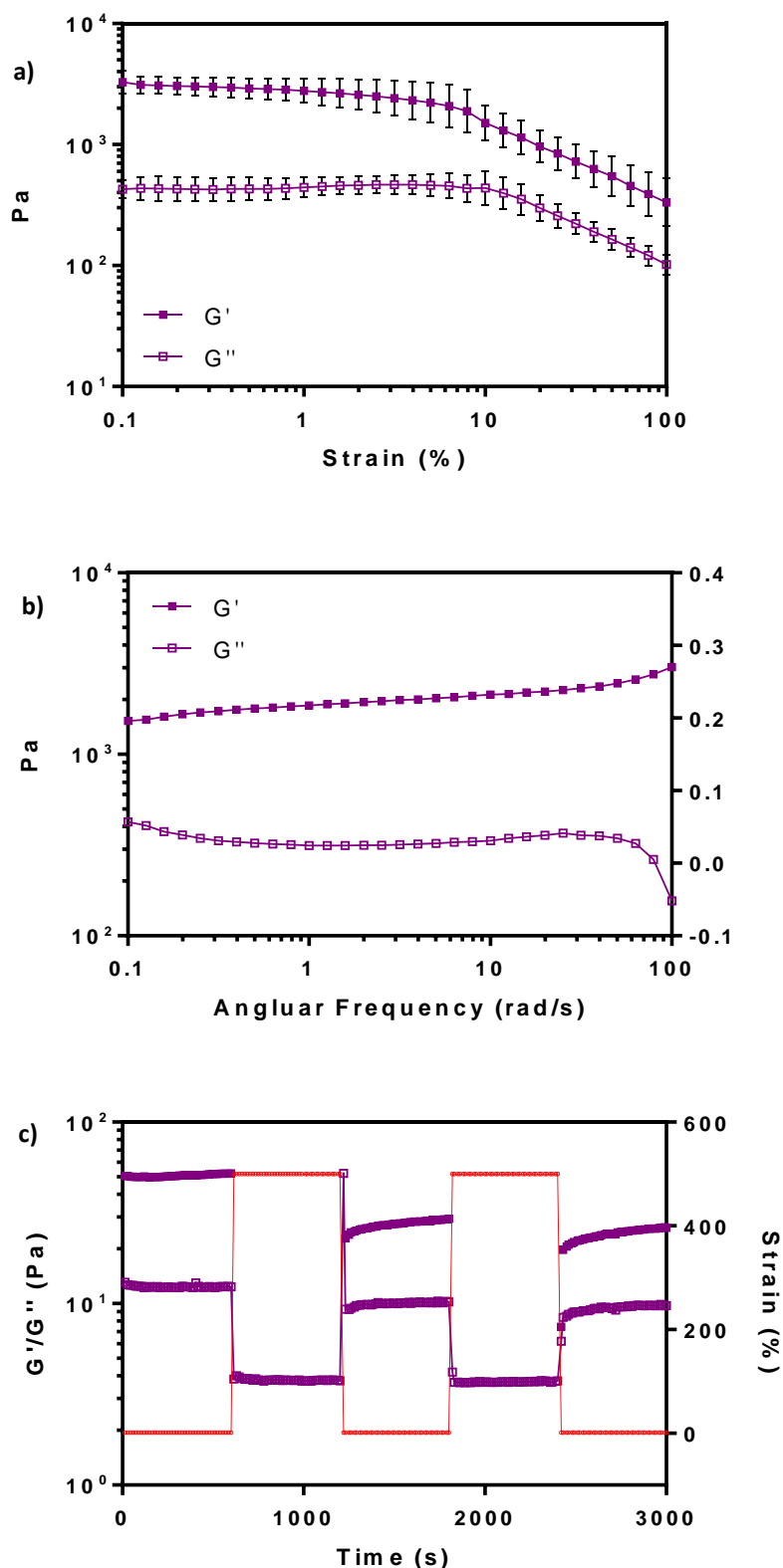
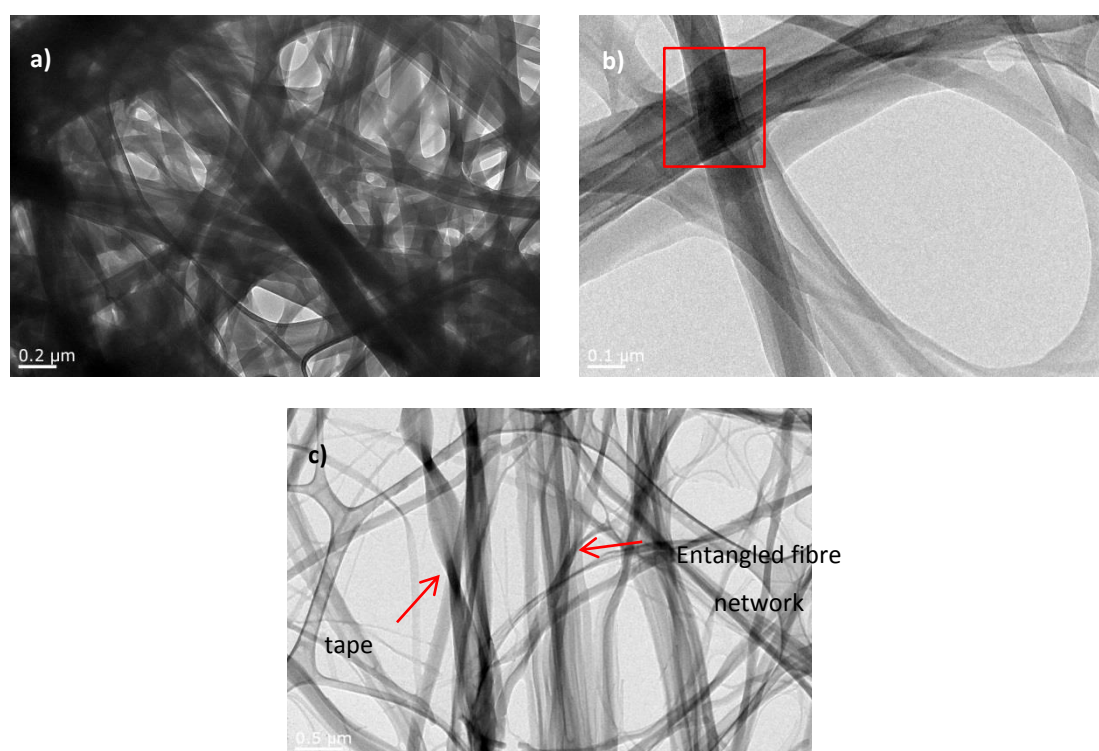


Figure 48: Rheological measurements (amplitude, frequency and recovery) for 51d  $\Phi_{EtOH}$  0.05 (0.5 % w/v).

a) Amplitude sweep carried out  $\gamma = 0.1 - 100$  %,  $\omega = 10$  rad/s, and  $T = 37$  °C. b) Frequency sweep carried out  $\omega = 0.1 - 100$  rad/s,  $\gamma = 1$  % and  $T = 37$  °C. Standard Deviation ( $G'$ )  $2040 \pm 620$  c) Strain/recovery sweep carried out  $\omega = 10$  rad/s,  $\gamma = 1$  % and  $T = 37$  °C. Each image is the result of  $n = 4$ . Standard Deviation ( $G'$ )  $75 \pm 25$  Pa.

#### 4.2.2.3. Transmission Electron Microscopy (TEM)

Based upon previous rheological measurements, the nanostructure of the gel (**51d**) was predicted to be a predominantly entangled fibrillar network with a few cross linking interactions present. Samples were imaged on graphene oxide lacey carbon grids (present as the structured artefact. **Figure 49a** shows a densely populated network of fibres, with open cavities seen between each strand whilst **Figure 49b** shows the cross-linked nature of the fibres. However, **Figure 49c** provides a more extensive overview of the differing morphologies and structure sizes observed during imaging, noticeable are both fibres and ribbons with some of the morphologies appearing cross linked. The majority of the structures were found to be entangled, which provides an explanation for the restricted recovery during the strain recovery experiment. Fibre diameters ranged from 1 nm to 35 nm and the lengths of fibres were measured to be up to 100's of  $\mu\text{m}$  which correlates to previous data of other gelators (**Section 2.2.3.1** and **3.2.3**)



**Figure 49: Transmission Electron micrographs of 51d  $\Phi_{\text{EtOH}}$  0.05 (0.5 % w/v)**

Transmission electron micrograph (TEM) images of 51d  $\Phi_{\text{EtOH}}$  0.05 (0.5 % w/v). a) Densely populated region of cross-linked nanofibre; scale bar 0.2  $\mu\text{m}$  b) shows the cross-linking of fibres; scale bar 0.1  $\mu\text{m}$  and c) Sample showing various morphologies (ribbons, fibres) and fibre sizes observed in sample; scale bar 0.5  $\mu\text{m}$ .

### 4.2.3. Gemcitabine-*N*-carbamates

#### 4.2.3.1. Stability to Inversion

Gelation of **52a** – **52c** was facilitated firstly using the ‘standard’ temperature mediated method; compounds (2.5 mg) were dissolved in an appropriate quantity of ethanol (**Table 6**) in a 1.5 mL sample vial and heated to 60 °C. pre-heated water (60 °C) was added and the samples left to cool to r.t over 18 h.

Based upon cLogP and predicted LogS<sub>w</sub> values (**Table 16**) all compounds were predicted to be stable to inversion, but owing to the increased cLogP value and potential favourable balance between lipophilicity and solubility it was predicted that **52c** (cLogP: 2.36, LogS<sub>w</sub>: -2.83) would present with the greatest stability to inversion under these conditions and at the lowest  $\Phi_{\text{EtOH}}$ . As the compounds also have a good degree of predicted water solubility, the gelation was again facilitated using less severe temperature requirements (~ 25 °C) and a mild sonication (~ 30 s) to further assess self-assembly capabilities as was suggested in **4.2.1.1**.

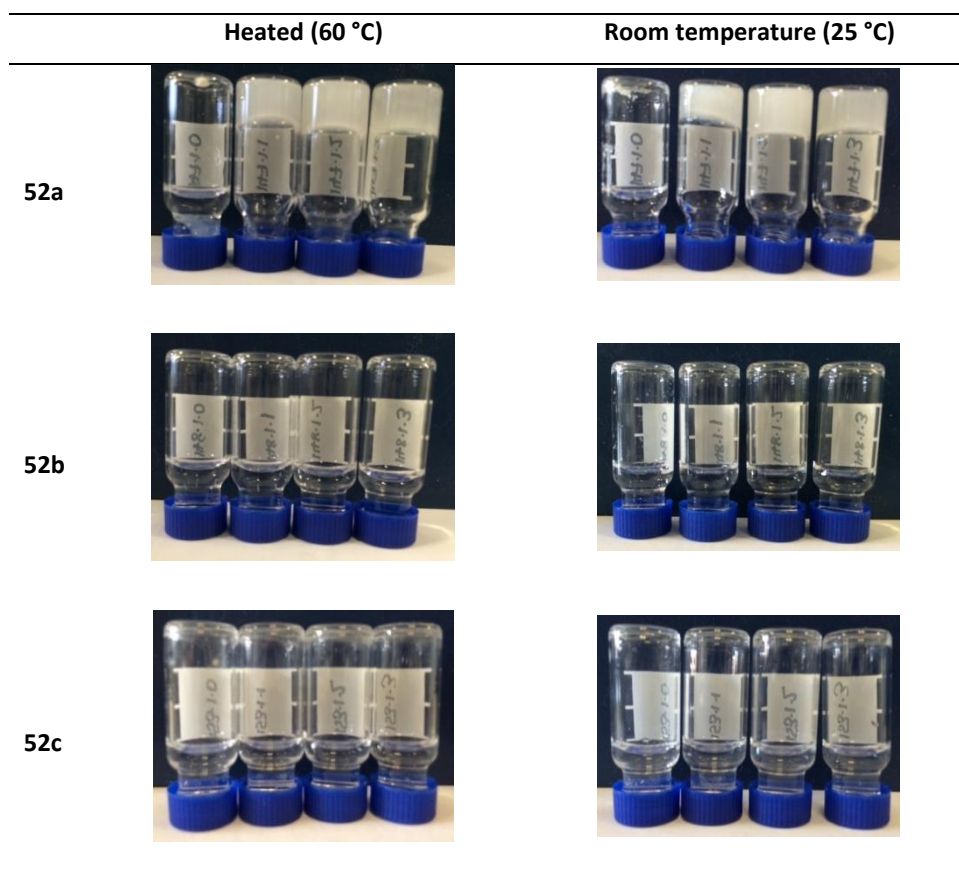
**Table 20** depicts the gelation of compounds **52a** – **52c** under the aforementioned conditions. **52b** and **52c** were found not to gel when using both the heating and sonication methods. The apparent water solubility and low cLogP values resulted in complete solubilisation of the compounds. However, gelation of **52a** mediated by both solvent and temperature switch and by sonication yielded gels with stability to inversion at  $\Phi_{\text{EtOH}}$  0.05, 0.10 and 0.20. Noted is the increased transparency of the samples facilitated by heating, which is likely due to the enhanced solubilisation of the compound prior to cooling and molecular reorganisation. Additionally, the gels derived from the sonication method were only partially stable under the influence of vial inversion.  $\Phi_{\text{EtOH}}$  0.05 and 0.20 can be classified as only partially stable owing to the ‘hanging’ edge of the sample at the point of contact with the glass sample vial.

Based upon these bench-top observations, it was decided that only the samples pertaining the greatest visible stability would be carried through to quantifiable mechanical testing. Therefore,  $\Phi_{\text{EtOH}}$  0.10 samples from both the heated and sonicated series’ were made on a larger 2 mL scale. Quantifying both of these

samples in parallel would allow easy comparison of the preparation methods at the molecular level.

**Table 20: Vial inversion of gels derived from 52a - 52c at 60 °C (left) and room temperature (right).**

In each case the images shown represent  $\Phi_{\text{EtOH}}$  0.00 to 0.20 (left to right). All gels were made to a final compound concentration of 0.5 % w/v and a final volume of 500  $\mu\text{L}$ . Each image is a representation of  $n = 3$



#### 4.2.3.2. Rheological Measurements

Stability of the gels (52a,  $\Phi_{\text{EtOH}}$  0.10) made at 60 °C and at 25 °C were quantified using amplitude sweeps; oscillatory measurements between a strain of  $\gamma = 0.1 - 100\%$  at a constant angular frequency ( $\omega = 10$  rad/s) and physiological temperature (37 °C). **Figure 50** shows the steady structural breakdown of both gels over the tested range. The opaque gel, derived from the 25 °C/sonication procedure produced the gel with the greatest mechanical stability. This is likely an artefact of the reduced solubilisation noted following the bench-top vial inversion. Precipitate often accrues additional strength in a sample owing to the increased viscosity it

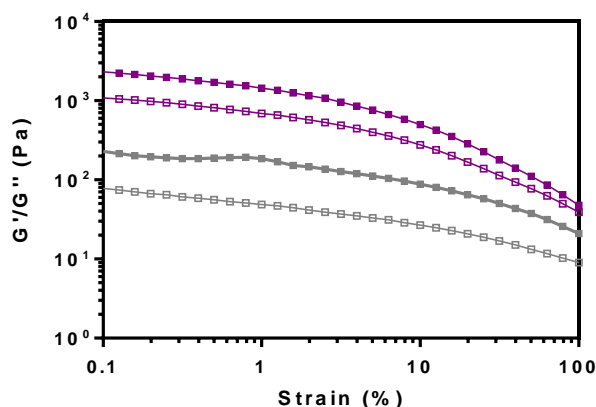


**Figure 50: Amplitude sweep of 52a (0.5 % w/v,  $\Phi_{\text{EtOH}}$  0.10)**

Sample prepared at 25 °C (purple) and 60 °C (grey). Solid data points represent  $G'$  and hollowed points represent  $G''$ . All data is representative of at least 4 repeats from freshly prepared gel samples. Standard Deviation ( $G'$ ); 25 °C:  $1708 \pm 768$  Pa and r.t:  $188 \pm 71$  Pa.

contributes to the overall system. The sample prepared at the elevated temperature maintains a consistent relationship between  $G'$  and  $G''$ . However, assessing the overall appearance of the sample, it is apparent that neither sample responds well to strain, with both gels losing mechanical stability at a steady rate, this is suggestive of an entangled network rather than a cross-linked network as neither of the gels fully breakdown i.e. the  $G'$  and  $G''$  values don't intersect at any point in the observable range. Further evidence to support the theory of an entangled network is the absence of a degree of magnitude between  $G'$  and  $G''$  in either sample. As there was no visible linear viscoelastic (LVE) region i.e. no independence to deformation in either sample, frequency sweeps were eliminated from the experimental programme. Instead TEM imaging was used to support the previous observations.

#### 4.2.3.3. Transmission electron microscopy (TEM)

Samples of both gels were imaged (**Figure 51**) as per the procedure described in section 4.2.2.3. Unlike previous samples where a highly cross-linked nanofibrillar structure (**51d**) was observed, in this instance there seemed to be an overwhelming dominance of tape like structures (**Figure 51a**), particularly in the heated sample,

with the nano-architecture displaying a wide yet shallow structure and with significantly shorter fragment lengths than fibres noted previously. Additional observations made during imaging were the brittle nature of the structures. **Figure 51b** shows the fractured end of one of the tapes following exposure to the electron beam of the microscope. **Figure 51c** represents the nanostructure of the sample prepared at room temperature aided by sonication. Although tapes are again present, there is additional thicker material that corresponds to the opacity noted during vial inversion. This is likely a direct result of the gelation process, the limited solubility achieved during sonication of relatively lipophilic compound results in the formation of thicker aggregates. Additionally the tape like architecture of these samples could provide the explanation for the lack of stability seen during amplitude sweeps above, the weak/thin nature of the samples, allows for rapid deformation under minimal external strain.

This data correlated to another similar monosaccharide-carbamate derived LMW

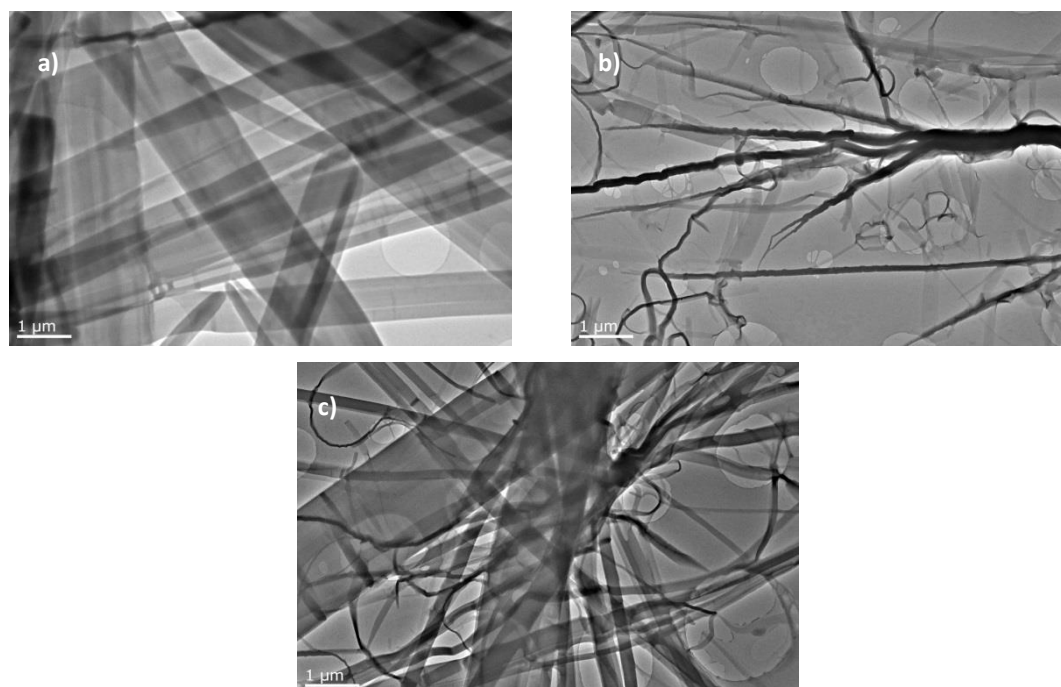


**Figure 51: Transmission electron micrograph images of 52a 0.5 % w/v,  $\Phi_{\text{EtOH}}$  0.10.**

a) Tape like nanostructure of sample prepared *via* heating (60 °C) method b) imaging showing fragile nature of sample prepared by heating and c) image showing nanostructure of sample prepared at 25 °C and sonication. Samples are representative of the system as a whole.

gelator formed in an aqueous mixture of ethanol.<sup>55</sup> The group observed that gels formed under these conditions produced fibrous assemblies similar to the ones seen above, however the rheological data was not reported and so cannot be directly compared.

#### 4.2.4. Gemcitabine-*N*-ureas

##### 4.2.4.1. Stability to Inversion

The final series based upon functionalisation by acylation was the urea series (**53a** – **53e**). Gelation once again was carried out at an elevated 60 °C and at 25 °C aided by minimal sonication to generate gels with a final compound concentration of 0.5 % w/v and a final gel volume of 500 µL. **Table 21** illustrates the results of gelation of compounds **53a** – **53e** under these conditions. Each image depicts a solvent volume fraction from  $\Phi_{\text{EtOH}}$  0.00 – 0.20.

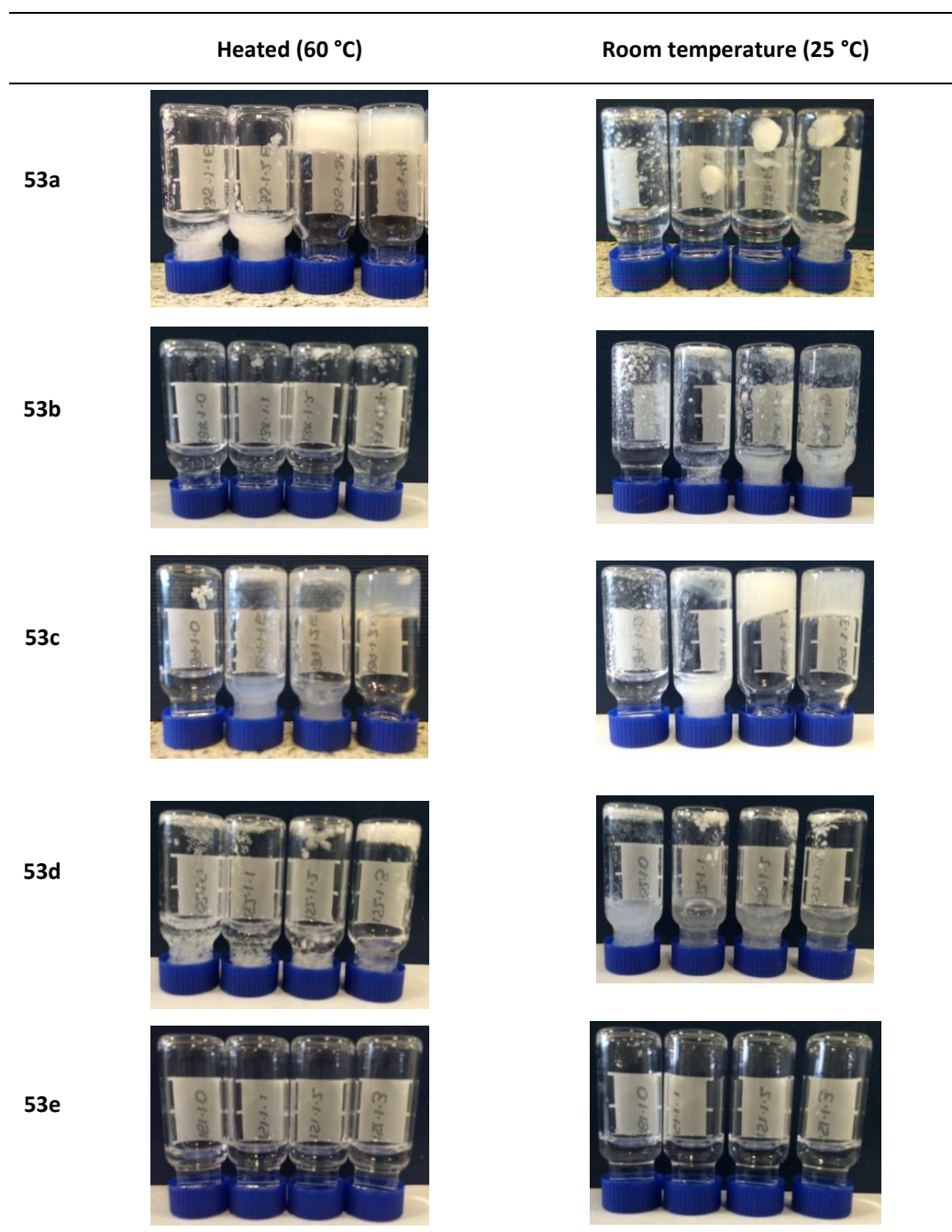
Based upon the previous predictions (**Table 16**) stability to inversion was anticipated from **53d** (cLogP: 2.21, LogS<sub>w</sub>: -2.62) with potential gelation predicted from **53c** (cLogP: 3.26, LogS<sub>w</sub>: -3.45) and **53e** (cLogP: 1.15, LogS<sub>w</sub>: -1.79).

In contrast to the majority of previous samples, in this instance the gelation could not be predicted. Although **53a** appeared to be stable to inversion when gelation was heat activated, the ‘gels’ were found to be rapidly crystallising metastable materials, quickly losing any apparent stability and becoming increasingly precipitous. No gel like character was observed in **53d**, conflicting with the original prediction. Given the seemingly ideal gelator characteristics the sample possessed, including the urea functionality (for stabilising hydrogen bonds), complimentary lipophilicity and associated water solubility, this result was unforeseen. **53e** was conversely found to be too hydrophilic in nature to aggregate and form any stabilising interactions, revealed by the complete solubilisation in the ethanol/water mixtures at both 60 °C and 25 °C. The only visually stable gels were found from **53c**, where both heat activation and sonication were found to be successful gelation promoting techniques.

Samples were observed towards the higher end of the tested solvent volume fractions in both cases, with gelation seen at  $\Phi_{\text{EtOH}}$  0.20 at 60 °C and  $\Phi_{\text{EtOH}}$  0.10 and

**Table 21: Vial inversion of gels derived for 53a - 53e,  $\Phi_{\text{EtOH}}$  0.00 – 0.20**

Samples prepared at 60 °C (left) and at room temperature (right). In each case the images shown represent  $\Phi_{\text{EtOH}}$  0.05 to 0.20 (left to right). All gels were made to a final compound concentration of 0.5 % w/v and a final volume of 500  $\mu\text{L}$ . Each image is a representation of n = 3



0.20 at 25 °C. However, the sample derived *via* the heating method appears to contain an undesirable aggregate, this is likely due to incomplete solubilisation and was observed in each of the repeat samples therefore this sample was ruled out of further testing. A similar conclusion was drawn for the  $\Phi_{\text{EtOH}}$  0.10 sample found in the gels prepared from sonication at 25 °C. Visually the gel wasn't as stable and therefore was characterised as a partial gel. Samples were observed towards the higher end of the tested solvent volume fractions in both cases, with gelation seen at  $\Phi_{\text{EtOH}}$  0.20 at 60 °C and  $\Phi_{\text{EtOH}}$  0.10 and 0.20 at 25 °C. However, the sample derived *via* the heating method appears to contain an undesirable aggregate, this is likely due to incomplete solubilisation and was observed in each of the repeat samples therefore this sample was ruled out of further testing. A similar conclusion was drawn for the  $\Phi_{\text{EtOH}}$  0.10 sample found in the gels prepared from sonication at 25 °C. Visually the gel wasn't as stable and therefore was characterised as a partial gel. A similar observation was made during a study for other acyl urea containing *N*-acetylglucosamine LMW gelator<sup>222</sup> and a more recent tyrosine kinase gelator.<sup>168</sup>

The only visually stable gel was  $\Phi_{\text{EtOH}}$  0.20 from the 25 °C sample set. This was taken through to quantification by rheology.

#### 4.2.4.2. Rheological Measurements

Amplitude sweeps were used to determine overall mechanical strength of the gel ( $\Phi_{\text{EtOH}}$  0.20). Samples were run in triplicate at  $\gamma = 0.1 - 100$  %,  $\omega = 10$  rad/s and at physiologically relevant temperature of 37 °C. **Figure 52a** shows the measured mechanical strength of the gel; immediately apparent is the shortened duration of the LVE region. Upon reaching a strain of 2 % the sample had reached the point of impending deformation whereby the  $G'$  and  $G''$  had intersected and the  $G''$  had become the dominant parameter indicating that the material was on the border between gel and liquid-like states. The material demonstrated an order of magnitude difference in  $G'$  and  $G''$  prior to yield point, this is suggestive of weak cross linking interactions.

Frequency sweep measurements can validate this result and provide an indication of network morphology. Samples were run at  $\omega = 0.1 - 100$  rad/s and constant

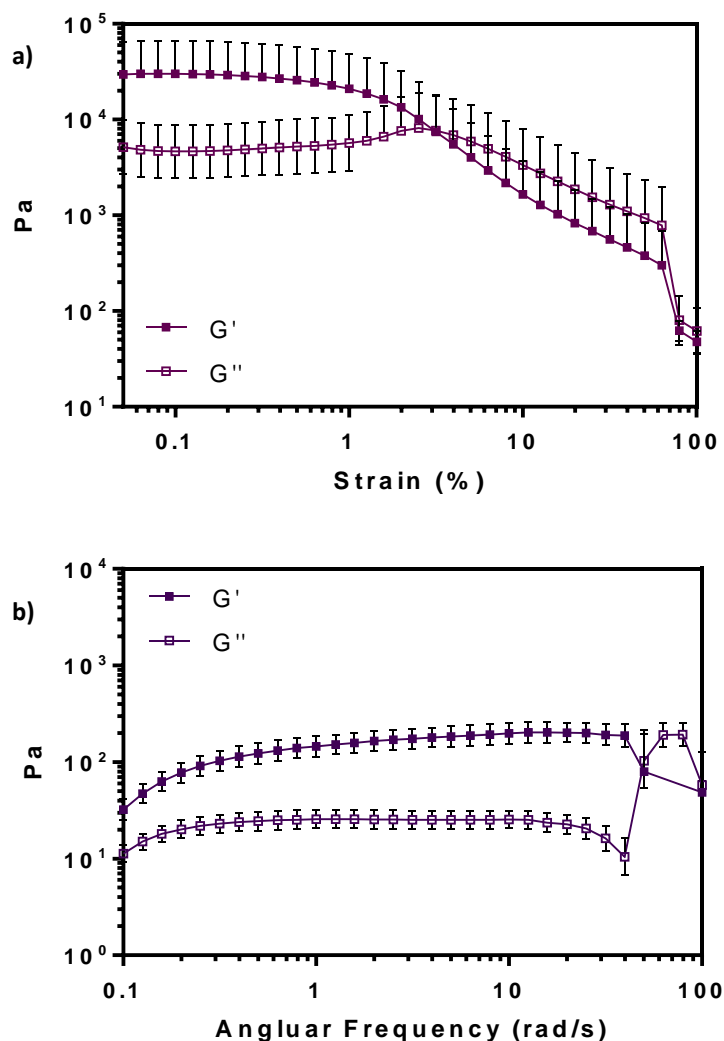


Figure 52: Amplitude and frequency sweep for 53c  $\Phi_{\text{EtOH}}$  0.20 at 25 °C

a) Amplitude sweep and b) angular frequency sweep. Solid data points represent  $G'$  and hollowed points represent  $G''$ . All data is representative of at least 3 repeats from freshly prepared gel samples. With a final compound concentration of 0.5 % w/v and a final gel volume of 2 mL

strain, based upon LVE calculations of 0.2 % and a temperature of 37 °C. **Figure 52b** displays the results from triplicate angular frequency sweep measurements, there is a sustained linear region seen at lower frequencies, however frequency dependency is noted at the higher frequencies (> 20 rad/s). Therefore the sample can be considered to have low degree of cross-linking behaviour, with increasing frequencies the  $G'$ -curve displays a gradual slope upwards before reaching a plateau. The  $G''$  curve slopes up towards a maximum before falling away again.<sup>178</sup>

Further characterisation using a fresh gel sample was carried out to determine the morphology of the nanostructure using TEM imaging.

#### 4.2.4.3. Transmission Electron Microscopy (TEM)

TEM imaging was carried out on holey carbon grids, with the gel (**53c**) samples being prepared 24 h in advance of imaging. Following rheological measurements the gel structure was predicted to be sparingly cross-linked and fibrillar in nature. However, the TEM imaging (**Figure 53**) exposed a nanofibrillar structure with crystalline aggregates present throughout the network. This is not an uncommon realisation; many gels suffer from long term instability, slowly developing into heterogeneous systems whereby large crystals co-exist in the fibrous gelator network.<sup>223</sup> Metastability usually arises from variable cooling rates, however, as these gels were formed at an ambient temperature this suggests that the crystal formation may be due to an inherent defect in the fibre network or even multiple packing morphologies that allow crystal formation. There is no study to date that conclusively explains observed experimental metastability.

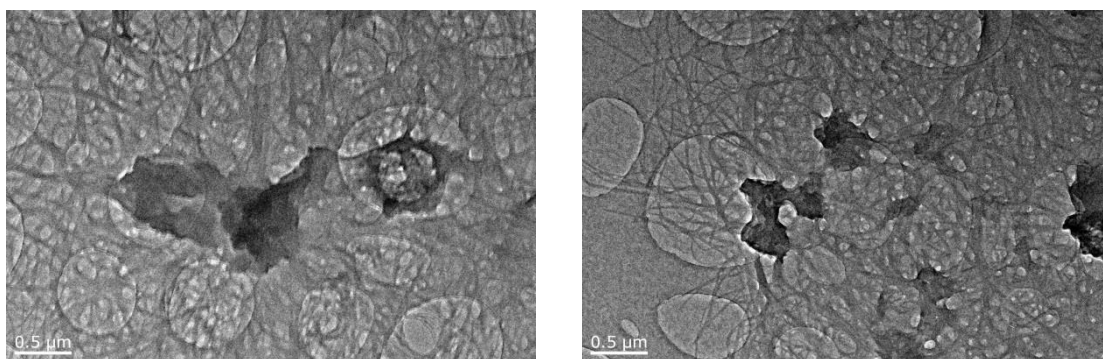


**Figure 53:** Transmission electron micrograph images of 53c 0.5 % w/v,  $\Phi_{\text{EtOH}}$  0.20 prepared at 25 °C. Samples were prepared 24 h in advance of imaging.

#### 4.2.5. Summary

There was limited stability noted from the majority of gels derived from acyl series' **50 – 53**. The successful gelators are summarised in **Table 22**. The esters (**50a – 50e**) displayed enhanced solubility owing to the presence of a free primary amine on the cytosine nucleobase, even at increased cLogP values and therefore produced no gels capable of retaining stability to inversion. The amide series (**51a - 51e**) proffered multiple gels with the ability to stabilise a gel network, however one gel stood out over and above the rest, **51d**  $\Phi_{\text{EtOH}}$  0.05 was found to have a reasonable LVE region, independency to angular frequency and was found to recover 50 % of its original mechanical strength following complete network deformation by oscillation. The carbamate series (**52a – 52c**) afforded one gelating compound (**52a**), however the sample didn't display an LVE region by amplitude sweep, which was attributed to the thin tape like architecture found on the TEM imaging. The final series afforded yet another single gelating compound (**53d**), however this time the gel was found to be metastable, crystallising in the 24h period following gelation.

Although only one successful molecular gel (**51d**) was discovered following all of 'stability to inversion', rheology and TEM studies, it can be noted that each of the compounds that displayed initial 'stability to inversion' fell within the parameters mentioned previously. This data is suggestive that a cLogP is a relevant consideration for gelation and that self-assembly in a binary system is more likely to occur when the cLogP of the final compound falls between 1 and 3.

**Table 22: cLogP and predicted water solubility values for successful gelating compounds 51d, 52a and 53c.**

Compound	n	cLogP
<b>48d</b>	6	1.44
<b>30</b>	-	-0.71
<b>51d</b>	6	2.62
<b>52a</b>	5	2.36
<b>53c</b>	8	3.26

#### 4.2.6. Fmoc-protected Gemcitabine-*N*-amino acids

The other synthesised compounds (**66** - **69**) were based upon the assumption that conjugating existing lipophilic gelating entities to the hydrophilic gemcitabine could facilitate gelation.

##### 4.2.6.1. Stability to Inversion

Gelation was facilitated using a temperature and solvent mediated approach. Samples were dissolved in a minimal amount of ethanol ( $\Phi_{\text{EtOH}}$  0.05 - 0.50) at 60 °C before the addition of pre heated water (60 °C) facilitated the gelation process. Gels were made to a final compound concentration of 0.5 % w/v and a final volume of 500  $\mu\text{L}$ .

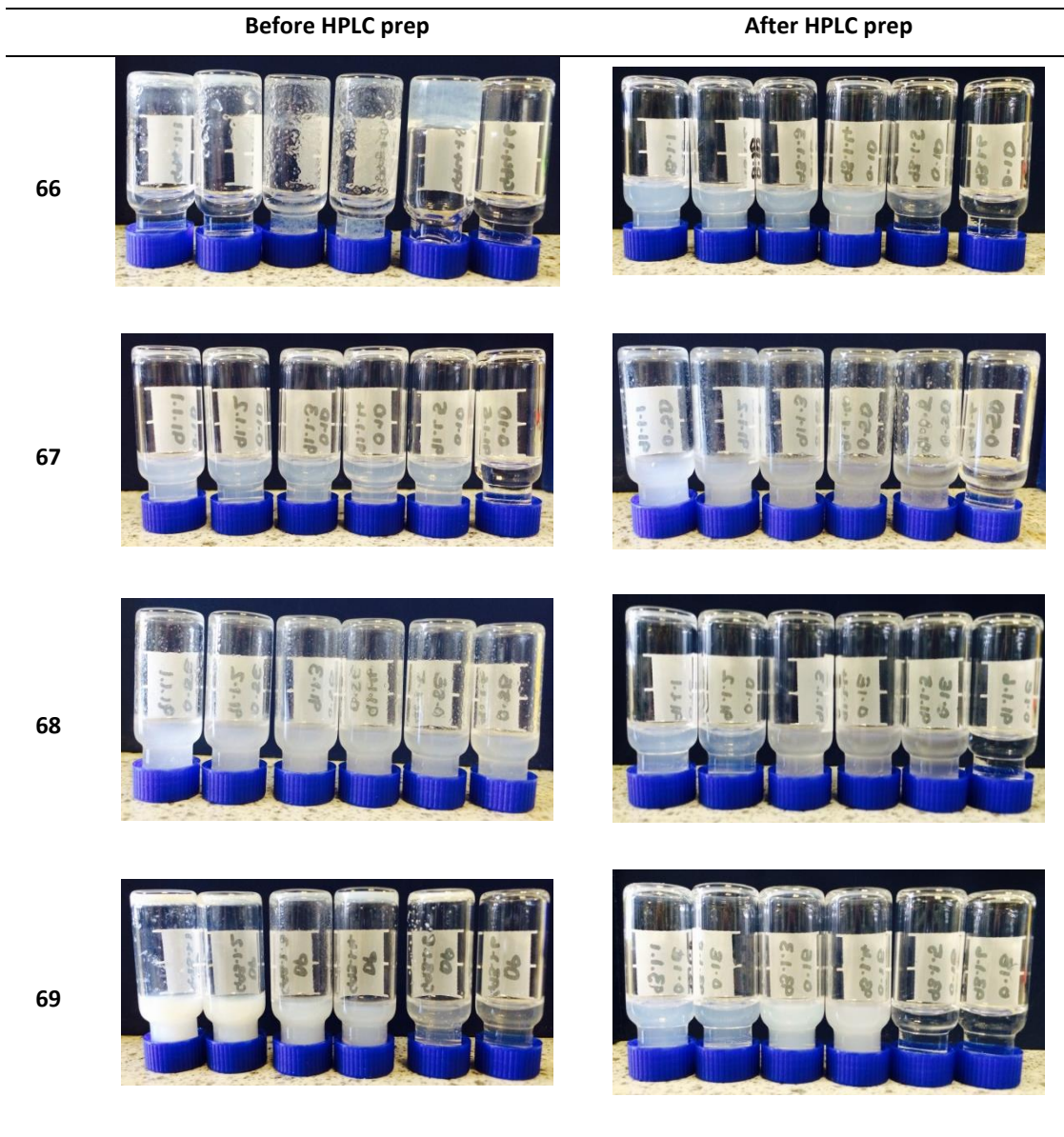
**Table 23** depicts the results of gelation pre- and post-preparative HPLC. Following synthesis and standard purification with a silica column the purity of the resultant compounds was ~ 90 %. Gelation was carried out with the gels at this purity to determine how the stability was affected by the presence of impurities including tetramethylurea from HATU coupling. Only one gel was found using these conditions **66**  $\Phi_{\text{EtOH}}$  0.40 demonstrated sustained stability to inversion. Unfortunately all other sample was found to be precipitous in nature.

Following preparative HPLC gelation was facilitated once more using the aforementioned method; however the increased purity of the samples resulted in the formation of precipitous suspensions for every sample at all tested solvent volume fractions, implying that the previous observed gel was stabilised predominantly through strong hydrogen bonding interaction between the urea based impurities.

It is therefore conclusive from this small study that the conjugation of existing gelators to gemcitabine to facilitate gelation is a likely to be unsuccessful. This may be down purely to the solubility of the resulting compounds; although gemcitabine itself is highly hydrophilic it does not contribute enough hydrophilicity to force the solubility driven gelation process towards the formation of a self-supporting gel network.

**Table 23: Vials inversion of gels derived from 66 -69**

Samples prepared prior to preparative HPLC are shown on the left and samples prepared following purification are depicted on the right. All gels were made to a final compound concentration of 0.5 % w/v and a final volume of 500  $\mu$ L. Each image is representative of n=3



### 4.3. Determining the Cytotoxic Nature of the Molecular Gels

The therapeutic molecular gels may show a certain degree of mechanical strength and present with the nanofibrillar/tape structure, however they have little application as a drug therapy if they are not biologically active. Owing to the highly lipophilic nature of the Fmoc-amino acid derivatives, they were not examined in this study as the conjugates could not be solubilised to the desired concentrations.

#### 4.3.1. Growth Inhibition Studies

A colorimetric cell proliferation assay (MTT) was used to evaluate *in vitro* anti-tumour activity of the parent compound, gemcitabine (**30**) against the synthesised conjugates **50d**, **51d**, **52a** and **53c** to determine the 50 % growth inhibition concentration (GI<sub>50</sub>). As gemcitabine is indicated as a first line treatment against gastric and pancreatic cancer, growth inhibition studies were carried out using MIA PaCa-2 (pancreatic adenocarcinoma) and MKN-7 (gastric adenocarcinoma) cell lines. To confirm the selectivity of the compounds towards both of these cells lines an additional fibroblast cell line was employed (MRC-5 foetal lung fibroblast).

The cells were seeded into a nuncwell 96 well plate (3000 cells/ well) and incubated for 24 h at 37 °C and a humidified atmosphere of 5 % CO<sub>2</sub> before introducing the test agent. The cells and test compound were incubated for a further 72 h before adding 3-(4,5-dimethylthiazol-2-yl)-2,5-diphenyltetrazolium bromide (MTT). Living cells were quantified by measuring UV absorbance; viable cells metabolise the yellow MTT to insoluble purple (E,Z)-5-(4,5-dimethylthiazol-2-yl)-1,3-diphenylformazan (formazan) crystals that can then be solubilised with DMSO and measured at 570 nm.

**Figure 54** depicts the results from the assays. MIA PaCa-2 and MKN-7 cells have both previously been reported to over express RRM2, a M2 subunit of ribonucleotide reductase and a key determinant in gemcitabine resistance,<sup>224,225</sup> with MIA PaCa-2.

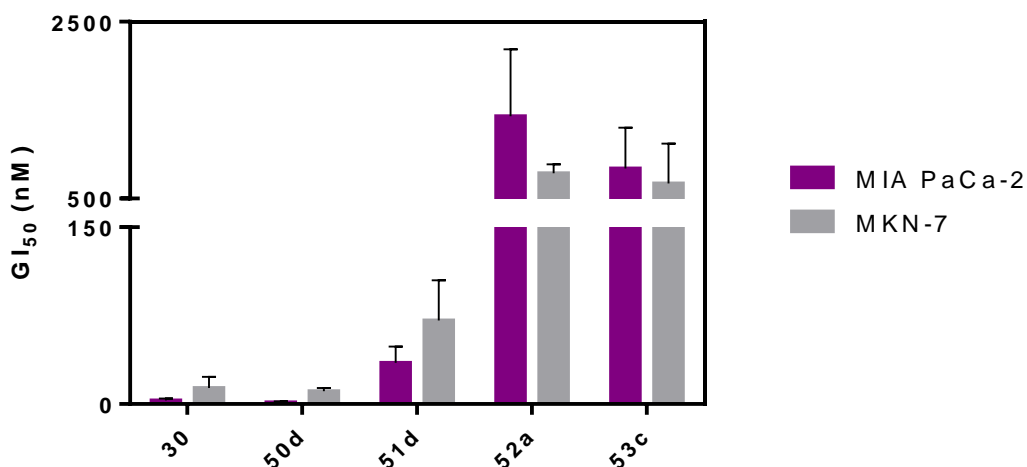


Figure 54: Growth inhibition studies of 30, 50d, 51d, 52a and 53c on Mia PaCa-2 (purple) and MKN-7 (grey) adenocarcinoma cell lines.

Each data point is a mean of  $n = 4$  and each one is representative of at least 3 repeat assays.

In MIA PaCa-2 cells the  $GI_{50}$  value (**Table 24**) of gemcitabine was found to be  $3.02 \pm 1.81$  nM. Of the other tested compounds **51d** was found to have reduced activity, displaying a 10-fold decrease in growth inhibition. **52a** and **53c** both displayed  $GI_{50}$  values in the micromolar range, a result consistent with recent findings.<sup>226</sup> In other words, the gemcitabine derivatives were less potent than gemcitabine. In contrast, **50d** demonstrated a  $GI_{50}$  of  $1.37 \pm 0.88$  nM, suggesting that the uptake is independent of the nucleoside transporter,<sup>227</sup> likely due to its increased lipophilicity, facilitating passive diffusion across the cell membrane. The prodrug is hypothesised to be metabolised intracellularly by intrinsic esterases.

A similar trend was observed in the MKN-7 cells; gemcitabine demonstrated a  $GI_{50}$  of  $13.52 \pm 9.66$  nM, 4× less potent than the growth inhibition seen in MIA PaCa-2. **50d** was the only compound found to have very similar activity when compared to gemcitabine ( $GI_{50}$  value 10.97 nM) likely due again to the increased lipophilicity of the compounds and once again suggesting that uptake is not receptor mediated and undergoes passive transport.

MRC-5 fibroblasts demonstrated the astounding selectivity of gemcitabine and its analogues towards the carcinoma cell lines, a 1000 fold decrease in selectivity was

demonstrated for **30**, **50d**, **52a** and **53d** and a 200 fold decrease was observed for **51d**. Whilst the selectivity cannot be qualified without further testing, these results validate these gelating entities as potential therapies for localised drug delivery.

**Table 24: Solution phase growth inhibition studies for gemcitabine (34) and conjugates 50d, 51d, 52a and 53c in MIA PaCa-2, MKN-7 and MRC-5 cells.**

Compound	GI <sub>50</sub> (nM)		
	MIA PaCa-2	MKN-7	MRC-5
<b>30</b>	3.02 ± 1.81	13.52 ± 9.66	> 10000
<b>50d</b>	1.37 ± 0.88	10.97 ± 2.65	> 10000
<b>51d</b>	34.91 ± 13.79	70.85 ± 34.26	2000 ± 560
<b>52a</b>	1430 ± 760	786 ± 100	> 10000
<b>53c</b>	840 ± 460	670 ± 450	> 10000

#### **4.4. Summary**

Designing a therapeutic molecular gel affords more challenges than it does solutions as the system needs to encompass both the properties of an efficacious chemotherapeutic agent and the stability of an injectable gel.

Gemcitabine was derivatised as esters, amides, carbamates and ureas. However, there was only one compound (**51d**) that possessed both of these properties. Although the compound can't necessarily be defined as a 'prodrug' because of the hydrolytic stability of the amide linkage, the compound demonstrated a nanomolar potency in both pancreatic (MIA PaCa-2) and gastric (MKN-7) adenocarcinoma cell lines, and demonstrated a selectivity towards the carcinomas over human fibroblasts. The compound was found to form a reasonably stable gel at a low solvent volume fraction ( $\Phi_{\text{EtOH}}$  0.05) when facilitated by a temperature mediated solvent switch.

**50d** was the best overall prodrug, the ester linkage provided the enhanced lipophilicity necessary to increase passive diffusion and the cleavable ester necessary to release the active compound. Unfortunately the compound failed to gel under temperature, solvent or salt mediated conditions. Neither **52a** nor **53c** provided significantly stable gels and when tested for growth inhibition displayed 100× lower activity than gemcitabine in the tested cell lines.

## 4.5. Materials and Methods

Gemcitabine was purchased from BePharm, Fmoc-protected amino acids were purchased from Bachem and all other chemicals and solvents were purchased from commercial suppliers and used without further purification.

1.5 mL sample vials and 7 mL Sterilin vials were purchased from Fischer Scientific, 7 mL aluminium rheology vials were purchased from Anton Paar GmbH and Transmission electron micrograph grids were purchased from EM Resolutions.

### 4.5.1. General Chemistry

TLC, HRMS, LC-MS and analytical RP-HPLC were all carried out as reported in **Section 2.6.1.**

<sup>1</sup>H NMR spectra were recorded on a Bruker 400 Ultrashield at 400.13 MHz at 25 °C. <sup>13</sup>C NMR spectra were recorded on a Bruker AV(III) at 500 MHz at 25 °C. Unless stated otherwise, solvent used for NMR analysis was DMSO-*d*<sub>6</sub> ((CHD<sub>2</sub>)<sub>2</sub>SO at δ<sub>H</sub> 2.50 ppm, (CD<sub>3</sub>)<sub>2</sub>SO at 39.52 ppm). Chemical shifts (δ) are recorded in parts per million (ppm). Coupling constants (*J*) are recorded in Hz (rounded to one decimal place) and any significant multiplicities described by singlet (s), doublet (d), triplet (t), quadruplet (q), broad (br), multiplet (m), doublet of doublets (dd) and doublet of triplets (dt). Spectra were assigned using COSY, distortionless enhanced polarisation transfer (DEPT) sequences and <sup>19</sup>F experiments.

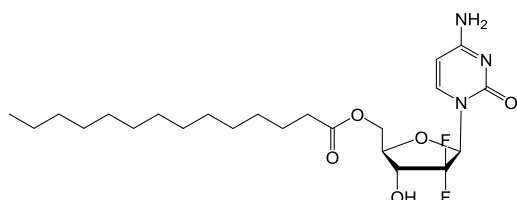
Preparative RP-HPLC was performed using a Phenomenex Luna reverse phase C<sub>8</sub> column (150 × 30 mm), a flow rate of 20 mL/min and UV detection of 254 nm.

### **General procedure for the 5'-OH-substitution of 4-amino-1-((2*R*,4*R*,5*R*)-3,3-difluoro-4-hydroxy-5-(hydroxymethyl)tetrahydrofuran-2-yl)pyrimidin-2(1*H*)-one**

Gemcitabine (**30**, 1 mmol, 1 eqv, 263 mg) and vinyl ester (12 mmol, 12 eqv) were made into a solution using hexane/pyridine (1:3, 10 mL). Lipase B *Candida Antarctica* (CAL-B)((500 units/mL) was added with stirring and the mixture heated to 50 °C for 6 h. Upon completion the mixture was cooled to room temperature and filtered to

remove enzyme. The solvent was evaporated *in vacuo* and was purified with silica column chromatography 0 – 10 % MeOH/CH<sub>2</sub>Cl<sub>2</sub> containing 0.05 % NH<sub>4</sub>OH.

**((2*R*,3*R*,5*R*)-5-(4-amino-2-oxopyrimidin-1(2*H*)-yl)-4,4-difluoro-3-hydroxytetrahydrofuran-2-yl) methyl tetradecanoate (50a)**



Vinyl tetradecanoate (12 mmol, 12 eqv, 3.51 mL)

**Yield:** 89.0 %

**HPLC purity:** 98.9 %

**HPLC t<sub>R</sub>:** 18.1 min

**<sup>1</sup>H NMR (DMSO-*d*<sub>6</sub>)** δ 0.85 (t, *J* = 6.8 Hz, 3H, CH<sub>3</sub>), 1.25 (br-m, 20H, CH<sub>2</sub>-(CH<sub>2</sub>)<sub>10</sub>-CH<sub>3</sub>), 1.45-1.60 (m, 2H, C=O-CH<sub>2</sub>-CH<sub>2</sub>), 2.35 (t, *J* = 7.4 Hz, 2H, C=O-CH<sub>2</sub>), 3.99 (ddd, *J* = 8.5, 6.0, 2.6 Hz, 1H, 4'-CH), 4.12-4.22 (m, 1H, 3'-CH), 4.25 - 4.38 (m, 2H, 5'-CH<sub>2</sub>), 5.79 (d, *J* = 7.5 Hz, 1H, 6-CH), 6.16 (t, *J* = 8.5 Hz, 1H, 1'-CH), 6.40 (d, *J* = 6.4 Hz, 1H, 3'-OH), 7.40 (d, *J* = 7.5 Hz, 2H, NH<sub>2</sub>), 7.50 (d, *J* = 7.5 Hz, 1H, 5-CH).

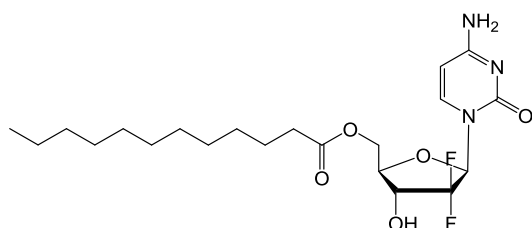
**<sup>13</sup>C NMR (DMSO-*d*<sub>6</sub>)** δ 13.95, 22.10, 24.35, 28.42, 28.68, 28.71, 28.86, 28.97, 29.01, 29.04, 31.30, 33.26, 62.48, 70.10, 77.37, 94.84, 122.67, 154.49, 165.62, 172.70

**<sup>19</sup>F NMR (DMSO-*d*<sub>6</sub>)** δ - 116.19

**m/z:** HRMS (TOF ES<sup>+</sup>) C<sub>23</sub>H<sub>38</sub>F<sub>2</sub>N<sub>3</sub>O<sub>5</sub> [M+H]<sup>+</sup> calculated 474.2774; found 474.1699

**m.p:** 120 – 123 °C

**((2*R*,3*R*,5*R*)-5-(4-amino-2-oxopyrimidin-1(2*H*)-yl)-4,4-difluoro-3-hydroxytetrahydrofuran-2-yl)methyl dodecanoate (50b)**



Vinyl dodecanoate (12 mmol, 12 eqv, 3.12 mL)

**Yield:** 76.9 %

**HPLC purity:** 97.6 %

**HPLC t<sub>R</sub>:** 15.9 min

**<sup>1</sup>H NMR (DMSO-*d*<sub>6</sub>)** δ 0.85 (t, *J* = 6.8 Hz, 3H, CH<sub>3</sub>), 1.25 (br-m, 16H, CH<sub>2</sub>-(CH<sub>2</sub>)<sub>8</sub>-CH<sub>3</sub>), 1.45-1.60 (m, 2H, C=O-CH<sub>2</sub>-CH<sub>2</sub>), 2.35 (t, *J* = 7.5 Hz, 2H, C=O-CH<sub>2</sub>), 3.99 (ddd, *J* = 8.5, 6.0, 2.6 Hz, 1H, 4'-CH), 4.12-4.22 (m, 1H, 3'-CH), 4.32 (ddd, *J* = 18.4, 12.4, 4.3 Hz, 2H, 5'-CH), 5.78 (d, *J* = 7.6 Hz, 1H, 6-CH), 6.16 (t, *J* = 8.4 Hz, 1H, 1'-CH), 6.40 (d, *J* = 6.5 Hz, 1H, 3'-OH), 7.40 (d, *J* = 6.1 Hz, 2H, NH<sub>2</sub>), 7.70 (d, *J* = 7.7 Hz, 1H, 5-CH).

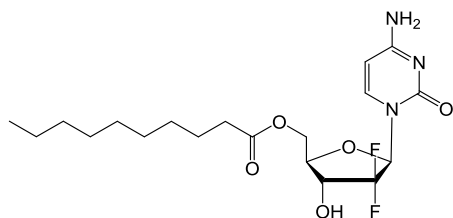
**<sup>13</sup>C NMR (DMSO-*d*<sub>6</sub>)** δ 13.95, 22.08, 24.34, 28.40, 28.66, 28.68, 28.85, 28.96, 28.97, 31.28, 33.25, 62.47, 69.91, 70.09, 70.27, 77.35, 94.82, 154.48, 165.62, 172.71

**<sup>19</sup>F NMR (DMSO-*d*<sub>6</sub>)** δ -116.17

**m/z:** HRMS (TOF ES<sup>+</sup>) C<sub>21</sub>H<sub>34</sub>F<sub>2</sub>N<sub>3</sub>O<sub>5</sub> [M+H]<sup>+</sup> calculated 446.2461; found 445.9998

**m.p:** 71 – 76 °C

**((2*R*,3*R*,5*R*)-5-(4-amino-2-oxopyrimidin-1(2*H*)-yl)-4,4-difluoro-3-hydroxytetrahydrofuran-2-yl)methyl decanoate (50c)**



Vinyl decanoate (12mmol, 12 eqv, 2.67 mL).  
product is a clear oil.

**Yield:** 65.7 %

**HPLC purity:** 98.3 %

**HPLC t<sub>R</sub>:** 13.7 min

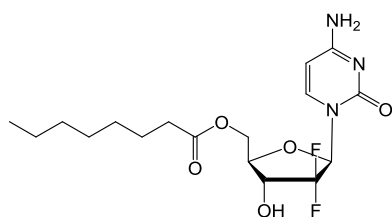
**<sup>1</sup>H NMR (DMSO-*d*<sub>6</sub>)** δ 0.85 (t, *J* = 6.9 Hz, 3H, CH<sub>3</sub>), 1.23 (br-m, 12H, CH<sub>2</sub>-(CH<sub>2</sub>)<sub>6</sub>-CH<sub>3</sub>), 1.45-1.60 (m, 2H, C=O-CH<sub>2</sub>-CH<sub>2</sub>), 2.35 (t, *J* = 7.4 Hz, 2H, C=O-CH<sub>2</sub>), 3.99 (ddd, *J* = 8.4, 6.0, 2.6 Hz, 1H, 4'-CH), 4.12-4.22 (m, 1H, 3'-CH), 4.32 (ddd, *J* = 18.4, 12.4, 4.3 Hz, 2H, 5'-CH<sub>2</sub>), 5.78 (d, *J* = 7.5 Hz, 1H, 6-CH), 6.16 (t, *J* = 9.3 Hz, 1H, 1'-CH), 6.40 (d, *J* = 6.4 Hz, 1H, 3'-OH), 7.40 (d, *J* = 5.9 Hz, 2H, NH<sub>2</sub>), 7.50 (d, *J* = 7.6 Hz, 1H, 5-CH).

$^{13}\text{C}$  NMR (DMSO- $d_6$ )  $\delta$  13.95, 22.07, 24.34, 28.40, 28.61, 28.66, 28.81, 31.25, 33.25, 62.47, 69.90, 70.09, 77.34, 94.82, 154.48, 165.62, 172.71

$^{19}\text{F}$  NMR (DMSO- $d_6$ )  $\delta$  -116.20

**m/z:** HRMS (TOF ES<sup>+</sup>) C<sub>19</sub>H<sub>30</sub>F<sub>2</sub>N<sub>3</sub>O<sub>5</sub> [M+H]<sup>+</sup> calculated 418.2148; found 418.1127

**((2R,3R,5R)-5-(4-amino-2-oxopyrimidin-1(2H)-yl)-4,4-difluoro-3-hydroxytetrahydrofuran-2-yl)methyl decanoate (50d)**



Vinyl octanoate (12 mmol, 12 eqv, 2.31 mL)

**Yield:** 95.0 %

**HPLC purity:** 99.2 %

**HPLC t<sub>R</sub>:** 11.6 min

$^1\text{H}$  NMR (DMSO- $d_6$ )  $\delta$  0.85 (t,  $J$  = 6.9 Hz, 3H, CH<sub>3</sub>), 1.23 (br-m, 8H, CH<sub>2</sub>-(CH<sub>2</sub>)<sub>4</sub>-CH<sub>3</sub>), 1.44-1.60 (m, 2H, C=O-CH<sub>2</sub>-CH<sub>2</sub>), 2.35 (t,  $J$  = 7.4 Hz, 2H, C=O-CH<sub>2</sub>), 3.99 (ddd,  $J$  = 8.5, 6.0, 2.6 Hz, 1H, 4'-CH), 4.11-4.22 (m, 1H, 3'-CH), 4.32 (ddd,  $J$  = 18.4, 12.4, 4.3 Hz, 2H, 5'-CH<sub>2</sub>), 5.79 (d,  $J$  = 7.5 Hz, 1H, 6-CH), 6.16 (t,  $J$  = 8.4 Hz, 1H, 1'-CH), 6.40 (d,  $J$  = 6.4 Hz, 1H, 3'-OH), 7.40 (d,  $J$  = 6.6 Hz, 2H, NH<sub>2</sub>), 7.50 (d,  $J$  = 7.5 Hz, 1H, 5-CH).

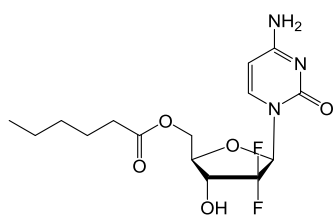
$^{13}\text{C}$  NMR (DMSO- $d_6$ )  $\delta$  13.91, 22.00, 24.35, 28.32, 28.36, 31.08, 33.25, 62.47, 69.91, 70.09, 70.28, 77.34, 94.82, 154.48, 165.62, 175.71

$^{19}\text{F}$  NMR (DMSO- $d_6$ )  $\delta$  -116.20

**m/z:** HRMS (TOF ES<sup>+</sup>) C<sub>17</sub>H<sub>26</sub>F<sub>2</sub>N<sub>3</sub>O<sub>5</sub> [M+H]<sup>+</sup> calculated 390.1835; found 390.4426

**m.p:** 65 – 67 °C

**((2R,3R,5R)-5-(4-amino-2-oxopyrimidin-1(2H)-yl)-4,4-difluoro-3-hydroxytetrahydrofuran-2-yl)methyl hexanoate (50e)**



Vinyl hexanoate (12 mmol, 12 eqv, 1.92 mL), product is an off-white oil.

**Yield:** 70.3 %

**HPLC purity:** 99.5 %

**HPLC  $t_R$ :** 9.4 min

**$^1\text{H}$  NMR (DMSO- $d_6$ )**  $\delta$  0.85 (t,  $J$  = 6.7 Hz, 3H,  $\text{CH}_3$ ), 1.24 – 1.29 (m, 4H,  $\text{CH}_2\text{-(CH}_2\text{)}_2\text{-CH}_3$ ), 1.50 -1.57 (m, 2H,  $\text{C=O-CH}_2\text{-CH}_2$ ), 2.35 (t,  $J$  = 7.4 Hz, 2H,  $\text{C=O-CH}_2$ ), 3.99 (ddd,  $J$  = 8.5, 6.0, 2.6 Hz, 1H, 4'- $\text{CH}$ ), 4.13 - 4.21 (m, 1H, 3'- $\text{CH}$ ), 4.32 (ddd,  $J$  = 18.4, 12.4, 4.3 Hz, 2H, 5'- $\text{CH}_2$ ), 5.79 (d,  $J$  = 7.6 Hz, 1H, 6- $\text{CH}$ ), 6.16 (t,  $J$  = 9.0 Hz, 1H, 1'- $\text{CH}$ ), 6.40 (d,  $J$  = 6.6 Hz, 1H, 3'- $\text{OH}$ ), 7.40 (d,  $J$  = 9.3 Hz, 2H,  $\text{NH}_2$ ), 7.50 (d,  $J$  = 7.5 Hz, 1H, 5- $\text{CH}$ ).

**$^{13}\text{C}$  NMR (DMSO- $d_6$ )**  $\delta$  14.26, 22.24, 24.50, 31.09, 33.69, 62.90, 70.37, 70.55, 70.73, 77.81, 95.30, 154.96, 166.09, 173.19

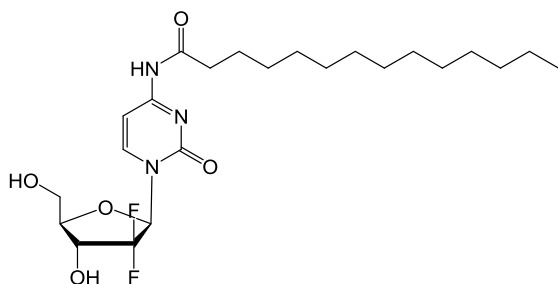
**$^{19}\text{F}$  NMR (DMSO- $d_6$ )**  $\delta$  -116.25

**$m/z$ :** HRMS (TOF  $\text{ES}^+$ )  $\text{C}_{15}\text{H}_{22}\text{F}_2\text{N}_3\text{O}_5$   $[\text{M}+\text{H}]^+$  calculated 362.1522; found 361.8756

**General procedure for the *N*-substitution of 4-amino-1-((2*R*,4*R*,5*R*)-3,3-difluoro-4-hydroxy-5-(hydroxymethyl)tetrahydrofuran-2-yl)pyrimidin-2(1*H*)-one**

To a solution of 2-chloro-4,6-dimethoxy-1,3,5-triazine (CDMT, **40**, 1 eqv) in anhydrous  $\text{CH}_2\text{Cl}_2$  at 0 °C, was added *N*-methylmorpholine (NMM, 1.36 eqv) with continuous stirring until a white suspension had formed. The mixture was then left to stir for 1 h. carboxylic acid (1 eqv) was added directly into the mixture as a solution in anhydrous DMF and stirred for 1 h at 0 °C. A solution of Gemcitabine (**30**, 1 eqv) in anhydrous DMF was made up at 0 °C. The cold triazine solution was added drop wise to the cooled gemcitabine solution over 30 mins, before heating to 50 °C and stirring for 14 - 24 h. The cooled solution was evaporated *in vacuo* and purified by silica column chromatography (0 – 10 % MeOH/  $\text{CH}_2\text{Cl}_2$ )

***N*-(1-((2*R*,4*R*,5*R*)-3,3-difluoro-4-hydroxy-5-(hydroxymethyl)tetrahydrofuran-2-yl)-2-oxo-1,2-dihydropyrimidin-4-yl)tetradecanamide (51a)**



CDMT (10 mmol, 1 eqv, 1.75 g), NMM (13.6 mmol, 1.36 eqv, 1.50 mL), CH<sub>2</sub>Cl<sub>2</sub> (30 mL). Tetradecanoic acid (10 mmol, 1 eqv, 2.28 g) in DMF (10 mL). Gemcitabine (10 mmol, 1 eqv, 2.63 g) in anhydrous DMF (20 mL).

**Yield:** 54.5 %

**HPLC purity:** 97.6 %

**HPLC t<sub>R</sub>:** 26.1 min

**<sup>1</sup>H NMR (DMSO-*d*<sub>6</sub>)** δ 0.85 (t, *J* = 6.9 Hz, 3H, CH<sub>3</sub>), 1.23 (br-m, 20H, CH<sub>2</sub>-(CH<sub>2</sub>)<sub>10</sub>-CH<sub>3</sub>), 1.53 (m, 2H, C=O-CH<sub>2</sub>-CH<sub>2</sub>), 2.39 (t, *J* = 7.3 Hz, 2H, C=O-CH<sub>2</sub>), 3.62 – 3.83 (m, 2H, 5'-CH<sub>2</sub>), 3.89 (dt, *J* = 5.9, 3.2 Hz, 1H, 4'-CH), 4.13 – 4.23 (m, 1H, 3'-CH), 5.29 (t, *J* = 5.5 Hz, 1H, 5'-OH), 6.17 (t, *J* = 7.3 Hz, 1H, 1'-CH), 6.31 (d, *J* = 6.5 Hz, 1H, 3'-OH), 7.28 (d, *J* = 7.8 Hz, 1H, 6-CH), 8.23 (d, *J* = 7.8 Hz, 1H, 5-CH), 10.97 (s, 1H, NH).

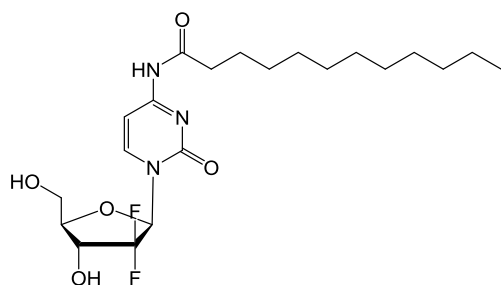
**<sup>13</sup>C NMR (DMSO-*d*<sub>6</sub>)** δ 14.37, 14.42, 22.56, 22.89, 23.71, 24.81, 29.47, 29.17, 31.16, 31.76, 36.85, 38.55, 49.06, 59.24, 67.87, 80.97, 81.00, 96.36, 129.13, 132.07, 154.67, 163.35, 174.57

**<sup>19</sup>F NMR (DMSO-*d*<sub>6</sub>)** δ -116.65

**m/z:** HRMS (TOF ES<sup>+</sup>) C<sub>23</sub>H<sub>38</sub>F<sub>2</sub>N<sub>3</sub>O<sub>5</sub> [M+H]<sup>+</sup> calculated 474.2774; found 474.2746.

**m.p:** 138 - 140 °C

***N*-(1-((2*R*,4*R*,5*R*)-3,3-difluoro-4-hydroxy-5-(hydroxymethyl)tetrahydrofuran-2-yl)-2-oxo-1,2-dihydropyrimidin-4-yl)dodecanamide (51b)**



CDMT (0.95 mmol, 1 eqv 167 mg), NMM (1.29 mmol, 1.36 eqv, 165  $\mu$ L),  $\text{CH}_2\text{Cl}_2$  (3.5 mL). Dodecanoic acid (0.95 mmol, 1 eqv, 190 mg) in DMF (1 mL). Gemcitabine (0.95 mmol, 1 eqv, 250 mg) in DMF (2 mL).

**Yield:** 22.5 %

**HPLC purity:** 98.6 %

**HPLC  $t_R$ :** 23.5 min

**$^1\text{H}$  NMR (DMSO- $d_6$ )**  $\delta$  0.85 (t,  $J$  = 6.9 Hz, 3H,  $\text{CH}_3$ ), 1.26 (br-m, 16H,  $\text{CH}_2$ -( $\text{CH}_2$ )<sub>8</sub>- $\text{CH}_3$ ), 1.54 (m, 2H,  $\text{C}=\text{O}$ - $\text{CH}_2$ - $\text{CH}_2$ ), 2.40 (t,  $J$  = 7.3 Hz, 2H,  $\text{C}=\text{O}$ - $\text{CH}_2$ ), 3.61 – 3.84 (m, 2H, 5'- $\text{CH}_2$ ), 3.89 (dt,  $J$  = 5.9, 3.2 Hz, 1H, 4'- $\text{CH}$ ), 4.18 (ddd,  $J$  = 19.6, 12.7, 7.2 Hz, 1H, 3'- $\text{CH}$ ), 5.29 (t,  $J$  = 5.5 Hz, 1H, 5'- $\text{OH}$ ), 6.17 (t,  $J$  = 7.5 Hz, 1H, 1'- $\text{CH}$ ), 6.31 (d,  $J$  = 6.5 Hz, 1H, 3'- $\text{OH}$ ), 7.28 (d,  $J$  = 7.6 Hz, 1H, 6'- $\text{CH}$ ), 8.23 (d,  $J$  = 7.6 Hz, 1H, 5'- $\text{CH}$ ), 10.97 (s, 1H,  $\text{NH}$ ).

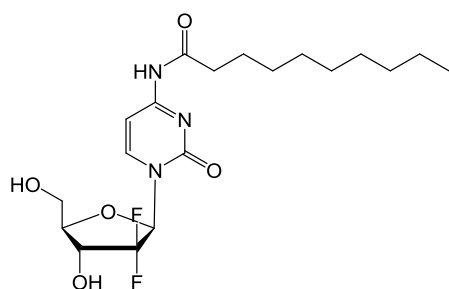
**$^{13}\text{C}$  NMR (DMSO- $d_6$ )**  $\delta$  13.95, 22.09, 24.34, 28.42, 28.70, 28.85, 28.97, 28.98, 31.28, 36.38, 58.78, 68.18, 68.36, 68.54, 80.97, 81.00, 95.89, 144.71, 154.20, 162.88, 174.10

**$^{19}\text{F}$  NMR (DMSO- $d_6$ )**  $\delta$  -116.33

**m/z:** HRMS (TOF ES<sup>+</sup>)  $\text{C}_{21}\text{H}_{34}\text{F}_2\text{N}_3\text{O}_5$  [M+H]<sup>+</sup> calculated 446.2461; found 446.3470

**m.p:** 134 – 137 °C

***N*-(1-((2*R*,4*R*,5*R*)-3,3-difluoro-4-hydroxy-5-(hydroxymethyl)tetrahydrofuran-2-yl)-2-oxo-1,2-dihydropyrimidin-4-yl)decanamide (51c)**



CDMT (0.95 mmol, 1 eqv, 167 mg), NMM (1.29 mmol, 1.36 eqv, 165  $\mu$ L),  $\text{CH}_2\text{Cl}_2$  (3.5 mL). Decanoic acid (0.95 mmol, 1 eqv, 164 mg) in DMF (1 mL). Gemcitabine (0.95 mmol, 1 eqv, 250 mg) in DMF (2 mL).

**Yield:** 40.9 %

**HPLC purity:** 98.8 %

**HPLC  $t_R$ :** 20.0 min

**$^1\text{H}$  NMR (DMSO- $d_6$ )**  $\delta$  0.85 (t,  $J$  = 6.8 Hz, 3H,  $\text{CH}_3$ ), 1.26 (br-m, 12H,  $\text{CH}_2$ - $(\text{CH}_2)_6$ - $\text{CH}_3$ ), 1.46 – 1.64 (m, 2H,  $\text{C}=\text{O}$ - $\text{CH}_2$ - $\text{CH}_2$ ), 2.40 (t,  $J$  = 7.3 Hz, 2H,  $\text{C}=\text{O}$ - $\text{CH}_2$ ), 3.60 – 3.84 (m, 2H,  $5'$ - $\text{CH}_2$ ), 3.86 - 3.91 (m, 1H,  $4'$ - $\text{CH}$ ), 4.18 (m, 1H,  $3'$ - $\text{CH}$ ), 5.29 (t,  $J$  = 5.4 Hz, 1H,  $5'$ - $\text{OH}$ ), 6.17 (t,  $J$  = 7.5 Hz, 1H,  $1'$ - $\text{CH}$ ), 6.31 (d,  $J$  = 6.5 Hz, 1H,  $3'$ - $\text{OH}$ ), 7.28 (d,  $J$  = 7.6 Hz, 1H, 6- $\text{CH}$ ), 8.23 (d,  $J$  = 7.6 Hz, 1H, 5- $\text{CH}$ ), 10.97 (s, 1H,  $\text{NH}$ ).

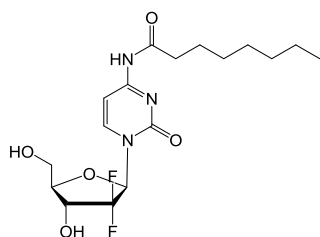
**$^{13}\text{C}$  NMR (DMSO- $d_6$ )**  $\delta$  13.95, 22.09, 24.34, 28.42, 28.64, 28.70, 28.82, 31.26, 36.39, 58.78, 68.18, 68.36, 68.54, 81.00, 95.90, 144.71, 154.20, 162.88, 174.10

**$^{19}\text{F}$  NMR (DMSO- $d_6$ )**  $\delta$  -116.90

**m/z:** HRMS (TOF ES<sup>+</sup>)  $\text{C}_{19}\text{H}_{30}\text{F}_2\text{N}_3\text{O}_5$   $[\text{M}+\text{H}]^+$  calculated 418.2148; found 418.3476

**m.p:** 136 - 140 °C

***N*-(1-((2*R*,4*R*,5*R*)-3,3-difluoro-4-hydroxy-5-(hydroxymethyl)tetrahydrofuran-2-yl)-2-oxo-1,2-dihydropyrimidin-4-yl)octanamide (51d)**



CDMT (1.53 mmol, 1 eqv, 217 mg), NMM (2.07 mmol, 1.36 eqv, 228  $\mu\text{L}$ ),  $\text{CH}_2\text{Cl}_2$  (6 mL). Octanoic acid (1.52 mmol, 1 eqv, 242  $\mu\text{L}$ ) in DMF (2 mL). Gemcitabine (1.53 mmol, 1 eqv, 400 mg) in DMF (4 mL).

**Yield:** 42.1 %

**HPLC purity:** 99.0 %

**HPLC  $t_R$ :** 17.1 min

**$^1\text{H}$  NMR (DMSO- $d_6$ )**  $\delta$  0.86 (t,  $J$  = 6.9 Hz, 3H,  $\text{CH}_3$ ), 1.25 (br-m, 8H,  $\text{CH}_2$ - $(\text{CH}_2)_4$ - $\text{CH}_3$ ), 1.46 – 1.62 (m, 2H,  $\text{C}=\text{O}$ - $\text{CH}_2$ - $\text{CH}_2$ ), 2.40 (t,  $J$  = 7.4 Hz, 2H,  $\text{C}=\text{O}$ - $\text{CH}_2$ ), 3.57 – 3.83 (m, 2H,

$^1\text{H}$  NMR (DMSO- $d_6$ )  $\delta$  3.87 - 3.91 (m, 1H, 4'-CH), 4.12 - 4.26 (m, 1H, 3'-CH), 5.29 (t,  $J$  = 5.4 Hz, 1H, 5'-OH), 6.17 (t,  $J$  = 7.5 Hz, 1H, 1'-CH), 6.31 (d,  $J$  = 6.5 Hz, 1H, 3'-OH), 7.28 (d,  $J$  = 7.6 Hz, 1H, 6-CH), 8.23 (d,  $J$  = 7.6 Hz, 1H, 5-CH), 10.97 (s, 1H, NH).

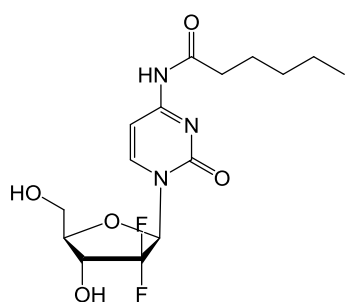
$^{13}\text{C}$  NMR (DMSO- $d_6$ )  $\delta$  13.93, 22.05, 24.36, 28.40, 31.10, 36.40, 58.78, 68.36, 81.01, 95.91, 122.94, 144.72, 154.21, 162.89, 174.12

$^{19}\text{F}$  NMR (DMSO- $d_6$ )  $\delta$  -116.91

m/z: HRMS (TOF ES<sup>+</sup>) C<sub>17</sub>H<sub>26</sub>F<sub>2</sub>N<sub>3</sub>O<sub>5</sub> [M+H]<sup>+</sup> calculated 390.1835 ; found 390.1537

m.p: 142 - 144 °C

***N*-(1-((2*R*,4*R*,5*R*)-3,3-difluoro-4-hydroxy-5-(hydroxymethyl)tetrahydrofuran-2-yl)-2-oxo-1,2-dihydropyrimidin-4-yl)hexanamide (51e)**



CDMT (1.50 mmol, 1 eqv, 214 mg), NMM (2.04 mmol, 1.36 eqv, 225  $\mu\text{L}$ ), CH<sub>2</sub>Cl<sub>2</sub> (6 mL). Octanoic acid (1.50 mmol, 1 eqv, 187  $\mu\text{L}$ ) in DMF (2 mL). Gemcitabine (1.50 mmol, 1 eqv, 395 mg) in DMF (4 mL)

**Yield:** 43.0 %

**HPLC purity:** 99.0 %

**HPLC t<sub>R</sub>:** 14.8 min

$^1\text{H}$  NMR (DMSO- $d_6$ )  $\delta$  0.86 (t,  $J$  = 6.9 Hz, 3H, CH<sub>3</sub>), 1.20 - 1.33 (m, 4H, CH<sub>2</sub>-(CH<sub>2</sub>)<sub>2</sub>-CH<sub>3</sub>), 1.51 - 1.58 (m, 2H, C=O-CH<sub>2</sub>-CH<sub>2</sub>), 2.40 (t,  $J$  = 7.4 Hz, 2H, C=O-CH<sub>2</sub>), 3.62 - 3.83 (m, 2H, 5'-CH<sub>2</sub>), 3.87 - 3.91 (m, 1H, 4'-CH), 4.12 - 4.26 (m, 1H, 3'-CH), 5.29 (t,  $J$  = 5.6 Hz, 1H, 5'-OH), 6.17 (t,  $J$  = 7.7 Hz, 1H, 1'-CH), 6.31 (d,  $J$  = 6.6 Hz, 1H, 3'-OH), 7.28 (d,  $J$  = 7.6 Hz, 1H, 6-CH), 8.23 (d,  $J$  = 7.6 Hz, 1H, 5-CH), 10.97 (s, 1H, NH).

$^{13}\text{C}$  NMR (DMSO- $d_6$ )  $\delta$  13.80, 21.83, 24.03, 30.65, 36.34, 58.77, 68.35, 81.00, 95.89, 144.72, 154.19, 162.87, 174.10

$^{19}\text{F}$  NMR (DMSO- $d_6$ )  $\delta$  -116.83

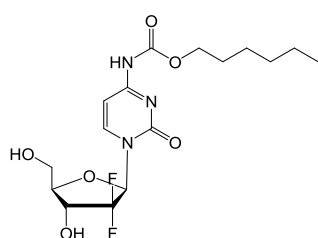
**m/z:** HRMS (TOF ES<sup>+</sup>) C<sub>15</sub>H<sub>22</sub>F<sub>2</sub>N<sub>3</sub>O<sub>5</sub> [M+H]<sup>+</sup> calculated 362.1522; found 361.9477

**m.p:** 152 – 153 °C

**General procedure for the *N*-carbamate-substitution of 4-amino-1-((2*R*,4*R*,5*R*)-3,3-difluoro-4-hydroxy-5-(hydroxymethyl)tetrahydrofuran-2-yl)pyrimidin-2(1*H*)-one**

Gemcitabine (**30**, 1 mmol, 1 eqv, 263 mg) was dissolved in anhydrous CH<sub>2</sub>Cl<sub>2</sub> (6 mL) at 0 °C, with continuous stirring. Anhydrous pyridine (2 mmol, 2 eqv, 161 μL) and acyl chloroformate (1.2 mmol, 1.2 eqv) were added and the reaction mixture stirred for 10 min at 0 °C. The temperature was increased to room temperature (~ 25 °C) and the reaction stirred for a further 4 h. The mixture was then evaporated *in vacuo* and purified by silica column chromatography 0 - 10 % MeOH/CH<sub>2</sub>Cl<sub>2</sub> containing 0.05 % NH<sub>4</sub>OH.

**Hexyl 1-((2*R*,4*R*,5*R*)-3,3-difluoro-4-hydroxy-5-(hydroxymethyl)tetrahydrofuran-2-yl)-2-oxo-1,2-dihydropyrimidin-4-yl)carbamate (**52a**)**



Hexyl chloroformate (1.2 mmol, 1.2 eqv, 196 μL)

**Yield:** 27.8 %

**HPLC purity:** 96.5 %

**HPLC t<sub>R</sub>:** 17.2 min

**<sup>1</sup>H NMR (DMSO-*d*<sub>6</sub>)** δ 0.87 (t, *J* = 6.9 Hz, 3H, CH<sub>3</sub>), 1.20 – 1.40 (m, 6H, CH<sub>2</sub>-(CH<sub>2</sub>)<sub>3</sub>-CH<sub>3</sub>), 1.54 -1.69 (m, 2H, C=O-CH<sub>2</sub>-CH<sub>2</sub>), 3.61 – 3.84 (m, 2H, 5'-CH<sub>2</sub>), 3.84 – 3.92 (m, 1H, 4'-CH), 4.11 (t, *J* = 6.7 Hz, 2H, C=O-O-CH<sub>2</sub>), 4.19 (td, *J* = 12.6, 7.1 Hz, 1H, 3'-CH), 5.29 (t, *J* = 5.5 Hz, 1H, 5'-OH), 6.16 (t, *J* = 7.5 Hz, 1H, 1'-CH), 6.31 (d, *J* = 6.5 Hz, 1H, 3'-OH), 7.10 (d, *J* = 7.6 Hz, 1H, 6-CH), 8.21 (d, *J* = 7.7 Hz, 1H, 5-CH), 10.82 (s, 1H, NH)

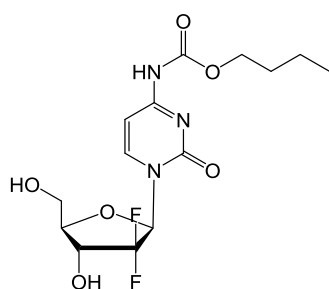
**<sup>13</sup>C NMR (DMSO-*d*<sub>6</sub>)** δ 14.34, 22.47, 25.29, 28.62, 31.22, 59.26, 65.83, 68.85, 81.44, 95.33, 124.38, 144.80, 150.09, 153.66, 154.49, 163.90

$^{19}\text{F}$  NMR (DMSO- $d_6$ )  $\delta$  -116.34

**m/z:** HRMS (TOF ES<sup>+</sup>) C<sub>16</sub>H<sub>24</sub>F<sub>2</sub>N<sub>3</sub>O<sub>6</sub> [M+H]<sup>+</sup> calculated 392.1628; found 391.9635

**m.p:** 94 – 97 °C

**Butyl (1-((2R,4R,5R)-3,3-difluoro-4-hydroxy-5-(hydroxymethyl)tetrahydrofuran-2-yl)-2-oxo-1,2-dihydropyrimidin-4-yl)carbamate (52b)**



n-butyl chloroformate (1.2 mmol, 1.2 eqv, 164 mg)

**Yield:** 29.0 %

**HPLC purity:** 95.3 %

**HPLC t<sub>R</sub>:** 12.8 min

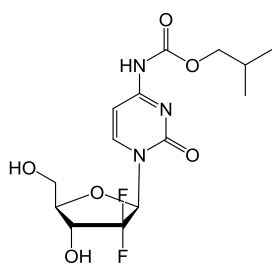
$^1\text{H}$  NMR (DMSO- $d_6$ )  $\delta$  0.90 (t,  $J$  = 7.4 Hz, 3H, CH<sub>3</sub>), 1.35 (dq,  $J$  = 14.5, 7.4 Hz, 2H, CH<sub>2</sub>-CH<sub>3</sub>), 1.48 - 1.67 (m, 2H, C=O-CH<sub>2</sub>-CH<sub>2</sub>), 3.60 – 3.84 (m, 2H, 5'-CH<sub>2</sub>), 3.84 – 3.92 (m, 1H, 4'-CH), 4.12 (t,  $J$  = 6.6 Hz, 2H, C=O-O-CH<sub>2</sub>), 4.07 - 4.25 (m, 1H, 3'-CH), 5.29 (t,  $J$  = 5.4 Hz, 1H, 5'-OH), 6.16 (t,  $J$  = 7.5 Hz, 1H, 1'-CH), 6.31 (d,  $J$  = 6.5 Hz, 1H, 3'-OH), 7.10 (d,  $J$  = 7.6 Hz, 1H, 6-CH), 8.21 (d,  $J$  = 7.6 Hz, 1H, 5-CH), 10.80 (s, 1H, NH)

$^{13}\text{C}$  NMR (DMSO- $d_6$ )  $\delta$  14.01, 18.92, 30.71, 59.27, 65.55, 81.44, 95.32, 121.36, 123.42, 125.47, 144.82, 153.66, 154.49, 163.89

$^{19}\text{F}$  NMR (DMSO- $d_6$ )  $\delta$  -116.75

**m/z:** HRMS (TOF ES<sup>+</sup>) C<sub>14</sub>H<sub>20</sub>F<sub>2</sub>N<sub>3</sub>O<sub>6</sub> [M+H]<sup>+</sup> calculated 364.1315; found 364.2564

**m.p:** 96 – 99 °C

***iso*-Butyl (1-((2*R*,4*R*,5*R*)-3,3-difluoro-4-hydroxy-5-(hydroxymethyl)tetrahydrofuran-2-yl)-2-oxo-1,2-dihydropyrimidin-4-yl)carbamate (52c)***i*-butyl chloroformate (1.2 mmol, 1.2 eqv, 164 mg)**Yield:** 25.6 %**HPLC purity:** 94.9 %**HPLC  $t_R$ :** 12.9 min

**$^1\text{H}$  NMR (DMSO- $d_6$ )**  $\delta$  0.91 (d,  $J = 6.7$  Hz, 3H, (CH $_3$ ) $_2$ ), 1.91 (m, 1H, CH-(CH $_3$ ) $_2$ ), 3.62 – 3.81 (m, 2H, 5'-CH $_2$ ), 3.84 – 3.91 (m, 1H, 4'-CH), 3.90 (d,  $J = 6.5$  Hz, 2H, O-CH $_2$ ), 4.12–4.23 (m, 1H, 3'-CH), 5.30 (t,  $J = 5.4$  Hz, 1H, 5'-OH), 6.16 (t,  $J = 7.3$  Hz, 1H, 1'-CH), 6.32 (d,  $J = 6.6$  Hz, 1H, 3'-OH), 7.08 (d,  $J = 7.7$  Hz, 1H, cytosine 6-CH), 8.21 (d,  $J = 7.6$  Hz, 1H, 5-CH), 10.80 (s, 1H, NH)

**$^{13}\text{C}$  NMR (DMSO- $d_6$ )**  $\delta$  14.02, 18.91, 30.71, 59.27, 65.55, 81.44, 95.32, 144.82, 153.66, 154.46, 163.89

**$^{19}\text{F}$  NMR (DMSO- $d_6$ )**  $\delta$  -116.53

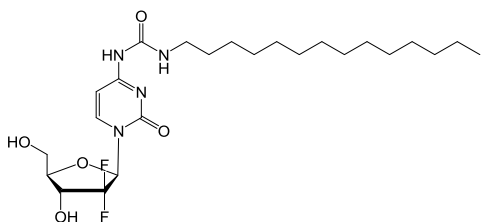
**$m/z$ :** HRMS (TOF ES $^+$ ) C $_{14}$ H $_{20}$ F $_2$ N $_3$ O $_6$  [M+H] $^+$  calculated 364.1315; found 364.1997

**$m.p$ :** 100 - 104 °C

**General procedure for the *N*-urea-substitution of 4-amino-1-((2*R*,4*R*,5*R*)-3,3-difluoro-4-hydroxy-5-(hydroxymethyl)tetrahydrofuran-2-yl)pyrimidin-2(1*H*)-one**

Gemcitabine (**30**, 1 mmol, 1 eqv, 263 mg) was dissolved in anhydrous DMF (21 mL) with stirring, under nitrogen. Acyl isocyanate (1 mmol, 1 eqv) in anhydrous DMF (1mL/10mg gemcitabine, 26.3 mL) was added dropwise under nitrogen and the mixture stirred at room temperature. Upon completion the mixture was evaporated *in vacuo* and purified with silica column chromatography, 0 - 12 % MeOH/CH $_2$ Cl $_2$ .

**1-((1-((2*R*,4*R*,5*R*)-3,3-difluoro-4-hydroxy-5-(hydroxymethyl)tetrahydrofuran-2-yl)-2-oxo-1,2-dihydropyrimidin-4-yl)-3-tetradecylurea (53a)**



Tetradecyl isocyanate was added in aliquots of 55  $\mu\text{L}$  (0.2 mmol, 0.2 eqv) at 1 h intervals, so that after 4 h a total of 275  $\mu\text{L}$  (1 mmol) had been added. Reaction stirred for 168 h.

**Yield:** 54.6 %

**HPLC purity:** 96.2 %

**HPLC  $t_R$ :** 24.6 min

**$^1\text{H}$  NMR (DMSO- $d_6$ )**  $\delta$  0.85 (t,  $J = 6.8$  Hz, 3H,  $\text{CH}_3$ ), 1.25 (br-m, 22H,  $(\text{CH}_2)_{11}\text{-CH}_3$ ), 1.42 - 1.45 (m, 2H,  $\text{C=O-CH}_2\text{-CH}_2$ ), 3.13 - 3.22 (m, 2H,  $\text{C=O-HN-CH}_2$ ), 3.58 - 3.82 (m, 2H, 5'- $\text{CH}_2$ ), 3.86 (dt,  $J = 8.4, 3.0$  Hz, 1H, 4'- $\text{CH}$ ), 4.10 - 4.24 (m, 1H, 3'- $\text{CH}$ ), 5.27 (t,  $J = 5.4$  Hz, 1H, 5'- $\text{OH}$ ), 6.13 (t,  $J = 7.6$  Hz, 1H, 1'- $\text{CH}$ ), 6.25 - 6.46 (s, 1H, 3'- $\text{OH}$ ), 6.29 (d,  $J = 6.5$  Hz, 1H, 6'- $\text{CH}$ ), 8.07 (d,  $J = 7.5$  Hz, 1H, 5'- $\text{CH}$ ), 8.86 (br-s, 1H,  $\text{NH-CH}_2$ ), 9.99 (s, 1H,  $\text{NH}$ )

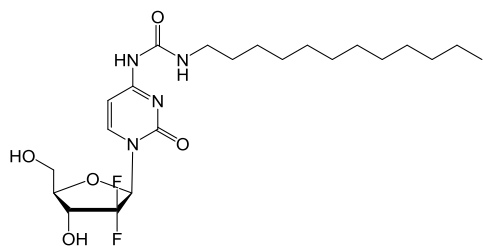
**$^{13}\text{C}$  NMR (DMSO- $d_6$ )**  $\delta$  14.43, 22.56, 26.81, 29.12, 29.17, 29.42, 29.47, 29.50, 29.70, 31.17, 31.76, 49.06, 59.27, 68.82, 81.39, 95.80, 123.42, 143.42, 153.67, 163.04

**$^{19}\text{F}$  NMR (DMSO- $d_6$ )**  $\delta$  -117.03

**m/z:** HRMS (TOF ES $^+$ )  $\text{C}_{24}\text{H}_{41}\text{F}_2\text{N}_4\text{O}_5$   $[\text{M}+\text{H}]^+$  calculated 503.3040; found 503.3099

**m.p:** 125 - 128  $^\circ\text{C}$

**1-(1-((2*R*,4*R*,5*R*)-3,3-difluoro-4-hydroxy-5-(hydroxymethyl)tetrahydrofuran-2-yl)-2-oxo-1,2-dihydropyrimidin-4-yl)-3-dodecylurea (53b)**



Dodecyl isocyanate (1 mmol, 1 eqv, 241  $\mu$ L).

Reaction stirred for 70 h.

**Yield:** 54.6 %

**HPLC purity:** 98.3 %

**HPLC  $t_R$ :** 22.9 min

**$^1\text{H NMR}$  (DMSO- $d_6$ )**  $\delta$  0.85 (t,  $J$  = 6.8 Hz, 3H,  $\text{CH}_3$ ), 1.25 (br-m, 22H,  $(\text{CH}_2)_{11}\text{-CH}_3$ ), 1.42 - 1.45 (m, 2H,  $\text{C=O-CH}_2\text{-CH}_2$ ), 3.13 - 3.22 (m, 2H,  $\text{C=O-HN-CH}_2$ ), 3.58 - 3.82 (m, 2H, 5'- $\text{CH}_2$ ), 3.86 (dt,  $J$  = 8.4, 3.0 Hz, 1H, 4'- $\text{CH}$ ), 4.10 - 4.24 (m, 1H, 3'- $\text{CH}$ ), 5.27 (t,  $J$  = 5.4 Hz, 1H, 5'- $\text{OH}$ ), 6.13 (t,  $J$  = 7.6 Hz, 1H, 1- $\text{CH}$ ), 6.25 - 6.46 (s, 1H, 3'- $\text{OH}$ ), 6.29 (d,  $J$  = 6.5 Hz, 1H, 6- $\text{CH}$ ), 8.07 (d,  $J$  = 7.5 Hz, 1H, 5- $\text{CH}$ ), 8.86 (br-s, 1H,  $\text{NH-CH}_2$ ), 9.99 (s, 1H,  $\text{NH}$ )

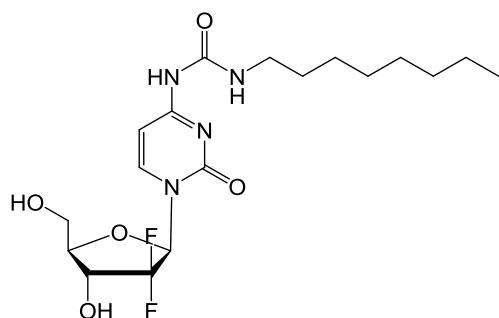
**$^{13}\text{C NMR}$  (DMSO- $d_6$ )**  $\delta$  14.42, 22.56, 26.80, 29.12, 29.17, 29.42, 29.47, 29.49, 29.70, 31.17, 31.76, 49.06, 59.27, 68.82, 81.39, 95.80, 123.42, 143.41, 153.67, 163.04

**$^{19}\text{F NMR}$  (DMSO- $d_6$ )**  $\delta$  -116.98

**m/z:** HRMS (TOF ES<sup>+</sup>)  $\text{C}_{22}\text{H}_{37}\text{F}_2\text{N}_4\text{O}_5$  [M+H]<sup>+</sup> calculated 475.2727; found 475.2956

**m.p:** 124 - 126  $^\circ\text{C}$

**1-(1-((2*R*,4*R*,5*R*)-3,3-difluoro-4-hydroxy-5-(hydroxymethyl)tetrahydrofuran-2-yl)-2-oxo-1,2-dihydropyrimidin-4-yl)-3-octylurea (53c)**



Octyl isocyanate (1 mmol, 1 eqv, 176  $\mu$ L).

Reaction stirred for 48 h

**Yield:** 53.4 %

**HPLC purity:** 95.7 %

**HPLC t<sub>R</sub>:** 21.1 min

**<sup>1</sup>H NMR** (DMSO-*d*<sub>6</sub>, 400 MHz) δ 0.85 (t, *J* = 6.9 Hz, 3H, CH<sub>3</sub>), 1.25 (br-m, 10H, (CH<sub>2</sub>)<sub>5</sub>-CH<sub>3</sub>), 1.39 -1.57 (m, 2H, C=O-CH<sub>2</sub>-CH<sub>2</sub>), 3.17 (m, 2H, C=O-HN-CH<sub>2</sub>), 3.58 – 3.83 (m, 2H, 5'-CH<sub>2</sub>), 3.87 (dt, *J* = 8.5, 3.1 Hz, 1H, 4'-CH), 4.10 - 4.24 (m, 1H, 3'-CH), 5.27 (t, *J* = 5.4 Hz, 1H, 5'-OH), 6.14 (t, *J* = 7.6 Hz, 1H, 1'-CH), 6.30 (d, *J* = 6.5 Hz, 1H, 6-CH), 6.31 (br-s, 1H, 3'-OH), 8.07 (d, *J* = 7.5 Hz, 1H, 5-CH), 8.86 (br-s, 1H, NH-CH<sub>2</sub>), 9.99 (s, 1H, NH)

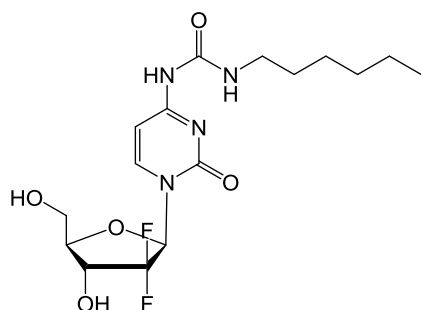
**<sup>13</sup>C NMR** (DMSO-*d*<sub>6</sub>, 100 MHz) δ 14.41, 22.54, 26.82, 29.10, 29.71, 31.68, 49.06, 59.27, 68.82, 81.39, 95.80, 123.43, 143.43, 153.67, 163.04

**<sup>19</sup>F NMR** (DMSO-*d*<sub>6</sub>) δ -116.86

**m/z:** HRMS (TOF ES<sup>+</sup>) C<sub>18</sub>H<sub>29</sub>F<sub>2</sub>N<sub>4</sub>O<sub>5</sub> [M+H]<sup>+</sup> calculated 419.2101; found 419.6169

**m.p:** 100 – 104 °C

**1-(1-((2*R*,4*R*,5*R*)-3,3-difluoro-4-hydroxy-5-(hydroxymethyl)tetrahydrofuran-2-yl)-2-oxo-1,2-dihydropyrimidin-4-yl)-3-hexylurea (53d)**



Octyl isocyanate (1 mmol, 1 eqv, 146 μL). Reaction stirred for 96 h

**Yield:** 36.1 %

**HPLC purity:** 97.3 %

**HPLC t<sub>R</sub>:** 19.8 min

**<sup>1</sup>H NMR** (DMSO-*d*<sub>6</sub>) δ 0.87 (t, *J* = 6.9 Hz, 3H, CH<sub>3</sub>), 1.29 (br-m, 6H, (CH<sub>2</sub>)<sub>3</sub>-CH<sub>3</sub>), 1.39 - 1.45 (m, 2H, C=O-CH<sub>2</sub>-CH<sub>2</sub>), 3.18 (dd, *J* = 12.7, 6.7 Hz, 2H, C=O-HN-CH<sub>2</sub>), 3.56 – 3.83 (m, 2H, 5'-CH<sub>2</sub>), 3.87 (dt, *J* = 8.4, 3.0 Hz, 1H, 4'-CH), 4.04 - 4.29 (m, 1H, 3'-CH), 5.27 (t, *J* = 5.4 Hz, 1H, 5'-OH), 6.14 (t, *J* = 7.6 Hz, 1H, 1'-CH), 6.30 (d, *J* = 6.5 Hz, 1H, 6-CH), 6.34 (br-s, 1H, 3'-OH), 8.07 (d, *J* = 7.5 Hz, 1H, 5-CH), 8.86 (br-s, 1H, NH-CH<sub>2</sub>), 9.99 (br-s, 1H, NH)

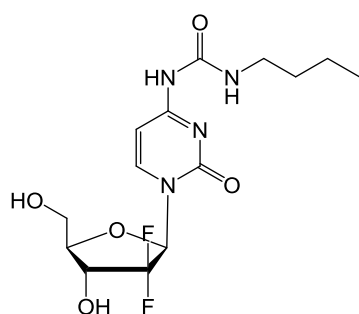
**<sup>13</sup>C NMR** (DMSO-*d*<sub>6</sub>) δ 14.37, 22.51, 26.50, 29.69, 31.37, 59.27, 68.82, 81.38, 95.80, 123.43, 143.42, 153.67, 163.04

$^{19}\text{F}$  NMR (DMSO- $d_6$ )  $\delta$  -117.01

**m/z:** HRMS (TOF ES $^+$ )  $\text{C}_{16}\text{H}_{24}\text{F}_2\text{N}_4\text{O}_5$  [M+H] $^+$  calculated 390.1715; found 390.4529

**m.p:** 116 – 120 °C

**1-butyl-3-(1-((2*R*,4*R*,5*R*)-3,3-difluoro-4-hydroxy-5-(hydroxymethyl)tetrahydro-furan-2-yl)-2-oxo-1,2-dihydropyrimidin-4-yl)urea (53e)**



*n*-butyl isocyanate (1 mmol, 1 eqv, 113  $\mu\text{L}$ ). Reaction stirred for 96 h

**Yield:** 26.0 %

**HPLC purity:** 96.4 %

**HPLC  $t_R$ :** 17.2 min

$^1\text{H}$  NMR (DMSO- $d_6$ )  $\delta$  0.90 (t,  $J$  = 7.3 Hz, 3H,  $\text{CH}_3$ ), 1.32 (m, 2H,  $\text{CH}_2\text{-CH}_3$ ), 1.40 -1.51 (m, 2H,  $\text{C=O-CH}_2\text{-CH}_2$ ), 3.18 (m, 2H,  $\text{C=O-NH-CH}_2$ ), 3.59 – 3.83 (m, 2H,  $5'\text{-CH}_2$ ), 3.87 (dt,  $J$  = 8.5, 3.1 Hz, 1H,  $4'\text{-CH}$ ), 4.16 (ddd,  $J$  = 14.3, 10.4, 4.9 Hz, 1H,  $3'\text{-CH}$ ), 5.27 (t,  $J$  = 5.4 Hz, 1H,  $5'\text{-OH}$ ), 6.14 (t,  $J$  = 7.6 Hz, 1H,  $1'\text{-CH}$ ), 6.30 (d,  $J$  = 6.5 Hz, 1H,  $6\text{-CH}$ ), 6.31 (br-s, 1H,  $3'\text{-OH}$ ), 8.07 (d,  $J$  = 7.5 Hz, 1H,  $5\text{-CH}$ ), 8.86 (br-s, 1H,  $\text{NH-CH}_2$ ), 9.99 (br-s, 1H,  $\text{NH}$ )

$^{13}\text{C}$  NMR (DMSO- $d_6$ )  $\delta$  13.62, 19.55, 31.37, 38.78, 48.59, 58.80, 68.35, 80.91, 95.34, 142.95, 153.31, 162.57

$^{19}\text{F}$  NMR (DMSO- $d_6$ )  $\delta$  -116.89

**m/z:** HRMS (TOF ES $^+$ )  $\text{C}_{14}\text{H}_{21}\text{F}_2\text{N}_4\text{O}_5$  [M+H] $^+$  calculated 363.1475; found 362.9986

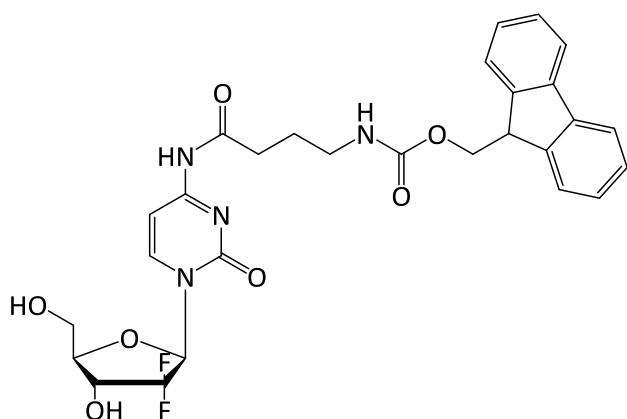
**m.p:** 120 - 124 °C

**General procedure for the *N*-peptide-substitution of 4-amino-1-((2*R*,4*R*,5*R*)-3,3-difluoro-4-hydroxy-5-(hydroxymethyl)tetrahydrofuran-2-yl)pyrimidin-2(1*H*)-one**

Fmoc-protected amino acid (1.1 mmol, 1.1 eqv) and HATU (1 mmol, 1 eqv, 380 mg) were solubilised in anhydrous DMF (10 mL) at 0 °C and stirred under nitrogen for 1 h.

Gemcitabine (**30**, 1 mmol, 1 eqv, 263 mg) and DIPEA (3 mmol, 3 eqv, 522  $\mu$ L) were made into solution in anhydrous DMF (10 mL) at 0°C. The flask containing the activated Fmoc-protected amino acid was added dropwise to the flask containing gemcitabine at 0 °C and stirred for a further h. The temperature was increased to room temperature (~ 25 °C) and the reaction monitored by TLC. Products were purified using preparative RP-HPLC. TFA salts were removed from post-purified products using an aqueous wash with CH<sub>2</sub>Cl<sub>2</sub>. Products were basified until neutral with Na<sub>2</sub>CO<sub>3</sub> and dried over Na<sub>2</sub>SO<sub>4</sub> and gravity filtered. All compounds were found to have a purity of > 99 %.

**(9H-fluoren-9-yl)methyl 4-((1-((2R,4R,5R)-3,3-difluoro-4-hydroxy-5-(hydroxymethyl) tetrahydrofuran-2-yl)-2-oxo-1,2-dihydropyrimidin-4-yl)amino)-4-oxobutyl) carbamate (66)**



Fmoc-gamma amino butyric acid (GABA)-OH (1.1 mmol, 1.1 eqv, 358 mg)

**Yield:** 67.1 %

**HPLC t<sub>R</sub>:** 16.28 min

**<sup>1</sup>H NMR (DMSO-*d*<sub>6</sub>)**  $\delta$  1.69 (m, 2H, C=O-CH<sub>2</sub>), 2.43 (t, *J* = 7.7 Hz, 2H, NH-CH<sub>2</sub>-CH<sub>2</sub>), 3.00 (q, *J* = 6.6 Hz, 2H, NH-CH<sub>2</sub>), 3.63 – 3.83 (m, 2H, 5'-CH<sub>2</sub>), 3.88 – 3.91 (m, 1H, 4'-H), 4.14 – 4.23 (m, 2H, NH-C=O-O, 3'-CH), 3.90 (m, 1H, CH<sub>3</sub>-CH) 4.30 (d, *J* = 7.1 Hz, 2H, O-CH<sub>2</sub>), 5.30 (t, *J* = 5.4 Hz, 1H, 5'-OH), 6.18 (t, *J* = 7.3 Hz, 1H, 1'-CH), 6.32 (d, *J* = 6.6 Hz, 1H, 3'-OH), 7.28 (d, *J* = 7.6 Hz, cytosine 6-H), 7.34 (t, *J* = 7.4 Hz, 2H, fluorenyl 4-H, 11-H), 7.42 (t, *J* = 7.6 Hz, 2H, fluorenyl 5-H, 10-H), 7.69 (d, *J* = 7.6 Hz, 2H, fluorenyl 3-H, 12-H), 7.90 (d, *J* = 7.6 Hz, 2H, fluorenyl 6-H, 9-H), 8.24 (d, *J* = 7.6 Hz, 1H, cytosine 5-H), 11.00 (s, 1 H, cytosine 4-NH)

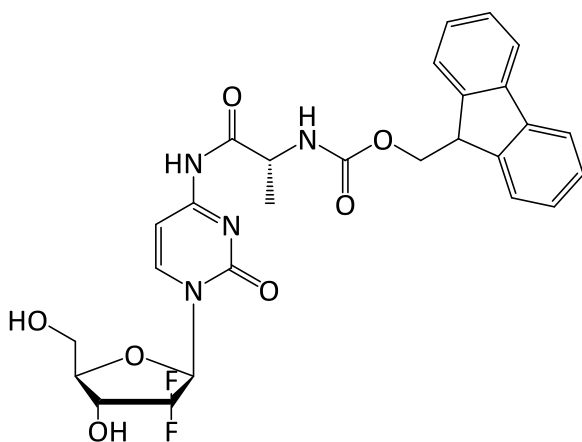
**<sup>13</sup>C NMR (DMSO-*d*<sub>6</sub>)**  $\delta$  25.04, 34.14, 47.23, 59.26, 65.69, 68.83, 81.48, 96.39, 120.59, 125.60, 127.53, 128.06, 141.21, 145.20, 154.67, 156.59, 163.32, 174.16

<sup>19</sup>F NMR (DMSO-*d*<sub>6</sub>) δ -116.89

m/z: HRMS (TOF ES<sup>+</sup>) C<sub>28</sub>H<sub>29</sub>F<sub>2</sub>N<sub>4</sub>O<sub>7</sub> [M+H]<sup>+</sup> calculated 571.1999; found 571.2853

m.p: 116 – 120 °C

(9H-fluoren-9-yl)methyl ((R)-1-((1-((2R,4R,5R)-3,3-difluoro-4-hydroxy-5-(hydroxymethyl)tetrahydrofuran-2-yl)-2-oxo-1,2-dihydropyrimidin-4-yl)amino)-1-oxopropan-2-yl)carbamate (67)



Fmoc-alanine (Fmoc-Ala-OH)(1.1 mmol, 1.1 eqv, 342 mg)

Yield: 77.0 %

HPLC t<sub>R</sub>: 19.0 min

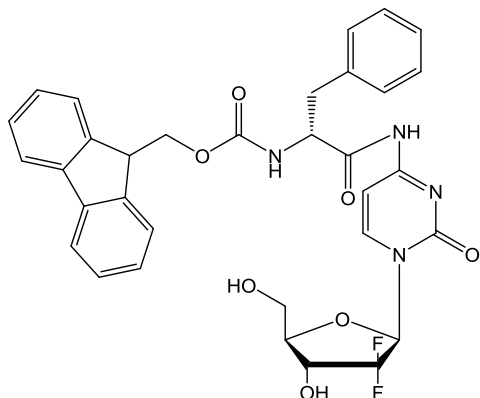
<sup>1</sup>H NMR (DMSO-*d*<sub>6</sub>) δ 1.30 (d, *J* = 6.9 Hz, CH<sub>3</sub>), 3.58 – 3.75 (m, 2H, 5'-CH<sub>2</sub>), 3.79 (m, 1H, 4'-H), 3.90, (m, 1H, CH<sub>3</sub>-CH), 4.16 – 4.31 (m, 5H, fluorenyl 1-H, O-CH<sub>2</sub>, 3'-H), 5.31 (t, *J* = 5.4 Hz, 1H, 5'-OH), 6.19 (t, *J* = 7.2 Hz, 1H, 1'-CH), 6.33 (d, *J* = 7.2 Hz, 1H, 3'-OH), 7.27 (d, *J* = 7.6 Hz, cytosine 6-H), 7.35 (m, 2H, fluorenyl 4-H, 11-H), 7.41 (m, 2H, fluorenyl 5-H, 10-H), 7.72 - 7.76 (dd, *J* = 6.5, 12.4 Hz, 3H, fluorenyl 3-H, 12-H, alanine N-H), 7.90 (d, *J* = 7.5 Hz, 2H, fluorenyl 6-H, 9-H), 8.28 (d, *J* = 7.5 Hz, 1H, cytosine 5-H), 11.11 (s, 1 H, cytosine 4-NH)

<sup>19</sup>F NMR (DMSO-*d*<sub>6</sub>) δ -116.90

m/z: HRMS (TOF ES<sup>+</sup>) C<sub>27</sub>H<sub>27</sub>F<sub>2</sub>N<sub>4</sub>O<sub>7</sub> [M+H]<sup>+</sup> calculated 557.1842; found 557.1844

m.p: 90 – 96 °C

**(9H-fluoren-9-yl)methyl ((S)-1-((1-((2R,4R,5R)-3,3-difluoro-4-hydroxy-5-(hydroxymethyl)tetrahydrofuran-2-yl)-2-oxo-1,2-dihydropyrimidin-4-yl)amino)-1-oxo-3-phenylpropan-2-yl)carbamate (68)**



Fmoc-phenylalanine (Fmoc-Phe-OH)(1.1 mmol, 1.1 eqv, 426 mg)

**Yield:** 53.3 %

**HPLC t<sub>R</sub>:** 21.6 min

**<sup>1</sup>H NMR (DMSO-*d*<sub>6</sub>, 400 MHz)** δ 2.78 – 3.10 (m, 2H, phenyl-CH<sub>2</sub>), 3.64 – 3.83 (m, 2H, 5'-CH<sub>2</sub>), 3.89 – 3.92 (m, 1H, 4'-H), 4.12 – 4.25 (m, 4H, fluorenyl 1-H, O-CH<sub>2</sub>, 3'-CH), 4.49 – 4.53 (m, 1H, NH-CH), 5.31 (t, *J* = 5.3 Hz, 1H, 5'-OH), 6.18 (t, *J* = 7.3 Hz, 1H, N-CH-O), 6.33 (d, *J* = 6.5 Hz, 1H, 3'-OH), 7.21 (d, *J* = 7.7 Hz, 1H, cytosine 6-H), 7.25 – 7.42 (m, 9H, fluorenyl 3-H, 4-H, 11-H, 12-H, phenyl 2-H, 3-H, 4-H, 5-H, 6-H), 7.60 – 7.65 (dd, *J* = 7.5, 16.9 Hz, 2H, fluorenyl 5-H, 10-H), 7.83 (d, *J* = 8.3 Hz, 1H, cytosine 5-H), 7.87 (d, *J* = 7.5 Hz, 2H, fluorenyl-6-H, 9-H), 8.29 (d, *J* = 7.6 Hz, 1H, NH), 11.38 (s, 1 H, cytosine 4-NH)

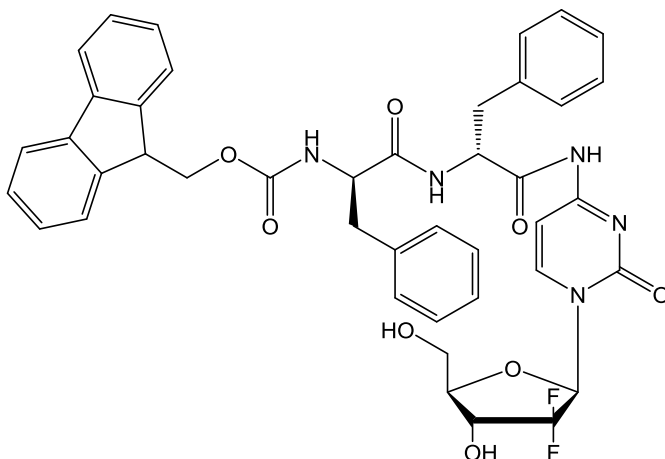
**<sup>13</sup>C NMR (DMSO-*d*<sub>6</sub>)** δ 31.24, 36.25, 46.99, 59.22, 66.17, 81.52, 96.42, 120.58, 125.70, 126.93, 127.51, 128.10, 128.53, 129.84, 138.03, 141.12, 144.16, 154.59, 156.48, 162.77, 163.37, 174.04

**<sup>19</sup>F NMR (DMSO-*d*<sub>6</sub>)** δ -116.93

**m/z:** HRMS (TOF ES<sup>+</sup>) C<sub>33</sub>H<sub>31</sub>F<sub>2</sub>N<sub>4</sub>O<sub>7</sub> [M+H]<sup>+</sup> calculated 633.2155; found 633.2098

**m.p:** 119 – 122 °C

(9H-fluoren-9-yl)methyl ((R)-1-(((R)-1-((1-((2R,4R,5R)-3,3-difluoro-4-hydroxy-5-(hydroxymethyl)tetrahydrofuran-2-yl)-2-oxo-1,2-dihydropyrimidin-4-yl)amino)-1-oxo-3-phenylpropan-2-yl)amino)-1-oxo-3-phenylpropan-2-yl)carbamate (69)



Fmoc-diphenylalanine (Fmoc-PhePhe-OH) (1.1 mmol, 1.1 eqv, 588 mg)

**Yield:** 59.8 %

**HPLC  $t_R$ :** 23.6 min

**$^1\text{H NMR}$  (DMSO- $d_6$ )  $\delta$**  1.87 – 2.19 (m, 2H, phenyl- $\text{CH}_2$ ), 2.78 – 3.14 (m, 2H, phenyl- $\text{CH}_2$ ),

3.63 – 3.82 (m, 2H, 5'- $\text{CH}_2$ ), 3.89 – 3.91 (m, 1H, 4'- $\text{H}$ ), 4.07 – 4.14 (m, 4H, fluorenyl 1-H, O- $\text{CH}_2$ , 3'- $\text{CH}$ ), 4.17 – 4.29 (m, 2H, 2(NH- $\text{CH}$ )), 5.30 (t,  $J = 5.4$  Hz, 1H, 5'-OH), 6.19 (t,  $J = 7.3$  Hz, 1H, 1'- $\text{CH}$ ), 6.33 (d,  $J = 6.5$  Hz, 1H, 3'-OH), 7.18 – 7.40 (m, 14H, fluorenyl 3-H, 4-H, 11-H, 12-H, 2(phenyl 2-H, 3-H, 4-H, 5-H, 6-H)), 7.15 (d,  $J = 7.6$  Hz, 1H, NH), 7.44 (d,  $J = 8.3$  Hz, 1H, cytosine 6-H), 7.60 – 7.65 (dd,  $J = 7.1, 12.5$  Hz, 2H, fluorenyl 5-H, 10-H), 7.87 (d,  $J = 7.5$  Hz, 2H, fluorenyl-6-H, 9-H), 8.29 (d,  $J = 7.6$  Hz, 1H, NH), 8.53 (d,  $J = 8.2$  Hz, 1H, cytosine 5-H), 11.38 (s, 1 H, cytosine 4-NH)

**$^{19}\text{F NMR}$  (DMSO- $d_6$ )  $\delta$**  -116.96

**m/z:** HRMS (TOF ES<sup>+</sup>)  $\text{C}_{42}\text{H}_{40}\text{F}_2\text{N}_5\text{O}_8$  [M+H]<sup>+</sup> calculated 780.2839; found 780.2634

**m.p:** 124 – 127 °C

#### 4.5.2. Physicochemical Characterisation

##### 4.5.2.1. Stability to Inversion

Stability to inversion was carried out by weighing samples (2.5 mg) using an A and D GR-202 semi micro-analytical balance into 1.5 ml sample vials.

**Temperature mediated solvent switch:** Compound was solubilised in ethanol (Table 6) at an elevated temperature (60 °C) using a bespoke aluminium heating apparatus. Pre heated (60 °C) water was added to generate a final sample volume of 500  $\mu$ L and the sample left to cool to room temperature for 18 h, prior to inversion.

**Room temperature/sonication mediated solvent switch:** Compound was dispersed in either water or sodium chloride (100 – 400 mM)(500  $\mu$ L) at room temperature. Samples were sonicated for 30 s to solubilise compound and left to stand for 18 h prior to inversion.

#### **4.5.2.2. Rheological Experiments**

Rheology was carried out using an Anton Paar MCR302 Modular Compact Rheometer. A four-bladed vane geometry was used with a diameter of 8.5 mm and length 8.5 mm in a cup with a diameter of 14.5 mm. The solution of gelator was prepared in a 7 mL aluminium sample vial to a final sample volume of 2 mL, as per the method mentioned in Section 4.5.2.1. Once the gel was prepared, the sample vial was mounted in the lower plate (cup) of the rheometer; the vane (attached to the upper part) was lowered into place, at a depth of 3 mm. This arrangement gave a total sample depth of approximately 16 mm in the 14.5 mm diameter cup which allowed positioning of the vane in the centre of the vial. All oscillatory experiments, unless stated otherwise were carried out at a physiologically relevant temperature of 37 °C.

Amplitude sweeps were carried out at a strain ( $\gamma$ ) of 0.1 – 100 % and a constant frequency ( $\omega = 10$  rad/s). Frequency sweeps were carried out at an angular frequency 0.1 – 100 rad/s and at a constant strain as determined by the centre of the linear viscoelastic region. Recovery measurements were carried out at constant strain ( $\gamma$ ) and frequency ( $\omega$ ) as determined by the amplitude and frequency measurements.

#### **4.5.2.3. Transmission Electron Microscopy (TEM)**

TEM imaging was carried out by dispersing a small amount of gel in 150  $\mu$ L of ultra-purified water and pipetting on to a graphene oxide, lacey carbon coated copper grid (No. 300). Excess sample was blotted with Whatman 50 filter paper. The grid was

subjected to high vacuum in a Gatan dry pumping station (model 655) prior to inserting into the machine and imaging at an accelerated voltage of 100 kV.

#### **4.5.3. *In vitro* Growth Inhibition Assays**

Human derived MIA PaCa-2 (pancreatic adenocarcinoma) and MKN-7 (gastric adenocarcinoma) cells were sub-cultured at 37 °C in an atmosphere of 5 % CO<sub>2</sub> in RPMI 1640 medium supplemented with 10 % foetal bovine serum and routinely sub-cultured twice weekly to maintain continuous logarithmic growth. Experimental agents were prepared at 10 mM stock solutions dissolved in DMSO and stored at 4 °C protected from light for a maximum of 2 weeks. MRC-5 (foetal lung fibroblast) cells were sub-cultured in modified eagles medium (MEM, containing sodium bicarbonate) supplemented with 10 % heat inactivate foetal calf serum, 1 % penicillin/streptomycin, 1 % L-glutamine (200 mM), 1 % non-essential amino acids (0.1 mM), 1 % HEPES buffer (1 M) and 1 % sodium bicarbonate (7.5 %). MTT was made in sterile PBS at a concentration of 2 mg/mL.

**Growth inhibition assays:** Cells were seeded into 96-well microtiter plates at a density of  $3 - 5 \times 10^3$  cells/well and allowed to adhere for 24 h prior to the addition of test agents (final concentration 500 pM – 100  $\mu$ M, n = 8). Serial dilutions were prepared in medium immediately prior to each assay. Viable cells at the time of drug addition, (time zero (T<sub>0</sub>)) and following 72 h incubation period with test agents, were determined by cell-mediated MTT reduction. MTT was added to each well (final concentration 400  $\mu$ g/mL) and the plates incubated at 37 °C, 5 % CO<sub>2</sub> for 2h to allow the reduction of MTT to an insoluble formazan, which was solubilised by DMSO (150  $\mu$ L). Cell growth and agent activity were determined by measuring absorbance at 550 nm using an Anthos Labtec systems plate reader. Non-linear regression analysis was used to calculate compound concentrations required to inhibit 50 % cell growth (GI<sub>50</sub>).

## 5. Conclusions and Future Work

---

### 5.1. General Conclusions

Using cytosine based nucleosides (Cytidine (**39**) and 2'-deoxycytidine (**46**) and gemcitabine (**30**)) three new low molecular weight gelating systems were developed for intra-tumoural drug delivery; **42c**, **48d** and **51d**, respectively. The systems were synthesised, characterised and tested *in vitro* for biological relevance and release efficiency.

#### 5.1.1. Modified Cytidine as a Drug Delivery Platform

Simple chemical modification of the 4-amino position on the cytosine nucleobase with a tetradecanoyl chain afforded a suitably amphiphilic compound (**42c**). Other analogues with longer and shorter chains were synthesised but when prompted by a change in solvent polarity, weren't able to successfully self-assemble. **42c** assembled in a rapid (instantaneous) gelation process resulting in the formation of a stable self-assembled cross-linked fibrillar network.

Rheological testing, TEM imaging and FTIR alluded to the importance of the solvent: water ratio to the self-assembly process; showing that a gel containing a solvent volume fraction,  $\Phi_{\text{EtOH}}$  0.40, enhanced self-assembly capabilities, allowing for arrangement into an ordered highly cross-linked fibrillar structure with an increased mechanical strength. FT-IR spectroscopy indicated the critical importance of the amide functionality in the self-assembly process, though it was not able to provide more information about the interaction on a molecular level beyond this.

The potential application of such gels as reservoirs for both large and small bio macromolecular therapeutics was fully demonstrated. And the biocompatibility of the solid compound explored using growth inhibition assays, thus validating this system as an 'inert molecular gel scaffold' for the diffusion mediated delivery of low molecular weight compounds intra-tumourally.

However, there are significant drawbacks to this gelator formulation; its increased ethanol concentration is a hindrance, particularly when considering this gelator/gel for drug delivery applications beyond intra-tumoural or topical drug delivery. Developing a gelator with minimal (< 5 %) or no solvent interference i.e. a complete hydrogel, would be a way to overcome this. This would require increasing the water solubility/hydrophilicity of the compound or conversely decreasing the amount of lipophilic character introduced during the conjugation.

### 5.1.2. A Tale of Refinement

Using the gelator **42c** found in **Chapter 2** as a foundation, modifications were made in an attempt to enhance aqueous solubility and to improve the self-assembly process by driving it towards hydro-gelation.

Initial findings confirmed the existing amide functionality of **42c** as a key functionality in the gelation process. Additional studies focused on chemical modification of **46** and **47**, to probe the role of ribose hydroxyls in the gelation process. **48d**, an octanoyl derivative of **46**, was found to self-assemble in a 100 % aqueous environment, undergoing a fast molecular reorganisation into an ordered cross-linked structure when gelation was promoted by temperature change. Quantification of the mechanical properties by rheology alluded to a mechanically strong and self-healing gel, mimicking the injectability required for intra-tumoural delivery.

TEM imaging and *in vitro* release studies once again demonstrated the application of the 'inert gel scaffold' *via* the diffusion mediated release of small molecular weight fluorescein from the gelator matrix. *In vitro* growth inhibition assays finally established the gelator compound and the gel scaffold as an inert matrix and thus validated the device for drug delivery.

### 5.1.3. Therapeutics Molecular Gels of Gemcitabine

Gemcitabine was derivatised as esters, amides, carbamates and ureas. However, only one compound (**51d**) possessed the properties of an efficacious chemotherapeutic agent and demonstrated the stability of an injectable gel. Although the compound can't necessarily be defined as a 'prodrug' because of the hydrolytic stability of the

amide linkage, the compound demonstrated a nanomolar potency in both pancreatic (MIA PaCa-2) and gastric (MKN-7) adenocarcinoma cell lines, and demonstrated a high selectivity (> 1000-fold) towards pancreatic and gastric carcinomas over human fibroblasts. The compound was found to form a reasonably stable gel at a low solvent volume fraction ( $\Phi_{\text{EtOH}}$  0.05) when facilitated by a temperature mediated solvent switch.

Based on *in vitro* assays alone, **50d** was the best overall prodrug, the ester linkage provided the enhanced lipophilicity necessary to increase passive diffusion and the cleavable ester necessary to release the active compound. Unfortunately the compound failed to gel under temperature, solvent or salt mediated conditions. Neither **52a** nor **53c** provided significantly stable gels and when tested for growth inhibition displayed 100× lower activity than gemcitabine in the tested cell lines.

## 5.2. Future Work

Work carried out thus far, has provided a good foundation for future development and progression of low molecular weight gelators as a depot for intra-tumoural delivery of chemotherapeutics.

### 5.2.1. Further functionalisation of nucleosides

As previously described in **Chapter 1**, there are multiple, complex functionalities that could be used to enhance the gelation process, including the already probed and well established peptide gelators. From the small library developed in this work, there is much scope for developing nucleoside peptides, both as inert gel scaffolds and therapeutic molecular gels. Aromaticity of the resulting systems will play a big role in the self-assembly process and so new libraries with both aromatic and non-aromatic amino acids should be considered.

Additionally in the case of therapeutic molecular gels, cleavable linkers should be a high priority, the above system could be used as a mode of functionalisation from the 5'-hydroxyl and has already found scope in literature as a therapeutic entity.<sup>228</sup>

### 5.2.2. *In vitro* release of therapeutics from inert-gel scaffold

Both **42c** and **48d** had been validated as scaffolds for diffusion controlled drug release, however, their efficiency towards therapeutics hadn't been considered. Particular consideration for gemcitabine release should be noted. Additional measures to support this data would be the release of a therapeutic from the gel *via in vitro* growth inhibition assays as previously described, and determination of the activity when mediated by diffusion.

### 5.2.3. *In vivo* imaging of drug release

Following the above tests, a more in depth study into the physiological relevance of the hydrogelating system of **48d** e.g. *via* an *in vivo* sub-cutaneous xenograft modelling fluorescent release in the cavity of a resected tumour.

#### **5.2.4. Determining the reason for selectivity seen in MRC-5 fibroblasts**

In **Chapter 4** was noted the parent gemcitabine and synthesised analogues all had astounding selectivity towards carcinoma cell lines over human fibroblast (healthy controls). This finding still remains unexplained. To probe this further more healthy cell lines would need to be tested and other complementary assay run to see if the selectivity was due to the presence or lack of specific tumour markers.

## References

---

- (1) Skilling, K. J.; Citossi, F.; Bradshaw, T. D.; Ashford, M.; Kellam, B.; Marlow, M. *Soft Matter* **2014**, *10*, 237.
- (2) Estroff, L. A.; Hamilton, A. D. *Chemical Reviews* **2004**, *104*, 1201.
- (3) Abdallah, D. J.; Weiss, R. G. *Journal of the Brazilian Chemical Society* **2000**, *11*, 209.
- (4) Terech, P.; Weiss, R. G. *Chemical Reviews* **1997**, *97*, 3133.
- (5) Sangeetha, N. M.; Maitra, U. *Chemical Society Reviews* **2005**, *34*, 821.
- (6) Vemula, P. K.; Wiradharma, N.; Ankrum, J. A.; Miranda, O. R.; John, G.; Karp, J. M. *Curr Opin Biotechnol* **2013**.
- (7) George, M.; Weiss, R. G. *Accounts of Chemical Research* **2006**, *39*, 489.
- (8) van Esch, J. H.; Feringa, B. L. *Angewandte Chemie-International Edition* **2000**, *39*, 2263.
- (9) *Functional Molecular Gels*; Escuder, B.; Miravet, J. F., Eds., 2014.
- (10) Lan, Y.; Corradini, M. G.; Weiss, R. G.; Raghavan, S. R.; Rogers, M. A. *Chemical Society Reviews* **2015**.
- (11) Weiss, R.; Terech, P. *Molecular Gels: Materials with Self-assembled fibrillar networks*; Springer, 2006.
- (12) Graham, T. *Phil. Trans. Roy. Soc* **1861**, *151*, 183.
- (13) Jordan Lloyd, D. *Colloid Chemistry* **1926**.
- (14) Gelbart, W. M.; Ben-Shaul, A. *The Journal of Physical Chemistry*<sup>®</sup> **1996**, *100*, 13169.
- (15) Flory, P. J. *Faraday Discussions* **1975**, *57*, 7.
- (16) Vintiloiu, A.; Leroux, J.-C. *Journal of Controlled Release* **2008**, *125*, 179.
- (17) Estroff, L. A.; Hamilton, A. D. *Angewandte Chemie International Edition* **2000**, *39*, 3447.
- (18) Raeburn, J.; Zamith Cardoso, A.; Adams, D. J. *Chemical Society Reviews* **2013**.
- (19) Israeachvilil, J.; Wennerstrom, H. *Journal of Physical Chemistry* **1992**, *96*, 520.
- (20) Aggeli, A.; Nyrkova, I. A.; Bell, M.; Harding, R.; Carrick, L.; McLeish, T. C. B.; Semenov, A. N.; Boden, N. *Proc Natl Acad Sci U S A* **2001**, *98*, 11857.
- (21) Van Esch, J.; Schoonbeek, F.; De Loos, M.; Kooijman, H.; Spek, A. L.; Kellogg, R. M.; Feringa, B. L. *Chemistry - A European Journal* **1999**, *5*, 937.
- (22) Liu, X. Y. In *Low Molecular Mass Gelators: Design, Self-Assembly, Function*; Fages, F., Ed. 2005; Vol. 256, p 1.
- (23) Liu, X. Y.; Sawant, P. D. *Applied Physics Letters* **2001**, *79*, 3518.

- (24) Liu, X. Y.; Sawant, P. D. *Angewandte Chemie-International Edition* **2002**, *41*, 3641.
- (25) Liu, X.; Sawant, P. *Advanced Materials* **2002**, *14*, 421.
- (26) Liu, X. Y.; Sawant, P. D.; Tan, W. B.; Noor, I. B. M.; Pramesti, C.; Chen, B. H. *J Am Chem Soc* **2002**, *124*, 15055.
- (27) Liu, X. Y.; Sawant, P. D. *Advanced Materials* **2002**, *14*, 421.
- (28) Pal, A.; Patra, T.; Dey, J. *Chemical Physics Letters* **2013**, *556*, 245.
- (29) Mukai, M.; Minamikawa, H.; Aoyagi, M.; Asakawa, M.; Shimizu, T.; Kogiso, M. *Soft Matter* **2012**, *8*, 11979.
- (30) Segarra-Maset, M.; Nebot, V.; Miravet, J.; Escuder, B. *Chemical Society Reviews* **2013**, *42*, 7086.
- (31) Zhang, Z.; Grelet, E. *Soft Matter* **2013**, *9*, 1015.
- (32) Brizard, A.; Oda, R.; Huc, I. In *Low Molecular Mass Gelator*; Springer Berlin Heidelberg: 2005; Vol. 256, p 167.
- (33) Hanabusa, K.; Maesaka, Y.; Kimura, M.; Shirai, H. *Tetrahedron Letters* **1999**, *40*, 2385.
- (34) Maitra, U.; Kumar Potluri, V.; Sangeetha, N. M.; Babu, P.; Raju, A. R. *Tetrahedron: Asymmetry* **2001**, *12*, 477.
- (35) Pham, Q. N.; Brosse, N.; Frochot, C.; Dumas, D.; Hocquet, A.; Jamart-Gregoire, B. *New Journal of Chemistry* **2008**, *32*, 1131.
- (36) Jokic, M.; Makarevic, J.; Zinic, M. *Journal of the Chemical Society, Chemical Communications* **1995**, *0*, 1723.
- (37) Engelkamp, H.; Middelbeek, S.; Nolte, R. J. M. *Science* **1999**, *284*, 785.
- (38) Skilling, K. J.; Ndungu, A.; Kellam, B.; Ashford, M.; Bradshaw, T. D.; Marlow, M. *Journal of Materials Chemistry B* **2014**, *2*, 8412.
- (39) Adams, D. J.; Butler, M. F.; Frith, W. J.; Kirkland, M.; Mullen, L.; Sanderson, P. *Soft Matter* **2009**, *5*, 1856.
- (40) Tang, C.; Smith, A. M.; Collins, R. F.; Ulijn, R. V.; Saiani, A. *Langmuir* **2009**, *25*, 9447.
- (41) Gao, J.; Wang, H.; Wang, L.; Wang, J.; Kong, D.; Yang, Z. *Journal of the American Chemical Society* **2009**, *131*, 11286.
- (42) Wang H; Wei J; Yang C; Zhao H; Li D; Yin Z; Yang, Z. *Bomaterials* **2012**, *33*, 5848.
- (43) Chen, L.; Raeburn, J.; Sutton, S.; Spiller, D. G.; Williams, J.; Sharp, J. S.; Griffiths, P. C.; Heenan, R. K.; King, S. M.; Paul, A.; Furzeland, S.; Atkins, D.; Adams, D. J. *Soft Matter* **2011**, *7*, 9721.
- (44) Ganji, F.; Vasheghani-Farahani, E. *Iranian Polymer Journal* **2009**, *18*, 63.
- (45) Kempe, S.; Mader, K. *Journal of Controlled Release* **2012**, *161*, 668.

- (46) Kloxin, A. M.; Kloxin, C. J.; Bowman, C. N.; Anseth, K. S. *Advanced Materials* **2010**, *22*, 3484.
- (47) Kavanagh, G. M.; Ross-Murphy, S. B. *Progress in Polymer Science* **1998**, *23*, 533.
- (48) Rogers, M. A.; Kim, J. H. J. *Food Research International* **2011**, *44*, 1447.
- (49) Mahler, A.; Reches, M.; Rechter, M.; Cohen, S.; Gazit, E. *Advanced Materials* **2006**, *18*, 1365.
- (50) Li, X.; Yi, K.; Shi, J.; Gao, Y.; Lin, H.-C.; Xu, B. *J Am Chem Soc* **2011**, *133*, 17513.
- (51) Raeburn, J.; Pont, G.; Chen, L.; Cesbron, Y.; Levy, R.; Adams, D. J. *Soft Matter* **2012**, *8*, 1168.
- (52) Adams, D. J.; Mullen, L. M.; Berta, M.; Chen, L.; Frith, W. J. *Soft Matter* **2010**, *6*, 1971.
- (53) Bildstein, L.; Pili, B.; Marsaud, V.; Wack, S.; Meneau, F.; Lepetre-Mouelhi, S.; Desmaele, D.; Bourgaux, C.; Couvreur, P.; Dubernet, C. *European Journal of Pharmaceutics and Biopharmaceutics* **2011**, *79*, 612.
- (54) J.J. Panda, A. M., A. Basu, V.S. Chauhan *Biomacromolecules* **2008**, *9*, 2244.
- (55) Wang, G.; Cheuk, S.; Yang, H.; Goyal, N.; Reddy, P. V. N.; Hopkinson, B. *Langmuir* **2009**, 8696.
- (56) Terech, P.; Friol, S.; Sangeetha, N.; Talmon, Y.; Maitra, U. *Rheologica Acta* **2006**, *45*, 435.
- (57) Heeres, A.; van der Pol, C.; Stuart, M.; Friggeri, A.; Feringa, B. L.; van Esch, J. J. *J Am Chem Soc* **2003**, *125*, 14252.
- (58) Fuhrhop, J. H.; Schnieder, P.; Rosenberg, J.; Boekema, E. *J Am Chem Soc* **1987**, *109*, 3387.
- (59) Terech, P.; de Geyer, A.; Struth, B.; Talmon, Y. *Advanced Materials* **2002**, *14*, 495.
- (60) Hirst, A. R.; Coates, I. A.; Boucheteau, T. R.; Miravet, J. F.; Escuder, B.; Castelletto, V.; Hamley, I. W.; Smith, D. K. *J Am Chem Soc* **2008**, *130*, 9113.
- (61) Banerjee, S.; Das, R. K.; Terech, P.; de Geyer, A.; Aymonier, C.; Loppinet-Serani, A.; Raffy, G.; Maitra, U.; Del Guerzo, A.; Desvergne, J.-P. *Journal of Materials Chemistry C* **2013**, *1*, 3305.
- (62) Lebel, O.; Perron, M.-E.; Maris, T.; Zalzal, S. F.; Nanci, A.; Wuest, J. D. *Chem Mater* **2006**, *18*, 3616.
- (63) Escuder, B.; Llusar, M.; Miravet, J. F. *The Journal of Organic Chemistry* **2006**, *71*, 7747.
- (64) Iqbal, S.; Rodriguez-Llansola, F.; Escuder, B.; Miravet, J. F.; Verbruggen, I.; Willem, R. *Soft Matter* **2010**, *6*, 1875.
- (65) Hanabusa, K.; Matsumoto, M.; Kimura, M.; Kakehi, A.; Shirai, H. *Journal of Colloid and Interface Science* **2000**, *224*, 231.

- (66) de Loos, M.; van Esch, J.; Kellogg, R. M.; Feringa, B. L. *Angewandte Chemie-International Edition* **2001**, *40*, 613.
- (67) George, M.; Weiss, R. G. *Langmuir* **2003**, *19*, 8168.
- (68) Suzuki, M.; Yumoto, M.; Kimura, M.; Shirai, H.; Hanabusa, K. *Helvetica Chimica Acta* **2003**, *86*, 2228.
- (69) Capitani, D.; Rossi, E.; Segre, A. L.; Giustini, M.; Luisi, P. L. *Langmuir* **1993**, *9*, 685.
- (70) Tata, M.; John, V. T.; Waguespack, Y. Y.; McPherson, G. L. *J Am Chem Soc* **1994**, *116*, 9464.
- (71) Celis, S.; Nolis, P.; Illa, O.; Branchadell, V.; Ortuno, R. *Organic & Biomolecular Chemistry* **2013**, *11*, 2839.
- (72) Hanabusa, K.; Yamada, M.; Kimura, M.; Shirai, H. *Angewandte Chemie-International Edition in English* **1996**, *35*, 1949.
- (73) Uhrich, K. E.; Cannizzaro, S. M.; Langer, R. S.; Shakesheff, K. M. *Chemical Reviews* **1999**, *99*, 3181.
- (74) Cui, H.; Webber, M. J.; Stupp, S. I. *Biopolymers* **2010**, *94*, 1.
- (75) Ulijn, R.; Bibi, N.; Jayawarna, V.; Thornton, P.; Todd, S.; Mart, R.; Smith, A.; Gough, J. *Materials Today* **2007**, *10*, 40.
- (76) Tian, R.; Chen, J.; Niu, R. *Nanoscale* **2014**, *6*, 3474.
- (77) Vegners, R.; Shestakova, I.; Kalvinsh, I.; Ezzell, R. M.; Janmey, P. A. *Journal of peptide science : an official publication of the European Peptide Society* **1995**, *1*, 371.
- (78) Nagai, Y.; Unsworth, L. D.; Koutsopoulos, S.; Zhang, S. *Journal of Controlled Release* **2006**, *115*, 18.
- (79) Koutsopoulos, S.; Unsworth, L. D.; Nagaia, Y.; Zhang, S. *Proceedings of the National Academy of Sciences of the United States of America* **2009**, *106*, 4623.
- (80) Sutton, S.; Campbell, N. L.; Cooper, A. I.; Kirkland, M.; Frith, W. J.; Adams, D. J. *Langmuir* **2009**, *25*, 10285.
- (81) Naskar, J.; Palui, G.; Banerjee, A. *Journal of Physical Chemistry B* **2009**, *113*, 11787.
- (82) Soukasene, S.; Toft, D. J.; Moyer, T. J.; Lu, H.; Lee, H.-K.; Standley, S. M.; Cryns, V. L.; Stupp, S. I. *ACS Nano* **2011**, *5*, 9113.
- (83) Murdan, S. *Expert opinion on drug delivery* **2005**, *2*, 489.
- (84) Penzes, T.; Blazso, G.; Aigner, Z.; Falkay, G.; Eros, I. *International Journal of Pharmaceutics* **2005**, *298*, 47.
- (85) Couffin-Hoarau, A. C.; Motulsky, A.; Delmas, P.; Leroux, J. C. *Pharmaceutical Research* **2004**, *21*, 454.
- (86) Motulsky, A.; Lafleur, M.; Couffin-Hoarau, A. C.; Hoarau, D.; Boury, F.; Benoit, J. P.; Leroux, J. C. *Biomaterials* **2005**, *26*, 6242.

- (87) Plourde, F.; Motulsky, A.; Couffin-Hoarau, A. C.; Hoarau, D.; Ong, H.; Leroux, J. C. *Journal of Controlled Release* **2005**, *108*, 433.
- (88) Bastiat, G.; Leroux, J.-C. *Journal of Materials Chemistry* **2009**, *19*, 3867.
- (89) Bastiat, G.; Plourde, F.; Motulsky, A.; Furtos, A.; Dumont, Y.; Quirion, R.; Fuhrmann, G.; Leroux, J.-C. *Biomaterials* **2010**, *31*, 6031.
- (90) Iwanaga, K.; Sumizawa, T.; Miyazaki, M.; Kakemi, M. *International Journal of Pharmaceutics* **2010**, *388*, 123.
- (91) Cui, H.; Webber, M. J.; Stupp, S. I. *Peptide Science* **2010**, *94*, 1.
- (92) Rautio, J.; Kumpulainen, H.; Heimbach, T.; Oliyai, R.; Oh, D.; Jarvinen, T.; Savolainen, J. *Nat Rev Drug Discov* **2008**, *7*, 255.
- (93) Kim, J.-K.; Anderson, J.; Jun, H.-W.; Repka, M. A.; Jo, S. *Molecular Pharmaceutics* **2009**, *6*, 978.
- (94) Van Bommel, K.; Stuart, M.; Feringa, B.; Van Esch, J. *Organic & Biomolecular Chemistry* **2005**, *3*, 2917.
- (95) Bhuniya, S.; Seo, Y. J.; Kim, B. H. *Tetrahedron Letters* **2006**, *47*, 7153.
- (96) Li Jiyang; Yi, K.; Shi, J.; Gao, Y.; Zhou, J.; Xu, B. *Beilstein Journal of Organic Chemistry* **2013**, *9*, 908.
- (97) Vemula, P. K.; Cruikshank, G. A.; John, G.; Karp, J. M.; Ieee *Enzyme Responsive Acetaminophen Hydrogels*, 2009.
- (98) Gao, Y.; Kuang, Y.; Guo, Z.-F.; Guo, Z.; Krauss, I. J.; Xu, B. *Journal of the American Chemical Society* **2009**, *131*, 13576.
- (99) Wang, H.; Yang, C.; Wang, L.; Kong, D.; Zhang, Y.; Yang, Z. *Chem Commun (Camb)* **2011**, *47*, 4439.
- (100) Wang, H.; Yang, Z. *Soft Matter* **2012**, *8*, 2344.
- (101) Li, X.; Yang, C.; Zhang, Z.; Wu, Z.; Deng, Y.; Liang, G.; Yang, Z.; Chen, H. *Journal of Materials Chemistry* **2012**, *22*, 21838.
- (102) Li, R.; Shu, C.; Wang, W.; Wang, X.; Li, H.; Xu, D.; Zhong, W. *Journal of Pharmaceutical Sciences* **2015**, *104*, 2266.
- (103) Webber, M. J.; Matson, J. B.; Tamboli, V. K.; Stupp, S. I. *Biomaterials* **2012**, *33*, 6823.
- (104) Xing, B. G.; Yu, C. W.; Chow, K. H.; Ho, P. L.; Fu, D. G.; Xu, B. *Journal of the American Chemical Society* **2002**, *124*, 14846.
- (105) Ellis-Behnke, R. G.; Liang, Y.-X.; You, S.-W.; Tay, D. K. C.; Zhang, S.; So, K.-F.; Schneider, G. E. *Proc Natl Acad Sci U S A* **2006**, *103*, 5054.
- (106) Matson, J. B.; Newcomb, C. J.; Bitton, R.; Stupp, S. I. *Soft Matter* **2012**, *8*, 3586.
- (107) Wang, H.; Lv, L.; Xu, G.; Yang, C.; Sun, J.; Yang, Z. *Journal of Materials Chemistry* **2012**, *22*, 16933.

- (108) Lee, J. B.; Peng, S.; Yang, D.; Roh, Y. H.; Funabashi, H.; Park, N.; Rice, E. J.; Chen, L.; Long, R.; Wu, M.; Luo, D. *Nat Nano* **2012**, *7*, 816.
- (109) Gellert, M.; Lipsett, M. N.; Davies, D. R. *Proceedings of the National Academy of Sciences of the United States of America* **1962**, *48*, 2013.
- (110) Sasisekharan, V.; Zimmerman, S.; Davies, D. R. *Journal of Molecular Biology* **1975**, *92*, 171.
- (111) Araki, K.; Yoshikawa, I. *Low Molecular Mass Gelators: Design, Self-Assembly, Function* **2005**, *256*, 133.
- (112) Moreau, L.; Barthélémy, P.; El Maataoui, M.; Grinstaff, M. W. *J Am Chem Soc* **2004**, *126*, 7533.
- (113) Iwaura, R.; Yoshida, K.; Masuda, M.; Yase, K.; Shimizu, T. *Chemistry of Materials* **2002**, *14*, 3047.
- (114) Park, S. M.; Lee, Y. S.; Kim, B. H. *Chemical Communications* **2003**, 2912.
- (115) Yun, Y. J.; Park, S. M.; Kim, B. H. *Chemical Communications* **2003**, 254.
- (116) Yoshikawa, I.; Yanagi, S.; Yamaji, Y.; Araki, K. *Tetrahedron* **2007**, *63*, 7474.
- (117) Simeone, L.; Milano, D.; De Napoli, L.; Irace, C.; Di Pascale, A.; Boccalon, M.; Tecilla, P.; Montesarchio, D. *Chemistry-a European Journal* **2011**, *17*, 13854.
- (118) Godeau, G.; Barthelemy, P. *Langmuir* **2009**, *25*, 8447.
- (119) Latxague, L.; Dalila, M.-J.; Patwa, A.; Ziane, S.; Chassande, O.; Godeau, G.; Barthelemy, P. *Comptes Rendus Chimie* **2012**, *15*, 29.
- (120) Wu, D.; Zhou, J.; Shi, J.; Du, X.; Xu, B. *Chem Commun (Camb)* **2014**, *50*, 1992.
- (121) Yuan, D.; Zhou, R.; Shi, J.; Du, X.; Li, X.; Xu, B. *RSC Advances* **2014**, *4*, 26487.
- (122) Park, S. M.; Y, S.; Kim, B. H. *Org Biomol Chem* **2007**, *5*, 610.
- (123) de Sousa Cavalcante, L.; Monteiro, G. *European Journal of Pharmacology* **2014**, *8*
- (124) Di, M.; Di, C.; Macchini; Nobili; Vecchiarelli; Brandi; Biasco *Oncology Reports* **2010**, *23*, 1183.
- (125) Bilimoria, K. Y.; Bentrem, D. J.; Ko, C. Y.; Stewart, A. K.; Winchester, D. P.; Talamonti, M. S. *Annals of Surgery* **2007**, *246*, 173.
- (126) Vincent, A.; Herman, J.; Schulick, R.; Hruban, R. H.; Goggins, M. *The Lancet*, *378*, 607.
- (127) Ritzel, M.; Ng, A.; Yao, S.; Graham, K.; Loewen, S.; Smith, K.; Hyde, R. J.; Karpinski, E.; Cass, C.; Baldwin, S. A.; Young, J. D. *Mol Membr Biol* **2001**, *18*.
- (128) Heinemann, V.; Hertel, L. W.; Grindey, G. B.; Plunkett, W. *Cancer Res* **1988**, *48*, 4024.
- (129) Bouffard, D. Y.; Laliberté, J.; Momparler, R. L. *Biochemical Pharmacology* **1993**, *45*, 1857.

- (130) Hu, R.; Lam, W.; Hsu, C.-H.; Cheng, Y.-C. *Plos One* **2011**, *6*, e19490.
- (131) Ruiz van Haperen, V. W. T.; Veerman, G.; Eriksson, S.; Boven, E.; Stegmann, A. P. A.; Hermsen, M.; Vermorken, J. B.; Pinedo, H. M.; Peters, G. J. *Cancer Res* **1994**, *54*, 4138.
- (132) Bergman, A. A.; Pinedo, H. A.; Peters, G. J. *Drug Resistance Updates* **2002**, *5*, 176.
- (133) Huang, P.; Chubb, S.; Hertel, L. W.; Grindey, G. B.; Plunkett, W. *Cancer Res* **1991**, *51*, 6110.
- (134) Huang, P.; Plunkett, W. *Seminars in Oncology* **1995**, *22*, 19.
- (135) Heinemann, V.; Xu, Y. Z.; Chubb, S.; Sen, A.; Hertel, L. W.; Grindey, G. B.; Plunkett, W. *Molecular Pharmacology* **1990**, *38*, 567.
- (136) Ferreira, C. G.; Span, S. W.; Peters, G. J.; Kruyt, F. A.; Giaccone, G. *Cancer Res* **2000**, *60*, 7133.
- (137) Nakashima, M.; Adachi, S.; Yasuda, I.; Yamauchi, T.; Kawaguchi, J.; Itani, M.; Yoshioka, T.; Matsushima-Nishiwaki, R.; Hirose, Y.; Kozawa, O.; Moriwaki, H. *Cancer Lett* **2011**, 218.
- (138) Walker, E. J.; Ko, A. H. *World Journal of Gastroenterology* **2014**, *20*.
- (139) Kleger, A.; Perkhofer, L.; Seufferlein, T. *Annals of Oncology* **2014**.
- (140) Nakano, Y.; Tanno, S.; Koizumi, K.; Nishikawa, T.; Nakamura, K.; Minoguchi, M.; Izawa, T.; Mizukami, Y.; Okumura, T.; Kohgo, Y. *British Journal of Cancer* **2007**, *96*, 457.
- (141) Mackey, J. R.; Mani, R. S.; Selner, M.; Mowles, D.; Young, J. D.; Belt, J. A.; Crawford, C. R.; Cass, C. E. *Cancer Res* **1998**, *58*, 4349.
- (142) Endicott, J. A.; Ling, V. *Annu Rev Biochem* **1989**, *58*, 137.
- (143) Grant, S.; Turner, A.; Nelms, P.; Yanovich, S. *Leukemia* **1995**, *9*, 808.
- (144) Zhang, Y.; Gao, Y.; Wen, X.; Ma, H. *Asian Journal of Pharmaceutical Sciences* **2014**, *9*, 65.
- (145) Bergman, A. M.; Kuiper, C. M.; Noordhuis, P.; Smid, K.; Voorn, D. A.; Comijn, E. M.; Myhren, F.; Sandvold, M. L.; Hendriks, H. R.; Fodstad, O.; Breistol, K.; Peters, G. J. *Nucleosides Nucleotides Nucleic Acids* **2004**, *23*, 1329.
- (146) Couvreur, P.; Stella, B.; Reddy, L. H.; Hillaireau, H.; Dubernet, C.; Desmaële, D.; Lepître-Mouelhi, S.; Rocco, F.; Dereuddre-Bosquet, N.; Clayette, P.; Rosilio, V.; Marsaud, V.; Renoir, J.-M.; Cattel, L. *Nano Letters* **2006**, *6*, 2544.
- (147) Wickremsinhe, E.; Bao, J.; Smith, R.; Burton, R.; Dow, S.; Perkins, E. *Pharmaceutics* **2013**, *5*, 261.
- (148) Fang, Y.; Du, F.; Xu, Y.; Meng, H.; Huang, J.; Zhang, X.; Lu, W.; Liu, S.; Yu, J. *Colloids and Surfaces B: Biointerfaces* **2015**, *128*, 357.
- (149) Song, X.; Lorenzi, P. L.; Landowski, C. P.; Vig, B. S.; Hilfinger, J. M.; Amidon, G. L. *Molecular Pharmaceutics* **2005**, *2*, 157.

- (150) Bergman, A. M.; Adema, A. D.; Balzarini, J.; Bruheim, S.; Fichtner, I.; Noordhuis, P.; Fodstad, O.; Myhren, F.; Sandvold, M. L.; Hendriks, H. R.; Peters, G. J. *Invest New Drugs* **2011**, *29*, 456.
- (151) Wu, W.; Sigmond, J.; Peters, G. J.; Borch, R. F. *J Med Chem* **2007**, *50*, 3743.
- (152) Orbach, R.; Adler-Abramovich, L.; Zigerson, S.; Mironi-Harpaz, I.; Seliktar, D.; Gazit, E. *Biomacromolecules* **2009**, *10*, 2646.
- (153) Chen, L.; Morris, K.; Laybourn, A.; Elias, D.; Hicks, M. R.; Rodger, A.; Serpell, L.; Adams, D. J. *Langmuir* **2010**, *26*, 5232.
- (154) Vilaca, H.; Pereira, G.; Castro, T. G.; Hermenegildo, B. F.; Shi, J.; Faria, T. Q.; Micaelo, N.; Brito, R. M. M.; Xu, B.; Castanheira, E. M. S.; Martins, J. A.; Ferreira, P. M. T. *Journal of Materials Chemistry B* **2015**, *3*, 6355.
- (155) Araki, K.; Yoshikawa, I. In *Low Molecular Mass Gelators: Design, Self-Assembly, Function*; Fages, F., Ed.; Springer-Verlag Berlin: Berlin, 2005; Vol. 256, p 133.
- (156) Guschlbauer, W.; J.F., C.; Thiele, D. *J Biomol Struct Dyn* **1990**, *8*, 491.
- (157) Godeau, G.; Bernard, J.; Staedel, C.; Barthelemy, P. *Chem Commun (Camb)* **2009**, 5127.
- (158) Godeau, G.; Brun, C.; Arnion, H.; Staedel, C.; Barthélémy, P. *Tetrahedron Letters* **2010**, *51*, 1012.
- (159) Wu, D.; Du, X.; Shi, J.; Zhou, J.; Xu, B. *Chinese Journal of Chemistry* **2014**, *32*, 313.
- (160) Andersen, N. K.; Spáčilová, L.; Jensen, M. D.; Kočalka, P.; Jensen, F.; Nielsen, P. *Nucleic Acids Symposium Series* **2008**, *52*, 149.
- (161) Dodd, D. W.; Jones, N. D.; Hudson, R. H. E. *Artificial DNA: PNA + XNA* **2010**, *1*, 90.
- (162) Thanassoulas, A.; Barthélémy, P.; Navailles, L.; Sigaud, G. *The Journal of Physical Chemistry B* **2014**, *118*, 6570.
- (163) Jin, Y. G.; Lian, Y. J.; Du, L. N. *Colloids and Surfaces a-Physicochemical and Engineering Aspects* **2012**, *393*, 60.
- (164) Chhikara, B. S.; Mandal, D.; Parang, K. *Eur J Med Chem* **2010**, *45*, 4601.
- (165) Kaminski, Z. J. *Biopolymers (Pept. Sci.)* **2000**, 140.
- (166) Rode, A. B.; Son, S. J.; Hong, I. S. *Bulletin of the Korean Chemical Society* **2010**, *31*, 2061.
- (167) Bandgar, B. P.; Pandit, S. S. *Tetrahedron Letters* **2003**, *44*, 3855.
- (168) Marlow, M.; Al-Ameedee, M.; Smith, T.; Wheeler, S.; Stocks, M. J. *Chem Commun (Camb)* **2015**, *51*, 6384.
- (169) Mahire, R. R.; Agrawal, D. S.; Patil, D. K.; More, D. H. *RSC Advances* **2014**, *4*, 33286.

- (170) Grunt, T. W.; Somay, C.; Pavelka, M.; Ellinger, A.; Dittrich, E.; Dittrich, C. *Journal of Cell Science* **1991**, 657.
- (171) McIntyre, L. J.; Kim, Y. S. *European Journal of Cancer Clinical Oncology* **1984**, 20, 265.
- (172) Rodrigues, M.; Calpena, A. C.; Amabilino, D. B.; Garduno-Ramirez, M. L.; Perez-Garcia, L. *Journal of Materials Chemistry B* **2014**, 2, 5419.
- (173) Joseph, T. R. In *Encyclopedia of Pharmaceutical Technology, Third Edition*; Taylor & Francis: 2013; Vol. null, p 806.
- (174) Allum, W.; Griffin, S.; Watson, A.; Colin-Jones, D. *Gut*. **2002**, 1-23.
- (175) Orbach, R.; Mironi-Harpaz, I.; Adler-Abramovich, L.; Mossou, E.; Mitchell, E. P.; Forsyth, V. T.; Gazit, E.; Seliktar, D. *Langmuir* **2012**, 28, 2015.
- (176) Smith, A. M.; Williams, R. J.; Tang, C.; Coppo, P.; Collins, R. F.; Turner, M. L.; Saiani, A.; Ulijn, R. V. *Advanced Materials* **2008**, 20, 37.
- (177) Zurcher, D. M.; McNeil, A. J. *The Journal of Organic Chemistry* **2015**, 80, 2473.
- (178) Mezger, T. G. *The Rheology Handbook*; 3rd Revised Edition ed.; Vincentz Network, 2011.
- (179) Raeburn, J.; Mendoza-Cuenca, C.; Cattoz, B. N.; Little, M. A.; Terry, A. E.; Zamith Cardoso, A.; Griffiths, P. C.; Adams, D. J. *Soft Matter* **2015**, 11, 927.
- (180) Ritger, P. L.; Peppas, N. A. *Journal of Controlled Release* **1987**, 5, 23.
- (181) Sutton, S.; Campbell, N. L.; Cooper, A. I.; Kirkland, M.; Frith, W. J.; Adams, D. J. *Langmuir* **2009**, 25, 10285.
- (182) Howe, R. C. T.; Smalley, A. P.; Guttenplan, A. P. M.; Doggett, M. W. R.; Eddleston, M. D.; Tan, J. C.; Lloyd, G. O. *Chemical communications (Cambridge, England)* **2013**, 49, 4268.
- (183) Awhida, S.; Draper, E. R.; McDonald, T. O.; Adams, D. J. *Journal of Colloid and Interface Science* **2015**, 455, 24.
- (184) Wang, Y.; Tang, L.; Yu, J. *Crystal Growth & Design* **2008**, 8, 884.
- (185) Cui, J.; Shen, Z.; Wan, X. *Langmuir* **2010**, 26, 97.
- (186) Van Roey, P.; Salerno, J. M.; Chu, C. K.; Schinazi, R. F. *Proc Natl Acad Sci U S A* **1989**, 86, 3929.
- (187) Shi, J.; Gao, Y.; Yang, Z.; Xu, B. *Beilstein Journal of Organic Chemistry* **2011**, 7, 167.
- (188) Draper, E. R.; McDonald, T. O.; Adams, D. J. *Chem Commun (Camb)* **2015**, 51, 6595.
- (189) Phadke, A.; Zhang, C.; Arman, B.; Hsu, C.-C.; Mashelkar, R. A.; Lele, A. K.; Tauber, M. J.; Arya, G.; Varghese, S. *Proceedings of the National Academy of Sciences* **2012**, 109, 4383.

- (190) Fang, Y.; Wang, C.-F.; Zhang, Z.-H.; Shao, H.; Chen, S. *Scientific Reports* **2013**, *3*, 2811.
- (191) Yan, C.; Pochan, D. J. *Chemical Society Reviews* **2010**, *39*, 3528.
- (192) Hirst, A. R.; Miravet, J. F.; Escuder, B.; Noirez, L.; Castelletto, V.; Hamley, I. W.; Smith, D. K. *Chemistry – A European Journal* **2009**, *15*, 372.
- (193) Smith, M. M.; Smith, D. K. *Soft Matter* **2011**, *7*, 4856.
- (194) Panda, J. J.; Mishra, A.; Basu, A.; Chauhan, V. S. *Biomacromolecules* **2008**, *9*, 2244.
- (195) Liebmann, T.; Rydholm, S.; Akpe, V.; Brismar, H. *Bmc Biotechnology* **2007**, *7*.
- (196) Ziane, S.; Schlaubitz, S.; Miraux, S.; Patwa, A.; Lalande, C.; Bilem, I.; Lepreux, S.; Rousseau, B.; Le Meins, J. F.; Latxague, L.; Barthelemy, P.; Chassande, O. *European Cells & Materials* **2012**, *23*, 147.
- (197) Wang, W. J.; Wang, H. M.; Ren, C. H.; Wang, J. Y.; Tan, M.; Shen, J.; Yang, Z. M.; Wang, P. G.; Wang, L. *Carbohydrate Research* **2011**, *346*, 1013.
- (198) Buerkle, L. E.; von Recum, H. A.; Rowan, S. J. *Chemical Science* **2012**, *3*, 564.
- (199) van den Bosch, E.; Gielens, C. *International Journal of Biological Macromolecules* **2003**, *32*, 129.
- (200) Beaumont, K.; Webster, R.; Gardner, I.; Dack, K. *Current Drug Metabolism* **2003**, *4*, 461.
- (201) Wu, W.; Sigmond, J.; Peters, G. J.; Borch, R. F. *J Med Chem* **2007**, *50*, 3743
- (202) Chhikara, B. S.; Mandal, D.; Parang, K. *Eur J Med Chem* **2010**, *45*, 4601.
- (203) Li, N.; Zong, M.-H.; Ma, D. *European Journal of Organic Chemistry* **2008**, *2008*, 5375.
- (204) Li, X. F.; Zong, M. H.; Zhao, G. L. *Bioorg Med Chem Lett* **2010**, *20*, 4125.
- (205) Katsoura, M. H.; Polydera, A. C.; Tsironis, L. D.; Petraki, M. P.; Rajačić, S. K.; Tselepis, A. D.; Stamatis, H. *New Biotechnology* **2009**, *26*, 83.
- (206) Pavlidis, I. V.; Vorhaben, T.; Tsoufis, T.; Rudolf, P.; Bornscheuer, U. T.; Gournis, D.; Stamatis, H. *Bioresour Technol* **2012**, *115*, 164.
- (207) Uppenberg, J.; Trier Hansen, M.; Patkar, S.; Jones, T. A. *Structure* **1994**, *2*, 293.
- (208) Uppenberg, J.; Ohrner, N.; Norin, M.; Hult, K.; Kleywegt, G. J.; Patkar, S.; Waagen, V.; Anthonsen, T.; Jones, T. A. *Biochemistry* **1995**, *34*, 16838.
- (209) Jin, Y.; Lian, Y.; Du, L. *Colloids and Surfaces A: Physicochemical and Engineering Aspects* **2012**, *393*, 60.
- (210) Dasari, M.; Acharya, A. P.; Kim, D.; Lee, S.; Lee, S.; Rhea, J.; Molinaro, R.; Murthy, N. *Bioconjug Chem* **2012**, *24*, 4.
- (211) Bender, D. M.; Bao, J.; Dantzig, A. H.; Diseroad, W. D.; Law, K. L.; Magnus, N. A.; Peterson, J. A.; Perkins, E. J.; Pu, Y. J.; Reutzel-Edens, S. M.; Remick, D. M.; Starling, J.

- J.; Stephenson, G. A.; Vaid, R. K.; Zhang, D.; McCarthy, J. R. *J Med Chem* **2009**, *52*, 6958.
- (212) Baker, B. C.; Acton, A. L.; Stevens, G. C.; Hayes, W. *Tetrahedron* **2014**, *70*, 8303.
- (213) Coyne, C. P.; Jones, T.; Pharr, T. *Bioorg Med Chem* **2011**, *19*, 67.
- (214) Mart, R. J.; Osborne, R. D.; Stevens, M. M.; Ulijn, R. V. *Soft Matter* **2006**, *2*, 822.
- (215) Adams, D. J. *Macromolecular Bioscience* **2011**, *11*, 160.
- (216) Al-Warhi, T. I.; Al-Hazimi, H. M. A.; El-Faham, A. *Journal of Saudi Chemical Society* **2012**, *16*, 97.
- (217) Zhang, L.; Wang, X.; Wang, T.; Liu, M. *Small* **2014**, n/a.
- (218) Imura, T.; Kawamura, D.; Ishibashi, Y.; Morita, T.; Sato, S.; Fukuoka, T.; Kikkawa, Y.; Kitamoto, D. *J. Oleo Sci.* **2012**, *61*, 659.
- (219) Naota, T.; Koori, H. *J Am Chem Soc* **2005**, *127*, 9324.
- (220) Cravotto, G.; Cintas, P. *Chemical Society Reviews* **2009**, *38*, 2684.
- (221) Zhang, M.; Meng, L.; Cao, X.; Jiang, M.; Yi, T. *Soft Matter* **2012**, *8*, 4494.
- (222) Goyal, N.; Cheuk, S.; Wang, G. *Tetrahedron* **2010**, *66*, 5962.
- (223) Terech, P. *Langmuir* **2009**, *25*, 8370.
- (224) Duxbury, M. S.; Ito, H.; Zinner, M.; Ashley, S. W.; Whang, E. E. *Oncogene* **2004**, *23*, 1539.
- (225) Morikawa, T.; Hino, R.; Uozaki, H.; Maeda, D.; Ushiku, T.; Shinozaki, A.; Sakatani, T.; Fukayama, M. *Human Pathology*, *41*, 1742.
- (226) Weiss, J. T.; Dawson, J. C.; Fraser, C.; Rybski, W.; Torres-Sánchez, C.; Bradley, M.; Patton, E. E.; Carragher, N. O.; Unciti-Broceta, A. *J Med Chem* **2014**, *57*, 5395.
- (227) Adema, A.; Smid, K.; Losekoot, N.; Myhren, F.; Sandvold, M.; Peters, G. *Cancer Res* **2008**, *68*, 5740.
- (228) Song, X.; Lorenzi, P. L.; Landowski, C. P.; Vig, B. S.; Hilfinger, J. M.; Amidon, G. L. *Molecular Pharmaceutics* **2004**, *2*, 157.

